MULTI-OBJECTIVE CONTROL ALLOCATION

Ramey Jamil
philosophiae doctor

Autonomous and Intelligent Systems
Department of Engineering Physics, School of Engineering
Cranfield University, Cranfield
United Kingdom

2012

I am, and ever will be, a white-socks, pocket-protector, nerdy engineer, born under the second law of thermodynamics, steeped in steam tables, in love with free-body diagrams, transformed by Laplace and propelled by compressible flow.

–Neil Armstrong 1930-2012

–To My Parents

Breviarium

Performance and redundancy requirements imposed on state-of-the-art unmmaned combat aerial vehicles often lead to over-actuated systems with a mix of conventional and novel moment generators. Consequently, control allocation schemes have become a crucial part of the flight control architecture and their design is now a growing problem. This thesis presents a four control allocation scheme designed to meet multiple objectives and resolve objective conflicts by finding the 'Pareto' optimal solution, namely; Weighted Control Allocation, Minimax Control Allocation, Canonical Control Allocation and Classical. This is defined as a solution to the multi-objective optimisation problem which is non-dominated for all objectives. The scheme is applied to a six degrees of freedom nonlinear simulation of an aircraft equipped with conventional control surfaces as well as fluidic thrust vectoring and circulation control. The results indicate a perfect allocation of the total control demand onto the actuator suite.

Agnitiones

The journey through academia is a long and arduous one. It delves into a myriad of abstract concepts and foreign territories to which only a few have ever tread. It can seem somewhat insurmountable if it were not for the help and support of one's colleagues and friends. I would hence like to take a moment to express my greatest gratitude to all who have helped me circumvent the turbulent ocean that is academia. First of all I would to thank my parents, Jamal Jamil and Mona Kidorey, their continued support has guided me though my entire life. They have yet to steer me wrong and I have and shall always hold the up-most respect for them both.

I am truly indebted to my fellow researchers with whom I have not only shared a *somewhat less that desirable office* but amounted innumerable experiences with. You all have played such a vital role in my Cranfield experience and I'd like to thank you all; Alicia Li, Henry Andres Porras, Samer Muhi, Marco Melega, Hakim Oheda, Baba Omar, Neil Panchal, Francis Salama, Saurav Agarwal, Pierre Jameson, Tareq Alawadi, Antonis Foivos, Hamid Alturbeh, Mudessier Lone, Hyondong Oh and Mark Picciani who, although was a late arrival has definitely had a positive influence on me.

With particular mention to Guido Monterzino whose knowledge of all things engineering has no bounds. I shall always hold a great fondness to the times we spent on Flaviir, the endless hours spent in the lab and our time away on flight trails. The Demon was a cruel but fair mistress (bloody hard work old friend). Leonardo Lopez whom sail ocean with me battling the demons of academia along the way. Your attention to detail, acute perception of obscure concept and calm exterior were and always shall be inspiring. Kashif Iqbal a mathematician lost in an engineer's world. Your relentless and sometime *repetitive* humour brightened up my day. I shall hold a great fondness for the times we spent in the office - our late night conversations which seemed to span all space and time from renaissance art to quantum physics to cultural diversity will remain with me through my life. Solange Baena who has been at the heart of every social event. I applaud your tireless efforts on coercing the fellow researchers to - just for a moment put aside their research, crawl out of their cave and enjoy each others company.

A special mention must go to my non-Cranfield friends; Daniel Watt, Rowena Brown, Daniel Grant, James Clark, Gareth Munkley, Lewis Read, Alex Leckie, Claire Leckie, Jason Nicholls and Eric Smith, whom too have

shared in the trials and tribulations of my PhD – as they were continually subjected to my incessant moaning. I thank you all for your continued support, but perhaps more importantly for simply keeping me sane.

Finally my greatest thanks goes to the academic professors and lecturers who have guided me throughout these years. James Whidborne who's unrivalled knowledge in control was vital to my PhD - To whom I hold the up-most respect and admiration . Ali Savvaris who has guided me throughout the entirety of my PhD and to whom I am eternally thankful . Annalisa Buonanno who introduced me to control allocation and guided me through the first crucial months. Craig Lawson whose leadership throughout FLAVIIR and Demon was inspiring - If it ever needs be I shall again follow him into battle without a moments though. With their help, dedication and guidance I shall forever be standing on the shoulders of giants.

Ramey Jamil

Indicem Contenta

Tabula Figurarum

Nomenclature

Aircraft Variables

$-h$	Altitude
α	Angle of attack
$\bar{L}$	Rolling moment
$\bar{q}$	Dynamic pressure
$\bar{Y}$	Lateral force
β	Side Slip
γ	Flight path angle
DCM	Direction cosine matrix
p	Position Vector
V	Velocity vector
ω	Angular velocity vector
Φ	Aircraft Attitudes
ϕ	Roll angle
ψ	Heading angle
ρ	Density
θ	Pitch angle
b	Body-fixed reference frame
$C\mu$	Dimensionless blowing coefficient
D	Drag force
e	Earth-fixed reference frame
F	Total force
F_T	Thrust component
g	Earth gravity 9.81
G_f	Control gain for fluidic controls
H	angular momentum
I	Inertial matrix
L	Lift force
M	Pitching moment
m	Aircraft mass
N	Yawing moment
p	Angular rate about the x_b axis
p_E	Position east
p_N	Position north
q	Angular rate about the y_b axis

r	Angular rate about the z_b axis
S	Wing surface area
$T^\dagger$	Total torque
T_A	Variant of the direction cosine matrix which relates the body axis to the wind axis.
T_m	Total moments
$u^\dagger$	Longitudinal velocity
$v^\dagger$	Lateral velocity
V_T	True airspeed
w	Wind-fixed reference frame
$w^\dagger$	Normal velocity
X	Longitudinal force
Y	Side force
Z	Down force

Demon Control Variables

η_{FTV}	Fluidic thrust vectoring
η_{Left}	Port side elevator
η_{Right}	Starboard side elevator
$\xi_{CC_{Left}}$	Port side circulation control device
$\xi_{CC_{Right}}$	Starboard side circulation control device
ξ_{Left}	Port side aileron
ξ_{Right}	Starboard side aileron
ζ	Rudder

Control Allocation

$\aleph$	Nullspace
ϵ	Prioritising Gain
γ	User Defined Weighting
λ	Lagrange Multiplier
Ω	Set of equality, inequality and linear constraints
ω	Solution to the generalised multi-objective optimisation problem
ω	The generalised solution to the Multi objective optimisation problem
ω^t	Efficient solution to the generalised multi objective optimisation problem
$\overline{u}$	Minimum actuator deflection
$\underline{u}$	Minimum actuator deflection
Υ	Demand subset
ϱ_l	Objective weighting with respect to the weighted control allocation method

Ξ	Control subset
A	State matrix
B	Control effectiveness matrix
B_k^κ	Generalised inverse
B_p^+	Position limit pseudo inverse
B_r^+	Rate limit pseudo inverse
B_u	Control matrix
B_v	Critical control matrix
F^*	Ideal solution to the multi-objective control allocation problem. The solution tends to lie outside of the attainable space
f_j^*	Respective components of the ideal point
G	Ganging Matrix
j	Objective number
j_h	High frequency low pass filter component
j_l	Low frequency low pass filter component
l	Order of successively solved single objectives
m	Number of actuators
n	Number of inputs
p	The order of the l_p norm
T	Sampling Time
u	Actuator inputs
$u(t-T)$	Solutions to the actuator input at the last time step
u^g	Design parameter for canonical control allocation method
u_d	Design parameter to which the solutions are to be drawn
u_p	Pseudo Controls
v	Total control effort
W_u	prioritisation control matrix
x	State variables

Acronyms

CC	Circulation Control
FDI	Failure Detection Isolation
FLAVIIR	Flapless Air Vehicle Integrated Industrial Research
FTV	Fluidic Thrust Vectoring
UAS	Unmanned Aerial System
UAV	Unmanned Aerial Vehicle

CHAPTER 1

Introduction

1.1 Introduction

IN an effort to increase the reliability of Unmanned Aerial Vehicles (UAVs), further redundant control surfaces coupled with innovative fluidic devices are being applied. The optimal utilisation of such a configuration provides a challenging problem, as questions begin to arise regarding the synchronic appropriation of both conventional and fluidic devices. The potential benefits of such a system can not only lead to enhanced mission performance but also reduce the probability of a catastrophic failure. A vital element in this venture is control allocation. Control allocation is used to determine which effector, or combination of effectors, is most appropriate to use. Control allocation can not only be utilised to optimise effector configurations but, in combination with a fault detection system, can also act as a fault tolerant system, providing mitigation for effector failures.

In traditional aircraft configurations, each of the three principal control surfaces, elevator, aileron and rudder produces a moment principally in one axis. However, if there are more than one effector for each moment, then the aircraft is over-actuated, and a decision about the effector combination must be made. For some aircraft, such as modern transport aircraft, this may be obvious. But where the effectors use different technologies, it is not and some methodical approach must be taken. This is the control allocation problem.

If, for a standard linear state variable description $G(s) = C(sI-A)^{-1}B_u$, if the number of columns of B_u is greater than the column rank of B_u, then the system is overactuated, and control allocation is required. To do this, the controller consists of two parts, as shown in figure 1.1:

1. A control law that specifies the total control effort to be produced (net torque, force, etc).

2. A control allocator that maps the total control demand onto individual effector settings (commanded aerosurface deflections, thrust forces, etc).

It is advantageous to have a separate control allocation for the following reasons:

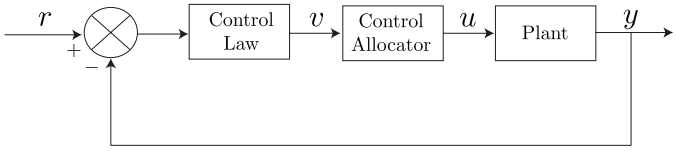

Figure 1.1: Control Allocation

- Actuator constraints can be taken into account. If one actuator saturates, and fails to produce its nominal control effect, another actuator may be used to make up the difference. This way, the control capabilities of the actuator suite are fully exploited before the closed loop performance is degraded. The way the system performance degrades can also be affected. For example, in flight control, it might be crucial to maintain yaw control performance to avoid yaw departure, while roll control may be less important.

- Controller reconfiguration can be performed if the effectiveness of the actuators change over time, or in the event of an actuator failure, without having to redesign the control law.

- Actuator utilisation can be treated independently and can be optimised for the application considered. The actuator redundancy can be used for several purposes. Most commonly, the extra degrees of freedom are used to optimise some objective, like total control surface deflections, drag, wing load, or radar signature in aircraft applications. In addition actuator utilisation can be optimised with respect to varying flight phases.

1.2 Novelty and Contribution

Typically control allocation schemes consider a single objective, although in many real-life situations this may not be ideal and multiple objectives need to be taken into account, especially in aerospace where objectives may not hold for the entirety of the mission. Dealing with multi-objective optimisation tends to be problematic, that is, generally as one objective is minimised it leads to the subsequent increase of another. The objectives are then said to be in conflict, and some trade-off is sought.

The trade-off attempts to find the best compromise solution between the objectives, yet questions arise regarding nature of the best compromise solution. For example, it may be deemed that the best solution for all objective lies at an ideal point - a point which lies outside of the attainable space due to the conflict that is caused by the objectives. Hence in this instance the best trade off would lie as close to the ideal point as possible while remaining within the feasible space. In other instances it may be required that certain

objectives would take prevalence over others, and there hence other objectives would remain diminished in their presence. Furthermore the user or decision maker may require that the solution is to be drawn to a pre defined point - a point which may have certain advantageous properties such a trim, or reduced drag.

This thesis presents four ***novel*** control allocation schemes which optimise for j-objectives while attempting to find the best compromise solution as mentioned above.

1.3 Aims and Objectives

The aim of the project is to develop a multi-objective control allocator that would accommodate for conflicting objectives while retaining reconfigurable flight control capabilities and maintaining a high level of designer preferences. The objectives can be treated as the following pragmatic items;

1. Design a multi objective control allocator which could account for j objectives while avoiding conflicts by means of a trade off.
2. Apply the multi objective control allocator to a high veracity simulation.
3. evaluate the capabilities of the allocators under normal and failure scenarios, by running controlled case scenarios.

1.4 Scope

The majority of this project shall be simulation based and shall be conducted on Matlab/Simulink. You will note the the thesis is inherently aerospace, but where possible the methodology shall aim to remain generalised, such that the methods and established framework, maybe applied to a number of systems with reasonable ease. The 'chosen' model for this thesis is the Demon UAV, a demonstrator vehicle developed at Cranfield University to illustrate the viability of fluidic devices. The model itself has been derived from wind tunnel testing and work produced During the FLAVIIR Project. In this thesis the model is hence given little attention as it has already been covered in the previous literature. The developed control allocators shall find the solution using numerical methods and to achieve this the Matlab/Simulink optimisation toolbox has been used. In addition to the optimisation toolbox the control systems toolbox has been used to aid in the development of the control algorithms.

1.5 Thesis Outline

Chapter 2 presents the mathematical framework upon which the demon model is based on. It defines the axis frames which are used to illustrate the aircraft's motion. It further goes on the define a number of preliminares which are need to be taken into consideration for the Demon model. This includes the description of the fluidic devices, Circulation Control and Fluidic Thrust vectoring and their subsequent modelling.

Chapter 3 establishes the control allocation problem for both linear and non linear systems. It goes on to list a number of optimial and non-optimal control allocation schemes, which are already in use, including; Dasiy chaining, Weighted pseudo inverse and Active set methods. Furthermore as a precursor to chapter 4 it attempts to identify some objectives which maybe used.

Chapter 4 formulates the multi-objective control allocation problem and outlines the principle concepts of multi-objective optimisation. Defining such concepts as Pareto optimal frontier, effectiveness and ideal points. It will go on to develop for novel control allocation schemes based on Weighted, Minimax, Classical and Canonical multi-objective optimisation methods.

Chapter 5 and **Chapter 6** applies the four allocators onto the high veracity 6Dof Demon model and subjects them to a case scenario. The results are presented under normal and effecter failure conditions respectively.

Chapter 7, Some conclusions are drawn and the thesis is brought to a close with possible future work.

1.6 List of Publications

The following is a list of published paper which directly related to the work outlined in this thesis.

Ramey Jamil, Al Savvaris. Reconfigurable Control Allocation for UAV with integrated Fluidic Devices. *25^{th} Bristol UAV Systems Conference*. Bristol University, Bristol, 2010

Ramey Jamil, Al Savvaris, James Whidborne. Effector Failure Mitigation by Control Allocation for UAV with Integrated Fludic Control Devices. *UKACC International Conference on CONTROL*. Coventry University, Coventry, 2010

Ramey Jamil, Francis Salama, Mudassir Lone, Al Savvaris, James Whidborne. Multi-objective Control Allocation With Conflict Resolution. *AIAA Guidance, Navigation, and Control Conference* Minneapolis - Minnesota, 2012

CHAPTER 2

Primer

IN order to build a suitable a mathematical model which encompasses all the aircraft dynamics and control systems, a secure foundation must first be establish. This foundation shall consist of a mathematical framework on which the equations of motion shall be develop upon. Since aircraft have somewhat relatively complex motion their dynamics are generally described by a number of variables related to their six degrees of freedom in an appropriate axis system. The following chapter shall consider the aircraft as a rigid body and outline the typical axis frames and variables used to depict the aircraft's motion within the general equations of motions. It shall go on to describe the control inputs for the "chosen" aircraft model along with a number of preliminaries which are required to understand the novelties which lie within the said model, particularly the CC devices and FTV Devices, see section 2.7.2. Within reason the thesis attempts to remain consistent with the mathematical framework and notions of those developed and denoted in [19] and [14].

Section 2.1 outlines the coordinate frames which are to be use to define the mathematical framework. Section 2.2 shall define the aircraft variables; defining Velocity, Position and Orientation. By assuming rigid body motion the equation of motion are developed in section 2.3 and gathered in section 2.5. The FLAVIIR program is outlined in section 2.6 and section 2.7 describes the Demon UAV.

2.1 Coordinate Frames

By convection the most frequent frames used to describe the aircraft motion are the Earth-fixed frame e, the Body-fixed b, and the Wind frame w. Typically with regards to the Earth-fixed axis a reference point o_e defined on the earth's surface projects a right handed, fixed frame orthogonal axis system where the $o_0\mathbf{x}_e$, $o_0\mathbf{y}_e$ and $o_0\mathbf{z}_e$ point north, east and downward respectively. In normal localised atmospheric flight a *flat earth* is assumed which lies tangential to the o_0 such that the vertical axis runs along the gravity vector, see figure 2.1. The body-fixed frame originates at the aircraft's center of gravity and protrudes forwards through the body, parallel to the horizontal fuselage datum $\mathbf{x}_b$, extends over the starboard wing $\mathbf{y}_b$, and directly downward $\mathbf{z}_b$. This frame tends to be useful in describing the aircraft's position and orientation, which shall be explained in greater detail in section 2.2. The wind

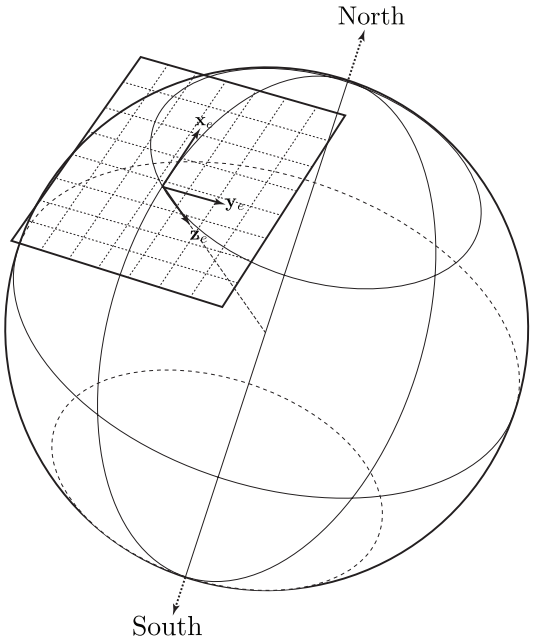

Figure 2.1: Conventional earth axis frame where the earth is considered as a flat surface

frame is directed along the velocity vector of the aircraft $\mathbf{V}$. The orientation of this frame is relative to the body-fixed frame and is determined by the angle of attack α and sideslip angle β, see figure 2.4.

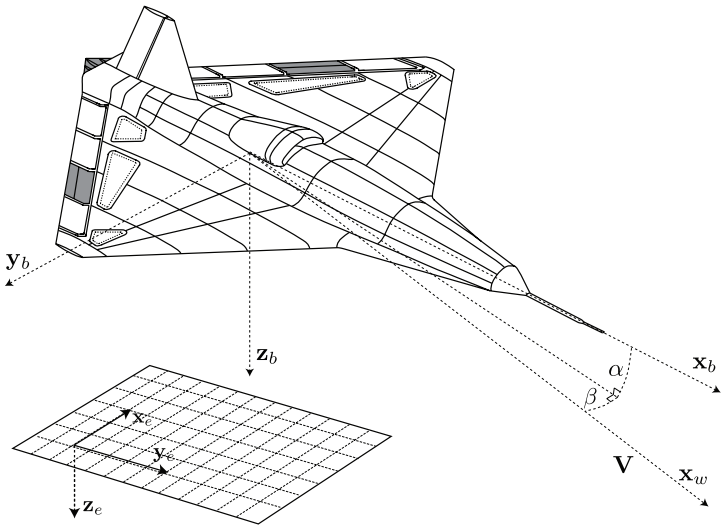

Figure 2.2: Earth-fixed coordinate frame e, and body fixed coordinate frame b, where α and β are both positive.

The components of the body axis b and wind axis w frame are related the

matrix T_A, where,

$$T_A = \begin{bmatrix} \cos\alpha\cos\beta & \sin\beta & \sin\alpha\cos\beta \\ -\cos\alpha\sin\beta & \cos\beta & -\sin\alpha\sin\beta \\ -\sin\alpha & 0 & \cos\alpha \end{bmatrix} \tag{2.1.1}$$

2.2 Aircraft Variables

The aircraft's motion can be described by velocity, position, orientation and angular velocity over time as follows,

Velocity

For a given true airspeed V_T,

$$V_w = \begin{bmatrix} V_T \\ 0 \\ 0 \end{bmatrix} \tag{2.2.1}$$

The components of the velocity vector $\mathbf{V}$ in the body axis can be describe as follows,

$$\mathbf{V} = \begin{bmatrix} u \\ v \\ w \end{bmatrix} \tag{2.2.2}$$

Where u is the longitudinal velocity, v is the lateral velocity and w is the normal Velocity, such that

$$\begin{bmatrix} u \\ v \\ w \end{bmatrix} = T_A \begin{bmatrix} V_T \\ 0 \\ 0 \end{bmatrix} \tag{2.2.3}$$

holds. Alternatively the true airspeed V_T can be considered,

$$V_T = \sqrt{(u^2 + v^2 + w^2)} \tag{2.2.4}$$

$$\alpha = \arctan\frac{w}{v} \tag{2.2.5}$$

$$\beta = \arcsin\frac{v}{V_T} \tag{2.2.6}$$

The flight path angle γ is defined as;

$$\gamma = \theta - \alpha \tag{2.2.7}$$

where θ is the pitch angle.

Position

The position of the aircraft in the earth reference frame can be described as components related to north, east and down.

$$\mathbf{p} = \begin{bmatrix} p_N \\ p_E \\ -h \end{bmatrix} \tag{2.2.8}$$

Where $\mathbf{p}$ is the position vector, p_N is position north, p_E is position east, and $-h$ is altitude.

Orientation

The aircraft attitude is defined as angular rotations of the body fixed frame, b which obey the commutative laws of Euler angles. They are thus described as,

$$\Phi = \begin{bmatrix} \phi \\ \theta \\ \psi \end{bmatrix} \tag{2.2.9}$$

Where ϕ corresponds to roll angle, θ corresponds to pitch and ψ to yaw, see figure 2.3.

Angular Velocity

The angular velocity vector denoted as ω is given by

$$\omega = \begin{bmatrix} p \\ q \\ r \end{bmatrix} \tag{2.2.10}$$

Where p is the roll rate, q is the pitch rate and r is the yaw rate, see figure 2.3.

2.2.1 Direction Cosine Matrix

It is often necessary to transform certain components from one axis to another, for example angular relationships used to describe attitudes may be generalised to describe orientation of one set of axis to with respect another. In this instance the *direction cosine matrix*[1] **DCM** can be used where,

$$DCM = \begin{bmatrix} \cos\theta\cos\psi & \cos\theta\sin\psi & -\sin\theta \\ \sin\phi\sin\theta\cos\psi & \sin\phi\sin\theta\sin\theta & \sin\phi\cos\theta \\ -\cos\phi\sin\psi & +\cos\phi\cos\phi & \\ \cos\phi\sin\theta\cos\psi & \cos\phi\sin\theta\sin\psi & \cos\psi\cos\theta \\ +\sin\phi\sin\psi & -\sin\phi\cos\psi & \end{bmatrix} \tag{2.2.11}$$

[1] T_A is a variant of the direction of cosine

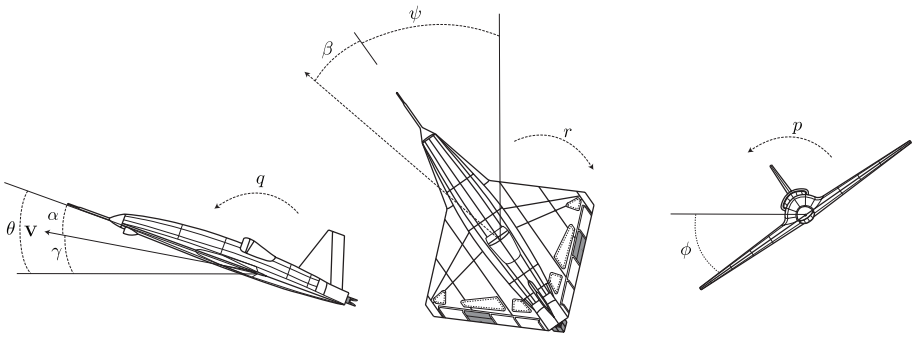

Figure 2.3: UAV orientation, ϕ, θ and ψ, aerodynamic angles, α and β, angular rates, p, q and r. Here all states are positive.

A full review of the direction cosine matrix can be found in [19].

2.3 Rigid Body Motion

By utilising Newtons's laws of motion the effects of the external force and moments acting on the vehicle can be investigated. In the body-fixed coordinate frame b, Newton's second law can be expressed as

$$F = \frac{d}{dt}|_b(mV) + \omega m\mathbf{V} \tag{2.3.1}$$

$$T^\dagger = \frac{d}{dt}|_b\mathbf{H} + \omega \times \mathbf{H} \tag{2.3.2}$$

where F = total force, $T^\dagger$ = total torque, m = aircraft mass, and H = angular momentum,

$$\mathbf{H} = I\omega \tag{2.3.3}$$

in this instant I is the inertial matrix,

$$I = \begin{pmatrix} I_x & 0 & -I_{xz} \\ 0 & I_y & 0 \\ -I_{xz} & 0 & I_z \end{pmatrix} \tag{2.3.4}$$

Equations 2.3.1 can be expressed in the terms of velocity and angular velocity as follows,

$$F = m(\dot{V} + \omega V) \tag{2.3.5}$$

$$T = I\dot{\omega} + \omega \times \omega \tag{2.3.6}$$

2.4 Forces and Moments

The total forces and moments acting on vehicle arise from three key areas; aerodynamic, engine and Gravity.

$$F = F_{aero} + F_{eng} + F_{grav} \tag{2.4.1}$$

$$T_m = T_{eng} + T_{aero} \tag{2.4.2}$$

The aerodynamic forces and moments as expressed in the body frame b are as follows

$$F_{aero} = \begin{pmatrix} X \\ \bar{Y} \\ Z \end{pmatrix} \qquad T_{aero} = \begin{pmatrix} \bar{L} \\ M \\ N \end{pmatrix} \tag{2.4.3}$$

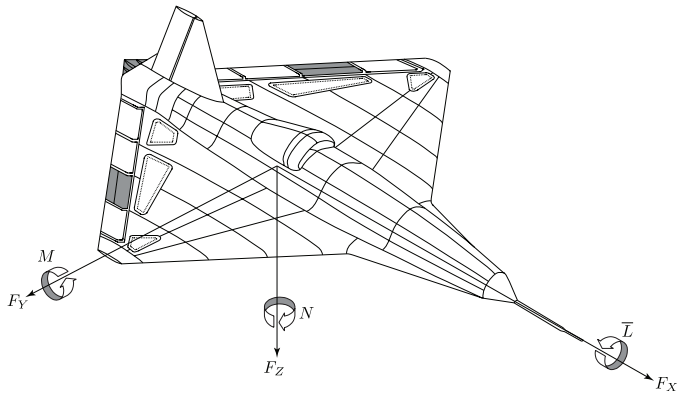

Figure 2.4: Earth-fixed coordinate frame e, and body fixed coordinate frame b. Where α and β are both positive.

Where

$$\begin{array}{cc} X = \bar{q}SC_x & \bar{L} = \bar{q}SbC_l \quad \text{Rolling Moment} \\ \bar{Y} = \bar{q}SC_y & M = \bar{q}S\bar{c}C_m \quad \text{Pitching Moment} \\ Z = \bar{q}SC_z & N = \bar{q}SbC_n \quad \text{Yawing Moment} \end{array}$$

The aerodynamic force as expressed in the wind-axes coordinate frame w are as follows

$$F_{aero} = \begin{pmatrix} -D \\ Y \\ -L \end{pmatrix} \quad \text{where} \quad \begin{array}{rcl} D &=& \bar{q}SC_D \\ Y &=& \bar{q}SC_Y \\ L &=& \bar{q}SC_L \end{array} \tag{2.4.4}$$

The relation of the force components between the two coordinate frames w and w is as follows

$$D = -X\cos\alpha\cos\beta - \bar{Y}\sin\beta - Z\sin\alpha\alpha\cos\beta \tag{2.4.5}$$

$$Y = -X\cos\alpha\sin\beta + \bar{Y}\sin\beta - Z\sin\alpha\alpha\cos\beta \tag{2.4.6}$$

$$L = X\sin\alpha - Z\cos\alpha \tag{2.4.7}$$

where $\bar{q}$ represents the dynamic pressure

$$\bar{q} = \frac{1}{2}\rho V_T^2 \tag{2.4.8}$$

Gravity

Gravity only acts upon the force component and in the body axis b is defined as,

$$F_{grav} = \begin{pmatrix} -\sin\theta \\ \sin\phi\cos\theta \\ \cos\phi\cos\theta \end{pmatrix} \tag{2.4.9}$$

it may also be transformed to the wind axis using T_A

Engine

The thrust force component denoted F_T, which acts directly along the x-axis yields;

$$F_{grav} = \begin{pmatrix} F_T \\ 0 \\ 0 \end{pmatrix} \tag{2.4.10}$$

Along with the engine position offset $\overline{x}_o$, the addition of a thrust vectoring device will induce a pitching moment which is directly related to the thrust component F_T,

$$T_{grav} = \begin{pmatrix} 0 \\ F_T\overline{x}_o + F_T\delta \\ 0 \end{pmatrix} \tag{2.4.11}$$

where u in this instant denotes the thrust line deflection[2].

[2]Note in Chapter 3, δ is denoted as a scaler within the input vector u, which is directly related to the deflection of the fluidic thrust vectoring

2.5 Equation of Motion

The equations of motion are expressed as follows

Body-Axes Force Equations

$$X - F_T - mg\sin\theta = m(\dot{u} + qw - rv) \quad (2.5.1)$$
$$\bar{Y} + mg\sin\phi\cos\theta = m(\dot{v} + ru - pw) \quad (2.5.2)$$
$$Z + mg\cos\phi\cos\theta = m(\dot{w} + pv - qu) \quad (2.5.3)$$

Body-Axes Moments Equations

$$L = I_x\dot{p} - I_{xz}\dot{r} + (I_z - I_y)qr - I_{xz}pq \quad (2.5.4)$$
$$M + F_{T\bar{x}} = I_y\dot{q} + (I_x - Iz)pr + I_{xz}(p^2 - r^2) \quad (2.5.5)$$
$$N = I_z\dot{r} - I_{xz}\dot{p} + (I_y - I_x)pq + I_{xz}qr \quad (2.5.6)$$

Wind-Axes Force Equations

$$\dot{V}_T = \frac{1}{m}(-D + F_T cos\alpha - mg\sin\gamma) \quad (2.5.7)$$
$$\dot{\alpha} = \frac{1}{cos\beta}(q_w + \frac{1}{mV_T}(-L - F_T\sin\alpha + mg)) \quad (2.5.8)$$
$$\dot{\beta} = -r_w + \frac{1}{mV_T}(Y - F_T\cos\alpha\sin\beta + mg) \quad (2.5.9)$$

Longitudinal Motion

$$\dot{V}_T = \frac{1}{m}(-D + F_T cos\alpha - mg\sin\gamma) \quad (2.5.10)$$
$$\dot{\alpha} = q + \frac{1}{mV_T}(-L - F_T\sin\alpha + mg\cos\gamma) \quad (2.5.11)$$
$$\dot{\gamma} = \frac{1}{mV_T}(L + F_T\sin\alpha - mg\cos\gamma) \quad (2.5.12)$$
$$\dot{q} = \frac{1}{I_y}(M + F_T z_{TP}) \quad (2.5.13)$$
$$\dot{\theta} = q\cos\phi - r\sin\phi \quad (2.5.14)$$

Lateral Motion

$$\dot{v} = \frac{\bar{Y}}{m} + g\sin\phi\cos\theta - ru + pw \tag{2.5.15}$$

$$\dot{p} = \frac{(I_z L + I_{xz} N - [I_{xz}\chi p + [I_{xz}^2 + I_z(I_z - I_y)]r]q)}{(I_x I_z - I_{xz}^2)} \tag{2.5.16}$$

$$\dot{r} = \frac{(I_{xz} L + I_x N - [I_{xz}\chi r + [I_{xz}^2 + I_x(I_x - I_y)]p]q)}{(I_x I_z - I_{xz}^2)} \tag{2.5.17}$$

$$\dot{\phi} = p + (q\sin\phi + r\cos\phi)\tan\theta) \tag{2.5.18}$$

$$\dot{\psi} = (q\sin\psi + r\cos\phi)\sec\theta \tag{2.5.19}$$

where,

$$\chi = (I_y - I_x - I_z) \tag{2.5.20}$$

2.6 FLAVIIR Program

The five year FLAVIIR (Flapless Air Vehicle Integrated Industrial Research) program investigates novel technologies for unmanned aerial systems (UASs), which could potentially be integrated onto next generation UASs. The program encompasses all aspects of aerospace engineering integration, including systems, structures, simulations and testing. Jointly funded by BAE systems and the Engineering and Physical Science and Research Council (EPSRC), the program led by Cranfield University embodies a consortium nine of universities, in major aspects of design, manufacture and testing. The program itself initially originated from BAE systems "Grand Challenge" which *challenged* universities;

> *"To develop technologies for maintenance free, low cost UAV without conventional control surfaces and without performance penalty over conventional craft"*

The most prominent goal of the FLAVIIR [39] program was to design, manufacture and fly a small but significantly representative vehicle - The Demon, which would house all the developed technologies within each specific research discipline, with focal interest revolving around the 'flapless' fliuidc controls namely the Circulation Control (CC) developed by Cranfield University and the Fluidic Thrust Vectoring (FTV) developed by Manchester University.

2.7 Demon UAV

The Demon aircraft is a light, tailless, cropped diamond wing plan-form configuration, powered by a single Titan gas turbine engine [3]. Due to the

small aspect ratio and large leading edge sweep the Demon configuration performs not unlike a conventional delta wing [40]. The $90kg$ UAV spans under three meters and holds a cruising speed of approximately $50m/s$. In September 2010 the Demon UAV completed it's second successful flight campaign at Walney island military proving ground [41] and hence holds the world record for the first aircraft to fly without the use of conventional surfaces, see figure 2.8. The Demon along with its health monitoring system [33], houses a full sensor suite which provides real time telemetry data of its states. The Demon UAV has two lanes of operation, a 'Manual' and 'Flight Control Computer' (FCC). The manual mode is essentially open loop and sends the signals directly to the surfaces, while the FCC mode direct the signals through the Flight Control Computer. This thesis shall assume that the Demon is operating in FCC mode throughout the entirety of the simulations. It is currently out-fitted with five trailing edge conventional control surfaces. See figure 2.5. With reference to the figure, η_{Left} and η_{Right} generally act as elevators, ξ_{Left} and ξ_{Right} act as ailerons and the rudder deflection is denoted by ζ. In addition to these effectors, the Demon incorporates newly integrated fluidic technologies, namely fluidic thrust vectoring (FTV), with actuation denoted by η_{FTV} and Circulation Control (CC) denoted by ξ_{CCLeft} and $\xi_{CCRight}$. The Demon has the ability to use a minimum of four devices (i.e. $zeta$, ξ_{CCLeft}, $\xi_{CCRight}$ and η_{FTV}) to achieve all three desired moments, where the remaining surfaces are defined as redundant. Likewise the Demon can alternate between conventional device mode and fluidic device modes. It is prominent to note that with the addition of a control allocator the control surface shall no longer act as conventional elevators, ailerons etc. but rather as coupled longitudinal and lateral moment generators.[3] The Demon 6 Dof model originally derived from the eclipse UAV [6, 13], encompasses the standard equation of motion and aerodynamic forces and moments obtain from wind tunnel testing. A full review of the development of the simulation model and control can be found in [4] and [2]

[3]Where the FTV will remain as a longitudinal moment generator as it can only act upon one axis.

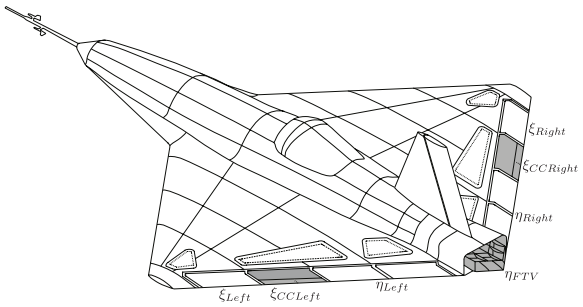

Figure 2.5: Demon's Control Devices

2.7.1 Control Variables

The Demon's control variables and position limits are as follows:

$$\begin{aligned}
-13^\circ \leq \quad & \eta_{FTV} & \leq 13^\circ \\
-30^\circ \leq \quad & \eta_{Left} & \leq 30^\circ \\
-30^\circ \leq \quad & \eta_{Right} & \leq 30^\circ \\
-1 \leq \quad & \xi_{CC_{Left}} & \leq 1 \\
-1 \leq \quad & \xi_{CC_{Right}} & \leq 1 \\
-30^\circ \leq \quad & \xi_{Left} & \leq 30^\circ \\
-30^\circ \leq \quad & \xi_{Right} & \leq 30^\circ \\
-30^\circ \leq \quad & \zeta & \leq 30^\circ
\end{aligned}$$

Where $\xi_{CCRight}$ and ξ_{CCLeft} dimensionless control inputs.

2.7.2 Fluidic Devices

As opposed to conventional controls which use a physical surface, the fluidic devices use jets of blown air to augment the pressure differential over a wing in order to induce the desired moment. These devices pose significant advantages over conventional controls in that they can offer reduced sizing which can allow for and increased storage for payload or systems, reduced maintenance and a reduced radar cross section.

The Demon's fluidic devices are based on the Coanda effect. This phenomenon occurs when a high pressured jet wall continues to remain attached around a curved surface [5]. As a fluid moves across a surface, skin friction amounts between the surface and the fluid, which tends to slow the moving flow. The resistance to the flow draws the fluid towards the surface, causing it to stick. Hence a fluid emerging from a nozzle can, depending on the curvature, follow a curved surface to the point of bending around corners. Application of Coanda effect involves converting the trailing edge

of the aerofoil into an enlarged rounded surface to which a jet of air adheres when blown tangentially from the upper and lower surfaces.

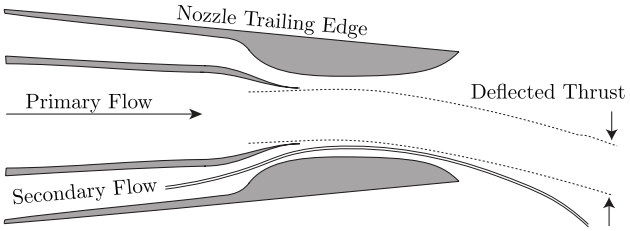

Figure 2.6: Demon's FTV Schematics

The FTV's construct is contrived such that, the flow acquired from engine bleeding is imparted to the FTV's upper and lower slots. The distribution of the flow at this point can be regulated through the use of actuated valves. The curvature of the nozzle trailing edge allows the occurrence of the Coanda effect; hence the flow exiting the FTV slots adheres to the nozzle trailing edge surface and as a result draws the thrust towards it, causing a pitching moment, [49] see figure 2.6.

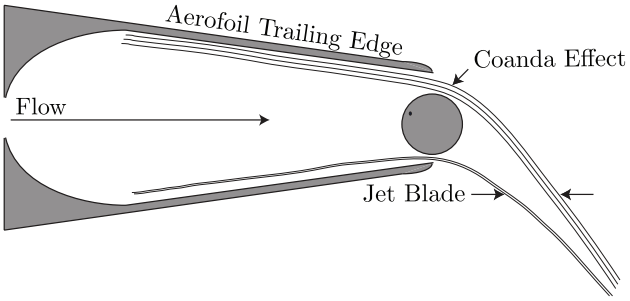

Figure 2.7: Demon's CC Schematics

The lateral fluidic device comprises of a dual slot circulation control allocator fully capable of proportional bi-directional control. Due to the temperature build up and further design issues, engine bleeding in this instance is not viable and hence the flow is derived from an auxiliary pressure unit [34]. The flow direction is augmented with the use a columnar Coanda surface actuated about an eccentric centre see figure 2.7, a full study was conducted by Buonanno in 2009 [4] and further literature can be found in [18, 17, 57, 16]

Due to this novel approach certain exigencies regarding the effectiveness of the devices have to be taken into consideration. Unlike conventional surfaces, where they become increasingly efficient with increasing airspeed, fluidic devices tend to behave to the contrary, i.e. they become more efficient with a reduction in speed.

2.7.3 A brief history of Circulation Control

The use of fluidic control devices has been an established research topic for over 90 years. The emergence of Circulation Control has been around since the early 1930's and has been demonstrated in 2000 by Englar *et al.* [27]. Exploratory investigation have demonstrated a threefold gain in lift over the conventional flapped surface [29] and at least have double the maximum lift coefficient for 3 dimensional aircraft configuration [28]. The main purpose of the Circulation Control integration has been to increase the lifting force of an aircraft at times when large lifting forces at slow speeds are required, such as take off and landing. Wing flaps which are currently use on modern aircraft tend to induce a high cost of drag. The benefit of Circulation control is that no extra drag is created and the lift coefficient is greatly increased. Furthermore the use of a Circulation Control systems eliminates the need for large complex components in the free stream such as flaps, greatly reducing the noise pollution of modern aircraft. The most dramatic impact of work into the field of Circulation Control was performed by Frith and Wood in 2004 [31], which focused its research interest on the use of Circulation Control devices for manoeuvring. The work established the principles for flight dynamic flapless control of air vehicles by replacing conventional ailerons with span-wise pairs of slots which permit differential operation sufficient for lateral control and without the adverse yaw effect of a flap surface. The devices which are currently housed on the Demon are a direct derivation of this work.

2.7.4 Fluidic Control modelling

The following section will briefly describe the modelling framework of the fluidic control devices - an excellent companion to this section, A.Bunnanno's Thesis [4] and [21] in which the design modelling and control is explained in concise and explicit detail.

A simple model for fluidic controls can be defined in analogy with conventional mechanical control motivators. Consider a conventional geometric control surface that produces a force output in response to a control surface deflection u. From basic aerodynamic theory, the change in local lift coefficient produced by the control input can be modelled simply as the product of a gain term (the rate of change of lift with control deflection) and the control deflection, or, in non dimensional form,

$$C_F = \frac{\partial C_F}{\partial u} u \tag{2.7.1}$$

Consider now a fluidic control that produces a force output in response to a momentum input. The force obtained by this control can be modeled as the product of a control gain and the control momentum. Expressing the control force as a dimensionless force coefficient, by dividing through by a

reference free stream momentum (free stream dynamic pressure multiplied by a suitable reference area), gives

$$C_f = G_f C_\mu \tag{2.7.2}$$

where G_f is the control gain and $C\mu$ is a dimensionless blowing coefficient, defined as the momentum flux exiting from the slot normalized by the free stream dynamic pressure and a reference area,

$$C_\mu = \frac{\dot{m}_j V_j}{q_{\inf} S} \tag{2.7.3}$$

For fluidic controls, Equation 2.7.3, the control input is now a dimensionless coefficient as opposed to a (dimensionless) angle. This means that the actual dimensional control input required to achieve a given control force coefficient is not independent of the reference momentum. Therefore, as the free stream speed increases, an increasing amount of input momentum is required to achieve a given force coefficient.

Experimental investigations have been conducted to inquiry the use of blown trailing edges and compare their effectiveness with conventional flaps. Details and results for the CC tests can be found in [4]. Preliminary static test have been conducted on a FTV system incorporating engine bleed from the compressor of a micro-jet turbine engine. Thrust vector angle and normal and longitudinal thrust components were measured at different engine operations. Details of the FTV test rig can be found in [49] and a computational fluid dynamics investigation can be found in [1].

2.8 State Space representation of DemonUAV

The mathematical model of the demon can be represented in the following state space representation,

$$\dot{x} = Ax + Bu \tag{2.8.1}$$
$$y = Cx + Du \tag{2.8.2}$$

The elements of the state matrix A represent the aerodynamic stability derivatives and are referred to in the body axis, in concise form. The coefficients of the input matrix B which represent the control derivatives are also in concise form. The derivatives can be referred to in the wind axes at $\theta_e = 0$, by making the following simplification; $sin\theta_e = 0$, $cos\theta_e = 1$ and $U_e = V_e$, where the subscript e indicates equilibrium. A complete list of longitudinal dimensionless aerodynamic stability and control derivatives referred to aircraft wind axis is provided in Tables 2.8.1, 2.8.1 and 2.8.1. The notations are consistent with [19].

2.8.1 Longitudinal Model

$$\underbrace{\begin{bmatrix} \dot{u} \\ \dot{w} \\ \dot{q} \\ \dot{\theta} \end{bmatrix}}_{\dot{x}} = \underbrace{\begin{bmatrix} X_u & X_w & X_q & X_\theta \\ Z_u & Z_w & Z_q & Z_\theta \\ M_u & M_w & M_q & M_\theta \\ 0 & 0 & 1 & 0 \end{bmatrix}}_{A} \underbrace{\begin{bmatrix} u \\ w \\ q \\ \theta \end{bmatrix}}_{x} + \cdots$$

$$\cdots \underbrace{\begin{bmatrix} X_{\eta_l} & X_{\eta_r} & X_{\xi_{CC_l}} & X_{\xi_{CC_r}} & X_{\xi_l} & X_{\xi_r} & X_{\eta_{FTV}} & X_\tau \\ Z_{\eta_l} & Z_{\eta_r} & Z_{\xi_{CC_l}} & Z_{\xi_{CC_r}} & Z_{\xi_l} & Z_{\xi_r} & Z_{\eta_{FTV}} & Z_\tau \\ M_{\eta_l} & M_{\eta_r} & M_{\xi_{CC_l}} & M_{\xi_{CC_r}} & M_{\xi_l} & M_{\xi_r} & M_{\eta_{FTV}} & M_\tau \\ 0 & 0 & 0 & 0 & 0 & 0 & 0 & 0 \end{bmatrix}}_{B} \underbrace{\begin{bmatrix} \eta_{Left} \\ \eta_{Right} \\ \xi_{CC_{Left}} \\ \xi_{CC_{Right}} \\ \xi_{Left} \\ \xi_{Right} \\ FTV \\ \tau \end{bmatrix}}_{u} \tag{2.8.3}$$

$$y = \underbrace{\begin{bmatrix} 1 & 0 & 0 & 0 \\ 0 & 1 & 0 & 0 \\ 0 & 0 & 1 & 0 \\ 0 & 0 & 0 & 1 \end{bmatrix}}_{C} \underbrace{\begin{bmatrix} u \\ w \\ q \\ \theta \end{bmatrix}}_{x} \tag{2.8.4}$$

where

$$D = [0] \tag{2.8.5}$$

Derivative	Description	Expression	Multiplier
X_u	Axial force due to velocity	$-2C_{De} + \frac{\partial T}{\partial V}\|_e \frac{1}{\frac{1}{2}\rho V_e S}$	$\frac{1}{2}\rho V_e S$
X_w	Axial force due to incidence	$Cle - \frac{\partial C_D}{\partial \alpha}\|_e$	$\frac{1}{2}\rho V_e S$
W_q	Axial force due to pitch rate	0	$\frac{1}{2}\rho V_e S\overline{c}$
$X_{\dot{w}}$	Axial force due to downwash	0	$\frac{1}{2}\rho S\overline{c}$
Z_u	Normal force due to velocity	$-2C_{le}$	$\frac{1}{2}\rho V_e S$
Z_w	Normal force due to incidence	$-C_{De} - D_{L\alpha}$	$\frac{1}{2}\rho V_e S$
Z_q	Axial force due to pitch rate	0	$\frac{1}{2}\rho V_e S\overline{c}$
$Z_{\dot{w}}$	Axial force due to downwash	$-C_{L_{\dot{\alpha}}}$	$\frac{1}{2}\rho S\overline{c}$
M_u	Pitching moment due to velocity	0	$\frac{1}{2}\rho V_e S\overline{c}$
M_w	Pitching moment due to incidence	$-C_{L_\alpha} K_n$	$\frac{1}{2}\rho V_e S\overline{c}$
M_q	Pitching moment due to pitch rate	C_{M_q}	$\frac{1}{2}\rho V_e S\overline{c}^2$
$M_{\dot{w}}$	Pitching moment due to downwash	$C_{M_{\dot{\alpha}}}$	$\frac{1}{2}\rho V_e S\overline{c}^2$

Table 2.1: Longitudinal aerodynamic stability derivatives referred to wind axis

Derivative	Description	Expression	Multiplier
X_{η_l}	Axial force due to port elevator	$-2KC_{L_{\eta_l}}$	$\frac{1}{2}\rho V_e^2 S$
X_{η_r}	Axial force due to starboard elevator	$2KC_{L_{\eta_r}}$	$\frac{1}{2}\rho V_e^2 S$
$X_{xi_{CC_l}}$	Axial force due to port CC device	$-2KC_{L_{xi_{CC_l}}}$	$\frac{1}{2}\rho V_e^2 S$
$X_{xi_{CC_r}}$	Axial force due to starboard CC device	$2KC_{L_{xi_{CC_r}}}$	$\frac{1}{2}\rho V_e^2 S$
X_{xi_l}	Axial force due to port aileron	$-2KC_{L_{xi_l}}$	$\frac{1}{2}\rho V_e^2 S$
X_{xi_r}	Axial force due to starboard aileron	$2KC_{L_{xi_r}}$	$\frac{1}{2}\rho V_e^2 S$
$X_{\eta_{FTV}}$	Axial force due to starboard aileron	$2KC_{L_{\eta_{FTV}}}$	$\frac{1}{2}\rho V_e^2 S$
Z_{η_l}	Normal force due to port elevator	$-C_{L_{\eta_l}}$	$\frac{1}{2}\rho V_e^2 S$
Z_{η_r}	Normal force due to starboard elevator	$C_{L_{\eta_r}}$	$\frac{1}{2}\rho V_e^2 S$
$Z_{xi_{CC_l}}$	Normal force due to port CC device	$-C_{L_{xi_{CC_l}}}$	$\frac{1}{2}\rho V_e^2 S$
$Z_{xi_{CC_r}}$	Normal force due to starboard CC device	$C_{L_{xi_{CC_r}}}$	$\frac{1}{2}\rho V_e^2 S$

Table 2.2: Longitudinal aerodynamic control derivatives referred to wind axis

Derivative	Description	Expression	Multiplier
Z_{xi_l}	Normal force due to port aileron	$-C_{L_{xi_l}}$	$\frac{1}{2}\rho V_e^2 S$
Z_{xi_r}	Normal force due to starboard aileron	$C_{L_{xi_r}}$	$\frac{1}{2}\rho V_e^2 S$
$Z_{\eta_{FTV}}$	Normal force due to starboard aileron	$C_{L_{\eta_{FTV}}}$	$\frac{1}{2}\rho V_e^2 S$
M_{η_l}	Pitching force due to port elevator	$-C_{L_{\eta_l}}(h_{cpe} - h_{cg})$	$\frac{1}{2}\rho V_e^2 S\overline{c}$
M_{η_r}	Pitching force due to starboard elevator	$C_{L_{\eta_r}}(h_{cpe} - h_{cg})$	$\frac{1}{2}\rho V_e^2 S\overline{c}$
$M_{xi_{CC_l}}$	Pitching force due to port CC device	$-C_{L_{xi_{CC_l}}}(h_{cpe} - h_{cg})$	$\frac{1}{2}\rho V_e^2 S\overline{c}$
$M_{xi_{CC_r}}$	Pitching force due to starboard CC device	$C_{L_{xi_{CC_r}}}(h_{cpe} - h_{cg})$	$\frac{1}{2}\rho V_e^2 S\overline{c}$
M_{xi_l}	Pitching force due to port aileron	$-C_{L_{xi_l}}(h_{cpe} - h_{cg})$	$\frac{1}{2}\rho V_e^2 S\overline{c}$
M_{xi_r}	Pitching force due to starboard aileron	$C_{L_{xi_r}}(h_{cpe} - h_{cg})$	$\frac{1}{2}\rho V_e^2 S\overline{c}$
$M_{\eta_{FTV}}$	Pitching force due to starboard aileron	$C_{L_{\eta_{FTV}}}(h_{cpe} - h_{cg})$	$\frac{1}{2}\rho V_e^2 S\overline{c}$

Table 2.3: Longitudinal aerodynamic control derivatives referred to wind axis continued

2.8.2 Lateral Model

$$\underbrace{\begin{bmatrix} \dot{v} \\ \dot{p} \\ \dot{r} \\ \dot{\phi} \end{bmatrix}}_{\dot{x}} = \underbrace{\begin{bmatrix} Y_v & Y_p & Y_r & Y_\phi \\ L_v & L_p & L_r & L_\phi \\ N_v & N_p & N_r & N_\phi \\ 0 & 1 & 0 & 0 \end{bmatrix}}_{A} \underbrace{\begin{bmatrix} v \\ p \\ r \\ \phi \end{bmatrix}}_{x} + \cdots$$

$$\cdots \underbrace{\begin{bmatrix} Y_{\eta_l} & Y_{\eta_r} & Y_{\xi_{CC_l}} & Y_{\xi_{CC_r}} & Y_{\xi_l} & Y_{\xi_r} & Y_\zeta \\ L_{\eta_l} & L_{\eta_r} & L_{\xi_{CC_l}} & L_{\xi_{CC_r}} & L_{\xi_l} & L_{\xi_r} & L_\zeta \\ N_{\eta_l} & N_{\eta_r} & N_{\xi_{CC_l}} & N_{\xi_{CC_r}} & N_{\xi_l} & N_{\xi_r} & N_\zeta \\ 0 & 0 & 0 & 0 & 0 & 0 & 0 \end{bmatrix}}_{B} \underbrace{\begin{bmatrix} \eta_{Left} \\ \eta_{Right} \\ \xi_{CC_{Left}} \\ \xi_{CC_{Right}} \\ \xi_{Left} \\ \xi_{Right} \\ \zeta \end{bmatrix}}_{u} \tag{2.8.6}$$

The coefficients of the state matrix represent the aerodynamic stability derivatives referred to in the body axes, in concise form. The coefficients of the input matrix B are the control derivatives are also in concise form. A complete list of dimensionless aerodynamic stability are given in table 2.8.2

Derivative	Description	Expression	Multiplier
Y_v	Side force due to side slip	$\frac{C_{Y_{\beta W}}}{C_L^2} C_{Le}^2 + C_{Y_\beta B} + C_{Y_{\beta V}}$	$\frac{1}{2}\rho V_e S$
Y_p	Side force due to roll rate	$\frac{C_{p_{\beta W}}}{C_L} C_{Le} + C_{Y_{pV}}$	$\frac{1}{2}\rho V_e S \frac{b}{2}$
Y_r	Side force due to yaw rate	$C_{Y_{rV}}$	$\frac{1}{2}\rho V_e S \frac{b}{2}$
L_v	Rolling moment due to side slip	$\frac{C_{LL_{\beta W}}}{C_L} C_{Le} + C_{LL_{\beta B}} + C_{LL_{\beta V}}$	$\frac{1}{2}\rho V_e S \frac{b}{2}$
L_p	Rolling moment due to roll rate	$C_{LL_{pW}} + C_{LL_{pV}}$	$\frac{1}{2}\rho V_e S \frac{b}{2}$
L_r	Rolling moment due to yaw rate	$\frac{C_{LL_{rW}}}{C_L} + C_{Le} + C_{LL_{rV}}$	$\frac{1}{2}\rho V_e S \frac{b}{2}$
N_v	Yawing moment due to side slip	$\frac{C_{N_{\beta W}}}{C_L^2} + C_{Le}^2 + C_{N_{\beta B}} + C_{N_{\beta V}}$	$\frac{1}{2}\rho V_e S \frac{b}{2}$
N_p	Yawing moment due to roll rate	$\frac{C_{N_{pW}}}{C_L} + C_{Le} + C_{N_{pV}}$	$\frac{1}{2}\rho V_e S \frac{b^2}{2}$
N_r	Yawing moment due to yaw rate	$\frac{C_{N_{pW}}}{C_L^2} + C_{Le}^2 + C_{N_{rV}}$	$\frac{1}{2}\rho V_e S \frac{b^2}{2}$

Table 2.4: Lateral aerodynamic stability derivatives referred to in the wind axis

Figure 2.8: Demon UAV at BAE Systems' military proving grounds

CHAPTER 3

Control Allocation

3.1 A Brief History of Control Allocation

CONTROL allocation originally stems from ganging or control effector mixing, early examples of the method relied upon demarcating a number of effectors into groups and engaging predetermined combinations of them to act upon a specific moments, an early example presented by Cunningham in 1982 [20] describes the use of a collective stabilises for pitch control, differential stabilisers and flaperons for roll control, and a rudder for yaw. These methods tended to rely on the designer's engineering judgement to assign specific commands to the actuator suite and hence by design may limit the control effector's full potential.

A number of different control allocation methods have been proposed over the last two decades. Control allocation methods can essentially be segregated into optimal and non-optimal methods. Non-optimal methods tend to be *ad hoc* solutions and simply attempt to find any solution within the feasible set – methods such as daisy chaining and explicit ganging fall into the non-optimal genre. A detailed description is given in section 3.3 and a further survey can be found in [53]. Optimal methods require an additional cost function to be minimised, as well as the saturation constraints being satisfied. Some examples include Beck [8] and Durham et al. [26].

Direct (or constrained) control allocation, see section 3.4.2, has been proposed by Durham in 1994 [23] as a method that can provide an optimal solution, in the sense of utilising the maximum capabilities of the controls. The method is reasonably straightforward in the 2D case [23], but considerably more complex for three dimensions [24]. The problem can be extended to dynamic control allocation [37], whereby the allocation can additionally take account of actuator rate constraints, allowing the actuators to operate at different parts of the frequency spectrum.The pseudo inverse method has perhaps now become the *defacto* solution of 'use', in which an analytical solution minimises the total defection within the system, the simplest formulation of this, is the non-saturated case. A number of other variants do exists, some of which are explained in this chapter – including the cascaded generalised inverse method, which was originally presented by Bordignon in 1996 [11]. At each time step a generalised inverse problem is solved and used to allocate the controls. Saturated controls are removed then from the problem and the process is repeated until all the control demand has been

allocated. Generally the simplest control allocation optimisation methods are based on unconstrained least squares algorithms, where modification of the method is typically aimed at accounting for rate and position limitations, [30, 55].

The existing literature is predominately aimed at solving the standardised control allocation problem for a *ad hoc* system, and little is concerned with different or *generalised* objectives. The following chapter shall attempt to collate a diverse number of methods, which will not only define means of computing the solution to the control allocation problem but also outline a number of objectives. Section 3.2 outlines the control allocation problem for both linear and non-linear systems and formulates the framework on which the problem lies. Some non optimal methods are describe in sections 3.3 followed by a number of optimal methods in section 3.4 which lists both analytical and numerical methods. Some active set methods are outlined in section 3.5.

3.2 Introduction to Control Allocation

When dealing with over-actuated systems, where more than one effector can achieve the same demand, some form of control allocation is generally required. A control allocator essentially apportions the total control demand among the individual actuators. The control law indicates the total control effort $v(t) \in \mathbb{R}^m$ which is required, and the control allocator will in turn distribute the control demand among the respective actuators $u(t) \in \mathbb{R}^m$, see figure 1.1. For example given $v(t)$, find $u(t)$ such that,

$$g(u(t)) = v(t) \tag{3.2.1}$$

where $g : \mathbb{R}^m \mapsto \mathbb{R}^n$ is the mapping from total control demand to the individual actuators in the system to be controlled.

Perhaps one of most the elegant ways of describing the control allocation problem was in this authors opinion adroitly presented in Harkegard's thesis [36] and can be seen below

Consider the following example,

$$\dot{x} = u_1 + u_2 \tag{3.2.2}$$

where the scalar x is a state variable and u_1 and u_2 are control inputs. We can consider x as some velocity or acceleration, which is directly affected by the net force of u_1 and u_2. If the net force required to accelerate this system is $u_1 + u_2 = 2$ then there are several ways of achieving it; for example we can utilise only the first effector so that $u_1 = 2$ and $u_2 = 0$. Alternatively we use both effectors, hence $u_1 = 1$ and $u_2 = 1$. Or we can even select a

completely different configuration such as $u_1 = -10$ and $u_2 = 12$, yet this may not be beneficial for most applications. The control allocation problems lies in attempting to select the most suitable solution.

3.2.1 Problem Statement

The standardised linear control allocation formulation can be stated as follows

$$Bu = v \tag{3.2.3}$$

where $v \in \mathbb{R}^n$ is the control output, $u \in \mathbb{R}^m$ is the effector input and $B \in \mathbb{R}^{n \times m}$ of rank n is the control effectiveness matrix relating v and u. The maximum and minimum values for u define a control subset Ξ ;

$$\Xi = \{u \in \mathbb{R}^m | \underline{u} \leq u \leq \overline{u}\} \subset \mathbb{R}^m \tag{3.2.4}$$

Since Ξ is closed bounded and convex, its image under B denoted by Υ, will also be closed, bounded and convex;

$$\Upsilon = \{v \in \mathbb{R}^n | Bu = v, u \in \Xi\} \subset \mathbb{R}^n \tag{3.2.5}$$

The solution to Equation 3.2.3 can have three possible outcomes: (1) an infinite number of solutions, (2) one unique solution or (3) have no solution at all [45].

In general control allocation attempts to contrive a function for mapping Υ to Ξ. When $m > n$ the system is over-actuated and some form of control allocation is required, such that $\mathbb{R}^n$ will produce a surjective mapping onto $\mathbb{R}^m$. There will exist a subspace of $\mathbb{R}^m$ that projects a zero dimensional space in $\mathbb{R}^n$, i.e. the null-space $\aleph(B)$ defined as:

$$u \in \aleph(B) = \{u \in \mathbb{R}^m | Bu \equiv 0\} \subset \mathbb{R}^m \tag{3.2.6}$$

Definition[51]: *Assuming two points x_1 and x_2 where $x_1 \neq x_2$ of form, $y = \mu x_1 + (1 - x_2)\mu$. $\mu \in \mathbb{R}$ forms a line which passes through x_1 and x_2. A set C is said to be convex if and only if for any $x_1, x_2 \in C$ and $0 \leq \mu \leq 1$,*

$$\mu x_1 + (1 - \mu)x_2 \in C \tag{3.2.7}$$

3.2.2 Geometric Representation

Perhaps the problem would be better understood if it were to be represented in a geometric matter. As dimensions greater than three tend to be difficult to visualise, consider a case where $v \in \mathbb{R}^2$ and $u \in \mathbb{R}^3$, so that $B \in \mathbb{R}^{2 \times 3}$. The controls are bounded to a three dimensional rectangular prism, where

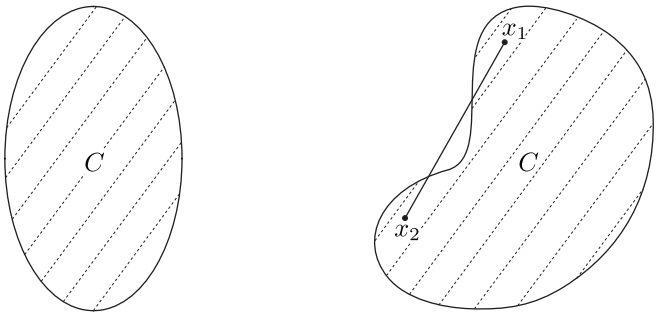

Figure 3.1: *Left:* A convex set *Right:* A non-convex set

the faces denote a single control at its saturation and the vertices indicate that all controls are at their limits. As $v \in \mathbb{R}^2$ B projects a prism onto a two dimensional plane creating the subset Υ. See Figure 3.2 [8].

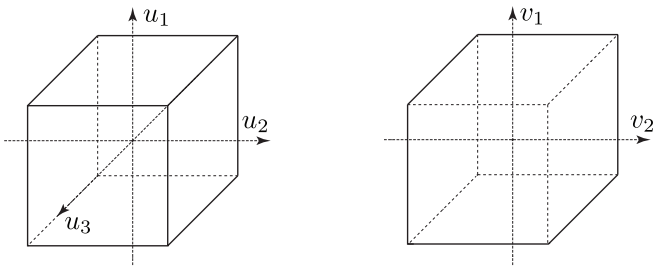

Figure 3.2: *Left:* The subset of Ξ *Right:* The subset Υ, contrived as a projection of Ξ in $\mathbb{R}^2$

Not all the points on the boundary of Ξ map to the boundary of Υ; instead some, map to the interior of Υ.

3.2.3 Linear Systems

Consider the following linear system;

$$\dot{x} = Ax + B_u u \tag{3.2.8}$$

Where the state vector is $x \in \mathbb{R}^k$, the control input is $u \in \mathbb{R}^m$, $A \in \mathbb{R}^{k\times k}$, and $B_u \in \mathbb{R}^{k\times m}$. Since the $m > n$ and $n = \text{rank}(B_u)$, then $\aleph(B_u) = (m-n)$, within which the control inputs can perturbed without affecting the $\dot{x}$, thus there arises a diverse number of control inputs which allow for the same system dynamics. As B_u is rank deficient it can factorised into

$$B_u = B_v B \tag{3.2.9}$$

where $B_v \in \mathbb{R}^{k\times n}$ and $B \in \mathbb{R}^{n\times m}$ both have rank n.

So by substituting equations 3.2.9 and 3.2.3 in to (3.2.8), it can be written as;

$$\dot{x} = Ax + B_v v \tag{3.2.10}$$

In the case where B_u is not rank deficient, yet ill conditioned, it has been suggested to use singular value decomposition, in order to approximate a factorised B_u [55], see appendix A.5.

3.3 Non-Optimal Control allocation methods

Non optimal methods go about attempting to find any feasible solution within the solution space. A number of methods have been developed over the years particularly with regards to aerospace. Some are described below,

3.3.1 Explicit Ganging

Perhaps one of the most simplest methods to implement is explicit ganging which goes about *'ganging'* or combining control effectors to produce a moment principally in one axis through an *ad hoc* distribution. In aerospace, generally and particularly with aircraft which posses reversible controls, ganging is accomplished though the means of pulleys, cables and mechanical systems. On modern fly-by-wire systems the following algorithm can be implemented,

$$u = Gu_p \tag{3.3.1}$$

Where u_p is a set of pseudo controls named so since some or all of the components in this vector are not necessary physical control, yet are linear combination of a number of controls u. G is the ganging matrix which relates the pseudo controls u_p to the control input u. Oppenhiemer *et al* [48] presents the following example,

$$\underbrace{\begin{bmatrix} u_1 \\ u_2 \\ u_3 \\ u_4 \end{bmatrix}}_{u} = \underbrace{\begin{bmatrix} 1 & 0 & 0 \\ 1 & 0 & 0 \\ 0 & 1 & 0 \\ 1 & 0 & 1 \end{bmatrix}}_{G} \underbrace{\begin{bmatrix} u_\phi \\ u_\theta \\ u_\psi \end{bmatrix}}_{u_p} \tag{3.3.2}$$

The ganging law above can be related to a light single prop aircraft, where $u_1, \ldots, u_4$, are left and right ailerons, elevator and rudder respectively. In this instance the pseudo roll control effector u_ϕ is a combination of left, right aileron and rudder inputs. Injecting equation 3.3.1 in to equation 3.2.3 yields,

$$\begin{aligned} v &= Bu \\ &= BGu_p \end{aligned} \tag{3.3.3}$$

and solving for u_p will thus reduce the control allocation problem to a unique solution.

Explicit Ganging Example

With respect to equations 3.3.2 consider a system where,

$$B = \begin{bmatrix} 2 & -2 & 0.5 & 0.2 \\ 1 & 1 & 2 & 0 \\ 0 & 0 & 0 & 2 \end{bmatrix} \; G = \begin{bmatrix} 1 & 0 & 0 \\ 1 & 0 & 0 \\ 0 & 1 & 0 \\ 1 & 0 & 1 \end{bmatrix} \; v = \begin{bmatrix} 1 \\ 2 \\ 3 \end{bmatrix} \tag{3.3.4}$$

such that equation 3.3.3 now takes the form of,

$$\begin{bmatrix} 1 \\ 2 \\ 3 \end{bmatrix} = \begin{bmatrix} 2 & -2 & 0.5 & 0.2 \\ 1 & 1 & 2 & 0 \\ 0 & 0 & 0 & 2 \end{bmatrix} \begin{bmatrix} 1 & 0 & 0 \\ 1 & 0 & 0 \\ 0 & 1 & 0 \\ 1 & 0 & 1 \end{bmatrix} \underbrace{\begin{bmatrix} u_\phi \\ u_\theta \\ u_\psi \end{bmatrix}}_{u_p} \tag{3.3.5}$$

and hence solving for u_p yields,

$$\begin{bmatrix} u_\phi \\ u_\theta \\ u_\psi \end{bmatrix} = \begin{bmatrix} -0.4 \\ 1.4 \\ 1.9 \end{bmatrix} \tag{3.3.6}$$

then by re-injecting u_p into equation 3.3.1 gives,

$$\begin{bmatrix} u_1 \\ u_2 \\ u_3 \\ u_4 \end{bmatrix} = \begin{bmatrix} 1 & 0 & 0 \\ 1 & 0 & 0 \\ 0 & 1 & 0 \\ 1 & 0 & 1 \end{bmatrix} \begin{bmatrix} -0.4 \\ 1.4 \\ 1.9 \end{bmatrix} \tag{3.3.7}$$

thus reducing the problem to a unique solution, such that

$$\begin{bmatrix} u_1 \\ u_2 \\ u_3 \\ u_4 \end{bmatrix} = \begin{bmatrix} -0.4 \\ -0.4 \\ 1.4 \\ 1.5 \end{bmatrix} \tag{3.3.8}$$

3.3.2 Daisy Chaining

Daisy chaining [15, 25] involves demarcating all available control devices into several groups such that the demand of the required moments may be generated individually from each groups. When responding to a moment demand, a particular group is first utilised, while the others remain dormant. As the initial group reaches saturation, it resides at $\overline{u}$ and the dormant groups are brought into action, thus allowing the system to continue to generate the desired moment, see figure 3.3. The daisy chaining method is as follows;

The control inputs and control effectiveness matrix initially need to be separated into respective group M

$$v = \begin{bmatrix} B_1 & B_2 & \dots & B_M \end{bmatrix} \begin{bmatrix} u_1 \\ u_2 \\ \vdots \\ u_M \end{bmatrix} \tag{3.3.9}$$

as already stated the primary set of controls u_1 in this situation must become saturated, before the secondary group of controls are brought to bear. So in a 2D case, before u_1 has reached $\overline{u}$:

$$\begin{aligned} u_1 &= B_1^{-1} v \\ u_2 &= 0 \end{aligned} \tag{3.3.10}$$

$$\tag{3.3.11}$$

Yet if the primary set of controls do reach $\overline{u}$, then:

$$u_1 = sat_{u_1}\left(B_1^{-1} v\right) \tag{3.3.12}$$

$$u_2 = sat_{u_2} B_2^{-1}\left(v - B_1 u_1\right) \tag{3.3.13}$$

hence u_M may presented as:

$$u_M = sat_{u_M}(B_M^{-1}(v - \sum_{i=1}^{M-1} B_i u_i)) \tag{3.3.14}$$

In this situation B_1 and B_2 are scalars and hence invertible, their inverses are unique, and the solutions obtained are unique for the particular control groupings.

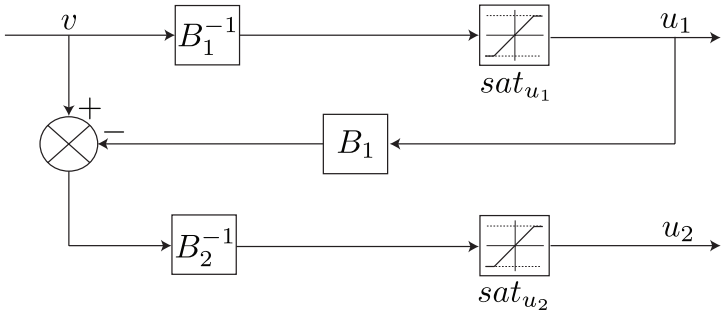

Figure 3.3: Daisy Chaining Control Allocation Case for Two Input Groups

Daisy Chaining Example

Lets consider a set of longitudinal controls, namely η_1 and η_2. For convenience the constrains shall be set to $-1 < \eta_1 < 1$ and $-1 < \eta_2 < 1$, with control effectiveness $B_1 = 3$ and $B_2 = 1$ respectively. If demand is $v = 1$

Then:

$$u_1 = sat_{u_1}(1 \cdot (\frac{1}{3} \cdot 1)) = \frac{1}{3} \tag{3.3.15}$$

$$u_2 = sat_{u_2}(1 - 3 \cdot \frac{1}{3}) = 0 \tag{3.3.16}$$

3.4 Optimal Control Allocation

In general optimal control allocation tends to revolve around the following interpretation. Given v determine u such that $Bu = v$. When a definite number of solution exists, select the most appropriate one. If no solution exists, determine u so that Bu approximates v.

Harkegard [36] describes the optimal control input as a two step optimisation problem;

$$\Sigma = \arg\min_{u \in \Xi}(||W_v(Bu - v)||_p) \tag{3.4.1}$$

$$\overline{u} = \arg\min_{u \in \Sigma}(||W_u(u)||_p) \tag{3.4.2}$$

Here p denotes the l_p norm, which can be used to denote how appropriate a solution is, see section A.2, and the weighting matrices W_v and W_u are design parameters which would prioritise certain objectives and controls over other ones respectively. Equation 3.4.1 can be interpreted as; given the set

Σ find the minimum control input u which minimises the euclidean distance between u and 0. Harkegard [36] also suggests to add an additional design parameter u_d so that u now becomes $u = \min ||W_u(u - u_d)||_p$. Attracting the solution of u to u_d if there is no unique solution to Σ.

3.4.1 Error Minimisation Problem

M.Bosden [10] suggests to reformulate equation 3.4.1 as a weighted optimisation problem, resulting in a far simpler single step optimisation,

$$u_w = \min_{u \in \Xi}(||W_u(u)||_p^p + \epsilon||W_v(Bu - v)||_p^p) \tag{3.4.3}$$

where if $p = 2$ then;

$$\lim_{\epsilon \mapsto \inf} u_w(\epsilon) = u_s \tag{3.4.4}$$

such that u_s is the solution to 3.4.1. [9]

3.4.2 Direct Control Allocation

Direct Control Allocation can be described as follows; given a virtual control demand v, find the feasible control input u^* that generates the virtual control input v^* of maximum magnitude in the direction of v, such that

$$v^* = Bu^* \tag{3.4.5}$$

Let

$$a = \frac{||v^*||_2}{||v||_2} \tag{3.4.6}$$

$$u = \begin{cases} \frac{1}{a}u^* & \text{if } a > 1 \\ u^* & \text{if } a \leq 1 \end{cases}$$

In instances where the control effector's position limits are defined such that they do no incur a sign change, i.e $-0.5 \leq u \leq -1$ where the origin of the control space would move out of the control subset. K Bordignon [11] Suggest to change the control limits, so that they are contained within the control subset. This may be achieved by adding some Δu to the control vector limits and changing the corresponding desired moment.

For example the control limits now become;

$$\underline{u} + \Delta u \leq u + \Delta u \leq \overline{u} + \Delta u \tag{3.4.7}$$

Define a new set of controls u^*, and a new moment demand v^*

$$
\begin{aligned}
u^* &= u + \Delta u && (3.4.8)\\
\Rightarrow u &= u^* - \Delta u && (3.4.9)\\
\Rightarrow v &= Bu = B(u^* - \Delta u) && (3.4.10)\\
&= Bu^* - B\Delta v \\
\Rightarrow v^* &= v + \Delta v = Bu^* && (3.4.11)
\end{aligned}
$$

and hence this shall guarantee that the origin of the moment space is contained within the moment subset.

3.4.3 Fix-Point Method

The fix point iteration method was purposed by Burken et al [42] for solving a weighted l_2-optimal control allocation problem, it is presented as follows;

$$u_i = \text{sat}((1-\gamma)\omega B^T Q_1 v - (\omega H - I)u^{k-1}),\ k = 1, \ldots, N \tag{3.4.12}$$

where N is the number of iterations,

$$\gamma = \frac{1}{\epsilon + 1} \tag{3.4.13}$$

$$
\begin{aligned}
Q_1 &= W_v^T W_v \\
Q_2 &= W_u^T W_u
\end{aligned}
$$

$$H = (1-\gamma)B^T Q_1 B + \gamma Q_2$$

and

$$\omega = ||H||_F^{-1} \tag{3.4.14}$$

in which $||\cdot||_F$ is considered to be the Euclidean norm, see section A.3. $\text{sat}(\cdot)$ is a vector saturator with components;

$$\text{sat}_i(u) = \begin{cases} \underline{u}_i, & u_i < \underline{u}_i \\ u_i, & \underline{u}_i \leq u_i \leq \overline{u}_i, \\ \overline{u}_i, & u_i > \overline{u}_i \end{cases} \tag{3.4.15}$$

and

$$i = 1, \ldots, m \tag{3.4.16}$$

Further references can be found in [7] and [47].

3.4.4 Weighted Pseudo-Inverse Method

Originally proposed by Durham in 1999 [25] the solution attempts to solve for u by employing a pseudo-inverse.

The problem is posed as such

$$\min_u \tfrac{1}{2} u^T R u \text{ subject to } Bu = v \tag{3.4.17}$$

Where R is a positive diagonal weighting matrix which prioritises a particular effector over another, see equation 3.4.27. The solution to weighted pseudo-inverse solution may be obtained by formulating the following augmented function, and utilising Lagrange multiplies,

$$\Lambda(u, \lambda) = a(u) \pm \lambda^T (c(u, v)) \tag{3.4.18}$$

where $a(u)$ is the objective and $c(u, v)$ is the constraint. The augmented function takes the form;

$$\Lambda(u, \lambda) = \frac{1}{2} u^T R u + \lambda^T (v - Bu) \tag{3.4.19}$$

By taking partial derivatives of Λ with respect to u and λ and setting them to zero in the normal fashion yields,

$$\frac{\partial J}{\partial u} = Ru - B^T \lambda = 0 \tag{3.4.20}$$

$$\frac{\partial J}{\partial \lambda} = v - Bu = 0 \tag{3.4.21}$$

Rearranging (3.4.20) such that;

$$u = R^{-1} B^T \lambda \tag{3.4.22}$$

and substitute (3.4.22) into (3.4.21) gives

$$v = B R^{-1} B^T \lambda \tag{3.4.23}$$

$$\lambda = (B R^{-1} B^T)^{-1} v \tag{3.4.24}$$

Substituting (3.4.24) into (3.4.20) gives

$$u = R^{-1} B^T (B R^{-1} B^T)^{-1} v \tag{3.4.25}$$

hence

$$u = W B^T (B W B^T)^{-1} v \tag{3.4.26}$$

where

$$R = \begin{bmatrix} \overline{u}_1 & 0 & 0 & 0 \\ 0 & \overline{u}_2 & 0 & 0 \\ 0 & 0 & \ddots & 0 \\ 0 & 0 & 0 & \overline{u}_i \end{bmatrix} \quad W = \begin{bmatrix} \frac{1}{\overline{u}_1} & 0 & 0 & 0 \\ 0 & \frac{1}{\overline{u}_2} & 0 & 0 \\ 0 & 0 & \ddots & 0 \\ 0 & 0 & 0 & \frac{1}{\overline{u}_i} \end{bmatrix} \tag{3.4.27}$$

The use of this weighting W results in the prime appropriation of the highly effective controls while minimising utilization of less effective controls.

It is prominent to note that Enns [30] proposes a control allocation scheme based on ellipsoidal constraints which can be reduced to the pseudo-inverse methods.

Furthermore it is beneficial to note that in the situations where control inputs exceed constraints, [44] suggests to either clip the individual control at the constraints or the entire vectors can be scaled such that no constraints are violated.

When considering reconfigurable flight control this generalised formulation easily allows for the removal of effectors from the active set of effectors by zeroing the weights associated with that effector.

The method is illustrated graphically by figure 3.4. Consider the case where $n = 3$ and $m = 2$. Then the problem can be regarded as a three dimensional ellipsoid problem, where the semi-axis are of lengths W_1u_1, W_2u_2 and W_3u_3. The surface of the ellipsoid represents constant values of the quadratic function u^TWu. The constraint $v-Bu$ represents a hyperplane which intersects the ellipsoid creating an ellipsis at which the solutions to u lie. The system is further constrained by the effectors position limits, represented as box. The point a which lies at the least distance from the origin is the solution to equation (3.4.26).

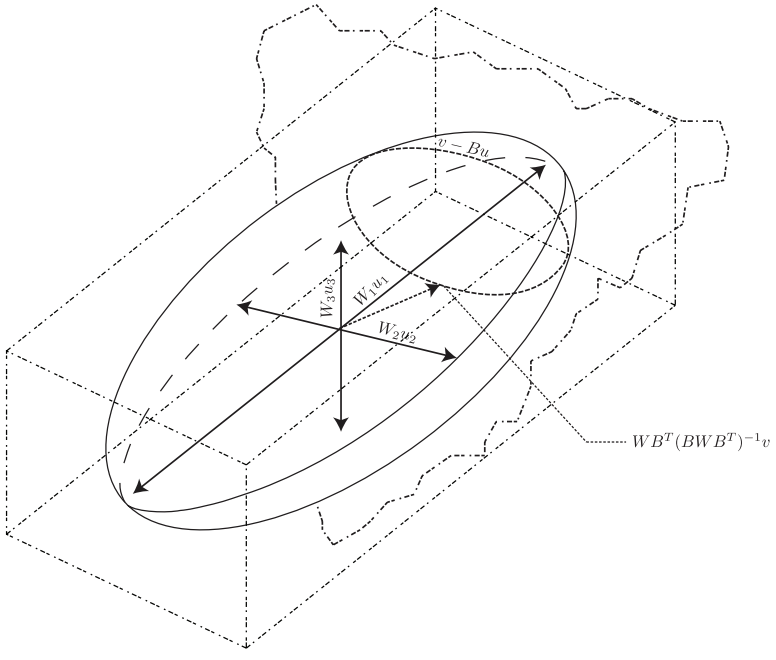

Figure 3.4: Geometric Representation of (3.4.19) and (3.4.26)

3.4.5 Cascaded Generalised Inverse Solutions

Bordignon [12] extends the pseudo inverse method to cascaded generalised inverse, he goes about attempting to solve a series of generalised inverses. At each step, a generalised inverse B_k^κ is used to allocate the control,

$$u_k = B^\kappa v_k \tag{3.4.28}$$

Controls in u, which exceed their control limits are held at their respective saturation limits and are systematically removed from B_{k+1} and v_{k+1}. The unattained moments are calculated

$$v_{k+1} = v_k - B_{k+1} u_k \tag{3.4.29}$$

Another generalised inverse is taken with reduced controls

$$u_{k+1} = B_{k+1}^\kappa v_{k+1} \tag{3.4.30}$$

This process is repeated until $v_{k+1} = 0$ or $m < n$.

3.4.6 Travel Deflection Rate

By adding the term $u(t-T)$ to equation 3.4.17 the control allocator shall now minimise the total deflection rate as opposed to the minimum deflection, where T is the sample time and $u(t-T)$ is the position of the actuator at the last time step and R_p is a positive diagonal weighting matrix similar to 3.4.27,

$$\min_{u \in \Xi} R_p ||u(t) - u(t-T)||_2 \tag{3.4.31}$$

The solution maybe be obtain in the same manner as to that of equation 5.3.1,

$$\Lambda = \frac{1}{2}(u - u_{t-T}) R_p (u - u_{t-T}) + \lambda^T (v - Bu) \tag{3.4.32}$$

by taking partials of u and λ with reference to equation 3.4.32 and equating them to zero gives,

$$\frac{\delta \Lambda}{\delta u} = R_p u - R_p u_{t-T} - B^T \lambda \Rightarrow u = u_{t-T} + R_p^{-1} B^T \lambda = 0 \tag{3.4.33}$$

$$\frac{\delta \Lambda}{\delta \lambda} = v - Bu = 0 \tag{3.4.34}$$

inject equation 3.4.33 in to equation 3.4.34 such that,

$$v = B(u_{t-T} + R_p^{-1} B^T \lambda) \Rightarrow \lambda = (B R_p^{-1} B^T)^{-1} (v - B u_{t-T}) \tag{3.4.35}$$

re-injecting λ into equation 3.4.33 gives

$$R_p(u) - R_p(u_{t-T}) - B^T(BR_p^{-1}B^T)^{-1}(v - Bu_{t-T}) = 0 \quad (3.4.36)$$

$$\Rightarrow u = u_{t-T} + R_p^{-1}B^T(BR_p^{-1}B^T)^{-1}(v - Bu_{t-T}) \quad (3.4.37)$$

$$= [I - R_p^{-1}B^T(BR_p^{-1}B^T)^{-1}B]u_{t-T} + R_p^1B^T(BR_p^{-1}B^T)^{-1}v \quad (3.4.38)$$

Since $W_p = R_p^{-1}$ then

$$u = [I - W_pB^T(BW_pB^T)^{-1}B]u_{t-T} + W_pB^T(BW_pB^T)^{-1}v \quad (3.4.39)$$

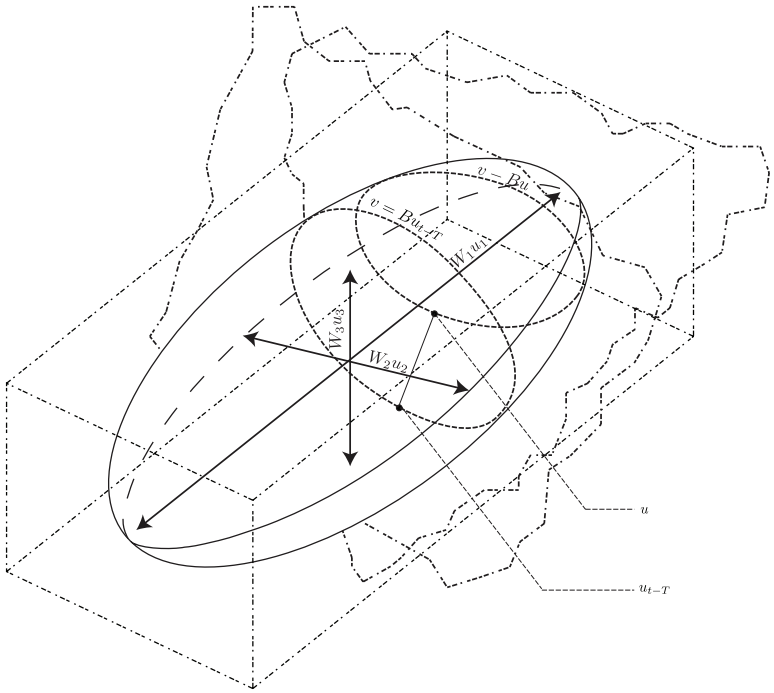

Figure 3.5: Graphical representation of equation 3.4.39

Figure 3.4.39 denotes a graphical representation of equation 3.4.32, in the same manner as equation 3.4.19. The semi-axis of the ellipsoid are of lengths W_1u_1, W_2u_2 and W_3u_3 and the hyperplanes $v - Bu$ and $v - Bu_{t-T}$ intersect the ellipsoid creating two ellipses to which all the solutions to u and u_{t-T} are bound. The solution to u is drawn to the $v - Bu_{t-T}$ hyperspace such that it lies at the point which is closest to u_{t-T}.

3.4.7 Frequency-Apportioned Control Allocation

Davidson [43] extends the Weighted Pseudo-inverse method to encompass frequency apportioned control allocation. The pseudo inverse method con-

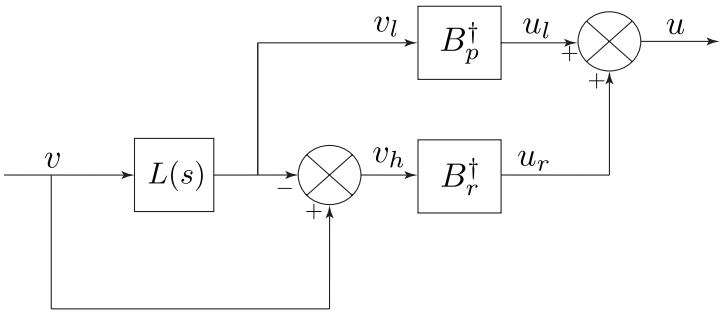

Figure 3.6: Frequency Apportioned Control Allocation Strategy

siders moments exhibited by individual effector. Yet if v changes aggressively slow reacting servos may saturate at their rate limits, which can introduce errors or time lags which could significantly degrade the closed loop performance. In order to over come this limitation frequency apportioned control allocation allots high-frequency commands to high rate effectors while distributing the lower frequency commands to highly effective controls, see figure 3.6. In order to achieve this, the total control demand must first be apportioned into high and low frequency components using a low pass filter.

$$j_l = L(s)v \tag{3.4.40}$$
$$j_h = (1 - L(s))v \tag{3.4.41}$$

where u_l refers to the low frequency component, u_h refers to the high frequency component and,

$$L(s) = \left(\begin{bmatrix} \frac{1}{T_M s+1} & 0 & 0 \\ 0 & \frac{1}{T_L s+1} & 0 \\ 0 & 0 & \frac{1}{T_N s+1} \end{bmatrix} \right) \tag{3.4.42}$$

The weighted pseudo-inverse is used to allocate the high and low frequency components in accordance with the individual effector rate and position limits,

$$u_l = B_p^+ j_l = B_p^+ v \tag{3.4.43}$$
$$u_h = B_r^+ j_h = B_r^+ v \tag{3.4.44}$$

Where B_p^+ and B_r^+ are position and rate limit pseudo inverses, such that

$$B_p^+ = W_p B^T (B W_p B^T)^{-1} \tag{3.4.45}$$
$$B_r^+ = W_r B^T (B W_r B^T)^{-1} \tag{3.4.46}$$

and W_p and W_r are positive diagonal weighting matrices similar to those expressed in equation 3.4.27. u is then given as,

$$u = u_l + u_h = [B_p^+ L + B_r^+ (1 - L)]v \tag{3.4.47}$$

As the time constants T_M, T_L and T_n in the low pass filters determine the frequency at which the total demand is passed on the to respective pseudo-inverse solutions, their selection plays a vital element in frequency apportioned control allocation. Davidson suggests to choose the time constant by determining the position and rate limits for u under a sinusoidal inputs and choose the time constant which yields the least restrictive boundary. For a full review see [43].

3.5 Active Set Methods For Control Allocation

Even though numerical approximation methods, like those mentioned in the previous sections, appear to provide an adequate solution to the control allocation problem, they are not necessary guaranteed to find the optimum in a finite number of iterations. Active set methods resemble iterative pseudo-inverse methods, in that inequality constraints are regarded; or disregard as equality constraints[35]. Yet active set methods do differ under the conditions to which the constraints are activated. This section shall outline a brief overview on active set methods for control allocation as well as introduce two methods namely Sequential Least Squares and Weighted Least Squares.

3.5.1 The Active Sets

To better understand the active set solution, it is required that we present a prolegomenon for the method to follow. All parameters such as B, u, W_u, W_v etc. may be changed to reflect the current state of the system. In this instance it will be necessary that the previous solution is feasible with respect to its new position constraints so that, $\underline{u}(t) \leq u(t - T) \leq \overline{u}$ holds, where T is the sampling time - and $u(t-T)$ is the solution at the last time step. The working set W_S is defined as the optimal active set of the previous sampling step. When the allocator is initialised, hence no previous solution is available then, $W_S = 0$ and $u^0 = (\underline{u} + \overline{u})/2$. The elements for u_i^0, for which $i = 1, \ldots, m$, are defined as such; if u_i was not met with a saturation then, $u_i^0 = u_i(t-T)$. Yet if $u_i(t-T)$ does saturate then $u_i^0 = \overline{u}(t)$ or $u_i^0 = \underline{u}$, depending on whether saturation occurred at its upper or lower bound. This ensures that if $u_i(t - T)$ presents an absolute value greater than the saturation limits,$\overline{u}_i(t)$, $\underline{u}_i(t)$, the starting point of the optimisation for the ith component resides at its physical position limit. The weighting matrices W_u, W_v are assumed to be non-singular. The non-singularity of W_u

ensures that the proposed optimisation problems both have unique optimal solution. See [38] for a full review.

3.5.2 The Least Squares Problem

Consider the following bounded constrained least squares problem

$$\begin{aligned} &\min_u ||Au - b|| \\ &Bu = v \\ &Cu \leq U \end{aligned} \tag{3.5.1}$$

Where $C = \binom{I}{-I}$, and $U = \binom{\overline{u}}{\underline{u}}$, such that $Cu \leq U$ is equivalent to $\underline{u} \leq u \leq \overline{u}$. Bjorck [9] solves 3.5.1 using a sequence of equality constraint problems where some inequality constraints are regarded as equalities and form the working set, while the other are disregarded [36]. For a full illustration of the algorithm See appendix B.1

3.5.3 Sequential Least Squares

The sequential least squares control allocation algorithm is as follows

1. Assign u^0 as described in section 3.5.1.
2. Solve

$$\begin{aligned} u_\Omega = \min_u &||W_v(Bu - v)||_p \\ &\underline{u} \leq u \leq \overline{u} \end{aligned}$$

   by using algorithm B.1 with the following modification; when the number of free variables exceed $k = dim v$ in which case the optimal perturbation p is not uniquely determined, pick the minimum perturbation.
3. $Bu_\Omega \neq v$, let $u = u_\Omega$, otherwise
4. Let $u^0 = u_\Omega$ and W_S be the resulting solution.
5. Solve

$$\begin{aligned} u = \min_u &||W_u(u - u_d)||_2 \\ &Bu = v \\ &\underline{u} \leq u \leq \overline{u} \end{aligned} \tag{3.5.2}$$

An investigation of Weighted least squares method can be found in [36]. Algorithms are also presented for the l_2-optimal control allocation problem 3.4.1

3.5.4 Weighted Least Squares

Consider the following problem,

$$u = \min_{u \in \Xi} ||W_u(u - u_d)||_2^2 + \gamma ||W_v(Bu - v)||_2^2 \tag{3.5.3}$$

Where γ should be assigned a value *great* enough, that the term $W_v(Bu - v)$ is minimised first.

Harkegard [35] reformulates problem 3.5.3 to,

$$||W_u u - W_u u_d||_2^2 + \gamma ||W_v B u - W_v v||_2^2 \tag{3.5.4}$$

$$= \left|\left|\begin{bmatrix} \gamma^{\frac{1}{2}} W_v B \\ W_u \end{bmatrix} u - \begin{bmatrix} \gamma^{\frac{1}{2}} W_v v \\ W_u u_d \end{bmatrix}\right|\right|_2^2 \tag{3.5.5}$$

By assuming that,

$$\begin{bmatrix} \gamma^{\frac{1}{2}} W_v B \\ W_u \end{bmatrix} \text{ is equivalent to } A, \quad \begin{bmatrix} \gamma^{\frac{1}{2}} W_v v \\ W_u u_d \end{bmatrix} \text{ is equivalent to } b \tag{3.5.6}$$

problem 3.5.3 can be solved using algorithm B.1.

The choice of γ in problem 3.5.3 is quite important. The corruptions of the first term, $||W_u(u - u_d)||_2^2$ with respect to the second term, $||W_v(Bu - v)||_2^2$, does not only depend on the values of B, W_u, W_v but also on γ. ie setting γ to 100 is equivalent to scaling W_v by 10 or W_u by $\frac{1}{10}$. Harkengard suggests to use the following algorithm to select the most appropriate γ,

$$\gamma = \gamma_d \frac{W_u^2}{(W_v B)^2} \tag{3.5.7}$$

where γ_d is a user defined weighting.

3.6 Dynamic Control Allocation

As opposed Davidson's method, seen in section 3.4.7, which use low pass filters to determine the frequency at which the total demand is passed on the a specific actuator. Harkegard [35] reformulates problem 3.4.1 to account for an additional term $||u(t) - u(t - T)||$ and hence,

$$u(t) = \min_{u(t) \in \Omega} ||W_p(u(t) - u_s(t)||_2^2 + ||W_r(u(t) - u(t - T)||_2^2 \tag{3.6.1}$$

where

$$\Omega = \min_{u(t) \in \Xi} ||v = Bu|| \tag{3.6.2}$$

and $u_s \in \mathbb{R}^m$ is the desired steady state control input. The weighting matrices W_r and W_p in this instance are considered to be symmetric, such that,

$$W_l = (W_p^2 + W_r^2)^{\frac{1}{2}} \tag{3.6.3}$$

is non-singular.

In comparison to equation 3.4.1, formulation 3.6.1 not only accounts for the position error - or minimum displacement, but the additional term $||u(t) - u(t-T)||$ also accounts for rate distribution.

Harkengard [35] reduces problem 3.6.1 to a simple non saturated case of form,

$$\min_{u(t)} ||W_p(u(t) - u_s(t)||_2^2 + ||W_r(u(t) - u(t-T)||_2^2 \tag{3.6.4}$$

$$\text{s.t.} Bu(t) = v(t) \tag{3.6.5}$$

Then equation 3.6.4 can be reformulated as such,

$$\begin{aligned} & (u(t) - u_s(t))^T W_p(u(t) - u_s(t)) + (u(t) - u(t-T))^T W_p(u(t) - u(t-T)) \\ = \; & u(t)^T(W_p + W_r)u(t) - u(t)^T(W_p u_s(t) + W_r u(t-T)) \\ & + u(t)^T W_p u_s(t) + u(t-T)^T W_r u(t-T) \\ & - (u_s(t)^T W_p + u(t-T)^T W_r)u_t \end{aligned} \tag{3.6.6}$$

The terms $u(t)^T W_p u_s(t)$ and $u(t-T)^T W_r u(t-T)$ do not have an effect on the minimisation and hence can be eliminated from the formulation, furthermore since $(u_s(t)^T W_p + u(t-T)^T W_r)u_t$ is equivalent to $u(t)^T(W_p u_s(t) + W_r u(t-T))$, then 3.6.6 can be express as follows,

$$\begin{aligned} & u(t)^T(W_p + W_r)u(t) - 2u(t)^T(W_p^2 u_s(t) + W_r^2 u(t-T)) \\ = \; & (u(t) - D)^T W_l(u(t) - D) \end{aligned}$$

where

$$D = W^{-2}(W_p^2 u_s(t) + W_r^2 u(t-T) \tag{3.6.7}$$

the formulation above is equivalent to[1]

$$\min ||W_l(u(t) + W_l^{-2}(W_p^2 u_s(t) + W_r^2 u(t-T))|| \tag{3.6.8}$$

Which problem can be solved through least squares minimisation, such that,

[1] A proof can be found in [35]

$$u(t) = (I - KB)W_l^{-2}W_p^2 u_s(t) + (I - KB)W^{-2}W_2^2 u(t-T) + Kv(t) \quad (3.6.9)$$

where

$$K = W_l^{-1}(BW_l^{-1})^\dagger \quad (3.6.10)$$

and † denotes a pseudo inverse operator see appendix A.6.

3.7 Discussion and Conclusions

A number of control allocation methods have been described in this chapter, depicting all manner of solutions to the control allocation problem including the Explicit Ganging,Pseudo Inverse, Active Set methods and Dynamic Control Allocation.

Explicit Ganging uses a set of pseudo control (control effector mixing) to reduce the control allocation problem to a feasible unique solution (non optimal solution). The method is perhaps one of the few control allocation schemes which maybe implemented onto an aircraft with reverse-able controls. Although as the common trend in aerospace is hugely sided towards fly-by-wire systems this method is becoming evermore obsolete.

Pseudo inverse solutions have, as previously stated, become the *de facto* method 'of use' and hence has been subject to extensive research. The pseudo inverse method cannot find a feasible solution for all attainable virtual control inputs v and certainly not for unattainable virtual control inputs [22]. A number of solutions have been proposed to resolve the said constraints. As seem in section 3.4.4 a simple solution is to weight each control input so that it is the inverse of the maximum saturation limit (assuming no rate limitations and symmetric position limits). Another alternative would be to truncate 3.4.26 by clipping those components which violate some constraints. In general, however, not all the control inputs saturate and hence the reaming control inputs may be utilised account for the remaining moments. Virnig et al [56] suggests that all control inputs which violate their bounds in the pseudo inverse solution are saturated and removed from the optimisation. Then, the control allocation problem is resolved with only the remaining free variable.

Active set methods are closely related to to the approximate pseudo inverse methods with are generally used in most modern aircraft control allocation schemes. As opposed to using heuristics, active sets methods use constrained programming to decided which actuators to saturate. The calculations performed at each iteration are consider to be computationally cheap since they mainly consist of solving, equity constrained least square problems. In a study conducted by Harkegard [36] it can be seen that feasible

non optimal solutions are produced at each time step which maybe used to further reduce the computation or if there is not enough time to compute the optimal solution.

Dynamic control allocation offers an extra degree of freedom in comparison to the pseudo inverse method described in section 3.4.4 and hence the allocation of the control effort among the effectors not need be the same for all frequency. In other words the allows slows effectors to be utilised to bare the low frequency components of the virtual control input, while the faster effectors may operate over the whole frequency range.

The dynamic control allocation can, in a manner of speaking, be conceived as a method for multi-objective control allocation, although in some respects is somewhat diminished. The method does give a trade off between the two objectives – $||W_p(u(t) - u_s(t))||_2$ and $||W_r(u(t) - u(t - T))$, yet the decision maker has no control over where the solution shall fall within the objective space. As the weightings within the minimisation tend to be assign arbitrary[2] values the solution can lie anywhere within the attainable set and hence is unlikely to be Pareto optimal, efficient or weakly efficient, (see section 4.3).The following chapter shall address this issue by developing a number of ***novel*** methods which would guarantee that the solution would lie of the Pareto optimal frontier.

[2]Arbitrary in the sense that they are not related to the multi-objective problem in anyway but instead are sized to, and are respective of, effector prioritisation

CHAPTER 4

Multi-Objective Control Allocation

4.1 Introduction

SO far, a number of optimal[1] control allocation schemes have been listed, including methods such as the 'Weighted Pseudo Inverse' in section 3.4.4 which employs Lagrange multipliers to attain to a global minima, to the 'Travel Deflection Rate' aptly described in section 3.4.6 which distributes the total control demand in accordance with the frequency components of the total control demand. Although each method has been proven to provide and adequate solution it is clear that each method is equipped to deal with only one objective, that is - the 'Weighted Pseudo inverse is designed to allocate the control demand such that the solution are drawn to zero (or a user defined point u_d) Hence evoking minimum displacement . While the 'Travel Deflection Rate' draws the solutions to the last time step - Minimum Rate.

In many real life scenarios a single objective does not suffice, particularly with in aerospace applications where certain objective may not hold for the entirety of the mission. For example whilst operating in hostile environment it may be necessary to reduce the radar cross section of the aircraft thereby it is required to minimise the control surface deflections and drawing the solutions to the neutral position. Although while on route to and from a mission, reduction of energy within the system becomes from prevalent. Generally, in a situation as this, a decision is to be made regarding which objective is to be used, thereby limit the operational envelope of the vehicle. Yet with the addition of a multi-objective control allocator, this is no longer necessary as it shall not only allow the user/designer to simply turn certain objectives "off" or "on" it can also provide a trade off between the objectives if necessary. That is to say the decision maker, during a mission has the ability to exaggerate certain objectives while diminishing others, regardless if the objective are said to be in conflict. A topic which has been little explored is multi-objective control allocation, which calls for the concurrent utilisation of a different objectives.

The following chapter shall introduce the principle concepts of Multi-objective optimisation and then move on to present four ***novel*** Multi objective control allocation methods; Simple Weighting, Minimax, and two which

[1] optimal in the sense of $Bu = v$ with a set of constraints on u

are based on Goal attainable methods - namely, Canonical Control Allocation and Classical Control Allocation.

This chapter is based on the following paper

Ramey Jamil, Francis Salama, Mudassir Lone, Al Savvaris, James Whidborne. Multi-objective Control Allocation With Conflict Resolution. *AIAA Guidance, Navigation, and Control Conference* Minneapolis - Minnesota, 2012

4.2 Multi-Objective Control Allocation

In order to completely understand the intricacies of Multi-objective control allocation a thorough understanding of Multi-objective optimisation must first be established. The generalised multi-objective optimisation problem may be presented as the following vector mathematical programme;

$$\text{optimise } F(\omega) = \{f_1(\omega) \dots f_j(\omega) \dots f_k(\omega)\} \tag{4.2.1}$$

$$\text{s.t } \omega \in \Omega \tag{4.2.2}$$

$$\Omega = \left\{ \omega \;\middle|\; \begin{array}{cc} g_i(\omega) \leq 0 & i = 1, \dots, m_1 \\ h_l(\omega) = 0 & l = 1, \dots, m_2 \\ \omega = [\omega_1 \dots \omega_n]^T & \end{array} \right\}$$

where ω denotes a solution to the Multi objective optimisation. Here the nonlinear objective functions $f_j(\omega)$ are assumed for minimisation or maximisation subject to a set of constraints Ω. Where $g_i(\omega)$ and $h_i(\omega)$ defines nonlinear inequality and equality constraint functions in Ω respectively. $F(\Omega)$ defines a projection of the objective set $F(\omega)$ on to the constraints Ω such that,

$$F(\Omega) = \{F(\omega) | \omega \in \Omega\} \tag{4.2.3}$$

Generally the objective functions $f_j(\omega)$ tend to be incommensurable and maybe in conflict with each other such that it is impossible to find a solution which can satisfy all j objective at their optimum. Therefore Multi objective schemes aim to find a point which best attains to the optimal solution or sets an appropriate trade off between them subject to designer's or decision makers preferences.

4.2.1 Preliminaries

The following section shall outline a number of preliminaries and define concepts which are necessary for Multi-objective optimisation. First consider the following single objective optimisation

Any two solution ω_1 and ω_2 in a single objective optimisation of form,

$$\min_{\omega \in \Omega} f(\omega) \tag{4.2.4}$$

where

$$\Omega = \left\{ \begin{array}{ll} h_i(\omega) = 0 & j = 1, 2, \ldots, m \\ g_j(\omega) \geq 0 & j = 1, 2, \ldots, l \end{array} \right\} \tag{4.2.5}$$

can be compared completely, expressly; either ω_1 is preferred to ω_2, if and only if $f(\omega_1) < f(\omega_2)$ or ω_2 is preferred to ω_1 if and only if $f(\omega_1) > f(\omega_2)$ or ω_1 is indifferent to ω_2 if and only if $f(\omega_1) = f(\omega_2)$. Therefore it is possible to find an optimal for which the objective is minimised.

per contra for a multi-objective optimisation of the form defined in equation 4.2.1, the solutions can not be compared completely, namely;

ω_1 dominates ω_2 if and only if $F(\omega_1) \leq F(\omega_2)$ (with strict inequality for at least one objective) – or in other words ω_1 is a better solution than ω_2 for all j objectives. ω_2 dominates ω_1 if and only if $F(\omega_1) \geq F(\omega_2)$ (with strict inequality for one objective) – or ω_2 is a better solution than ω_1 for all j objectives. ω_1 is indifferent to ω_2 if and only if $F(\omega_1) = F(\omega_2)$. ω_1 is non-dominate to ω_2 and ω_2 is non-dominate to ω_1 if and only if $F(\omega_1) <> F(\omega_2)$ - that is ω_1 outperforms ω_2 on some objectives but is worst on others.

Definition: *Assuming a solution ω^t, $F(\omega^t) \in F(\Omega)$ is said to be non dominated if there does not exist another vector, $F(\omega) \in F(\Omega)$ such that $F(\omega) \leq F(\omega^t)$ with at least one $f(\omega) \leq f(\omega) < f(\omega^t)$, otherwise, $F(\omega^t)$ is dominated* [32]

Generally in multi objective optimisation schemes, solutions which are dominated by other solution are not sought for. Furthermore it is not possible for a feasible solution to dominate all other solutions within the feasible set - as there would be no need for multi-objective optimisation. Hence it is required to find a solution that is non-dominated by all other solutions or is a Pareto optimal[2] solutions. Non-dominance results from the conflicts among objectives which are inherent in multiple objective optimisation – Pareto optimality is explained in greater detail in section 4.3.

Definition: *A solution $\omega^t \in \Omega$ is said to be a Pareto optimal or an efficient solution (respect. to weakly efficient solutions) of the multi-objective*

[2]Also referred to non-inferior, non-dominated and efficient

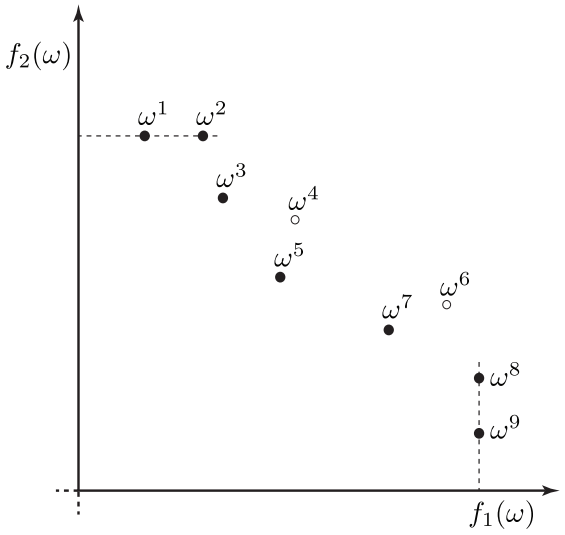

Figure 4.1: Efficient and weakly efficient solution examples, for two objectives [32]

problem if there does not exist any $\omega \in \Omega$, $\omega \neq \omega^t$ *such that* $F(\omega) \leq F(\omega^t)$ $(F(\omega) < F(\omega^t))$*and* $F(\omega) \neq F(\omega^t)$ *where* $F = \{f_1, f_2, \ldots, f_p\}$ *is the set of design objectives. The image of the efficient or Pareto optimal set by* F *is then referred to as the trade-off or Pareto optimal frontier.* [32]

It is easier to satisfy weakly efficiency than dominance since an efficient solution must be weakly efficient but a weakly efficient cannot be an efficient solution. G.P. Liu *et al* [32] represents the efficiency, weakly efficient problem' with a pragmatic 2D (two objective) graphical presentation see figure 4.1. ω^i for $i = \{1, \ldots, 9\}$ solution are presented in a discrete decision space - Here solutions ω^4 and ω^6 are noted as completely inefficient as they dominated by ω^5 and ω^7. The remaining solutions are denoted as weakly efficient, apart from ω^2 and ω^8 which are not efficient as they are weakly dominated by ω^1 and ω^9.

Definition: *A solution* ω^t *to problem 4.2.1 is said to be weakly efficient if there does not exist* $\omega \in \Omega(\omega \neq \omega^t)$ *such that* $F(\omega) < F(\omega^t)$. [32]

4.3 Pareto Optimality for Multi-Objective Control Allocation

Consider the following set of p conflicting design objectives of form $\{f_j(\omega) : j = 1 \dots p\}$ formulated as the general multi-objective optimisation problem:

$$\min_{\omega \in \Omega} \{f_j(\omega) \text{ for } j = 1 \dots p\} \tag{4.3.1}$$

where ω denotes a vector of decision variables and Ω denotes a set of design constraints.

For all intensive purpose it may appear that the definition for efficiency is the same as non-dominance, however strictly speaking efficiency tends to refer to the design variables and non dominance refers to the objective functions in $F(\Omega)$ [50]

The multi-objective optimisation must therefore select the desired solution within the set Ω that is said to be non-dominated for all objectives, i.e. the Pareto-optimal solutions. The Pareto optimal set is the collection of all efficient and weakly efficient solution of the feasible set.

For multi-objective optimisation, non-dominance implies that the improvement of some objective could only be achieved at the expense of another. As an example, assume the 2D case illustrated in Figure 4.2. The solution to the multi-objective optimisation problem must lie on the Pareto optimal frontier, where any point which lies within the attainable set is entirely sub-optimal. As the Pareto optimal solution sweeps across the frontier it is clear that a reduction in $f_2(\omega)$ leads to a the subsequent increase of $f_1(\omega)$.

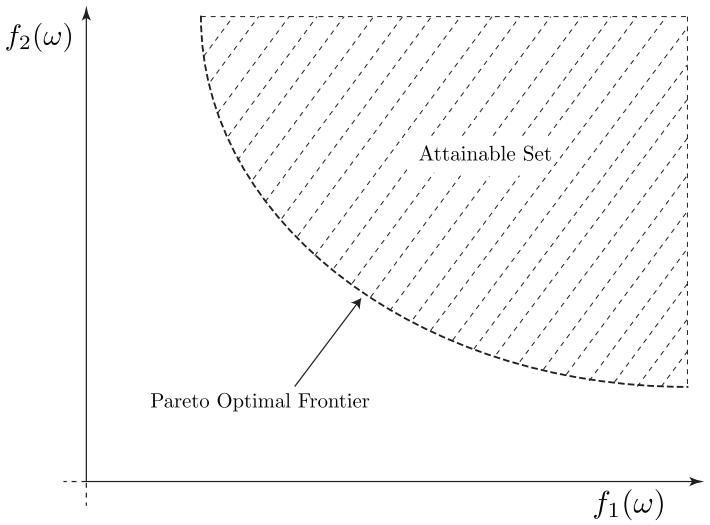

Figure 4.2: Pareto optimal frontier for two objectives[32].

4.4 Weighted Control Allocation for Two Objectives

The Simple Weighting control allocation scheme may be expressed as follows,

$$\min_{u\in\Omega} F(u) = \sum_{l=1}^{j} \varrho_l f_l(u) \tag{4.4.1}$$

As higher dimensions tend to be harder to visualise, assume a two objective optimisation of form,

$$\min_{u\in\Omega} F = \{f_1(u), f_2(u)\} \tag{4.4.2}$$

$$\text{where } \Omega = \left\{ \begin{array}{c} \underline{u} \leq u_i \leq \overline{u} \\ u(t-T) - T\dot{\mathbf{u}} \leq u_i \leq u(t-T) + T\dot{\mathbf{u}} \\ Bu = v \end{array} \right\} \tag{4.4.3}$$

Where $f_1(u)$ and $f_2(u)$ relates to any two objective function outlined in chapter 3. Ω defines a the set of constraints which must be met; encompassing the linear control allocation formulation $v = Bu$, the control subset Ξ and the dynamic constraint, $u(t-T) - T\dot{\mathbf{u}} \leq u_i \leq u(t-T) + T\dot{\mathbf{u}}$ which reduces the set to the maximum attainable subset which can be achieved within one time step. Where $\dot{\mathbf{u}} \in \mathbb{R}^m$ is a design parameter which depicts the maximum rate of the effectors. see figure 4.3.

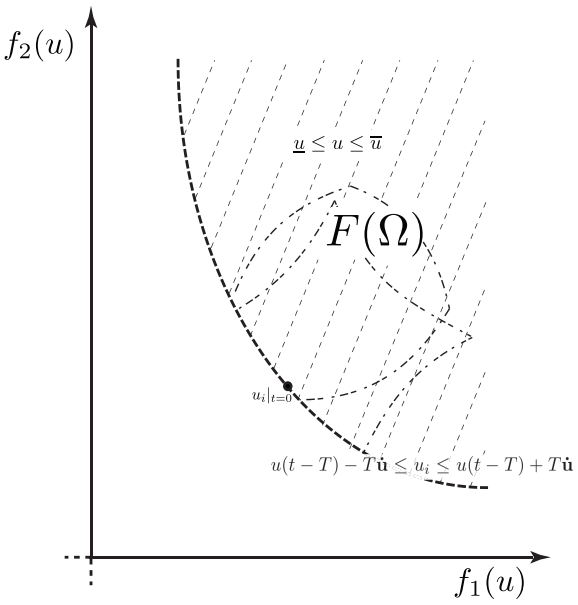

Figure 4.3: Set reduction

It is clear that if the problem is over constrained or Ω falls outside of the attainable set, it will result in an empty solution space. Care must be taken to ensure that Ω lies within the attainable set otherwise it will result in a diminished solution. This may be achieved by augmenting the weights in the single objectives as seen in section 3.4.4. Thereby shifting attainable set so that it lies within Ω

Equation 4.4.2 can be reformulated to the single objective function of form,

$$\min_{u \in \Omega} f(u) = \varrho_1 f_1(u) + \varrho_2 f_2(u) \tag{4.4.4}$$

$$\varrho_l \geq 0 \text{ for } l = 1, 2$$

where ϱ_l are weighting factors defined by the decision maker. Then by assuming that $\varrho > 0$ and dividing equation 4.4.4 by ϱ_1, will thus describe the following problem,

$$\min_{u \in \Omega} f(u, \varrho) = f_1(u) + \varrho f_2(u) \tag{4.4.5}$$

where,

$$\varrho = \frac{\varrho_2}{\varrho_1} \tag{4.4.6}$$

for any given ϱ the optimal solution to simple weighting problem defined by equation 4.4.2 is efficient.

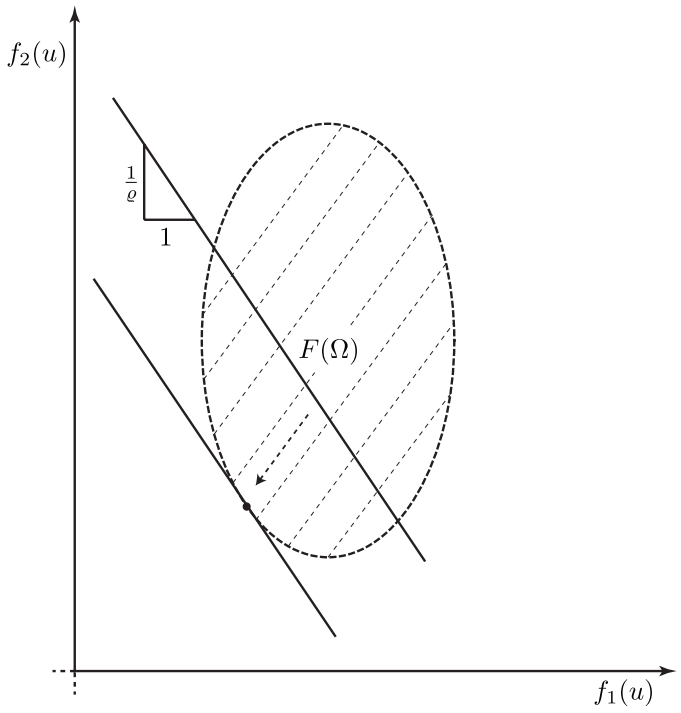

Figure 4.4: Simple weighted control allocation for two objectives

4.4.1 Understanding Simple weighting control allocation.

The contour of the equation 4.4.5 describes a linear indifference curve which intersect the objective space, $F(\Omega)$, at a slope of $\frac{1}{\varrho}$,

$$f_1 + \varrho f_2 = C \tag{4.4.7}$$

$$\Rightarrow \quad f_2 = -\frac{1}{\varrho} f_1 + \frac{C}{\varrho} \tag{4.4.8}$$

Where C is a constant. The solution to equation 4.4.4 shall draw the contour towards the minimum boundary until it lies tangent to the feasible objective space at a gradient of $\frac{1}{\varrho}$ – there shall lie the best compromise solution to the simple weighting control allocation problem defined in 4.4.2, see figure 4.4.1. As the decision maker varies ϱ the contour shall essentially rotate along the objective space's boundary or the pareto optimal frontier[3].

Figure 4.4.1 describes two variations, ϱ^1 and ϱ^2. ϱ^1 is defined such that $\infty > \varrho^1 > \varrho$, this will in-turn add a greater preference to f_2 and thus the solution will shift down the pareto optimal frontier - reducing f_2. conversely

[3]It is prominent to note that varying weights consistently will not generate an even distribution of pareto optimal solutions [50]

a reduction in ϱ to ϱ^2 such that $\varrho > \varrho^2 > 0$ will add a greater preference to f_1 and hence will cause the contour to shift upwards - reducing f_1.

Furthermore if the decision maker does not wish to consider f_1, then ϱ may be set such that $\varrho = \infty$ and hence f_2 shall only be minimised. Per contra if f_2 is to be no longer considered then ϱ is set so that $\varrho = 0$ and thus f_1 shall only be minimised, see figure 4.4.1

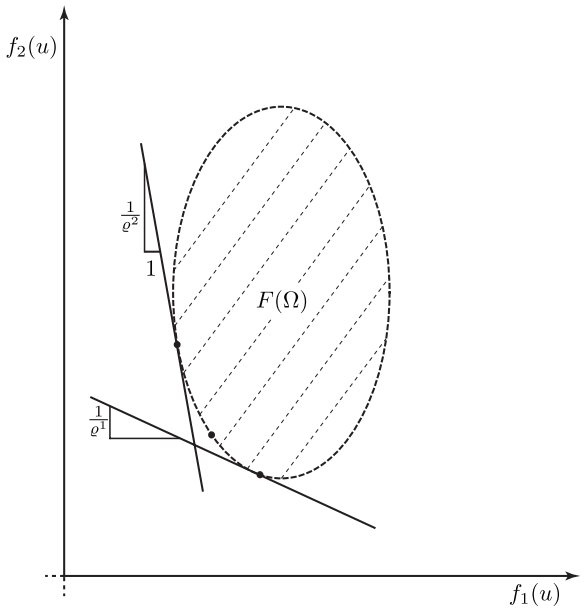

Figure 4.5: Varying the weightings ϱ^1 and ϱ^2 such that $\varrho > \varrho^2 > 0$ or $\infty > \varrho^1 > \varrho$ will cause the contour to shift up and down the frontier respectively

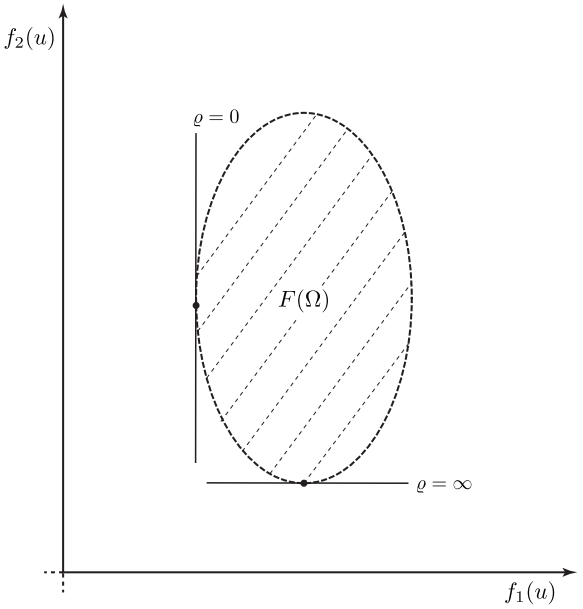

Figure 4.6: Objectives can be eliminated from the optimisation by setting $\varrho = \infty$ and $\varrho = 0$ accordingly

4.5 Minimax Control Allocation for two Objectives

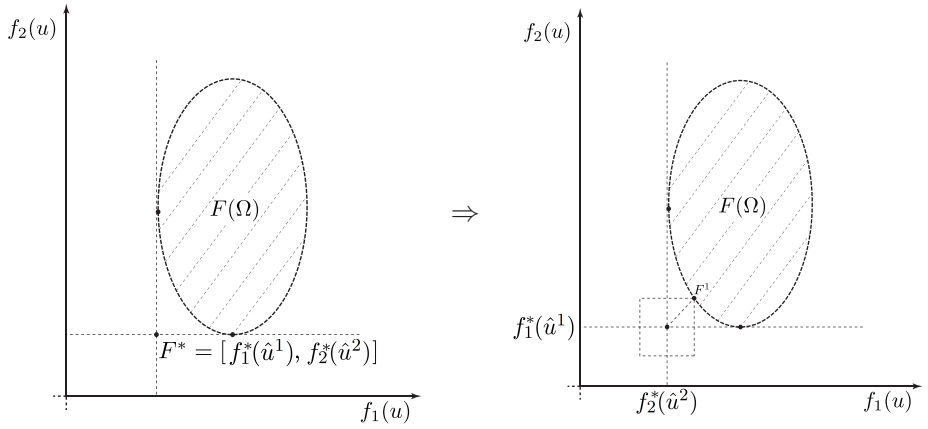

Figure 4.7: Minimax Ideal Point to Pareto-Optimal Solution

The Minimax control allocation scheme derived from the p-norm (See Appendix A) defines a ideal point to which the solutions are to tend to. The ideal point lies outside of the feasible objective space[4] and is determined by the optimal solutions of each single objective. The Minimax problem can be summarised with the follow pragmatic statement; given a set of weights determine the solution such that the ideal point and the feasible solutions are minimised - or in other words minimise the Euclidean distance between them. The multi-objective control allocation scheme maybe set up as an augmented Minimax problem, of the form seen in equation 4.2.1.
where $f_1(u), \ldots, f_j(u)$ relates to the objectives outlined in Chapter 3, v is the total demand and u is the true control input vector.

Definition: *A point F^* is said to be ideal if for each $i = \{1, 2, \ldots, j\}$, $F_i^* = \min_u\{F_i(u)|u \in \Omega\}$* [32]

Minimax Control Allocation Formulation

The minimax control allocation scheme may be formulated as follows;

Successively solve each objective $f(u)$ as a single objective optimisation problem and apply their respective weightings, W (as defined above) to the actuator suite. A number of single objective optimisations are applicable, for a full review see [32].

[4] if the contrary were true then the objectives would not be in conflict, and the problem would be trivial

$$\hat{u}^l = \begin{cases} \min\{f_l(u)\}, & \forall l \in \{1;2\} \\ u \in \Omega \end{cases} \tag{4.5.1}$$

where the optimal solution to the l^{th} objective function is $\hat{u}^l$, and the j^{th} objective $f_j(u)$ at $\hat{u}^l$ is denoted as:

$$f_j^{*l} = f_j(\hat{u}^l) \; ; \; \forall (j,l) \in \{1,2\} \times \{1,2\} \tag{4.5.2}$$

Then populate the classic pay-off table as such

	$f_1(u)$	$f_2(u)$	$\dots$	$f_j(u)$
$\hat{u}^1$	$f_1(\hat{u}^1)$	$f_2(\hat{u}^1)$	$\dots$	$f_j(\hat{u}^1)$
$\hat{u}^2$	$f_1(\hat{u}^2)$	$f_2(\hat{u}^2)$	$\dots$	$f_j(\hat{u}^2)$
$\vdots$	$\vdots$	$\vdots$	$\ddots$	$\vdots$
$\hat{u}^l$	$f_1(\hat{u}^l)$	$f_2(\hat{u}^l)$	$\dots$	$f_j(\hat{u}^l)$

$\Rightarrow$

	f_1	f_2
$\hat{u}^1$	$f_1(\hat{u}^1)$	$f_2(\hat{u}^1)$
$\hat{u}^2$	$f_1(\hat{u}^2)$	$f_2(\hat{u}^2)$

Define the ideal point in the feasible space $\underline{u} \leq u \leq \overline{u}$:

$$F^*(u) = \{f_1(\hat{u}^1), f_2(\hat{u}^2)\} \tag{4.5.3}$$

Then define the respective objective weightings,

$$\hat{w}_k, \; k \in \{1,2\} \tag{4.5.4}$$

such that

$$\hat{w}_k = \frac{w_k}{f_{\overline{k}} - f_k(\hat{u}^k)}, \; \forall k \in \{1,2\} \tag{4.5.5}$$

where w_k is the respective weighting given to the objective function $f_k(u)$ and $f_{\overline{k}}$ is the least optimal value (or worst solution) of $f_k(\hat{u}^l)$ denoted in the pay-off table. This is defined as:

$$f_{\overline{k}} = \max_{1 \leq l \leq 2} \{f_k(\hat{u}^l)\}; \; \forall k \in \{1,2\}; k \neq l \tag{4.5.6}$$

Formulate the multi-objective optimisation and solve for $u \in \Omega$ to find the pareto optimal solution, defined as:

$$\begin{cases} \min\{\lambda\} \\ \hat{w}_j(f_j(u) - f_j(\hat{u}^j)) \leq \lambda, \; j \in \{1;j\} \\ u \in \Omega \end{cases} \tag{4.5.7}$$

where λ is an auxiliary variable. In our case this is reformulated to:

$$\begin{cases} \min\{\lambda\} \\ \hat{w}_1(f_1(u) - f_1(\hat{u}^1) \leq \lambda, \\ \hat{w}_2(f_2(u) - f_2(\hat{u}^2) \leq \lambda, \\ u \in \Omega \end{cases} \tag{4.5.8}$$

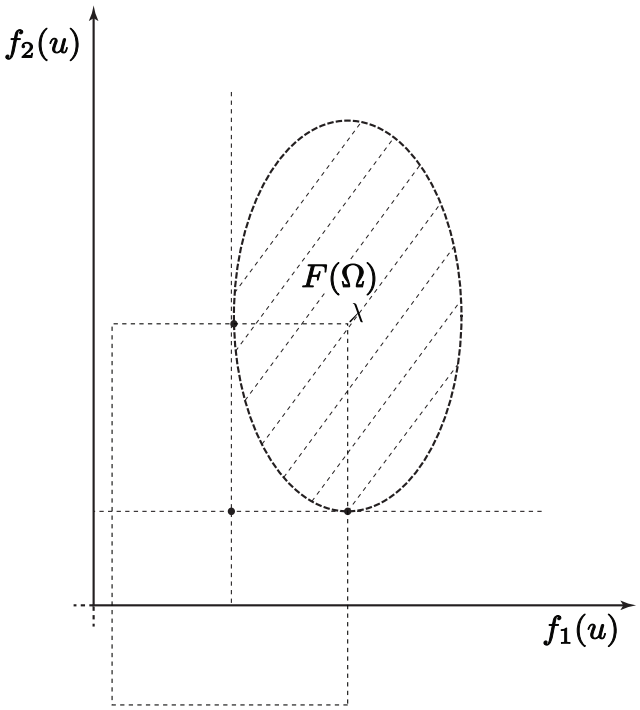

Figure 4.8: Minimax control allocation minimisation

4.5.1 Understanding Minimax control allocation

Figure 4.8 provides a geometric representation of minimax control allocation. λ defines a contour of hyper rectangles where the ideal point is at the center. Solving equation 4.5.8 minimises the contour until it just touches the Pareto optimal frontier at a vertex; denoted in the figure as $F^1 = \{f_1^1, f_2^2\}$. The line which passes through F^1 and F^* can be express as follows.

$$\hat{w}_1(f_1^1 - f_2^*) = \hat{w}_2(f_2^1 - f_2^*) \tag{4.5.9}$$

Minimax Example

Consider the following two objective linear optimisation Minimax example [32],

$$\begin{aligned} \text{Max} \quad & F = [f_1(u), f_2(u)] = [5u_1 - 2u_2, -u_1 + 4u_2] && (4.5.10) \\ \text{s.t} \quad & u \in \Omega && (4.5.11) \end{aligned}$$

where,

$$\Omega = \left\{ \begin{array}{c} -u_1 + u_2 \leq 3; u_1 + u_2 \leq 8 \\ u_1 \leq 6; u_2 \leq 4; u_1, u_2 \geq 0 \end{array} \right\} \tag{4.5.12}$$

By supposing that both objectives are of equal importance, the each single is optimised individually. Maximising the first objective in Ω yields $\hat{u}^1 = [6, 0]$ so that $f_1(\hat{u}^1) = 30$; then maximising the second objective subject to Ω gives $\hat{u}^2 = [1, 4]$ and $f_2(\hat{u}^2) = 15$. Then the minimax problem may be constructed as follows,

$$\begin{aligned} \text{Min} \quad & d_\infty && (4.5.13) \\ \text{s.t} \quad & 30 - 5u_1 + 2u_2 \leq d_\infty && (4.5.14) \\ & 15 + u_1 - 4u_2 \leq d_\infty && (4.5.15) \\ & u \in \Omega && (4.5.16) \end{aligned}$$

So the optimal solution may be given by,

$$\hat{u}^3 = [\hat{u}_1^3, \hat{u}_3^3] = [2.25, 2.75] \tag{4.5.17}$$

$$f_1(\hat{3}) = 20.75 \text{ and } f_1(\hat{3}) = 5.75 \tag{4.5.18}$$

which is the efficient solution of problem 4.5.10

4.6 Canonical Control Allocation

Contrary to the Minimax control allocation sheme which is based on the assumptions that the optimal compromise between the objectives is drawn to the ideal point F^*, the Canonical method allows the designer/decision maker to specify a preferred point to which the solutions are drawn to. This preferred point is a design parameter and can be based on a number of factors including trim, minimising induced drag or radar signature. The

formulation of the Goal attainable methods will provide a best compromise solution which is sensitive to the respective weights and preferred point.

Assuming the same multi-objective problem defined in equation 4.4.2, the single objective can be solved and the classic pay off table can be populated in the same manner as the Minimax formulation. Now suppose then that the decision maker provides a preferred solution u^g, and noted that

$$F^d = \{f_1^g, f_2^g, \ldots, f_j^g\} \tag{4.6.1}$$

where

$$f_j^d = f_j(u_g) \forall k \text{ objectives } j \in \{1;2\} \tag{4.6.2}$$

The following canonical weights can be defined for each of the objectives

$$w_j^t = \frac{1}{f_j^d - f_j^*}; \text{ where } j \in \{1;2\} \tag{4.6.3}$$

and where f_j^* are the respective components of the ideal point $F^* = \{f_1^*, f_2^*, \ldots, f_k^*\}$ for each objective. So the optimal compromise solution closest to the preferred goal at the following calculation step (u^{t+1}), for the multi objective problem defined in equation 4.4.2 is the given by the following minimax problem formulation using the above defined canonical weights,

$$u_g^{t+1} = \begin{cases} \min d\infty \\ w_j^t(f_j(u) - f_j^*) \leq d\infty \ , \ j \in \{1;2\} \\ u \in \Omega \end{cases} \tag{4.6.4}$$

where d_∞ represents the ∞-norm of the ideal point F^*.

As all the objective constraints for the solution, (u_g^{t+1}) are binding, the point $F(u_g^{t+1}) = \{f_1(u_g^{t+1}) \ldots f_k(u_g^{t+1})\}$ must lie on the line which passes through the two points F_* and F^d, defined in the objective space by,

$$w_1^t(f_1(u) - f_1^*) = w_j^t(f_j(u) - f_j^*) = w_1^k(f_k(u) - f_k^*) \tag{4.6.5}$$

4.7 Classical Goal Attainable

Alternatively in a more classical approach the goal attainable problem can be related to the minimax problem resulting in a simpler formulations of the multi-objective minimisation problem. This reduced formulation requires the decision maker to provide not only a desired goal solution u^g but also a set of weights $w = \{w_1, w_2 \ldots w_k\}$ corresponding to the k different objectives.

Assuming the multi-objective control allocation problem defined in equation 4.4.2 the single objectives can be solved and the pay-off table populated in the same manner as the minimax and classical control allocation methods.

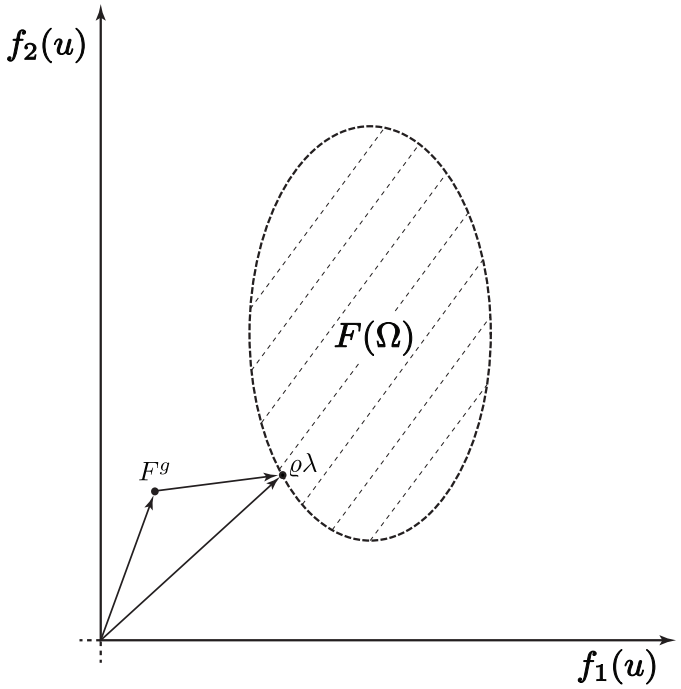

Figure 4.9: Goal Attainable methods

The goal attainment problem can then be reformulated without the use of canonical weights, as follows

$$u_g^{t+1} = \begin{cases} \min \lambda \\ f_j(u) - w_j \lambda_j^d \ \forall j \in \{1:k\} \\ u \in \Omega \end{cases} \tag{4.7.1}$$

where λ is an auxiliary variable unrestricted in sign, and where the set of weights w is normalised such that

$$\sum_{j=1}^{k} w_j = 1 \tag{4.7.2}$$

If an objective expected to be under-attained against the desired value a smaller weight is assigned to it. If it is required to be over-attained a larger weight should be assigned to it.

Understanding Goal Attainable methods

Figure 4.7 provides a graphical representation of the Goal attainable control allocation methods. It is noted that the direction of the preferred solution is determined by F^g and $\varrho \in \mathbb{N}$. λ is its minima when $F^g + \varrho\lambda$ intersects the pareto optimal frontier.

4.8 Discussion and Conclusions

Let us draw this chapter to a close with some brief conclusions. Four ***novel*** formulations for multi-objective control allocation have been proposed. In general the proposed methods outline a two objective case yet it is clear that all can be extended to accommodate for further objectives. Each method attempts to find the best compromise solution which lies on the Pareto optimal frontier. The Simple weightings method allows the decision maker to sweep across the Pareto frontier by utilising weightings; diminishing or exaggerating certain objective. It can further allow for objectives to be 'turned on' or 'off'. The minimax method attains to the ideal point at all times F^*. The minimax methods projects a contour of hyper rectangles where the ideal point is at the center. The problem goes about minimising the hyper rectangle until one vertex just touches the Pareto optmial frontier. This thereby finds the best compromise solution which is closest to the Ideal point.

Minimax can be extend to the Goal Attainable where canonical weights are used to represent the decision maker's preferences. thereby instead of attaining to the ideal point, the solution is draw to a user defined point u_g. This point is essentially similar to the term u_d, although it has the added benefit that it shall not be corrupted by other objectives in the minimisation.

The preference of a particular scheme as opposed to another lies on the requirements of the system, the heterogeneity of its effector suite and the preference if the user/ decision maker. These encompass the need for a preferred operating point to which solution is to be drawn to, such as, trim, endurance, drag performance or minimal radar signature. Furthermore the user's ability to prioritise certain objectives over others or alternatively leave it to the algorithms to determine the optimal compromise between the objectives within the feasible space. The respective strengths of the four featured algorithms and the way to determine which method best suits a specific application is summarised in table 4.1

Desired Allocation Solution	Preferred Goal Point to attain towards	No preferred operating point for the actuator suite
User defined objective weightings	Classical weights Goal Attainable	Simple Weighted Method
Ideal compromise between objectives	Canonical weights Goal Attainable	Minmax Formulation

Table 4.1: Control allocation algorithm selection table.

Another attribute the designer may take into consideration is the compu-

tational time. This of course depends on a number of factors, including the specifications of the embedded system, the programming language and the number of objectives used. The nature of the formulations in this instance can shed some light on the computational load. By far the simplest solution is the Simple Weighting method and hence it is quite clear that it shall have the least computational load. The Minimax on the other hand shall consume the most computational time due to the fact that it needs to compute the ideal point. This is closely followed by the goal attainable formulation as it has a given preferred point u_g thereby forgoing the computation of the ideal point.

CHAPTER 5

Simulation of Results

5.1 Introduction

IN the proceeding chapter we have established four ***novel*** methods for multi-objective control allocation. In the following chapter the methods shall be applied to the high veracity Demon 6Dof simulation and subjected to a set of commanded manoeuvres.

The case simulations are set so that they mimic standard operation of the vehicle with in its flight envelope. The simulations shall validate the control allocation algorithms by determining whether the effector distribution adheres to perfect allocation while at no point violating the constraints it is subjected to.

Each simulation shall exhibit properties which is to be consistent with the theory described in Chapter 4. That is to say that the Simple weighting method should provide a solution based on the respective weightings provided. The Minimax should adhere to the ideal point, while it is expected that the goal attainable method will display a somewhat 'held back' response, due to the user defined goal point.

An investigation in computational load is also conducted. Yet since computation time is subject to a number of factors, such as processing speed, system complexity, programming language and optimisation of the code its self. The investigation compares the number of iterations required to determine a Pareto optimal solution in an effort to maintain comparability for future research.

The simulations ought to provide a further insight into the use of heterogeneous controls with multi-objective control allocation. Giving a clearer understanding of which devices would be use under certain circumstances and the effect of the different multi-objective control allocation schemes upon the effector distribution.

Section 5.2 shall provide a brief description of the high veracity simulation model. Sections 5.5, 5.6, 5.7 and 5.8 present the Weighted, Minimax, Canonical and Classical control allocation respectively. Some conclusions are drawn in section 5.10.

5.2 Demon Model

The high veracity non-linear Demon Model was based on the Demon UAV aptly describe in section 2.7. The Model encompasses all the standard equation of motion as presented in chapter 2 and those encoded into Matlab/Simulink, subsuming the wind tunnel data and some critical data acquired from the two flight campaigns. The Demon UAV currently has three control law at its disposal, Linear Parameter Varying (LPV), $H\infty$ and Stability Augmentation System (SAS). The simulation variant which has been used through the entirety of this work is an attitude hold SAS control law.

5.3 Objectives

As previously stated, the majority of the literature tends to provide an *ad hoc* solution to the control allocation problem, and hence along with it a set of purpose built objectives, examples of this can be seen in [54].

In an effort to maintain a generalised approach to the problem and further to promote comparability between the cases, the following objectives shall be use for the simulations.

The variants themselves have been thoroughly study in the literature and a number of solution have been proposed (single objective optimisation). Each objectives has an analytical solution which thereby will reduce the computation load on the algorithm, partially when attempting to find the ideal point and populating the pay-off table.

As seen in section 5.3.1 these objectives are in conflict with each other and hence they do not have a unique minima. Noting that if the opposite where true the problem would be trivial.

Furthermore each objective defines a unique attribute which is beneficial in most applications, in that the "Minimum Travel" objective tends to, in a manner of speaking reduce energy within the system, while the "Total Defection" adds a specific design parameter which holds the solutions back to their neutral position.

Total Deflection

$$f_1(p) = \min W_p||u - u_d||_2 \tag{5.3.1}$$

Objective function (5.3.1) minimises the *total* displacement of the control effector. u_d is a design parameter to which the solution is drawn to if it falls out of the objective space. u_d can be set to minimum drag, trim conditions or a minimum radar signature,. W_u is a positive diagonal weighting matrix, through which a particular effector can be prioritised or diminished to the preference of the application.

Minimum Travel

$$f_2(u) = \min W_r||u(t) - u(t-T)||_2 \tag{5.3.2}$$

Objective function (5.3.2) minimises the total travel per step, where T is the sample time and $u(t-T)$ is the position of the actuator at the last time step. W_r is a positive diagonal weighting matrix, similar to W_u

5.3.1 Projection of the objectives in $F(u)$

Due to the quadratic form of the objective functions, $f_1(u)$ and $f_2(u)$ when represented in the objective space, denote a convex set. Figure 5.1 shows the Pareto optimal frontier for a given v and B.

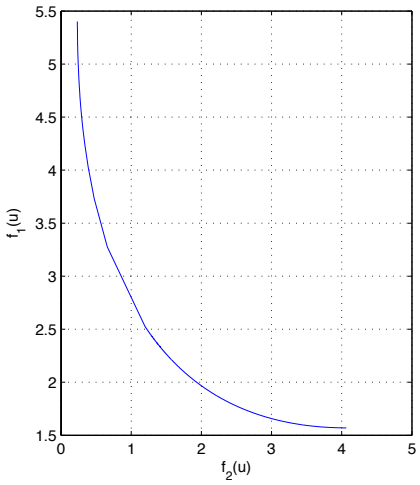

Figure 5.1: Pareto frontier for objective functions 5.3.1 and 5.3.2. The projection was obtained by use of the weighted control allocation method, i.e. the values of v and B were held and solutions were sought for a set of ϱ

5.4 Case Simulations

The following simulations where all initialised at a cursing speed $50m/s$, $200m$ above sea level and set to run for 40 seconds. At $t = 10$ the vehicle attempts to perform a pitch up manoeuvre, such that $r_\theta = 25$ and at $t = 20$ the aircraft performs a roll manoeuvre such that $r_\phi = -30$. Figure 5.4 shows the projected trajectory. The following simulations illustrate as simple manoeuvre to which does not place the aircraft out side of its flight envelope.

This shall provide consistency when comparing the different methods and shall not introduce any disparities with regards to behavioural dynamics and there hence shall not contaminate the comparison. A successful allocation will result in u directly mapping on to v. In all the following simulations, the mapping can be seen in figures 5.6, 5.10, 5.14 and 5.17, such that if the

trend Bu directly resembles v then the allocation is considered perfect. If there was an instance that $v \neq Bu$ then it would be likely due to a number of constraints being violated or the solution falling outside of the attainable moment set.

Assuming perfect allocation, the resulting states for all simulations should produce similar dynamics. Minor dissimilarities in the dynamics may become apparent, due to lags in computational time and or the use of slower effectors causing delayed dynamics. The states can be seen in figures 5.5, 5.9,5.13 and 5.16.

As previously mentioned the Demon UAV utilises a number of effectors (including non conventional devices) to achieve the demands. All the effectors can operate on both longitudinal and lateral axis apart from $\eta_F TV$ which can only operate along the longitudinal axis and ζ which can only operate along the lateral. Furthermore by design the vehicle has extended elevator surfaces, as seen in figure 2.5, hence it is prominent to note that deflection along the longitudinal axis tend to be quite small. The Demon model was linearised using Taylor series expansion, see appendix A.1 at trim conditions for a set velocities, such that $30 \leq V \leq 60$, where any velocity below $30m/s$ is assumed to stall speed.

Figures 5.4, 5.8, 5.12 and 5.15 shows the effector suite deployment over the extent of the simulation. The figures denotes the dynamic constraints evolution with respect to the effector distribution. When considering the results, it is perhaps more important to note the trend of the effector deployment as opposed to the absolute values to which the effectors adheres to. Note should be taken on the nature of peaks produced by the effector trend, where a dramatic peak indicate the use of f_1, and prolonged, extended peaks denotes that the comprise solution lies closer to f_2. Furthermore a diminished response indicates that the solution is attempting to adhere to the given goal point u_g.

The methods where applied to the case simulations and were run accordingly. Each multi-objective solution was subjected to a stopping function – a function that determines the accuracy of the solution and terminates the iterations once the solutions are deemed precise enough. In this instance the tolerance for termination of the solution u was set to 1×10^{-3}. This tolerance is far greater than the accuracy required to operate the Demon's effector suite.

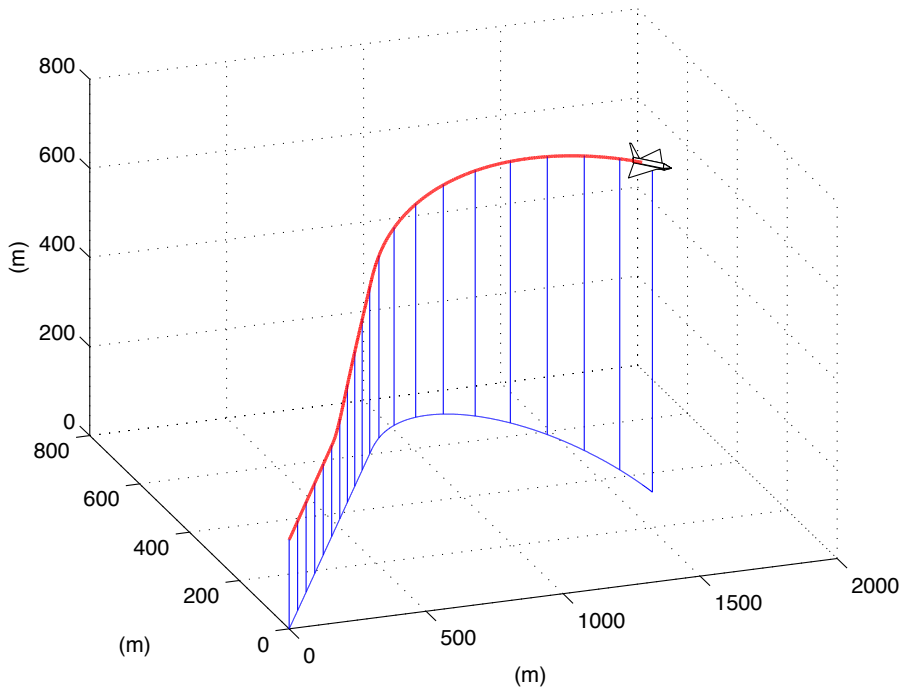

Figure 5.2: Trajectory

5.5 Simulation of Weighted Method

The Weighted Control allocator was applied to the Demon Model as depicted in figure 5.3 and initialised as stated in section 5.4. u_d has been set to 0 hence $f_1(u)$ is to draw the solutions to their neutral position and the respective weightings for each objective function, where set to the values of $\varrho_1 = 1$ and $\varrho_2 = \frac{1}{2}$, such that, with reference to equation 4.4.4 the weighted control allocator takes the form,

$$\min_{u\in\Omega} f(u) = \varrho_1 f_p(u) + \varrho_2 f_r(u) \tag{5.5.1}$$

where

$$\Omega = \left\{ \begin{array}{c} \underline{u} \leq u_i \leq \overline{u} \\ u(t-T) - T\dot{u} \leq u_i \leq u(t-T) + T\dot{u} \\ Bu_i = v \end{array} \right\} \tag{5.5.2}$$

and

$$W_p = \begin{bmatrix} \frac{1}{\overline{u}_1} & 0 & 0 & 0 \\ 0 & \frac{1}{\overline{u}_2} & 0 & 0 \\ 0 & 0 & \ddots & 0 \\ 0 & 0 & 0 & \frac{1}{\overline{u}_i} \end{bmatrix} \quad W_r = \begin{bmatrix} \frac{1}{\overline{u}_1} & 0 & 0 & 0 \\ 0 & \frac{1}{\overline{u}_2} & 0 & 0 \\ 0 & 0 & \ddots & 0 \\ 0 & 0 & 0 & \frac{1}{\overline{u}_i} \end{bmatrix} \tag{5.5.3}$$

The results can be seen in figures 5.4, 5.5 and 5.6. The figures depict the response of the control suite, states and mapping from v to Bu respectively. The red dashed line represents the dynamic constraints outlined in section 4.4,

$$u(t-T) - T\dot{u} \leq u_i \leq u(t-T) + T\dot{u} \tag{5.5.4}$$

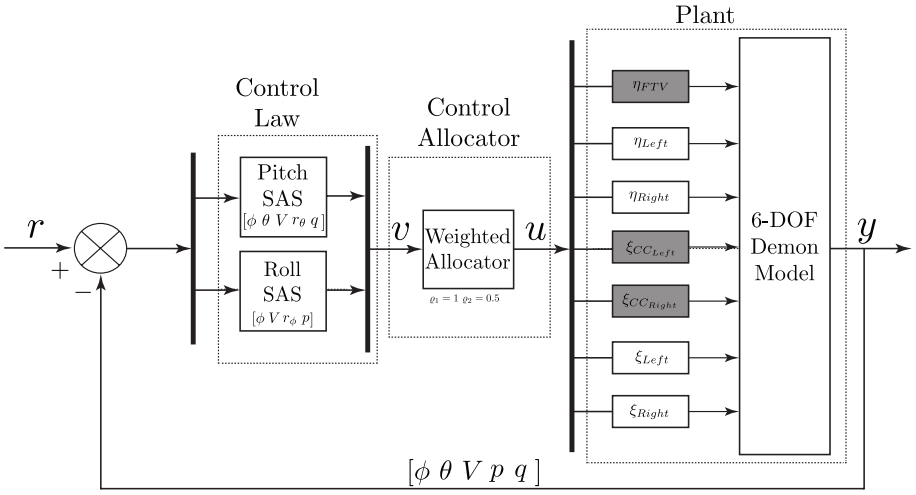

Figure 5.3: Weighted control allocation applied to the Demon 6DOF model.

5.5.1 Brief Discussion

Note that at $t = 10$ the control allocator employs all the conventional surfaces to meet the demand, designating the fluidic devices as redundant. In this instance you can see that η_{Left} and η_{Right} symmetrically deflect to 5° along with ξ_{Left} and ξ_{Right}. The FTV maintains the trim setting. At $t = 20$ the allocator utilises all its surfaces to meet the high moment demand. Figure 5.5 indicates that r_ϕ is met within 1 second. Furthermore it is clear from figure 5.6 that $v = Bu$ throughout the entirety of the simulation, indicating perfect allocation.

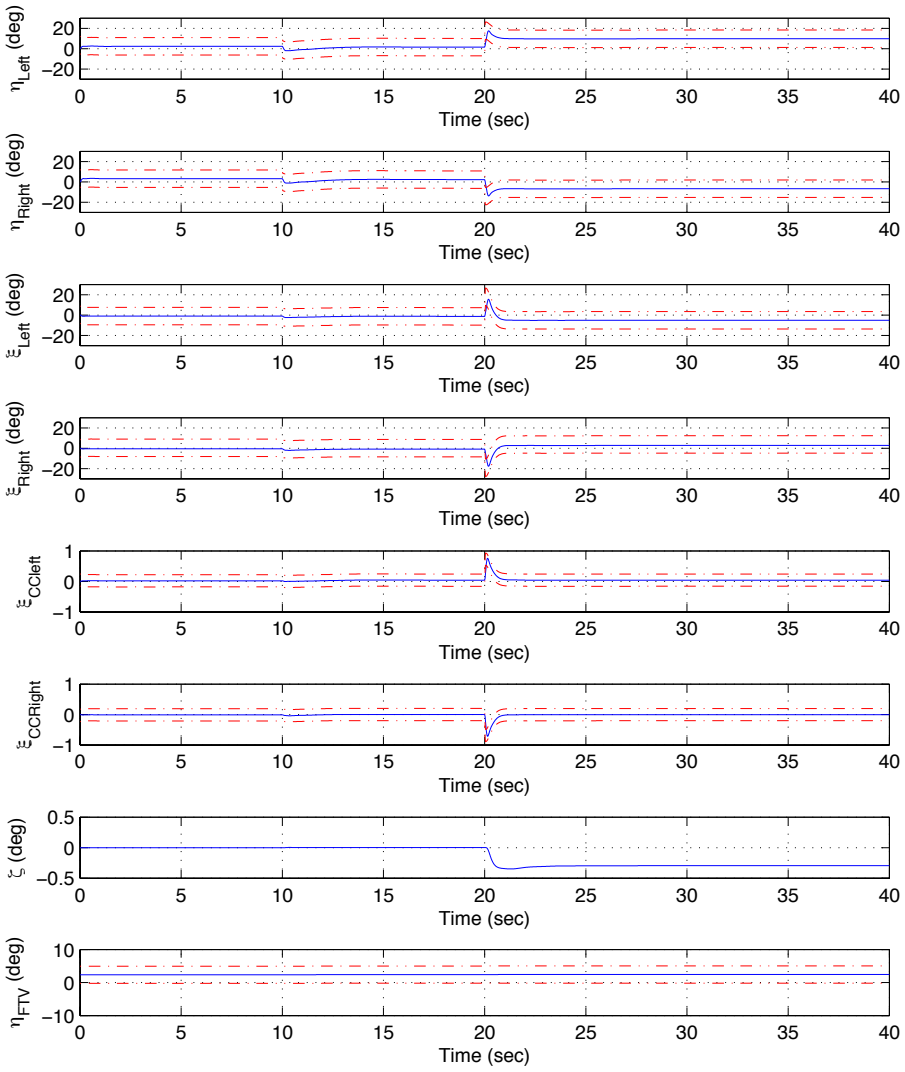

Figure 5.4: Effector Deflections for Weighted Control Allocation

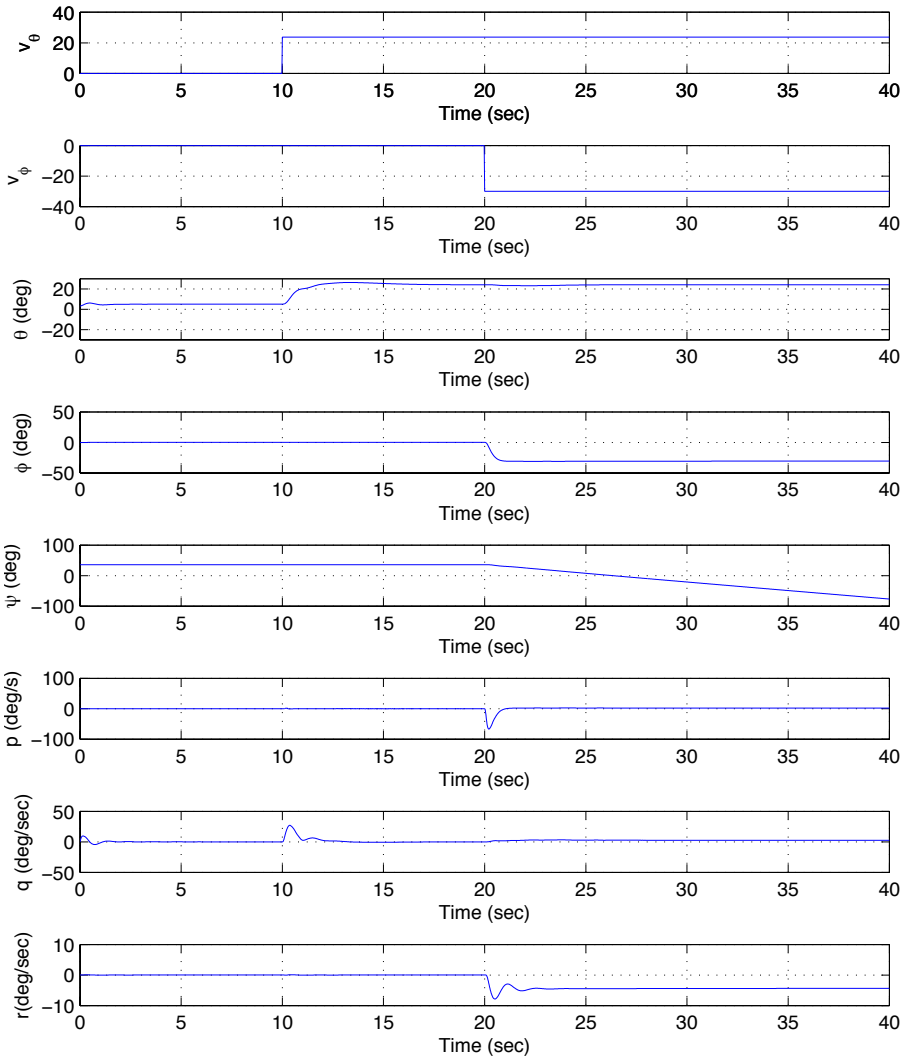

Figure 5.5: States for Weighted Control Allocation

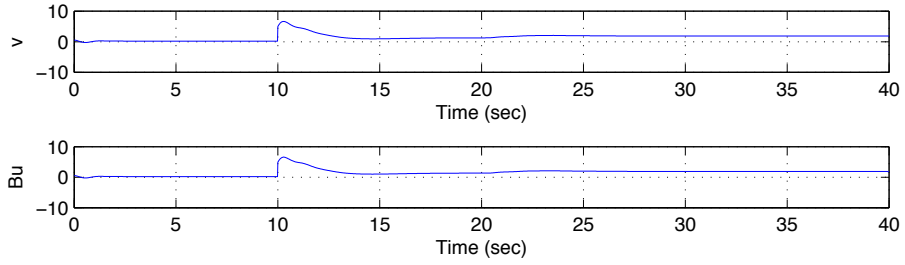

Figure 5.6: v,Bu for Weighted Control Allocation

5.6 Simulation of Minimax Method

The Minimax Control allocator was applied to the Demon Model as depicted in figure 5.7 and initialised as stated in section 5.4. u_d has been set to 0. With reference to equation 4.5.1, the Minimax control allocator takes the form,

$$\min_{uin\Omega} F(u) = \{f_p(u),\ f_r(u)\} \tag{5.6.1}$$

where Ω is denoted in equation 5.5.2 and the weightings W_p and W_r are set as in equation 5.5.3. The single objectives are solved analytically as outlined in sections 3.4.4 and 3.4.6, such that the optimal solution for each objective becomes,

$$f_r(\hat{u}^1) = W_p B^T (B W_p B^T)^{-1} v = f_p^{*1} \tag{5.6.2}$$

$$f_p(\hat{u}^1) = [I - W_r B^T (B W_r B^T)^{-1} B] u_{t-T} + W_r B^T (B W_r B^T)^{-1} v = f_r^{*2} \tag{5.6.3}$$

and hence the least optimal solution for each objective, pragmatically speaking, is the solution of the optimal value at the opposing objective, or,

$$f_p(f_r^{*2}) \text{ and } f_r(f_p^{*1}) \tag{5.6.4}$$

The results can be seen in figures 5.8, 5.9 and 5.10. The figures depict the response of the control suite, states and mapping from v to Bu respectively.

5.6.1 Brief Discussion

You will note that in a similar manner to weighted control allocation the minimax methods utilises all conventional surfaces to meet the longitudinal moment demand at $t = 10$. At $t = 20$, along with the conventional surfaces both CC devices ξ_{CCLeft} and $\xi_{CCRight}$ are utilised to meet the lateral moment demand while the FTV maintains the trim settings, see figure 5.8. The longitudinal, r_θ and Lateral r_ϕ attitudes are met within 3 and 1 seconds respectively as denoted in figure 5.9. Figure 5.10 denotes perfect allocation.

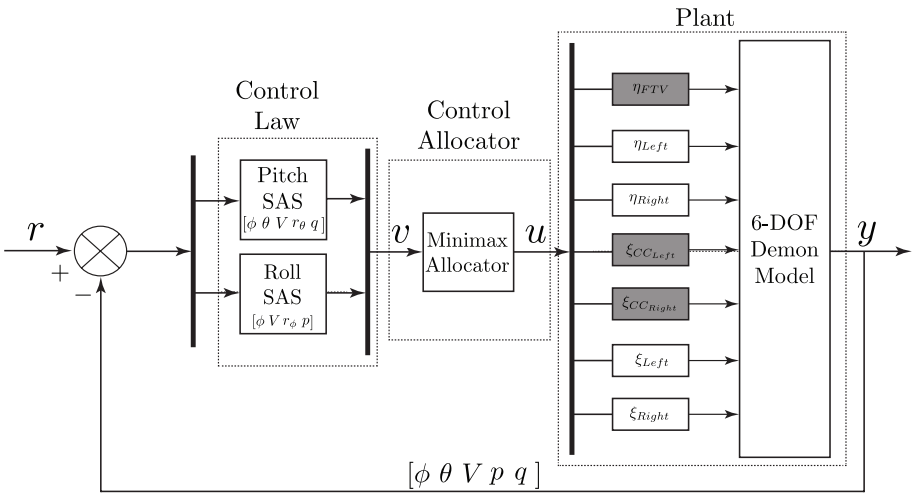

Figure 5.7: Minimax control allocation applied to the Demon 6DOF model.

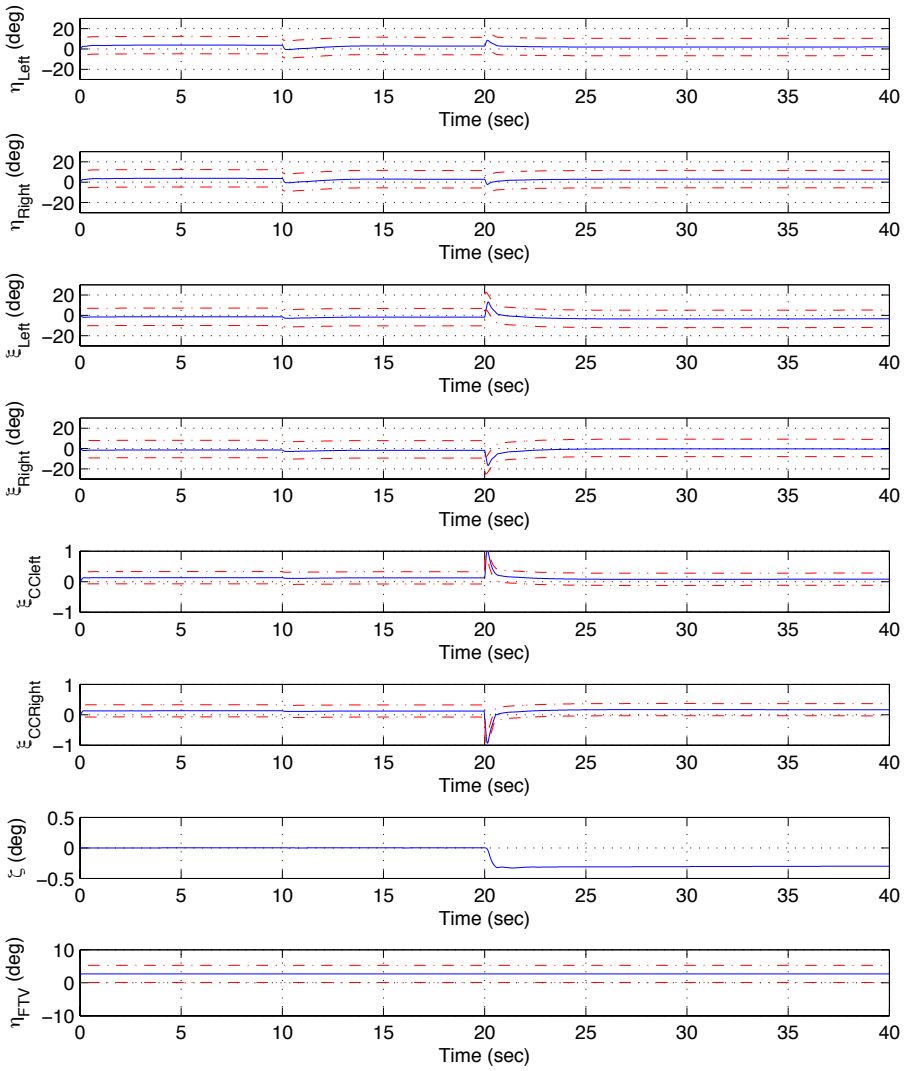

Figure 5.8: Effector Deflections for MiniMax Control Allocation

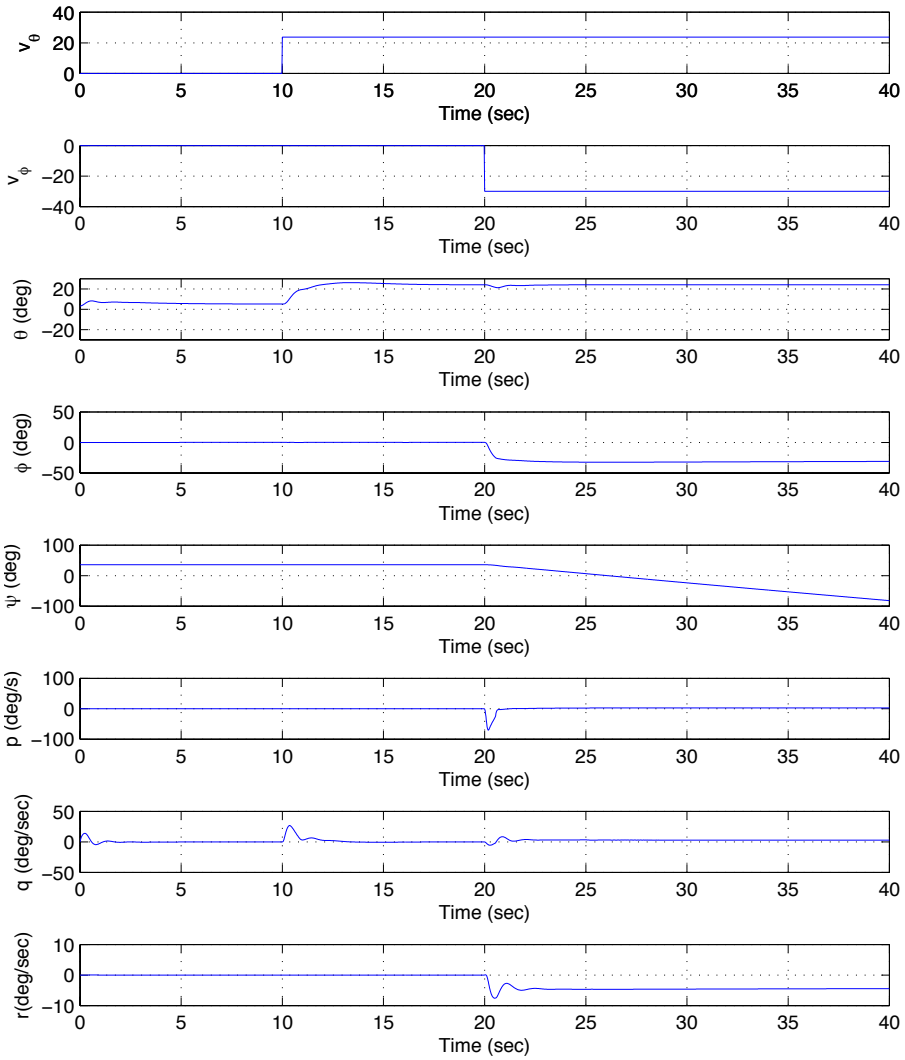

Figure 5.9: States for MiniMax Control Allocation

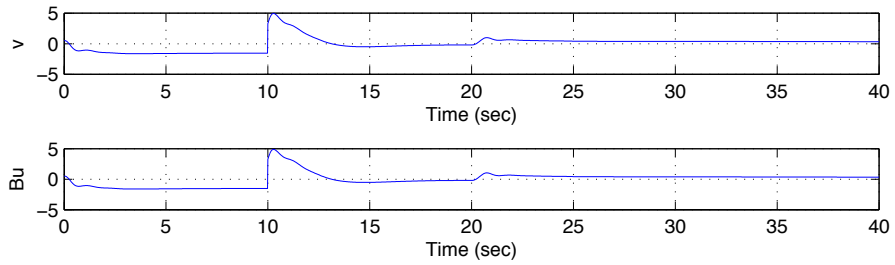

Figure 5.10: v,Bu for MiniMax Control Allocation

5.7 Simulation of Canonical Control Allocation

The Canonical Control allocator was applied to the Demon Model as depicted in figure 5.11 and initialised as stated in section 5.4. u_d has been set to 0. The single objective have been solved analytically in the same manner as the minimax control allocator (see section 5.6) and the pay-off table was constructed accordingly. u_g was set to attain to the trim positions. The results can be seen in figures 5.12, 5.13 and 5.14. The figures depict the response of the control suite, states and mapping from v to Bu respectively.

where

$$u_g = \begin{bmatrix} \eta_{Left} \\ \eta_{Right} \\ \xi_{Left} \\ \xi_{Right} \\ \xi_{CCLeft} \\ \xi_{CCRight} \\ \eta_{FTV} \end{bmatrix} = \begin{bmatrix} 2.695 \\ 2.695 \\ 0.485 \\ 0.485 \\ 0.00845 \\ 0.00845 \\ 1.348 \end{bmatrix} \tag{5.7.1}$$

5.7.1 Brief Discussion

In a similar manner to the Minimax and Weighted control allocation it is clear that the control allocator utilises all the conventional control surfaces for the longitudinal motion at $t = 10$ and utilises all the control devices with the exception of the FTV for the lateral manoeuvre at $t = 20$. Although in this instance there is an inherent difference in the trends in comparison to the preceding methods. With the addition of the term u_g you will note that as oppose to describing peaks the deflections are held back or 'draw' towards the trim settings.

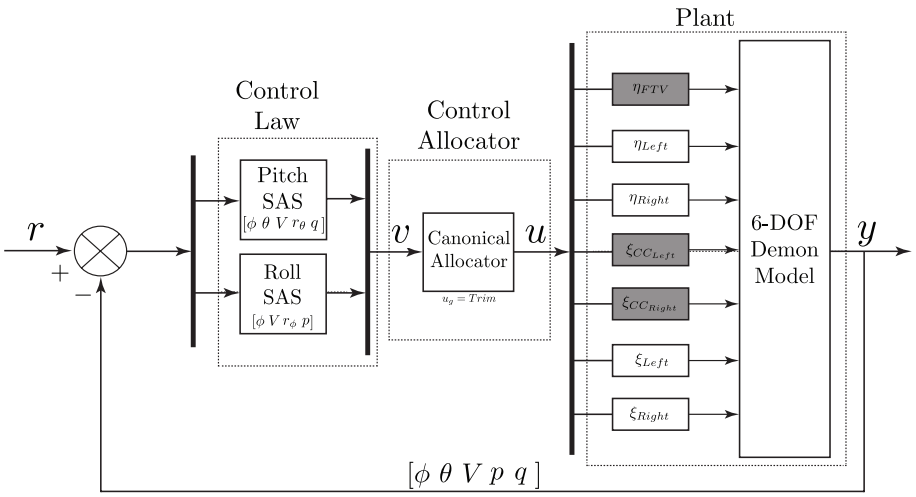

Figure 5.11: Canonical control allocation applied to the Demon 6DOF model.

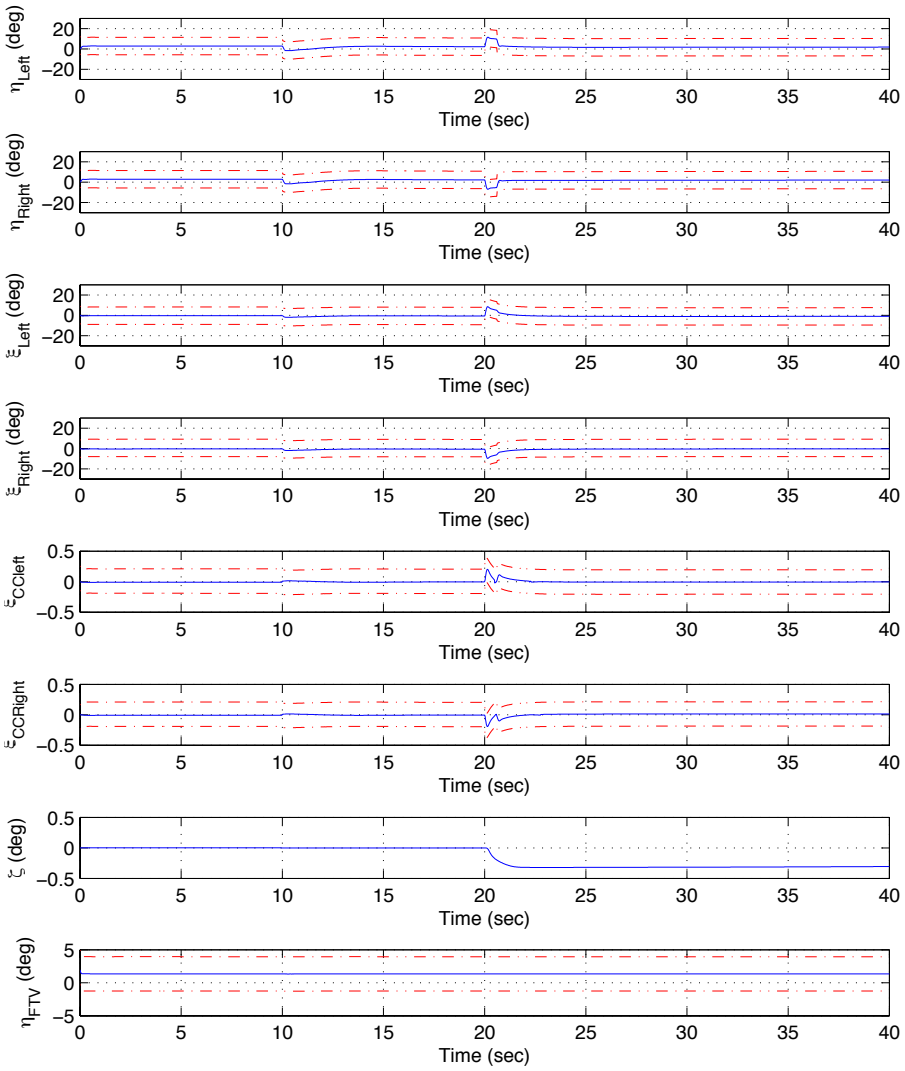

Figure 5.12: Effector Deflections for Canonical Control Allocation

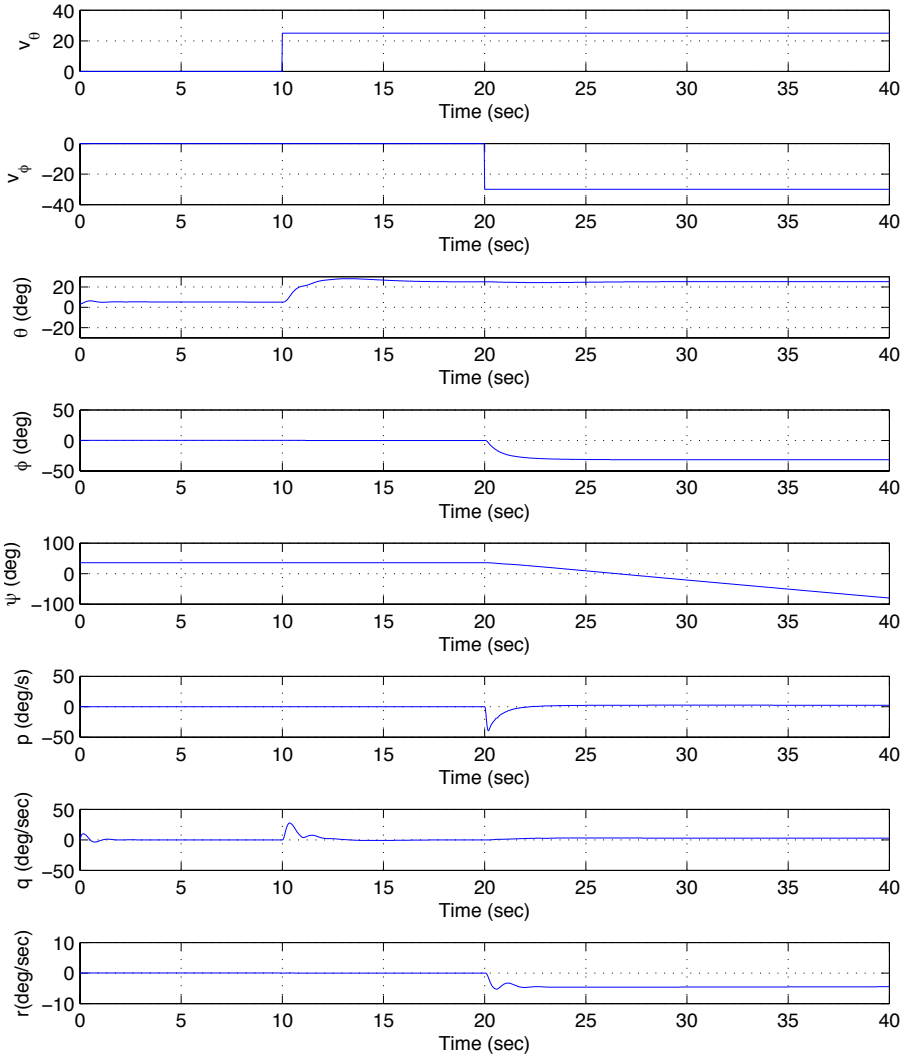

Figure 5.13: States for Canonical Control Allocation

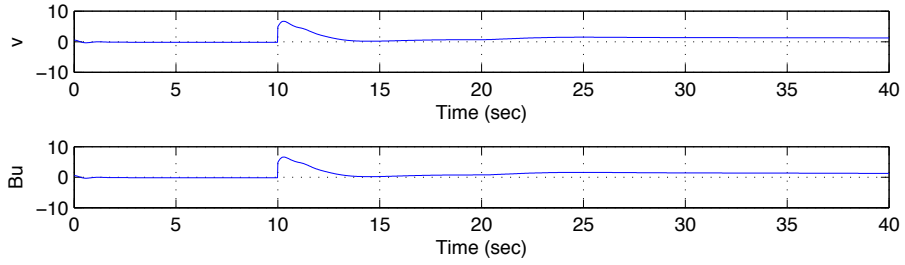

Figure 5.14: v,Bu for Canonical Control Allocation

5.8 Simulation of Classical Control Allocation

The Classical Control allocator was applied to the Demon Model in a similar manner to Canonical control allocation depicted in figure 5.11 and initialised as stated in section 5.4. u_d has been set to 0. The single objective have been solved analytically in the same manner as the minimax control allocator (see section 5.6) and the pay-off table was constructed accordingly. u_g was set to attain the trim positions. The respective weightings where set such that $w_p = 0.2$ and $w_r = 0.8$ The results can be seen in figures 5.15, 5.16 and 5.17. The figures depict the response of the control suite, states and mapping from v to Bu respectively.

5.8.1 Brief Discussion

The allocator describes the same trends as the previous methods, with an inherent difference, you will note that at $t = 10$ the distribution of the control effectors exhibit the same behaviour as the Canonical method, such that the solutions are drawn towards the trim positions, While at $t = 20$ the trend indicates peaks similar to the minimax method, see figure 5.15. The longitudinal, r_θ and Lateral r_ϕ attitudes are met within 3 and 1 seconds respectively as denoted in figure 5.16. Figure 5.17 denotes perfect allocation throughout the entirety on the simulation.

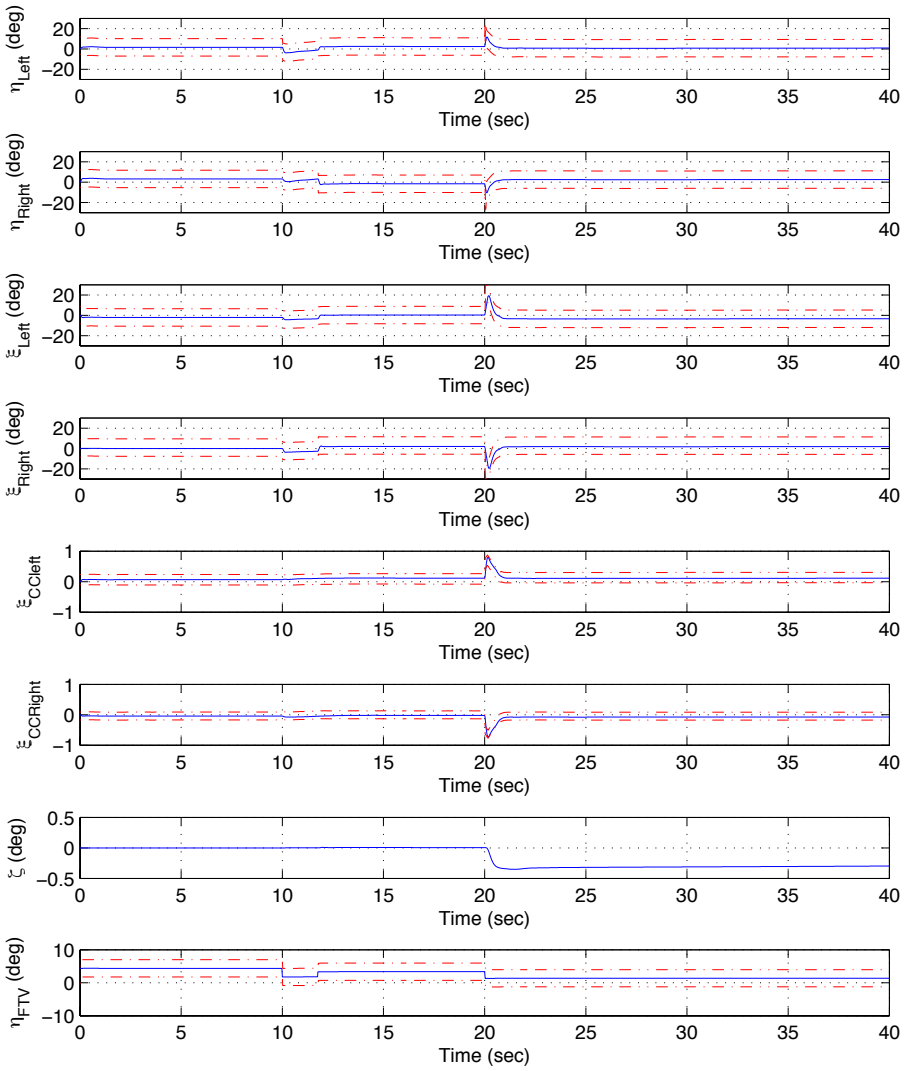

Figure 5.15: Effector Deflections for Classical Control Allocation

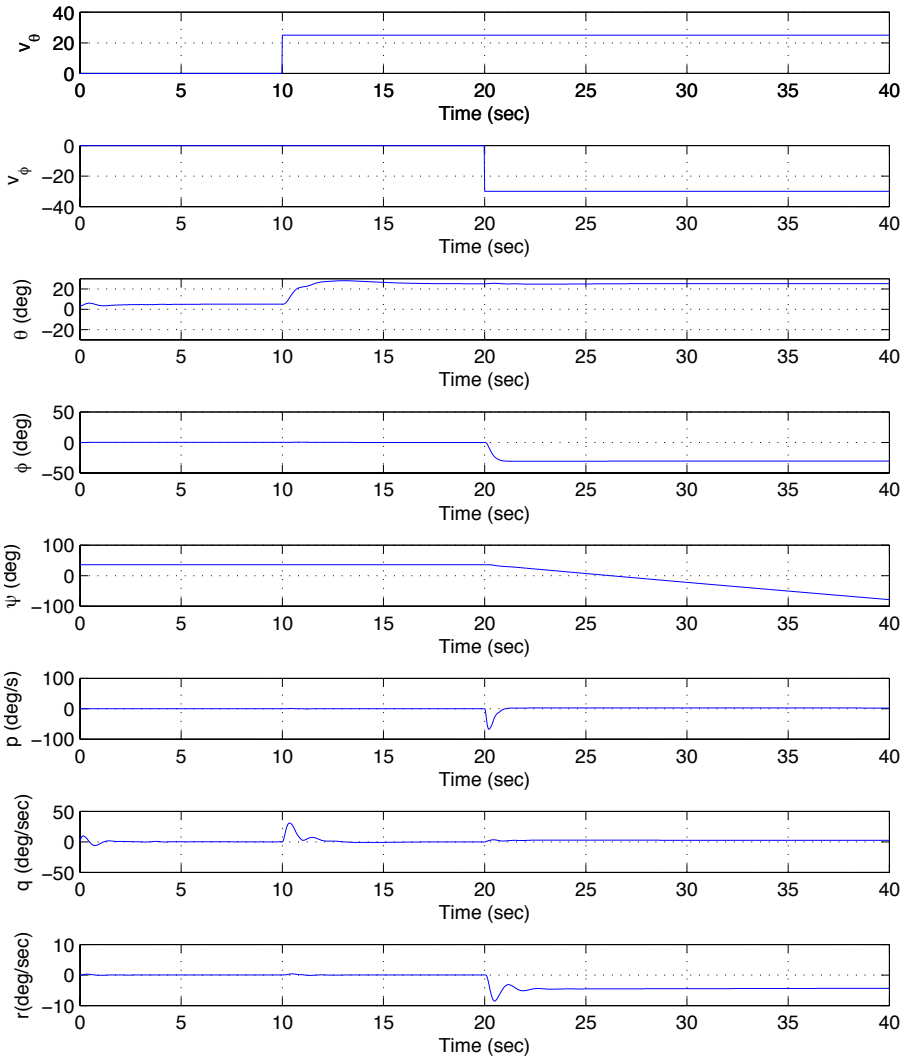

Figure 5.16: States for Classical Control Allocation

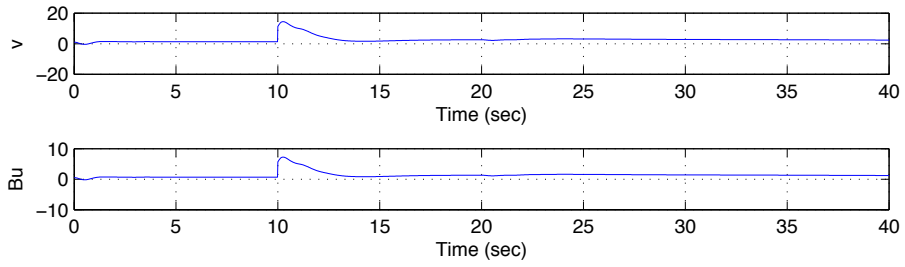

Figure 5.17: v,Bu for Classical Control Allocation

5.9 Evaluation of Methods

The methods where further subjected to vigorous simulation cases in order to determine their validity under extreme circumstances. So as not to contaminate the results, the allocators where initialised with the same parameters as depicted herein this chapter. Each formulation was run a total of 5 times, whereby the allocators where primarily subjected to decoupled Lateral and Longitudinal inputs at cruise speed, $V = 50m/s$ (the inputs can be seen in figure 5.18). Then subsequently the motions where coupled and run at speeds of $V = 50m/s$ (cruise speed), $V = 65m/3$ (maximum speed) and $V = 35m/s$ (minimum speed where stall is considered to be at $V = 32m/s$). This chose of inputs highlights a diverse cross coupling of lateral and longitudinal dynamics thereby subjecting the allocator to extreme conditions. The allocators can be compared to the single objective methods, namely the Minimum Travel as seen in section 3.4.4 and minimum Rate allocators, see section 3.4.6 . These too have been subjected to the same conditions as the multi-objective allocations and can be compared directly. The weightings for the conventional control allocators can been seen in equation 5.9.1.

$$W_p = W = \begin{bmatrix} \frac{1}{\overline{u}_1} & 0 & 0 & 0 \\ 0 & \frac{1}{\overline{u}_2} & 0 & 0 \\ 0 & 0 & \ddots & 0 \\ 0 & 0 & 0 & \frac{1}{\overline{u}_8} \end{bmatrix} \tag{5.9.1}$$

The single objective case essentially depicts the multi-objective case with either objective turn 'off', i.e having no resulting effect on the global solution. By inspecting the results, it is clear that the multi-objective formulation thereby give a appropriate trade off between the two objectives. Apart from the intrinsic parameters of the multi-objective allocators, the greatest impact on the solutions is the velocity. This is primarily due the B matrix' inherent dependency on velocity. It is seen that as the velocity is varied, the trend of the solution is maintained yet the extremum - so to speak is exaggerated. Throughout the entirety of the case study, v does in fact equal Bu and hence the solutions do attain the appropriated dynamics. The results have been conglomerated in Appendix C and are indexed in tables 5.9 and 5.9.

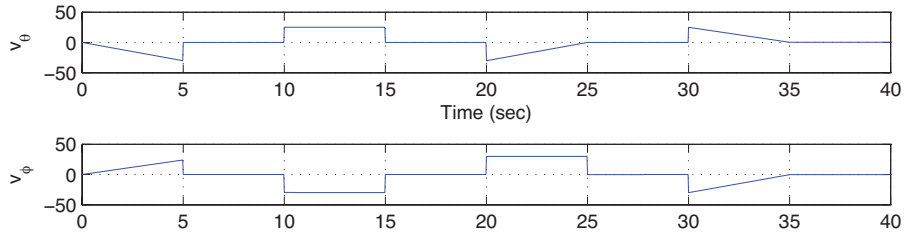

Figure 5.18: Lateral and longitudinal inputs

Method	Case	Figures
Minimum Deflection	Lateral $V = 50m/s$	C.1,C.2, C.3
	Longitudinal $V = 50m/s$	C.4,C.5, C.6
	Coupled Lateral and Longitudinal $V = 50m/s$	C.7,C.8, C.9
	Coupled Lateral and Longitudinal $V = 35m/s$	C.11,C.10, C.12
	Coupled Lateral and Longitudinal $V = 65m/s$	C.13,C.14, C.15
Minimum Rate	Lateral $V = 50m/s$	C.16,C.17, C.18
	Longitudinal $V = 50m/s$	C.19,C.20, C.21
	Coupled Lateral and Longitudinal $V = 50m/s$	C.22,C.23, C.24
	Coupled Lateral and Longitudinal $V = 35m/s$	C.25,C.26, C.27
	Coupled Lateral and Longitudinal $V = 65m/s$	C.28,C.29, C.30
Weighted	Lateral $V = 50m/s$	C.31,C.32, C.33
	Longitudinal $V = 50m/s$	C.34,C.35, C.36
	Coupled Lateral and Longitudinal $V = 50m/s$	C.37,C.38, C.39
	Coupled Lateral and Longitudinal $V = 35m/s$	C.40,C.41, C.42
	Coupled Lateral and Longitudinal $V = 65m/s$	C.43,C.44, C.45

Table 5.1: Index of extreme simulation scenarios

Method	Case	Figures
Minimax	Lateral $V = 50m/s$	C.46,C.47, C.48
	Longitudinal $V = 50m/s$	C.49,C.50, C.51
	Coupled Lateral and Longitudinal $V = 50m/s$	C.52,C.53, C.54
	Coupled Lateral and Longitudinal $V = 35m/s$	C.55,C.56, C.57
	Coupled Lateral and Longitudinal $V = 65m/s$	C.58,C.59, C.60
Classical	Lateral $V = 50m/s$	C.61,C.62, C.63
	Longitudinal $V = 50m/s$	C.64,C.65, C.66
	Coupled Lateral and Longitudinal $V = 50m/s$	C.67,C.68, C.69
	Coupled Lateral and Longitudinal $V = 35m/s$	C.70,C.71, C.72
	Coupled Lateral and Longitudinal $V = 65m/s$	C.73,C.74, C.75
Canonical	Lateral $V = 50m/s$	C.76,C.77, C.78
	Longitudinal $V = 50m/s$	C.79,C.80, C.81
	Coupled Lateral and Longitudinal $V = 50m/s$	C.82,C.83, C.84
	Coupled Lateral and Longitudinal $V = 35m/s$	C.85,C.86, C.87
	Coupled Lateral and Longitudinal $V = 65m/s$	C.88,C.89, C.90

Table 5.2: Index of extreme simulation scenarios

5.10 Discussion and Conclusion

In this chapter the four ***novel*** control allocators where tested on a high veracity non-linear simulation. In general they all appear to follow a similar trend but exhibit unique properties. It is clear from figures 5.6, 5.10, 5.14 and 5.15 that they all attained perfect allocation, as v directly maps onto Bu.

By looking at the allocation response of the four algorithms to the pitch control demand at $t = 10s$, Notice that the three first allocation schemes namely Simple Weighted, Minimax and Canonical Goal Attainable display very similar effector distributions. The conventional physical control surfaces are much more utilised, while the fluidic circulation control or FTV effectors are hardly called upon and remain dormant, close to their trim positions. This can be attributed to the fact that, by design, the vehicle features extended conventional elevator surfaces (see figure 2.5), η_{Left} and η_{right}, therefore providing those effectors with higher longitudinal effectiveness making them preferred candidates for demand allocation along that axis.For the same reason, one will note that deflection commands for longitudinal manoeuvres tend to be quite small. The one algorithm that proposes a notably different control distribution to meet the pitch demand is the Classical weight formulation of the Goal Attainable method. For which, in addition to the conventional surfaces being kept at a lesser deflection angle for longer compared to the other schemes, the fluidic FTV actuator is also put to contribution to meet the demand. Although it is expected that the Goal Attainable is to perform similarly to the Simple Weighted method, both of them being algorithms which rely mainly on user defined objective weightings. This actually illustrates the fact that the Simple Weighted method weights were setup to prioritise the first objective: minimum deflection, thus making its solutions tend to an ideal compromise similar to those given by the Minimax scheme. Whereas the Classical Goal Attainable weights were set to prioritise the second objective: the travel deflection rate, thus minimising the deflection changes from one time step to the next and hence, the longer deflection times and the discrepancy.

At $t = 20$ where the vehicle preforms a combined pitch and roll command, it can be noted that that the Simple Weighted and Classical Goal Attainable algorithms display very similar control distribution patterns, where all the control surfaces are deployed to meet the pitch and roll high moment demands. The only noticeable difference between the solutions lies in the use of the FTV actuation by the Classical Goal Attainable formulation. This can as previously, be attributed to the different objective weights not prioritising the same objective for the two methods. On the other hand, one can notice that the allocation response given by the Minimax algorithm differs from the three other schemes in the sense that its proposed deflections for the conventional control surfaces are of lesser amplitude, rather

distributing more of the control demand to the fluidic circulation control devices ξ_{CCLeft} and $\xi_{CCRight}$. This trend can be attributed to two reasons, first the increase of control effectiveness of these lateral fluidic devices with the velocity reduction caused by the pitching manoeuvre; and secondly their positioning along the Demon's wings, which makes them ideal compromising controls between lateral and longitudinal moment generators. Meaning that their deflection can produce a moment about both axis simultaneously, which coupled with their improved effectiveness, makes them ideal candidates for the solution to tend towards the ideal point compromise between objectives. The greater use of the CC devices to respond to the combined moment demand is also what induced the undesired pitch oscillations displayed by the Minimax simulation pitch rate response q, at $t = 20s$. Finally, when comparing the responses of the Minimax and Canonical Goal Attainable methods, which both attempt to tend to the ideal point solution, it can be noticed that; although the proportions of distributed demand to the respective actuators remain similar, that is to say it prefers the use of the CC devices, the Canonical Goal Attainment solution does not present the same deflection peaks as the Minimax does. Instead, the addition of the u_g goal point, causes the deflection solutions to be held back or drawn to the preferred trim settings – hence the smoother and square looking actuation pattern described by its solutions. This is also the cause of the leaner slope in the variations of the roll angle ϕ over a longer period of time displayed by the simulation states of this algorithm compared to the three others.

Furthermore the Weighted Control Allocation method generally exhibits peaks at the demand. This attribute was mimicked by the Minimax method which indicates a beneficial property to the Weighted control allocation method. That is to say in the event that processing power is an issue and the chosen objectives are all quadratic, such that they project a convex set in the objective space, the Weighted control allocator, with a reasonable degree of accuracy can be tuned to resemble the Minimax allocator thus foregoing the computational cost required to calculate the ideal point F^*. The Canonical method does attain to u_g such that at the demand the control is essentially 'held back' and applied for longer periods, this capability be beneficial to maintaining the aircraft's radar cross section. The Classical method too attained to u_g at $t = 10$ but alternatively indicated peaks at $t = 20$. This indicates the fact that the classical method is more likely to disregard the goal point u_g.

All the simulations ran in real time and the minimisation exhibited a reasonable degree of accuracy – producing solutions to four significant figures (this is a far greater degree of accuracy than is require to operate the full actuator suite on the Demon UAV).

Figure 5.19 provides a mean average of the number of iteration that are required to reach the Pareto optimal solution. It gives an indication of computational load exhibit by each method. It is quite clear and that the

Weighting method exhibits the least computational load while the Minimax is, by far the most computationally demanding algorithm, this may be attributed to the fact F^* is used as the focal point of the minimisation. Per contra the Canonical and Classical are given u_g and hence exhibit a lower computational time. During the entirety of the simulation, the Canonical and Classical algorithms remain within a reasonable of measure of each other. These results are consist with the theory depicted in Chapter 4.

As already stated, these simulation where conducted and developed in Matlab/Simulink and hence are somewhat unoptimised for this application. It is hence in this author's opinion that if the algorithms where to be developed in C/C++/Fortran and optimised accordingly such that they are to be complied onto an embedded platform, then the algorithms would consume far less processing power.

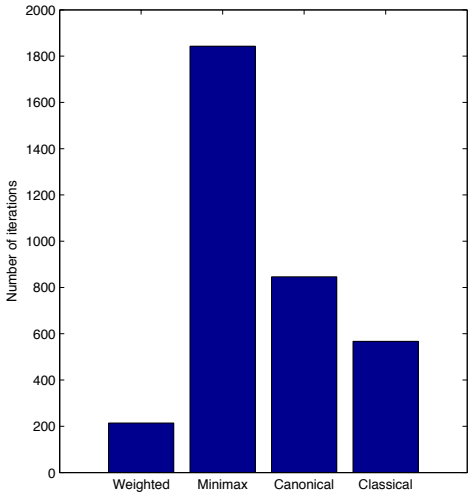

Figure 5.19: Computation load of each method

In conclusion the allocators all provided prefect allocation. Exhibiting a number of different attributes and properties which can be beneficial to a number of applications and missions. The implementation of the control allocators where applied to Demon Model with a reasonable ease, and further retained a high amount flexibility with regards to properties, objectives and the location of the solution along the pareto frontier[1]. Non of the imposed constraints where violated during the simulations and hence the allocator ran within operational limits.

With the addition of a Failure Detection and Isolation system, the following chapter shall investigate the allocators capability to mitigate effector

[1]Achieved by the altering the respective weights of each objective.

failures. The Demon UAV will be subjected to a hard failure at $t = 5$ and there-in expected to follow the same trajectory as seen in figure 5.4.

CHAPTER 6

Reconfigurable Flight Control

6.1 Introduction

THE main motivation behind research into control allocation was generally attributed to its capability to be augmented into a reconfigurable flight control system. Typically two types of failures can manifest themselves, neutral failure, which would hold the effector at its neutral position resulting in a zero effectiveness with respect to its state variable, or a hard[1] failure where the effector would reside at a some position, resulting in undesired longitudinal and, or lateral transients which could lead to a catastrophic failure[2]. In the event of a failure the control allocator would go about redistributing the the total commands onto the working effectors before the closed loop performance has degraded. Application of fault tolerant system primarily relies on two main aspects: (i) a control allocator and (ii) a Failure Detection and Isolation system (FDI), See Figure 6.1.

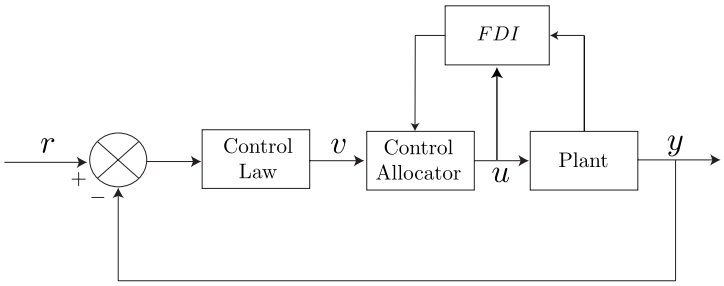

Figure 6.1: Reconfigurable Flight Control Architecture

For example the pseudo inverse control allocator, described in section 3.4.4, contains a set of weighting W, which would generally be used to prioritise certain effectors. In the event of a failure the respective weighting would be 'zeroed' and hence the the total demand would then be redistributed among the remaining effectors. Other approaches involve reducing the dimensions of the control space Ξ such that failed actuator is no longer considered in the optimisation.

The following chapter briefly describes FDI systems and go on to investigate the capability of the four ***novel*** methods described in chapter 4 to

[1] Denoted as hardover if the effector resides at its saturation

[2] Loss of aircraft, Loss of life [52]

mitigate effector transients when subjected to a hard failure.

6.2 Failure Detection and Isolation

Over the last two decades Failure Detection and Isolation systems have be the subject of considerable work, while some utilise neural networks [46], most employ actuator models and compare the input/out response;

Since most effector tend to exhibit higher order dynamics, detection of a failure can not simply be assumed by comparing the feedback and commanded positions. As the output differs during most transients, a high frequency of false negatives will be declared; that is unless, the threshold of failure is set undesirably high (which could result in a number of 'missed' failure) . It has been suggested to use a Model-based FDI [44] where the system employs a model of the actuator to predict the control device's behaviour and hence if the model is perfect; accurate detection of failures may be accomplished by comparing outputs from the model with feedbacks from the actuators, as shown in figure 6.2. In the instance that the model is not entirely accurate, nominal residuals can be overcome through the use of an appropriate threshold.

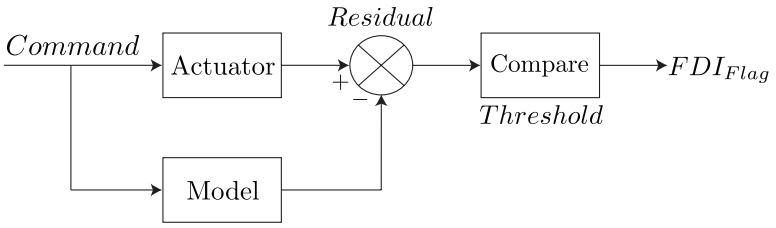

Figure 6.2: Model-based Failure Detection Isolation

6.3 Failure Simulations

The FDI was applied to the high veracity demon 6DoF simulation as described in chapter 5 and subjected to a Hard failure. The objective functions where set to equations 5.3.1 and 5.3.2 such that they denote a convex set in the objective space $F(u)$, as can be seen in figure 5.1. The methods were all contrive in the manner described in chapter 5. In the event of a failure the FDI_{Flag} would indicate a failed effector and the respective weightings in W_p and W_r would be set to zero. The total demand would then be redistributed to the remaining actuators in the following time step. The simulations where initialised at a cruising speed of $50m/s$ and altitude of $200m$ above sea level. At $t = 10$ the vehicle attempts to perform a pitch up manoeuvre, such that $r_\theta = 25$ and at $t = 20$ the aircraft performs a roll manoeuvre such that $r_\phi = -30$. At $t = 5$ the starboard side aileron

is subjected to a 10° hard failure and such that $\xi_{Right} = 10$ and continues to reside at this state throughout the entirety of the simulation. Figure 6.3 shows the desired path of the simulation and point '▽' indicates the start of the failure. The results for Weighted control allocation can be seen in figures 6.4, 6.5 and 6.6. The Minimax control allocator results are described in figures 6.7, 6.8 and 6.9. The Canonical control allocator results are denoted in figures 6.10, 6.11 and 6.12. The Classical control allocator's resluts can be seen in figures 6.13, 6.14 and 6.15. The all the figures denote the trends for the control deflection, states and mapping from v to Bu respectively.

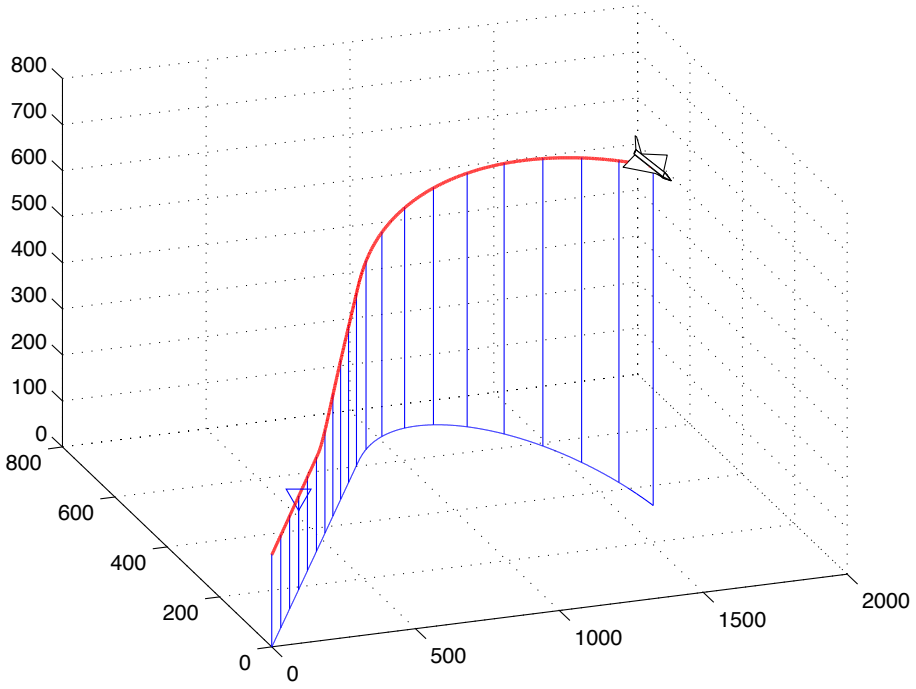

Figure 6.3: Desired Path

6.4 Discussions and Conclusions

It is clear that at $t = 5$ is the vehicle exhibits undesired transients which can be seen in all simulations (see figures 6.5, 6.8, 6.11 and 6.13). Due the nature of and geometry of the failed actuator these transients act on all three axis, x, y and z and their effects can be seen the resulting accelerations in p, q and r. Had these transient not been mitigated it is likely that the close loop performance would degrade to a unrepairable state. Yet with the application of the multi-objective control allocator the remaining effectors are untilised to mitigate the resulting transients. The effector distrubtion can been seen in figures 6.4, 6.7, 6.10 and 6.13.

In general the methods retained the same attributes as those seen in chapter 5. For the weighted control allocator, at $t = 5$ the allocator immediately deploys η_{Right} along with ξ_{Left}, $\xi_{CCRight}$ and ξ_{CCLeft} to counteract the resulting dynamics from the failed starboard side aileron ξ_{Right}. - culminating in a asymmetric distribution in the actuator suite. ξ_{Left} in this instance has the greatest effectiveness to counteract the failure, and along with the others is held at this solution. At $t = 10$, η_{Right} and η_{Left} are asymmetrically deployed to meet the longitudinal demand, which you will note that the attitude is met within 3 seconds. At $t = 20$ the allocator utilises all the remaining actuators to meet lateral demand. You will note that η_{Left} is held at approximately 20° to counter the continuing moment which is begin being generated from the fail actuator. It would seem that due to the fact that η_{Left} is being used to counter the undesired dynamic, η_{FTV} has been brought to bear to maintain the longitudinal attitude. The lateral attitude demand was met within 1 second, which is similar to the non-failure case in section 5.5. The minimax allocator, for the first ten seconds of the simulation produces similar solutions to the Weighted control allocator, yet at $t = 20$ the resultings peaks which appeared in the un-failed case in section 5.6 have now diminished and instead both solutions are attaining a greater ideal point F^*. Both $\xi_{CCRight}$ and η_{Right} were held at an offset position to counter the undesired transients being generated by ξ_{Right}. The FTV was again utilised to maintain the demanded attitude. The Canonical solution too exhibited the same trend as the proceeding methods with the exception that at $t = 20$ the solutions resembled the non-failure case. $\xi_{CCRight}$ and η_{Right} were held to counter the undesired dynamics which were being generated by ξ_{Right}. The attitude demand where again met within 1 and 3 seconds. In general the Classical trend resembled the Canonical method although exhibiting a somewhat more drastic peaks, which is consistent with the non-failure case. The solutions again held $\xi_{CCRight}$ and η_{Right} to counter the undesired dynamics which were being generated by ξ_{Right}.

An interesting resolution from these results is the fact that as opposed to the un-failed case, in all simulations the fluidic devices are (generally speaking) utilise more often as opposed to exaggerating the use of the conventional devices (attaining to high deployment). This in turn sheds some light upon the attributes of the control allocators in that despite a failed actuator the algorithms are still attaining to the ideal or user defined points where possible.

In conclusion all the methods retained their properties and aided in the mitigation of a single effector failure while maintaining perfect allocation, that is to say v directly maps to Bu. It can be seen that in all cases the no constraint is violated and the vehicle remains within operational limits and only minor transients occurred from the failed actuator. As the vehicle did not go unstable these transient are deemed acceptable.

An investigation into the computational time adheres with the results

shown in figure 5.19 which is to be expected as no constraints were violated and it is clear that the solution remained with the attainable set.

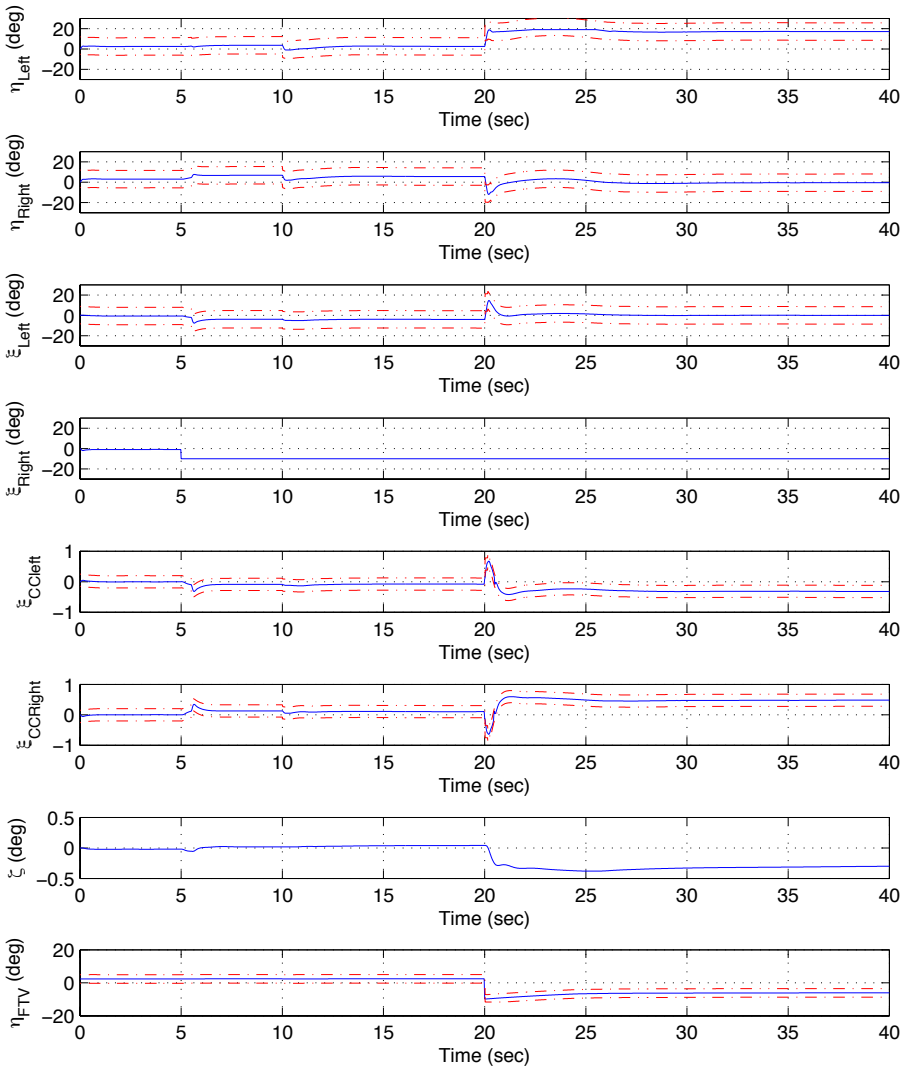

Figure 6.4: Failure Simulation for Weighted Allocator, Controls

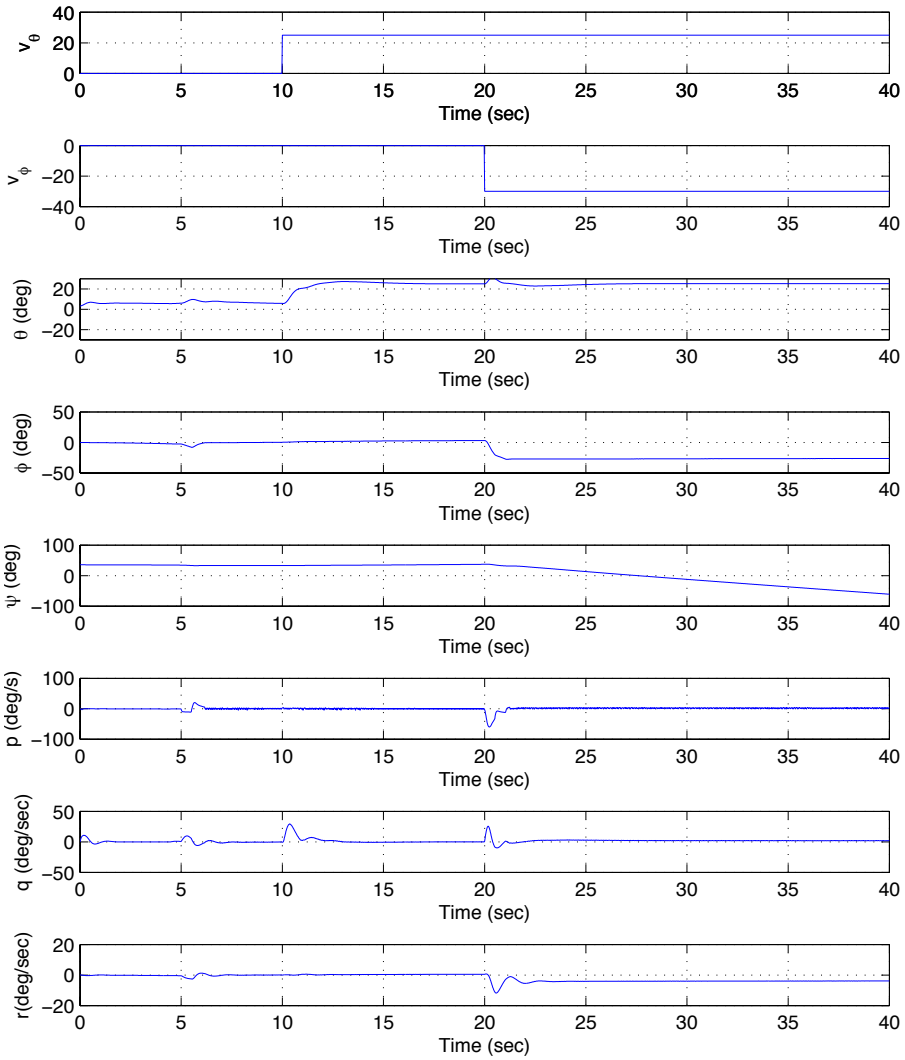

Figure 6.5: Failure Simulation for Weighted Allocator, States

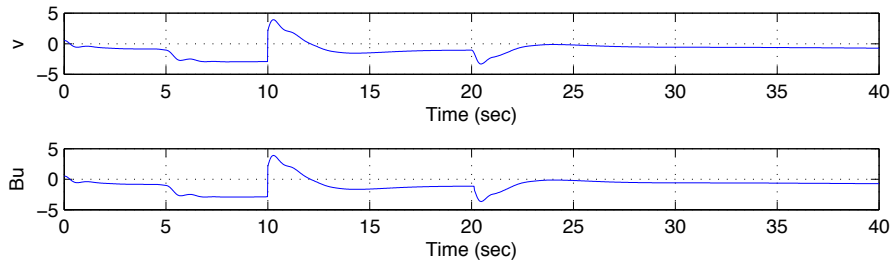

Figure 6.6: Failure Simulation for Canonical Allocator, v, Bu

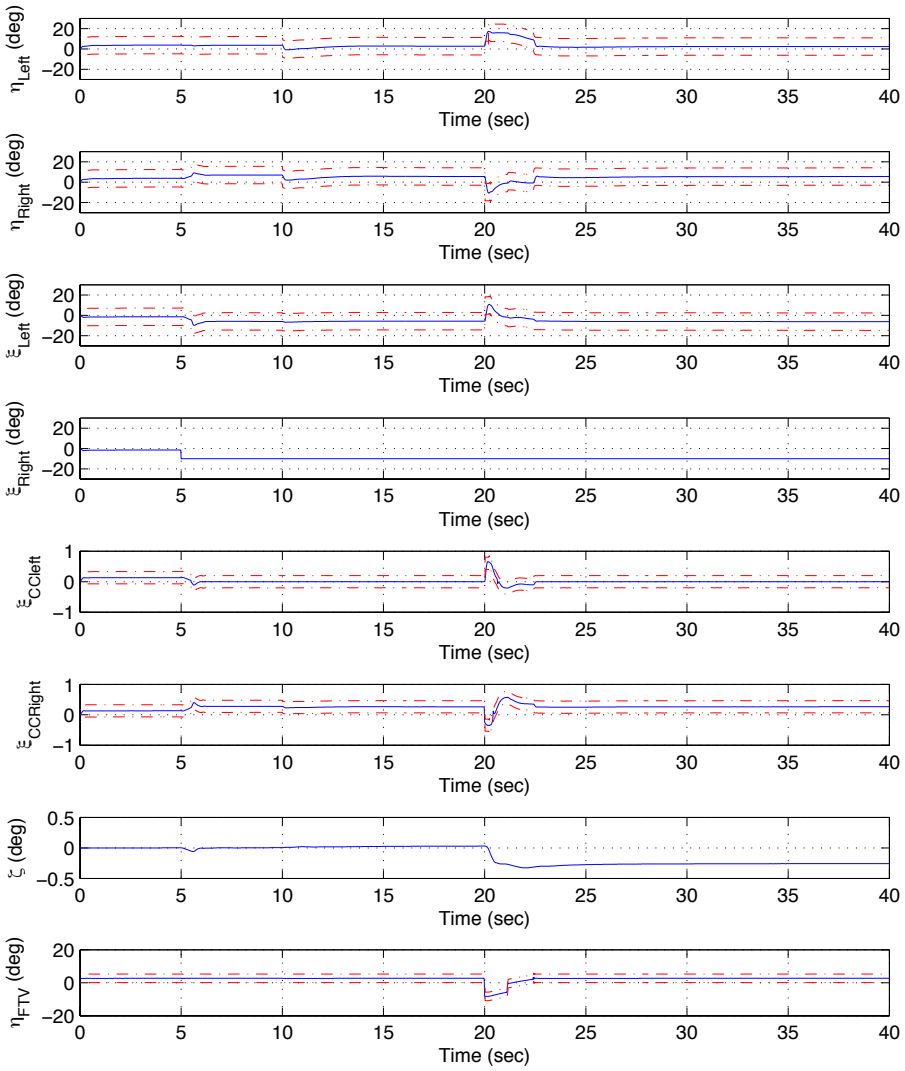

Figure 6.7: Failure Simulation for Minimax Allocator, Controls

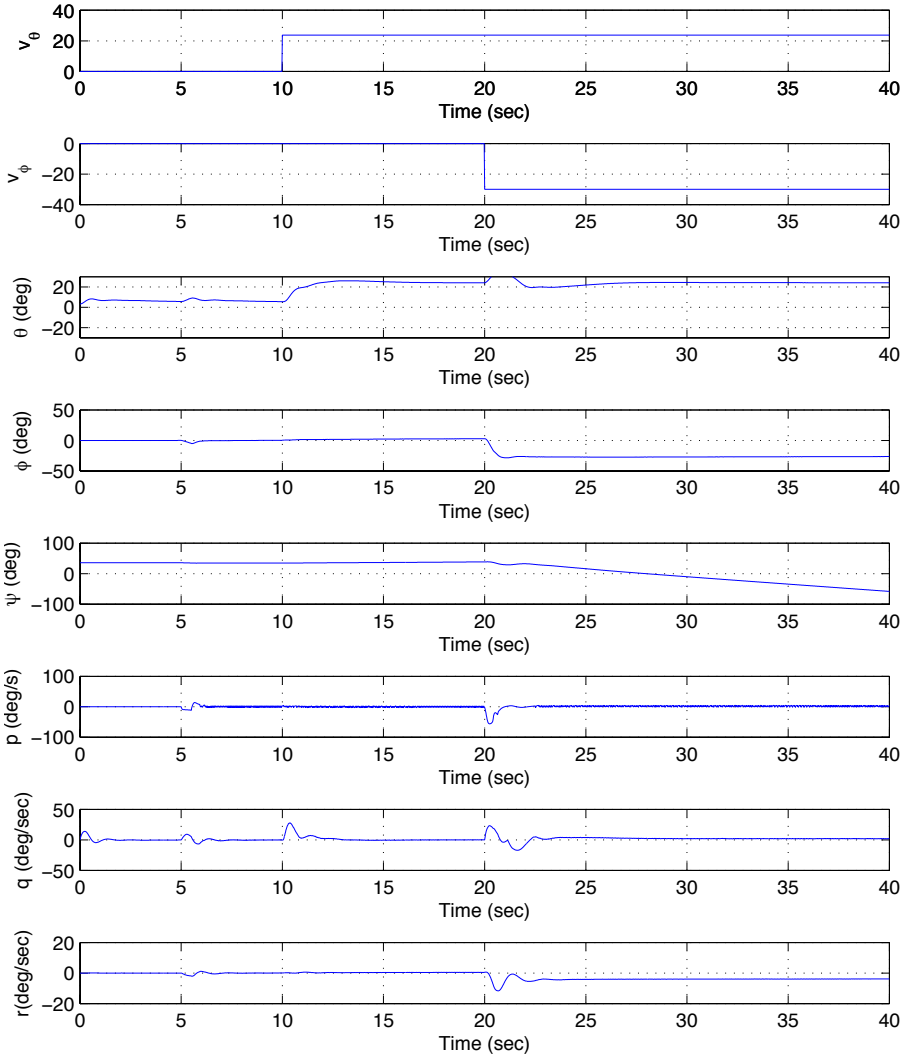

Figure 6.8: Failure Simulation for Minimax Allocator, States

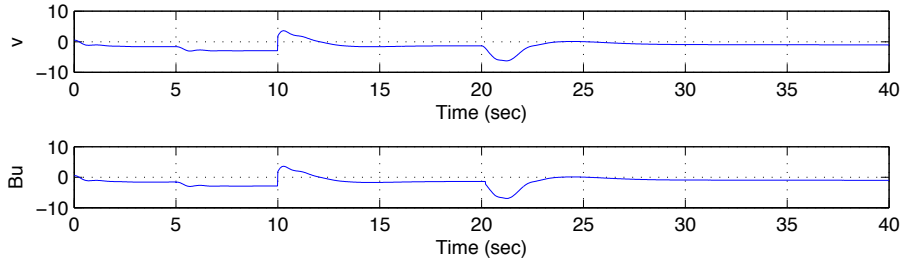

Figure 6.9: Failure Simulation for Canonical Allocator, v, Bu

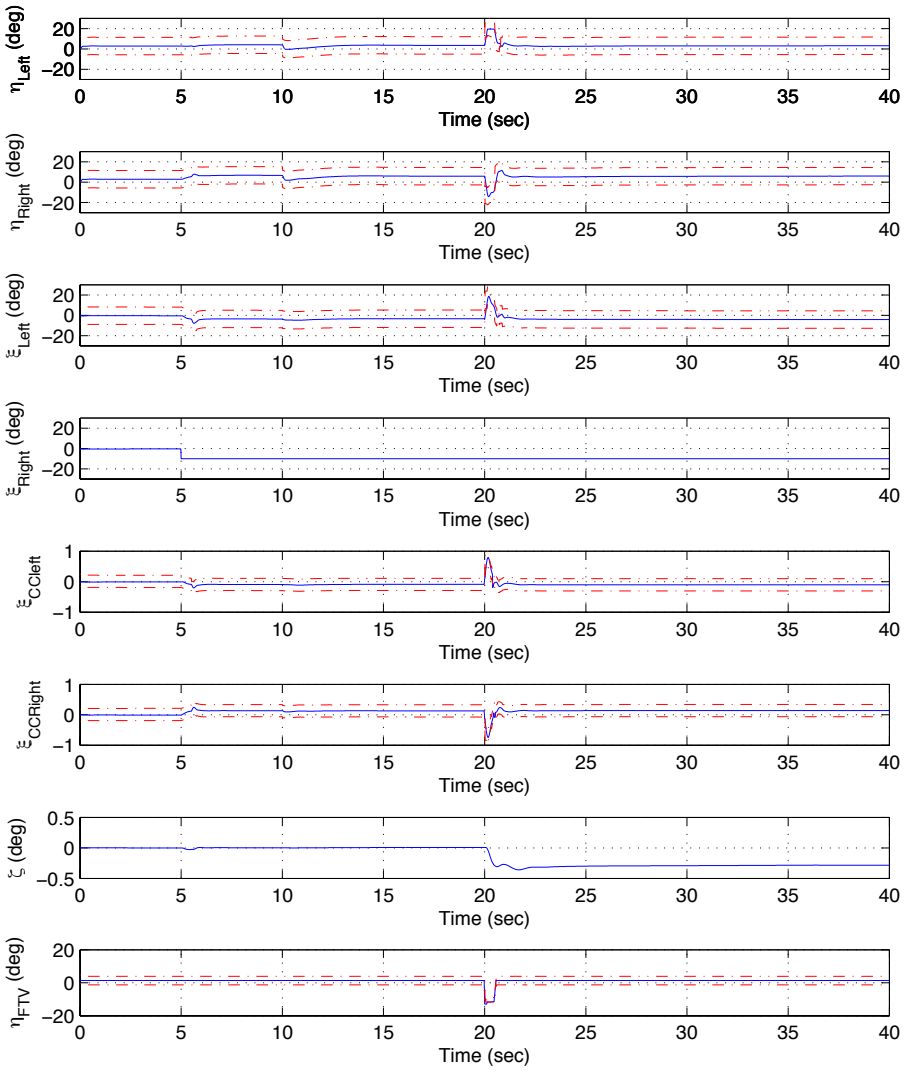

Figure 6.10: Failure Simulation for Canonical Allocator, Controls

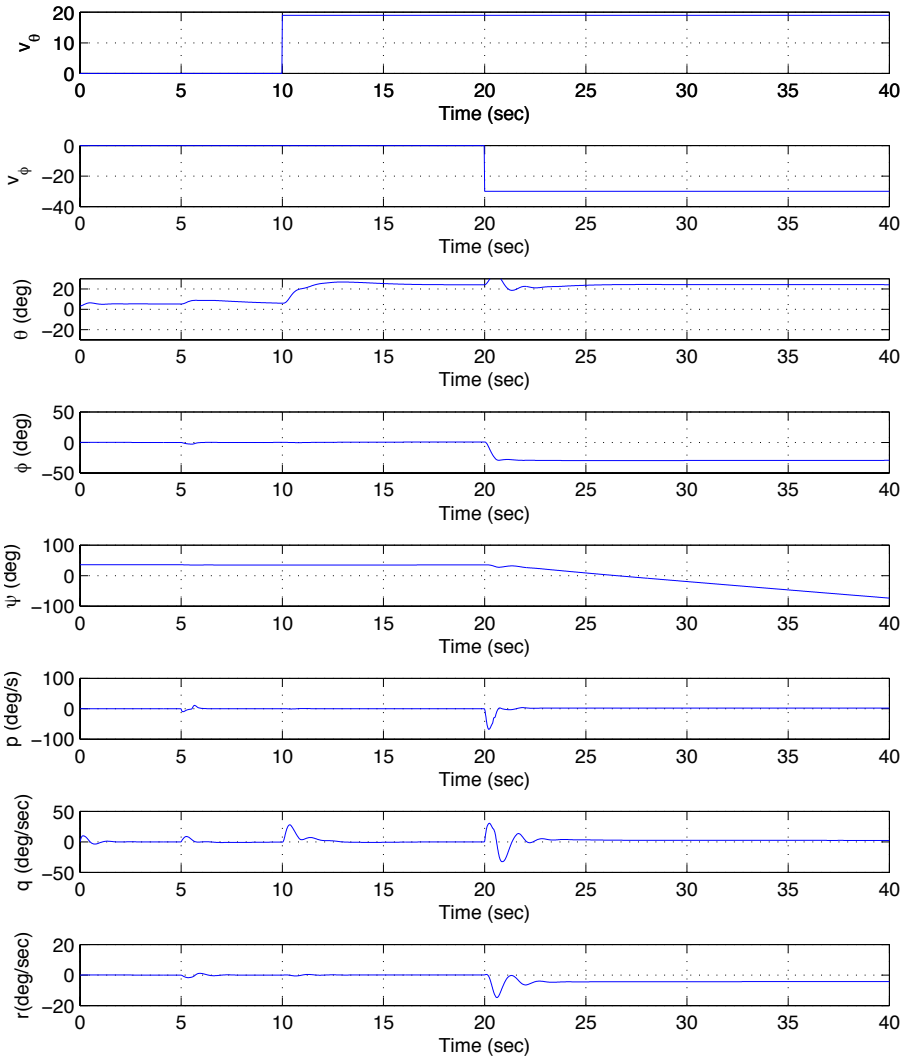

Figure 6.11: Failure Simulation for Canonical Allocator, States

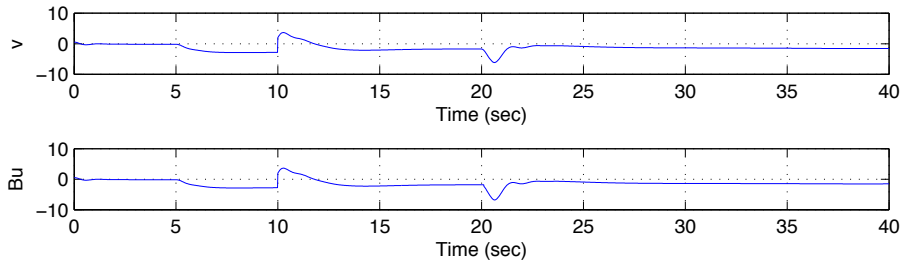

Figure 6.12: Failure Simulation for Canonical Allocator, v, Bu

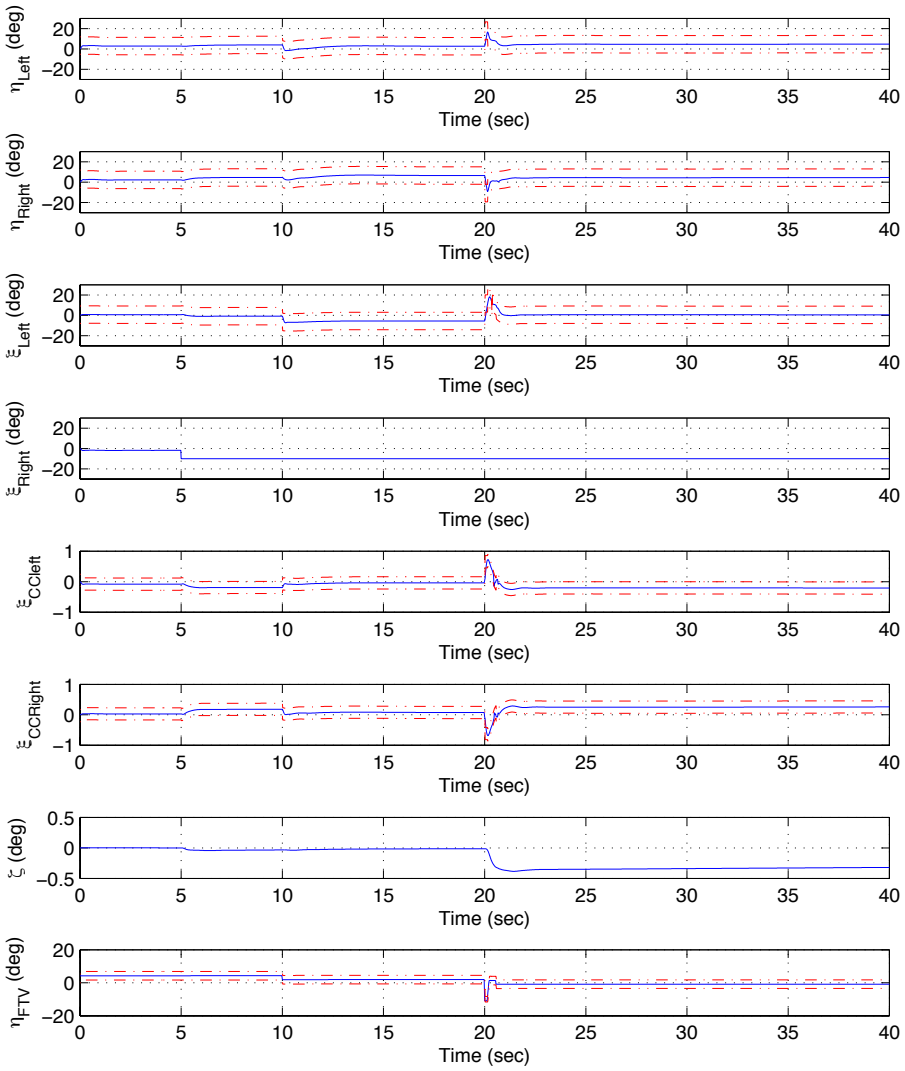

Figure 6.13: Failure Simulation for Classical Allocator, Controls

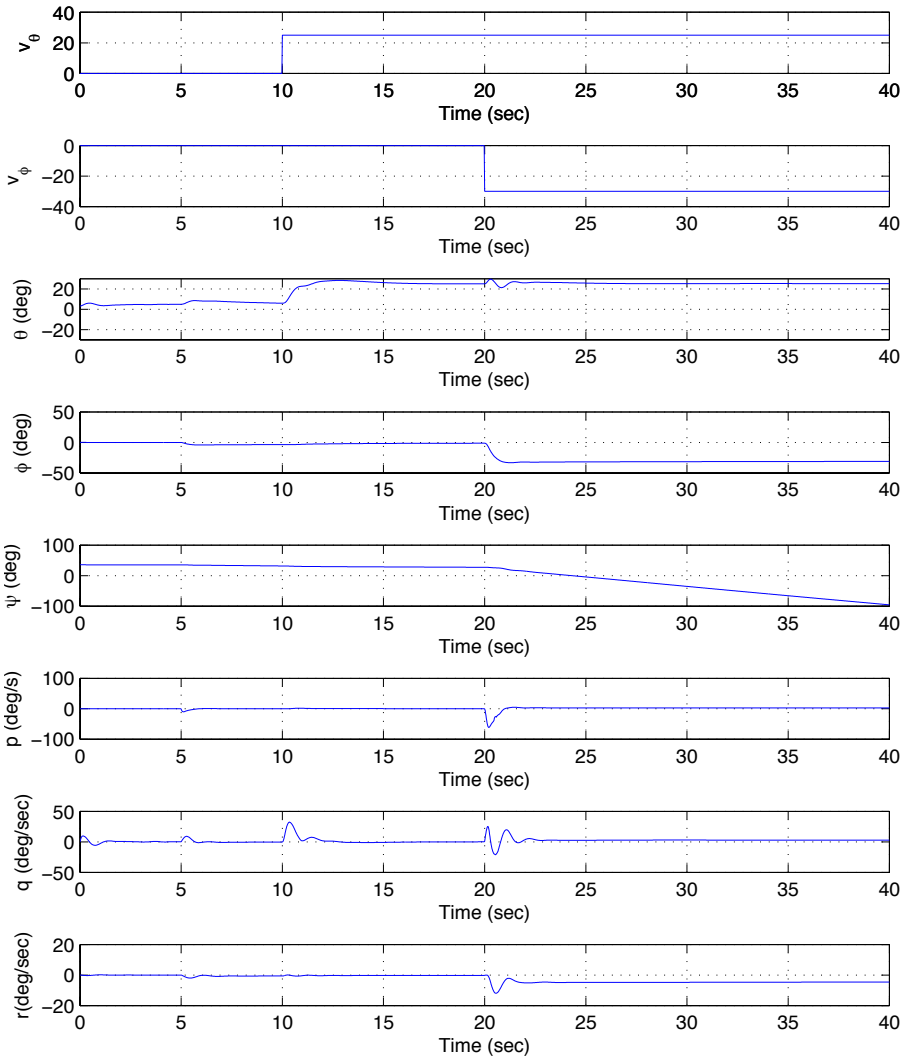

Figure 6.14: Failure Simulation for Classical Allocator, States

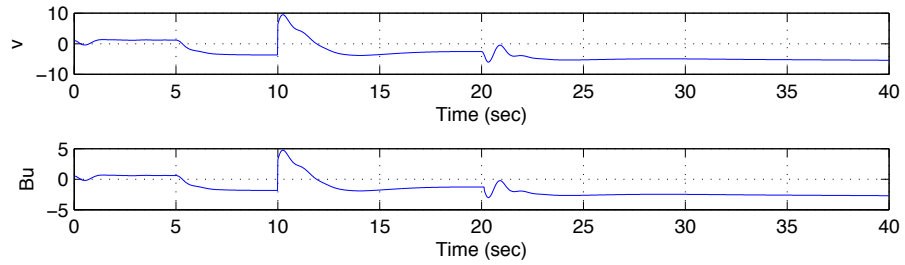

Figure 6.15: Failure Simulation for Classical Allocator, v, Bu

CHAPTER 7

Conclusions and Future Work

7.1 Conclusions

Let us draw this thesis to a close with some overall conclusions. Four ***novel*** methods for multi-objective control allocation have been developed. The methods were subjected to a number of conflicting objectives and found the Pareto optimal solution. It is clear that the methods can be extended to a greater number of objective, where the Minimax, Canonical and Classical are non-prejudice towards the projection of the objectives in the objective space being convex or non-convex. Each method provides a number of inherent properties which can be beneficial to certain mission and/or application. The Weighted method by far provides the most simplest formulation although must be performed under a convex set for j objectives. The Minimax method draws the solution towards the ideal point while the Goal attainable methods allows the decision maker to define a point outside of the attainable space to which the solutions are to be drawn to. The Goal Attainable methods contain inherent differences in the way they weight their objectives, where the Classical method is more likely to disregard the goal point u_g at higher values of v. They were all applied to a 6 DoF high veracity simulation based on the Demon UAV and were subjected to a set of predetermined manoeuvres. All the methods produced 'perfect' allocation, that is, in all cases v directly maps onto Bu. The control allocators where then subjected to a set of hard failures and produced solutions which mitigated the resulting transients. In conclusion the allocators produced an adequate effector distribution which was consistent with the theory.

It is difficult and somewhat inappropriate to elect a single method as superior over the others. This, as always must fall to the designer's engineering judgement – taking into account the computational load, mission, preferences and system complexity.

7.2 Future Work

As Multi-objective control allocation, remain is in its infancy, there are a number of ways it could be investigated further.

Computational time for lightweight systems tends to be an issue and the minimisation could further be investigated. Throughout this thesis, all the investigation and test cases were simulation based, the investigation of

the methods could further be applied to an embedded platform and perhaps flight tested. This would of course require thorough system ID investigation as the inaccuracies in the B matrix shall cause it to act as a high or low gain.

Currently two objectives have been applied to the method and both were solved analytically, a suggestion would be to add further objectives onto the methods as well as investigating other means of computing the single objective solution.

An area which is of most interest to me particularly, is to solve the Multi-objective control allocation with Pareto optimality analytically. That is to say, assuming a quadratic formulation of the single objectives, they shall always project a ellipsoidal convex set in the objective space $F(u)$. As the minima for each single objective is known, a fairly accurate approximation of the Pareto optimal frontier can be made and as such the problem becomes somewhat trivial. From there, methods can be derived which resemble the Weighed, Minimax and Goal Attainable.

Bibliography

[1] C Papachristou A Savvaris C Vamvakoulas C Warsop A Buonanno, D Drikakis. Computational investigation of the demon unmanned air vehicle thrust vectoring system. *Proceedings of the Institution of Mechanical Engineers, Part G: Journal of Aerospace Engineering*, 2009.

[2] S. D. Erbsloeh. A. Buonanno, M.V. Cook. Flight dynamic simulation of a flapless flight control uav. *25th International Congress of the Aeronautical Sciences*, 2006.

[3] J.P. Fielding A. Yarf-Abbasi. Design integration of the eclipse and demon demonstrator uavs. In *AIAA Aviation Technology and Operation Conference(ATIO)*, page 10, Belfast Northern Ireland, 2007.

[4] A.Buonanno. *Aerodynamic Circulation Control for Flapless Flight Control of an Unmanned Air Vehicle*. PhD thesis, Cranfield University, 2009.

[5] S.D.Erbsloeh A.Buonanno, M. V. C. Differental criculation control for flapless flight control of uav. In *Bristol UAV System Conference*, 2007.

[6] G Allegri. *Flight Dynamics of the Eclipse-Based Unmanned Platforms.* Flaviir, Cranfield University,UK, internal report inr151206 edition, 2006.

[7] R. D. Barnard. Continuous-time implementation of optimal-aim controls. *IEEE Transactions on Automatic Control*, 2001.

[8] Roger E. Beck. *Application of Control Allocation Methods to Linear Systems with Four or More Objectives*. PhD thesis.

[9] Ake Bjorck. *Numerical Methods for Least Squares Problems*. Siam, volume 1 edition, 1996.

[10] M. Bodson. Evaluation of optimization methods for control allocation. *J. Guid. Control Dyn.*, 25:703–711, 2002.

[11] Kenneth A. Bordignon. *Constrained Control Allocation for Systems with Redundant Control Effectors*. PhD thesis.

[12] Kenneth A. Bordignon and Wayne C. Durham. Closed-form solutions to constrained control allocation problem. *Journal of Guidance Control, and Dynamics*, 1995.

[13] K. Bradbrook. *Contribution to the Aerodynamic design for the Eclipse*. PhD thesis, University of Cranfield, 1999.

[14] Frank Lewis Brian Stevens. *Aircraft Control and Simulation*. John Wiley and Sons, New Jersey,USA, second edition, 2003.

[15] J. M. Buffington and D. F. Enns. Lyapunov stability analysis of daisy chain control allocation. *J. Guid. Control Dyn.*, 19:1226–1230, 1996.

[16] Cook M.V. Buonanno, A. and S. D. Erbsloeh. Development of a bi-directional circulation control actuator. *2nd European Conference for Aerospace Sciences*, 2007.

[17] Buonanno A. Cook, M.V and S. D Erbsloeh. Experimental determination of the aerodynamic performance of a dual slot circulation control actuator. *Journal of Aircraft*, 2008.

[18] Buonanno A. Cook, M.V and S. D Erbsloeh. A circulation control actuator for flapless flight control. *The Aeronautical Journal*, 2008, August.

[19] Micheal V. Cook. *Flight Dynamics Principles*. Butterworth-Heinemann, second edition, 2007.

[20] T.B Cunningham. Robust reconfiguration for high reliability and survivability for advanced aircraft. In *Restructurable Controls, NASA Conference Publication 2277*, 1982.

[21] I Postlethwaite D-W Gu, K Natesan. Modelling and robust control of fluidic thrust vectoring and circulation control for unmanned air vehicles. In *Proceedings of the Institution of Mechanical Engineers*, 2008.

[22] W. C. Durham. Attainable moments for the constrained control allocation problem. *J. Guid. Control Dyn.*, 17:1371–1373, 1994.

[23] W. C. Durham. Constrained control allocation. *J. Guid. Control Dyn.*, 16:717–725, 1994.

[24] W. C. Durham. Constrained control allocation - 3-moment problem. *J. Guid. Control Dyn.*, 17:330–336, 1994.

[25] W. C. Durham. Efficient, near-optimal control allocation. *J. Guid. Control Dyn.*, 22:369–372, 1999.

[26] W. C. Durham, J. G. Bolling, and K. A. Bordignon. Minimum drag control allocation. *J. Guid. Control Dyn.*, 20:190–193, 1997.

[27] R.J Englar. Circulation control pneumatic aerodynamics: Blown force and moment augmentation and modification; past, present and future. In *AIAA Paper 2000-2541, Fluids 2000, Denver, Colorado, 2000*, 2000.

[28] R.J. Englar and R.A Hemmerly. Design of the circulation control wing stol demonstrator aircraft. In *Journal of Aircraft, Vol. 18, No. 1, pp. 51 -58, 1981*, 1981.

[29] R.J. Englar and G.G. Huson. Development of adavanced circulation wing high lift airfoils. In *Journal of Aircraft, Vol. 21, No. 7, pp. 476-483, 1983*, 1983.

[30] D. Enns. Control allocation approaches. In *Proc AIAA Guid., Nav. and Control Conf.*, pages 98–108, Boston, MA, 1998.

[31] S. P. Frith and N.J. Wood. Effect of trailing edge geometry on a circulation control delta wing. In *AIAA Paper 2003-3797, 21st applied Aerodynamics Conference, Orlando, Florida, 2003.*, 1983.

[32] J.F. Whidborne G.P. Liu, JB. Yang. *Multiobjective Optimisation and Control*. Research Studies Press LTD, Hertfordshire,UK, first edition, 2003.

[33] C.P. Lawson Guido A. I. Monterzino. Design manufacturing and flight testing of a health monitoring system for prototype uavs. In *Elsevier Journal - Sensors and Actuators*, 2012.

[34] Craig P. Lawson Guido A. I. Monterzino. Development of a pneumatic system to enable flight without conventional control surfaces. *27th International Congress of the Aeronautical Sciences*, 2010.

[35] O. Harkegard. Efficient active set algorithms for solving constrained least squares problems in aircraft control allocation. *In Proc. of the 41st IEEE Conference on Decision and Control*, 2002.

[36] O Harkegard. *Backstepping and Control Allocation with Application to Flight Control*. PhD thesis, Linkoping University, 2003.

[37] O. Harkegard. Dynamic control allocation using constrained quadratic programming. *J. Guid. Control Dyn.*, 27:1028–1034, 2004.

[38] S. J. Wright J. Nocedal. *Numerical Optimization*. Springer, volume 1 edition, 1999.

[39] Howard Smith J. P. Fielding. Flaviir, an innovative university/industry research program for collaborative research and demonstration of uav technologies. In *25th International Congress of the Aeronautical Sciences*, 2006.

[40] R. M. Martins-Pires G. A. I. Monterzino J. P. Fielding, C. P. Lawson. Design, build and flight of the demon demonstrator uav. In *AIAA, Virginia Beach*, 2011.

[41] R. Pires G. Monterzino J. P. Fielding, C. P. Lawson. Development of the demon technology demonstrator uav. In *27th International Congress of the Aeronautical Sciences*, 2010.

[42] Z. Wu J.J. Burken, P. Lu and C. Bahm. Two reconfigurable flight – control methods: Robust servomechanism and control allocation. *Journal of Guidance Control, and Dynamics*, 2001.

[43] Frederich Lallman John B Davidson and Thomas Bundick. Integrated reconfigurable control allocation. *Journal of Guidance Control, and Dynamics*, 2001.

[44] W. T. B. John B. Davidson, F. J. L. Integrated reconfigurable control allocation. In *Guidance, Navigation and Control Conference and Exhibit*, pages 5499–5504, Montreal, Canada, 2001.

[45] Colin N. Jones. *Reconfigurable Flight Control First Year Report*. PhD thesis, University of Cambridge, 2005.

[46] Lopez-Mejia Henry Leonardo. *Aircraft damage detection and reconfiguration using artificial neural networks*. PhD thesis, Cranfield University, 2010.

[47] P. Lu. Constrained tracking control of non-linear systems. *System and Control Letters*, 1996.

[48] M.W. Oppenheimer, D.B. Doman, and M.A. Bolender. Control allocation for over-actuated systems. In *14th Mediterranean Conference on Control and Automation*, pages 1 –6, june 2006.

[49] S.N Michie W.J. Crowther P.I.A. Wilde, K. G. Integrated design of fluidic flight controls for flapless aircraft. In *AIAA, Nevada*, 2008.

[50] J.S Arora R.T. Marler. Survey of multi-objective optimization methods of engineering. *Structural and Multidisciplinary Optimization*, 2004.

[51] L Vandenberghe S Boyd. *Convex Optimization*. Cambridge University Press, Cambridge,UK, first edition, 2004.

[52] NATO Standardization. Stanag 4586. Technical report, NATO, 1998.

[53] Fossen T.I. and Johansen T.A. A survey of control allocation methods for ships and underwater vehicles. In *14th Mediterranean Conference on Control and Automation*, pages 1–6, Ancona, Italy, 2006.

[54] Petter Tondel Tor A. Johansen, Thomas P. Fuglseth. Optimal constrained control allocation in marine surface vessels with rudders. *Control Engineering Practice*, 2008.

[55] J.C. Virnig and D.S. Bodden. Mulitvariable control allocation and control law conditioning when control effectors limit. *Guidance, Navigation, and Control Conference and Exhibit*, 1994.

[56] J.C. Virnig and D.S. Bodden. Multivariable control allocation and control law conditioning when control effectors limit. In *Proc AIAA Guid., Nav. and Control Conf.*, pages 98–108, Scottsdale, AZ, 1998.

[57] Buonanno A. Crowther B. Wilde, P. and A. Savvaris. Aircraft control using fluidic maneuver effectors. *26th AIAA Applied Aerodynamics Conference*, 2008.

APPENDIX A

Matrix Theory

A.1 Non-linear linearisation via Taylor Series

Consider the following model;

$$\dot{x} = f(x, u) \tag{A.1.1}$$

where $x = (x_1, x_2, \ldots, x_n)$ and $u = (u_1, u_2, \ldots, u_m)$. Suppose that the equilibrium points are given by $\overline{x}$ and $\overline{u}$, so that linearisation of $f(x, u)$ about the equilibrium points is given by;

$$f(x,u) \approx \sum_{i=1}^{n} \frac{\partial f}{\partial x}\bigg|_{x_i=\overline{x}_i} (x_i - \overline{x}_i) + \sum_{i=1}^{m} \frac{\partial f}{\partial u}\bigg|_{u_i=\overline{u}_i} (u_i - \overline{u}_i) \tag{A.1.2}$$

by defining the states and inputs as $\partial x_i = x_i - \overline{x}_i$ (for $1 \leq i \leq n$) and $\partial u_i = ui - \overline{u}_i$ (for $1 \leq i \leq m$) the linearised dynamics of state x are given by

$$\partial x = \sum_{i=1}^{n} \frac{\partial f}{\partial x}\bigg|_{x_i=\overline{x}_i} \partial x_i + \sum_{i=1}^{m} \frac{\partial f}{\partial u}\bigg|_{u_i=\overline{u}_i} \partial u_i \tag{A.1.3}$$

A.2 l_p norm of a vector

Assume a vector $u \in \mathbb{R}^x$ can be defined as such

$$||u||_p = \left(\sum_{i=1}^{x} |u_i|^p \right)^{\frac{1}{p}} \text{ for } 1 \leq p \leq \infty \tag{A.2.1}$$

A.3 Euclidean norm of a matrix

The Euclidean norm, also known as Frobenius norm, of a matrix A is defined as the square root of the sum of the absolute squares of its elements,

$$||A||_F = \left(\sum_{i=1}^{m} \sum_{j=1}^{n} |a_{ij}|^2 \right)^{\frac{1}{2}} \tag{A.3.1}$$

A.4 QR Decomposition

Assume a non square matrix $A \in \mathbb{R}^{m \times n}$ with $m \geq n$. Matrix A can then be decomposed into its Q and R components such that,

$$A = QR \tag{A.4.1}$$

where $Q \in \mathbb{R}^{m \times m}$ defines an orthogonal matrix and $Rin\mathbb{R}^{m \times n}$ is upper triangle. If A is of full rank n then,

$$A = (Q_1 \; Q_2) \begin{pmatrix} R_1 \\ 0 \end{pmatrix} \tag{A.4.2}$$

A.5 Singular Value Decomposition

Assume matrix $A \in \mathbb{R}^{m \times n}$ with rank r Then the singular value decomposition of A can be defined as

$$A = U \Sigma V^T = U \begin{pmatrix} \Sigma_r & 0 \\ 0 & 0 \end{pmatrix} V^T \tag{A.5.1}$$

where $U \in \mathbb{R}^{m \times m}$ and $V \in \mathbb{R}^{n \times n}$ are orthogonal and

$$\Sigma_r = \text{diag}(\sigma_1, \sigma_2, \ldots, \sigma_r) \tag{A.5.2}$$

contains the nonzero singular values of A

A.6 Pseudo Inverse

Consider the follow,

$$y = Ax \tag{A.6.1}$$

Given A and y find x. Where $x \in \mathbb{R}^n$, $y \in \mathbb{R}^m$ and $A \in \mathbb{R}^{m \times n}$ such that $m > n$ and $\text{rank}(A) = m$. As $m > n$ the is no unique solution to A.6.1. The pseudo inverse[1] picks the unique minimum norm as such,

$$A^\dagger y = x \tag{A.6.2}$$

where

$$A^\dagger = A^T (A A^T)^{-1} \tag{A.6.3}$$

and $\dagger$ is a pseudo inverse operator.

[1] Also referred to as the *Moore-Penrose inverse*

A.7 Least Squares Problem

Assume the follow minimisation,

$$\min_x ||W(x - x_0)|| \tag{A.7.1}$$
$$\text{s.t. } y = Ax \tag{A.7.2}$$

where W is non singular. The least squares solution to x is as follows[2]

$$x = I - KAx_0 + Ky \tag{A.7.3}$$
$$K = W^{-1}(AW^{-1})^{\dagger} \tag{A.7.4}$$

[2] a proof can be found in Harkengard[36]

APPENDIX B

B.1 Algorithm for Sequential Least Squares

Let u_0 be a feasible starting point, and the working set W_S contain the active inequality constraint at u^0

for $i = 0, 1, 2, \ldots$

Given a suboptimal u^i, find the optimal perturbation p, considering the inequity in the working set as equity constraints and disregarding the remaining inequality constraints. Solve

$$\begin{aligned} c \quad & \min_p ||A(u^i + p) - b||_2 \\ & Bp = 0 \\ & p_i = 0, \ i \in W_S \end{aligned} \tag{B.1.1}$$

if $u^i + p$ is feasible, Set $u^{i+1} = u^i + p$ and compute the Lagrange multipliers.

if all $\lambda \geq 0$, u^{i+1} is optimal, so then let $u = u^{i+1}$

else Remove the constraint association with the most negative λ from the working set W_S.

else Determine the maximum step length α such that $u^{i+1} = u^i + \alpha p$is feasible. Add the bounding constraint at u^{i+1} to the working set.

end

APPENDIX C

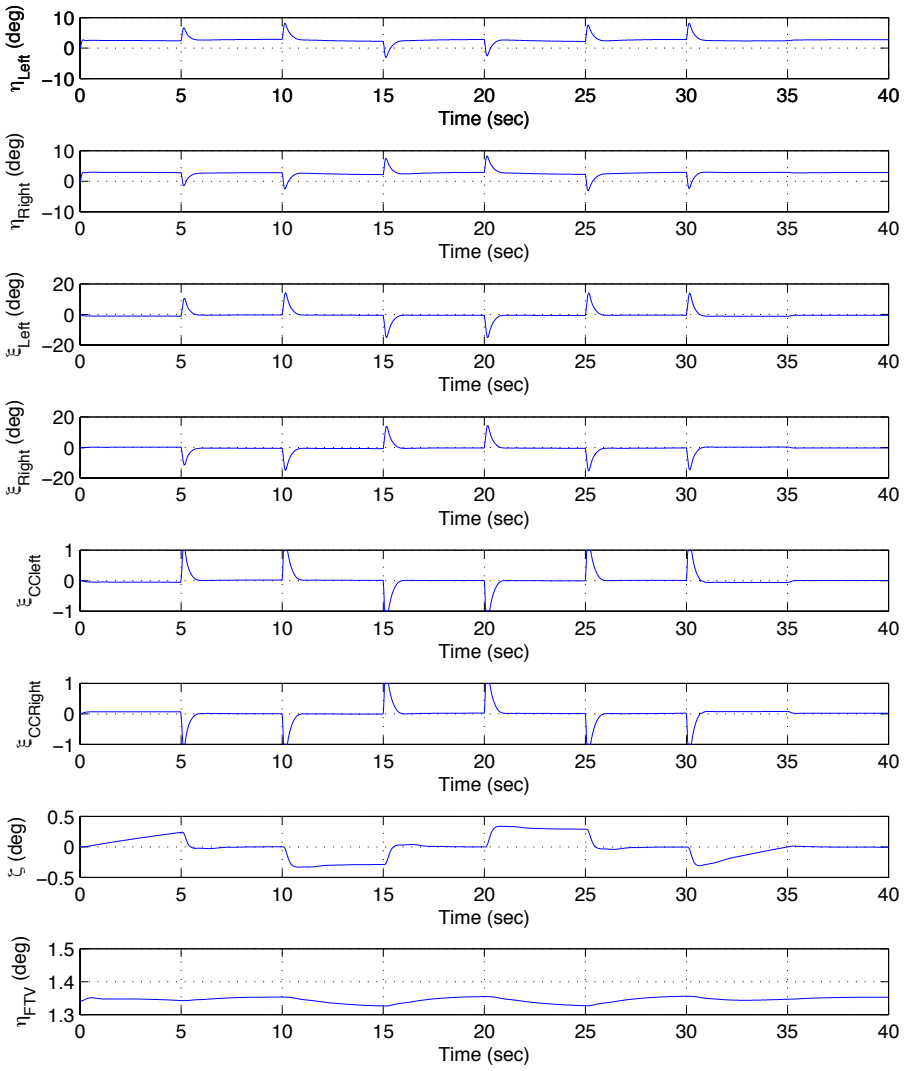

Figure C.1: Effector distribution for Minimum Deflection Control Allocation Method - Simulation 1

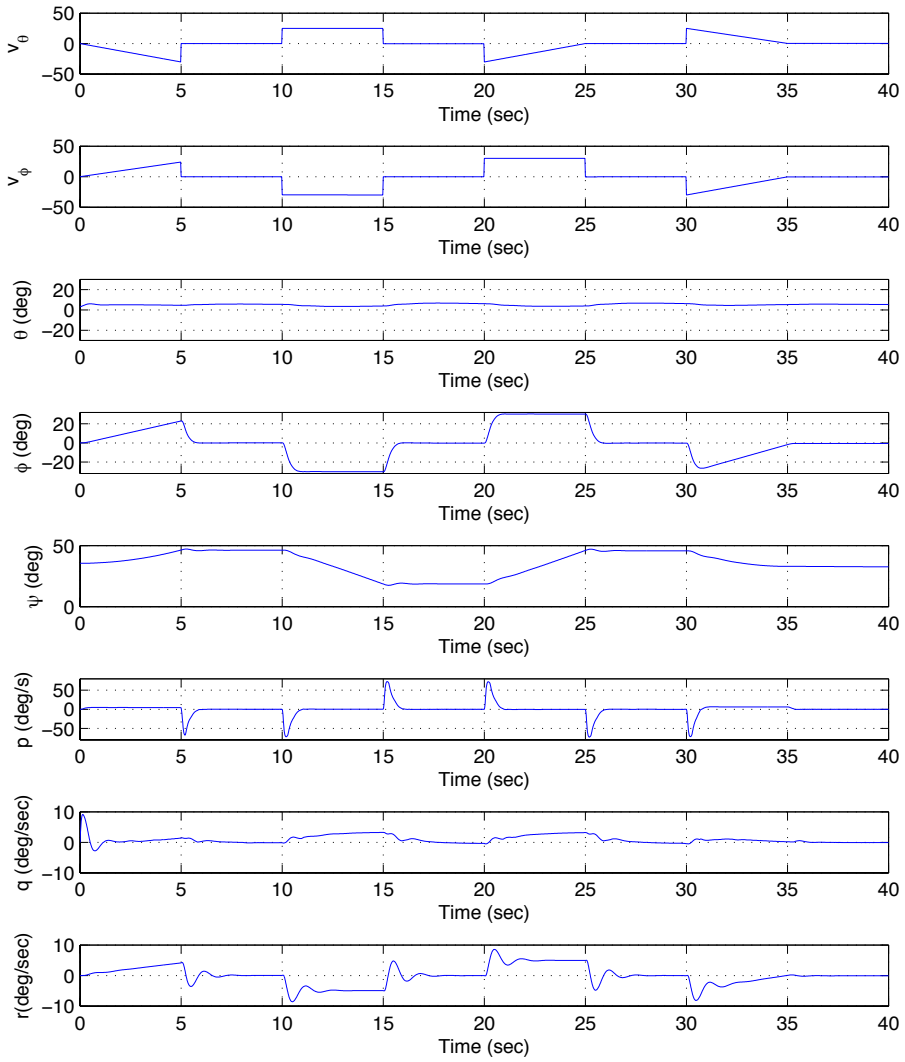

Figure C.2: States for Minimum Deflection Control Allocation Method - Simulation 1

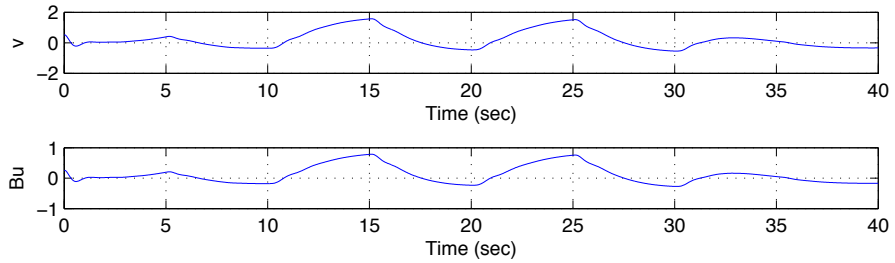

Figure C.3: v,Bu for Minimum Deflection Control Allocation Method - Simulation 1

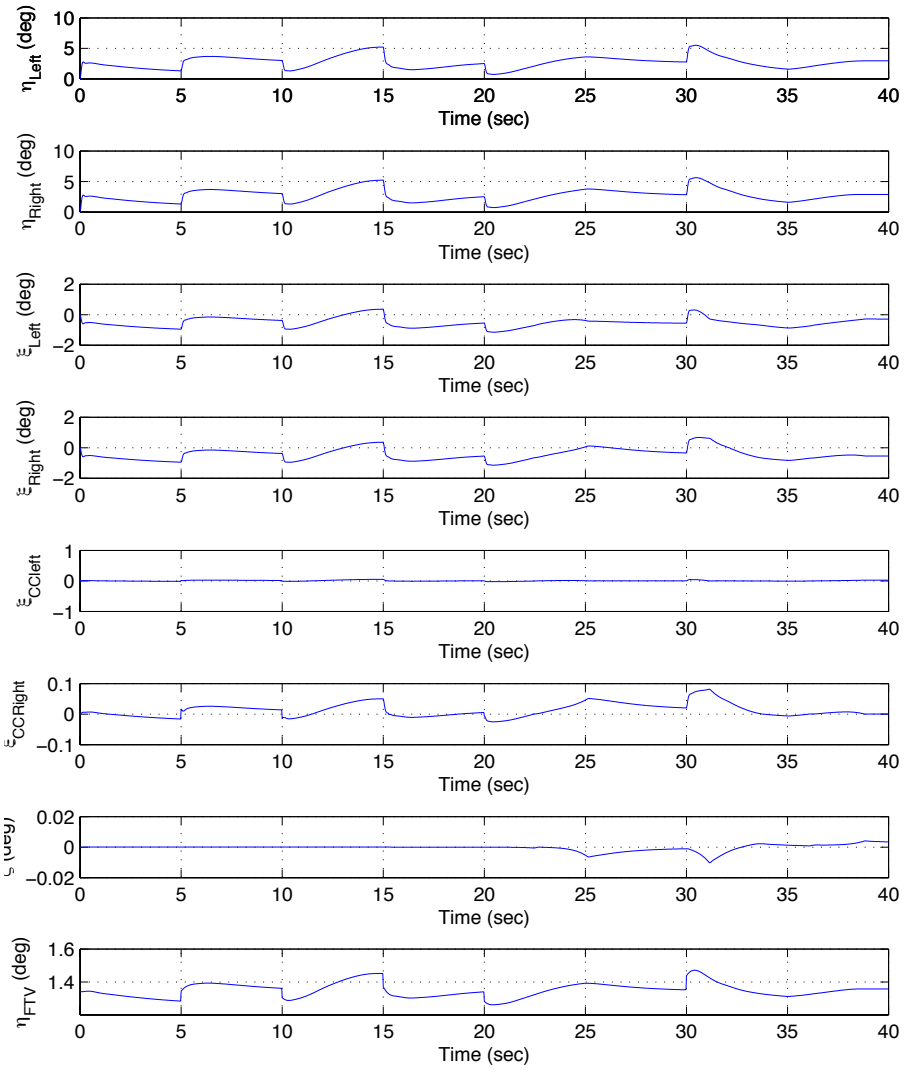

Figure C.4: Effector distribution for Minimum Deflection Control Allocation Method - Simulation 2

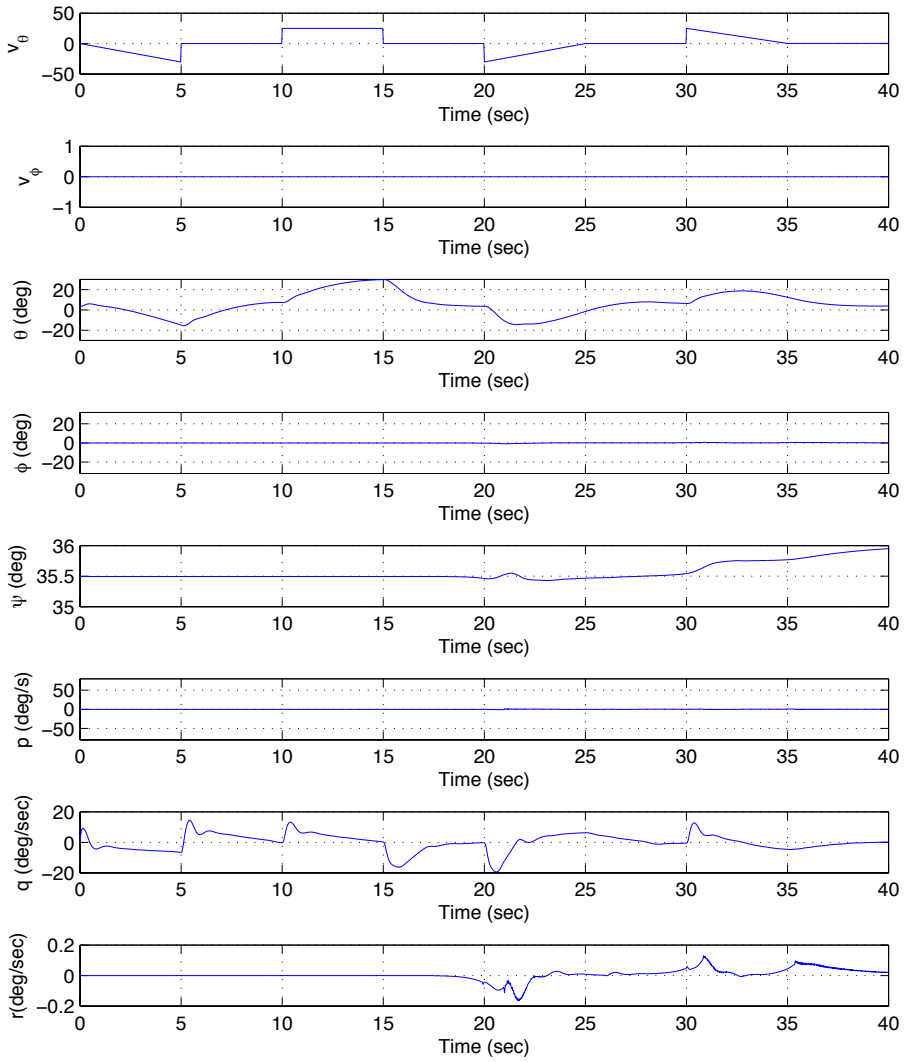

Figure C.5: States for Minimum Deflection Control Allocation Method - Simulation 2

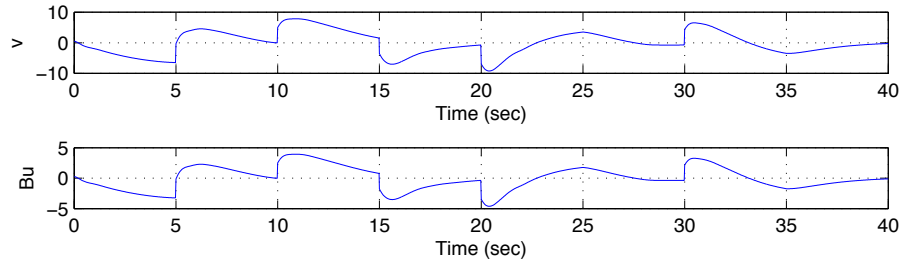

Figure C.6: v,Bu for Minimum Deflection Control Allocation Method - Simulation 2

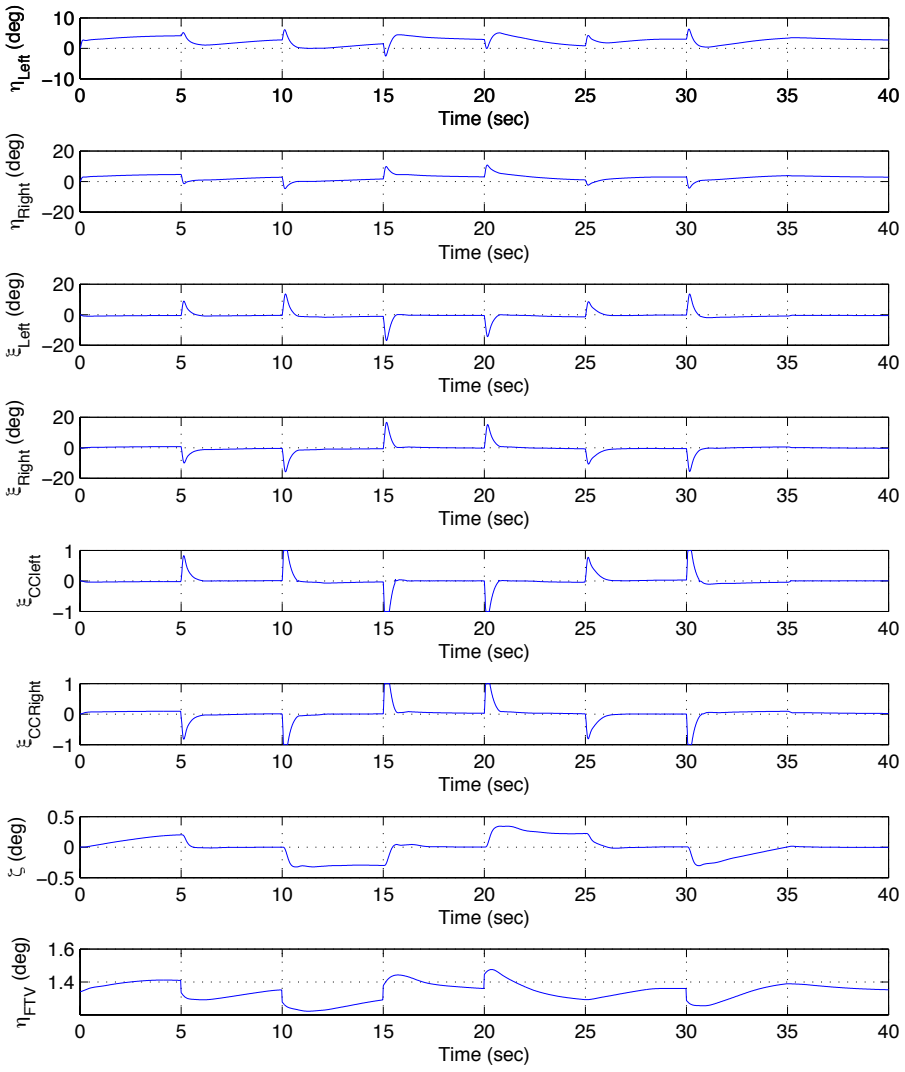

Figure C.7: Effector distribution for Minimum Deflection Control Allocation Method - Simulation 3

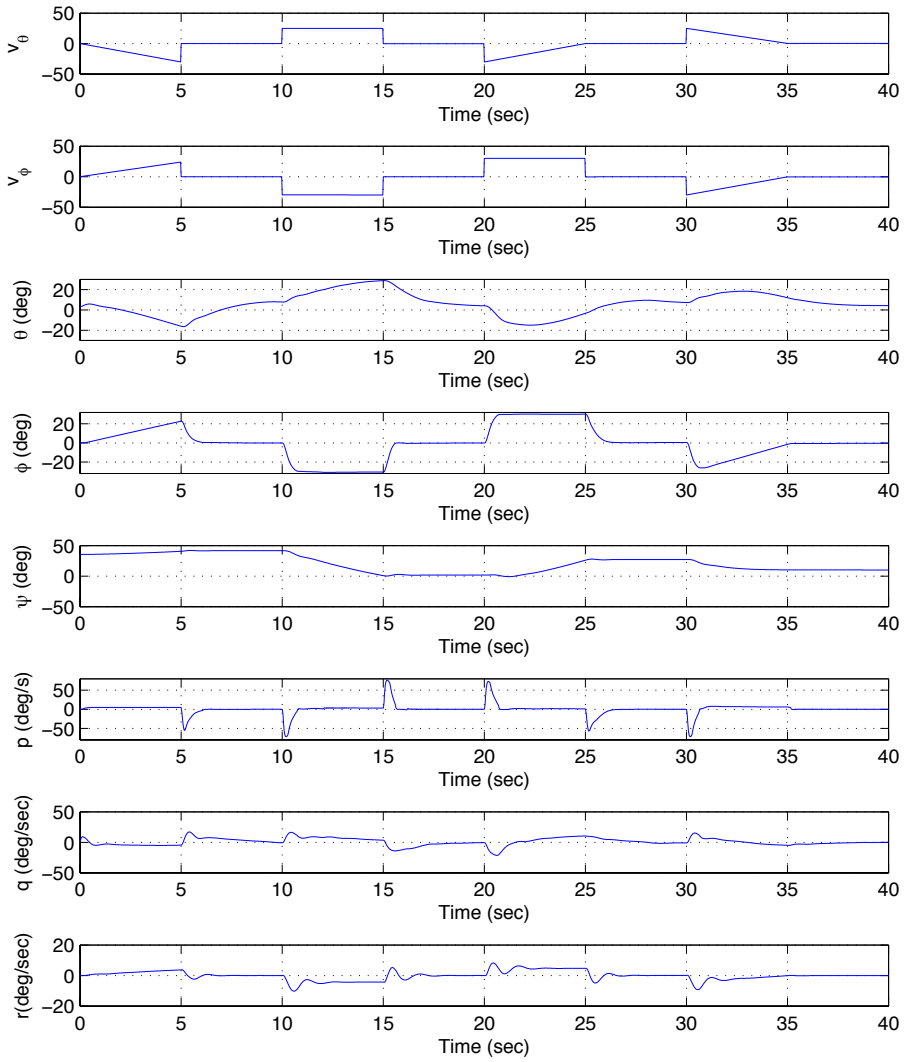

Figure C.8: States for Minimum Deflection Control Allocation Method - Simulation 3

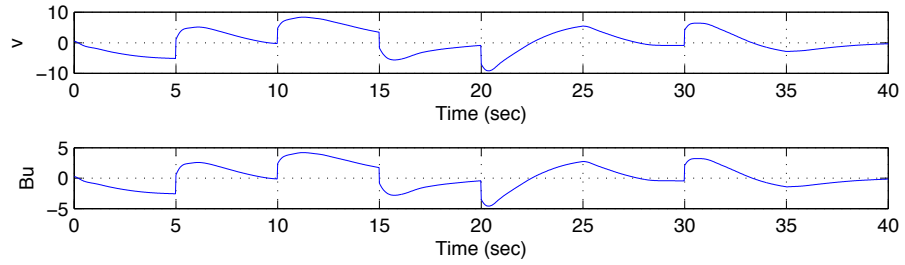

Figure C.9: v,Bu for Minimum Deflection Control Allocation Method - Simulation 3

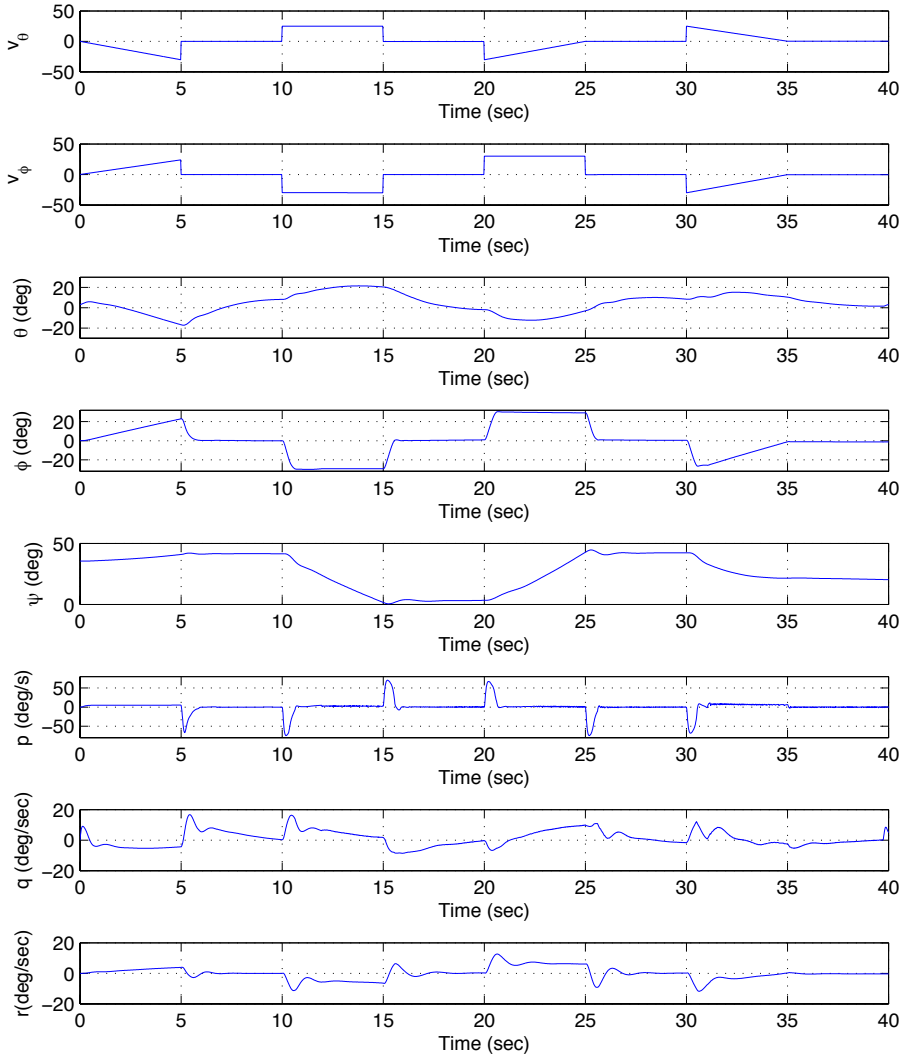

Figure C.10: Effector distribution for Minimum Deflection Control Allocation Method - Simulation 4

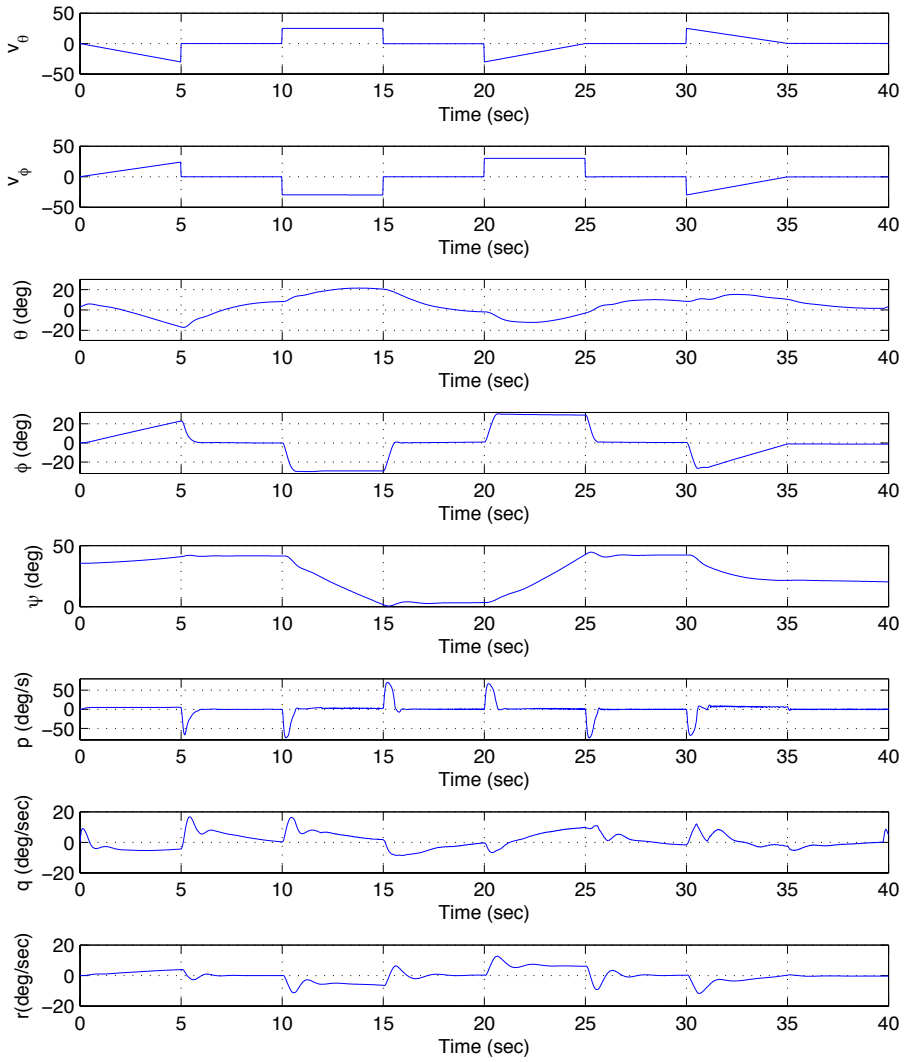

Figure C.11: States for Minimum Deflection Control Allocation Method - Simulation 4

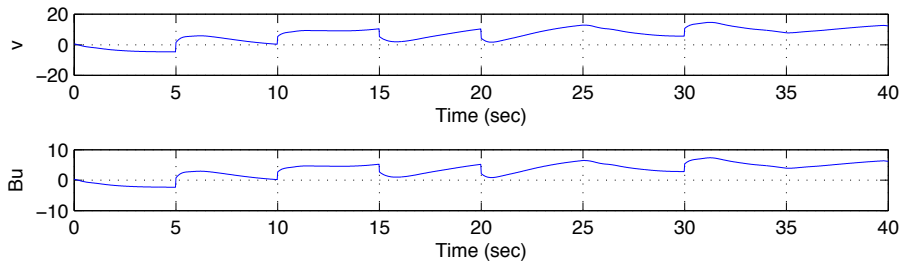

Figure C.12: v,Bu for Minimum Deflection Control Allocation Method - Simulation 4

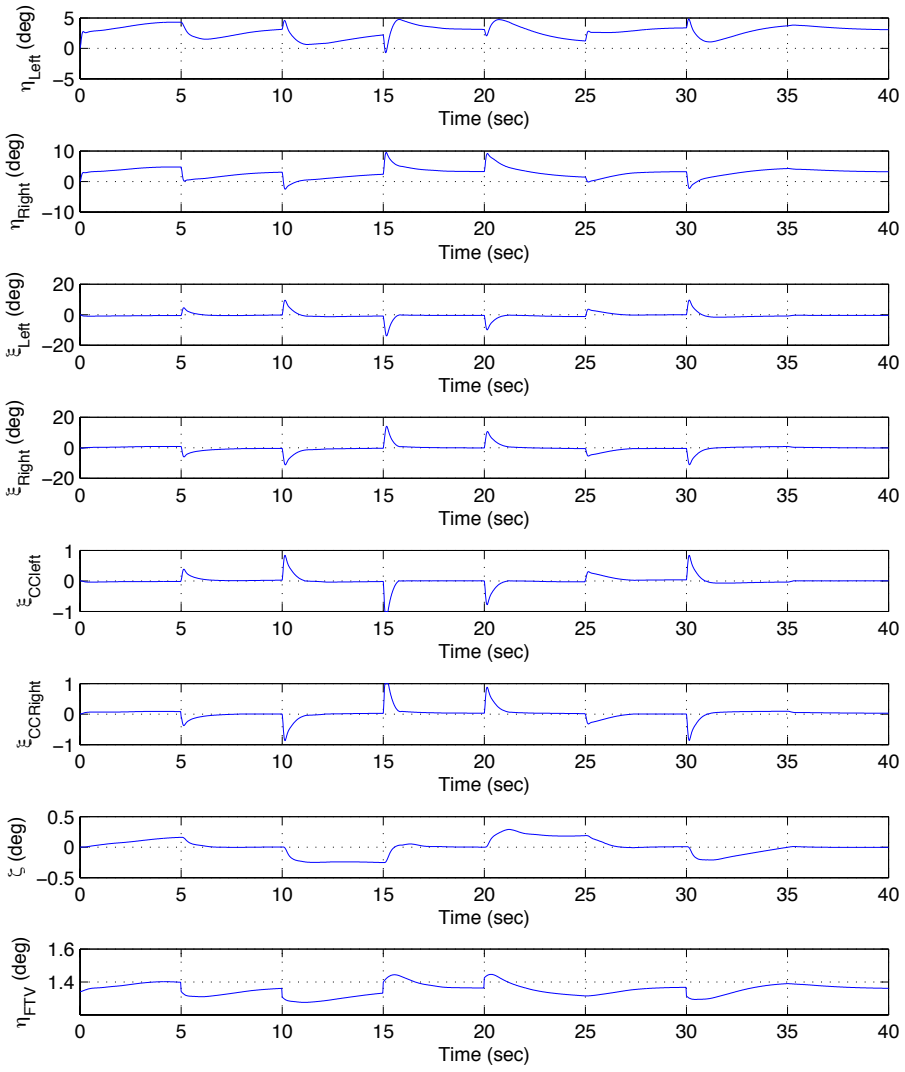

Figure C.13: Effector distribution for Minimum Deflection Control Allocation Method - Simulation 5

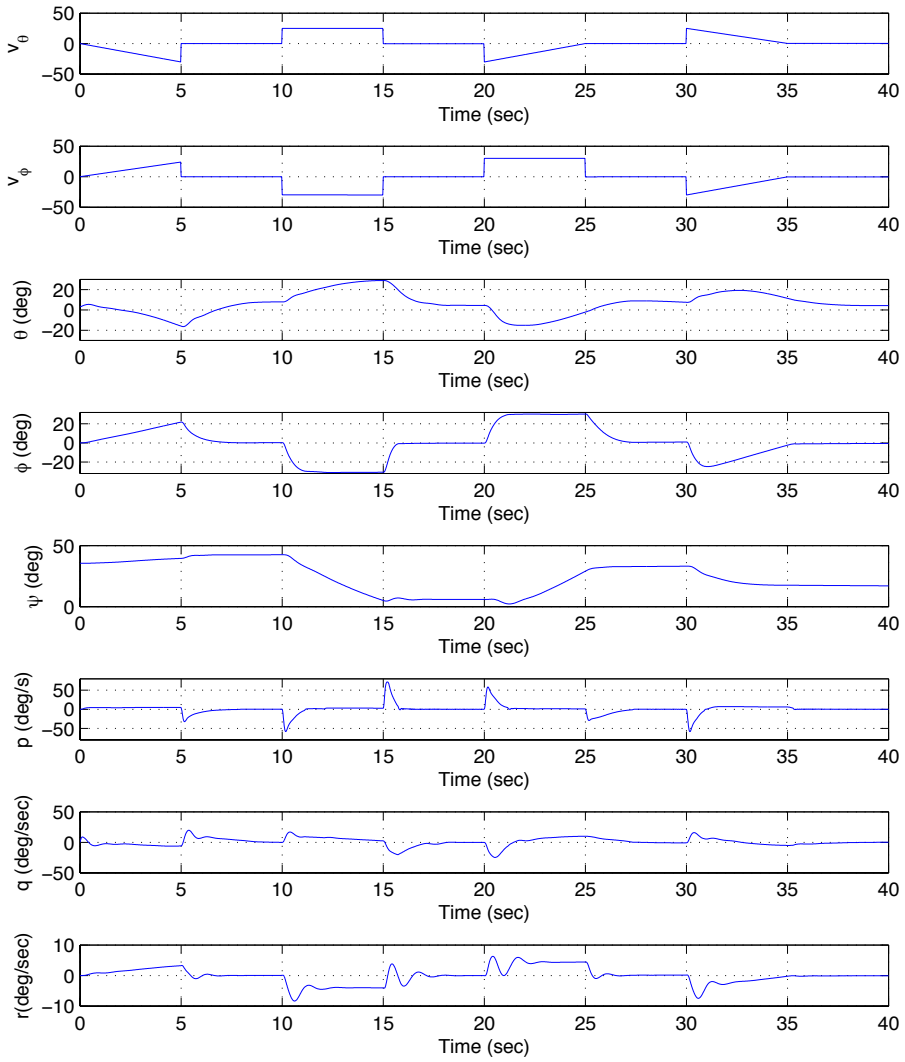

Figure C.14: States for Minimum Deflection Control Allocation Method - Simulation 5

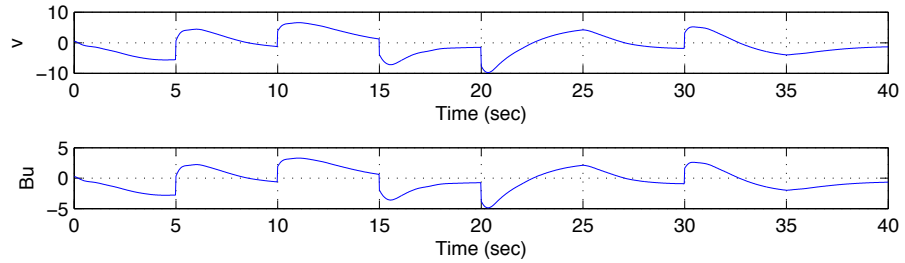

Figure C.15: v,Bu for Minimum Deflection Control Allocation Method - Simulation 5

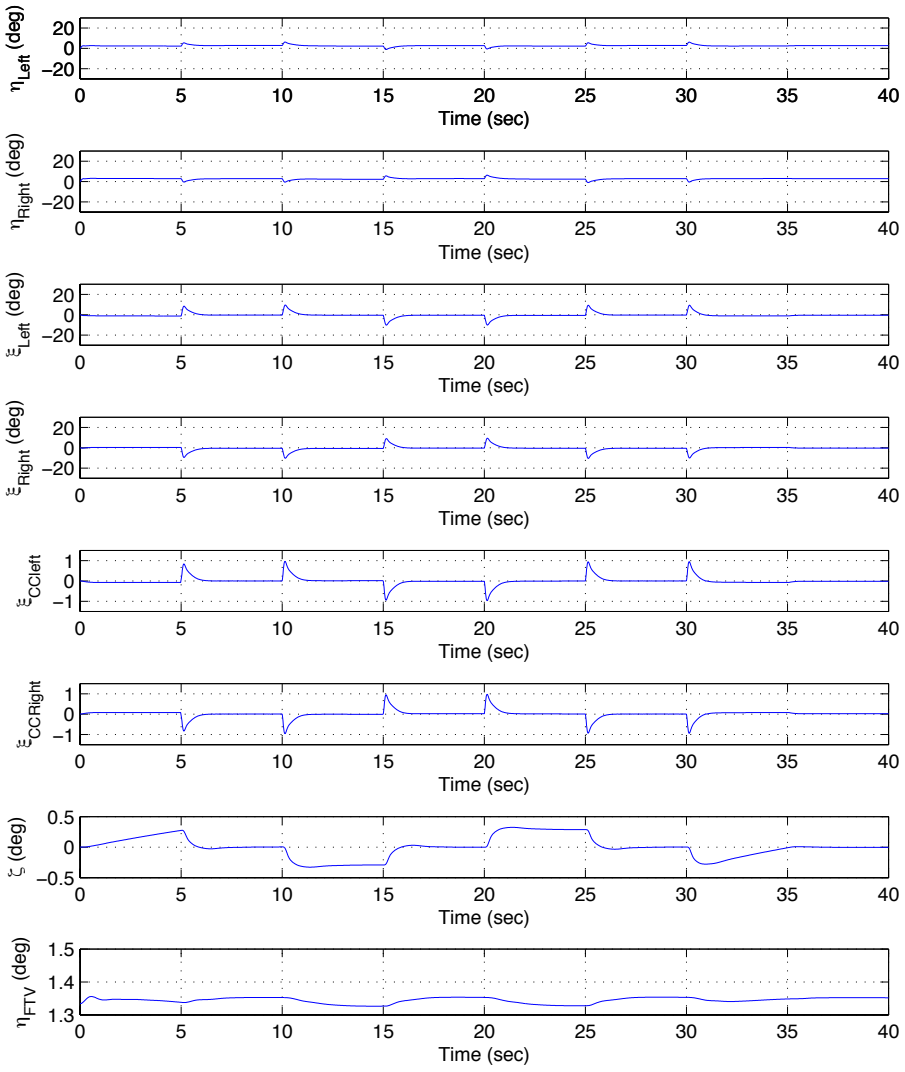

Figure C.16: Effector distribution for Rate Deflection Control Allocation Method - Simulation 6

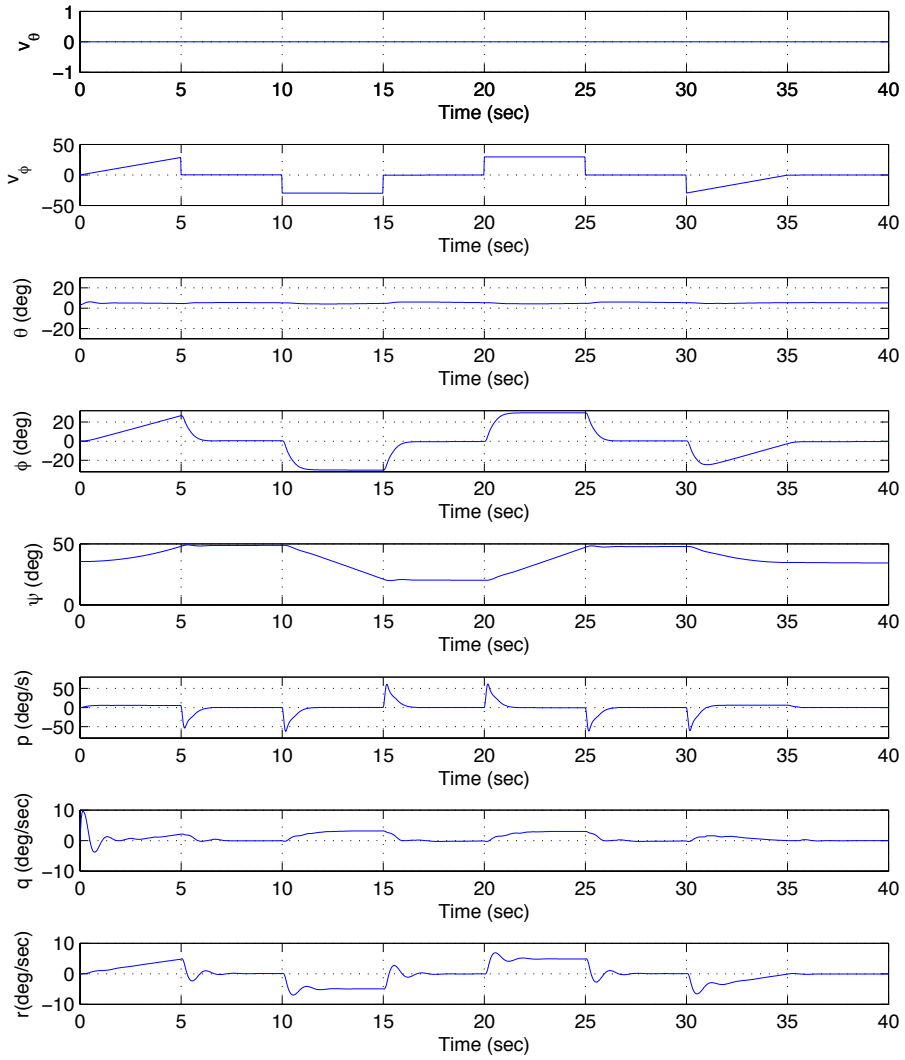

Figure C.17: States for Minimum Rate Control Allocation Method - Simulation 6

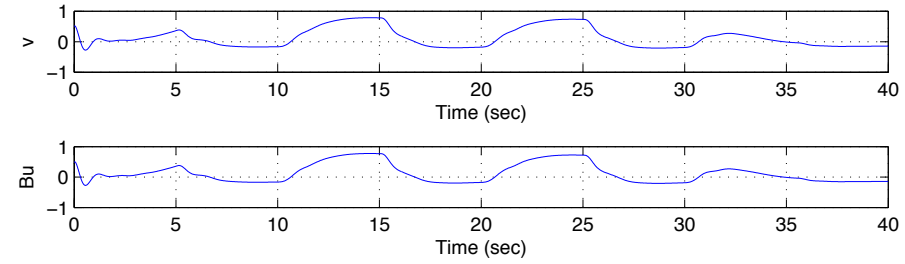

Figure C.18: v,Bu for Minimum Rate Control Allocation Method - Simulation 6

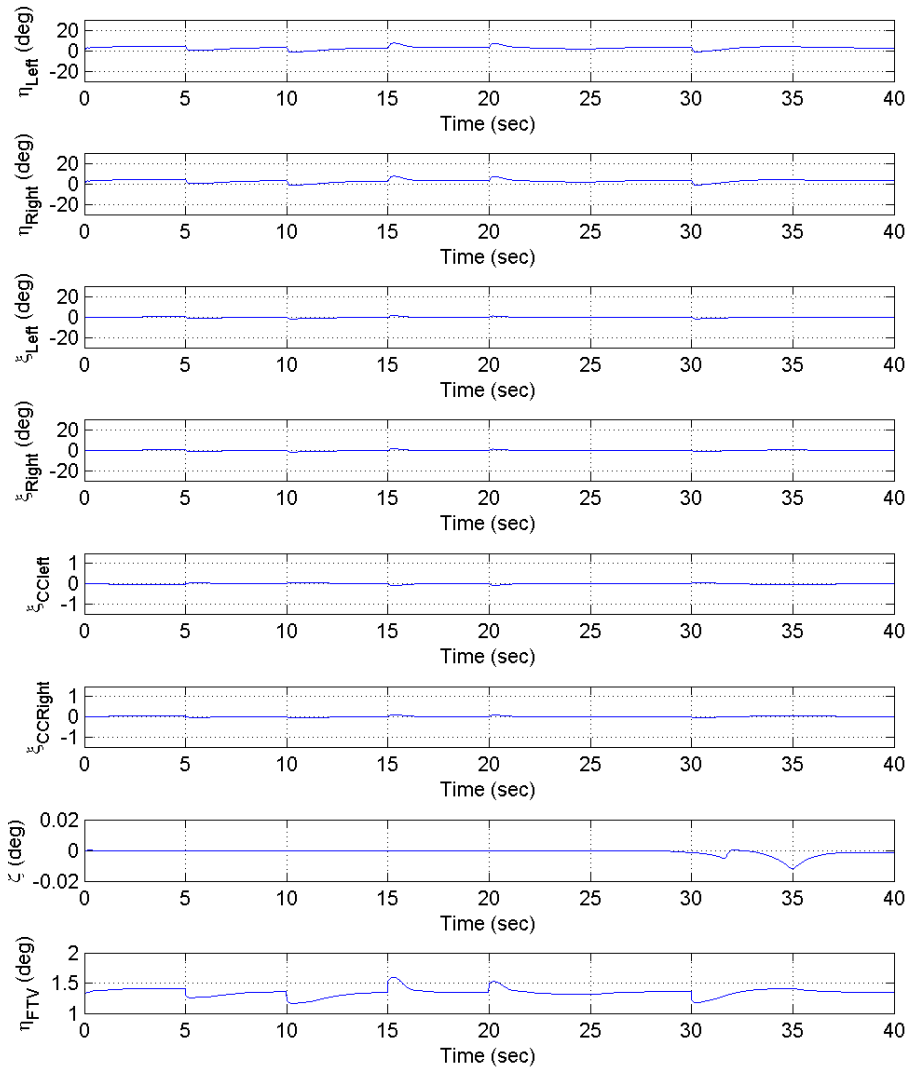

Figure C.19: Effector distribution for Rate Deflection Control Allocation Method - Simulation 7

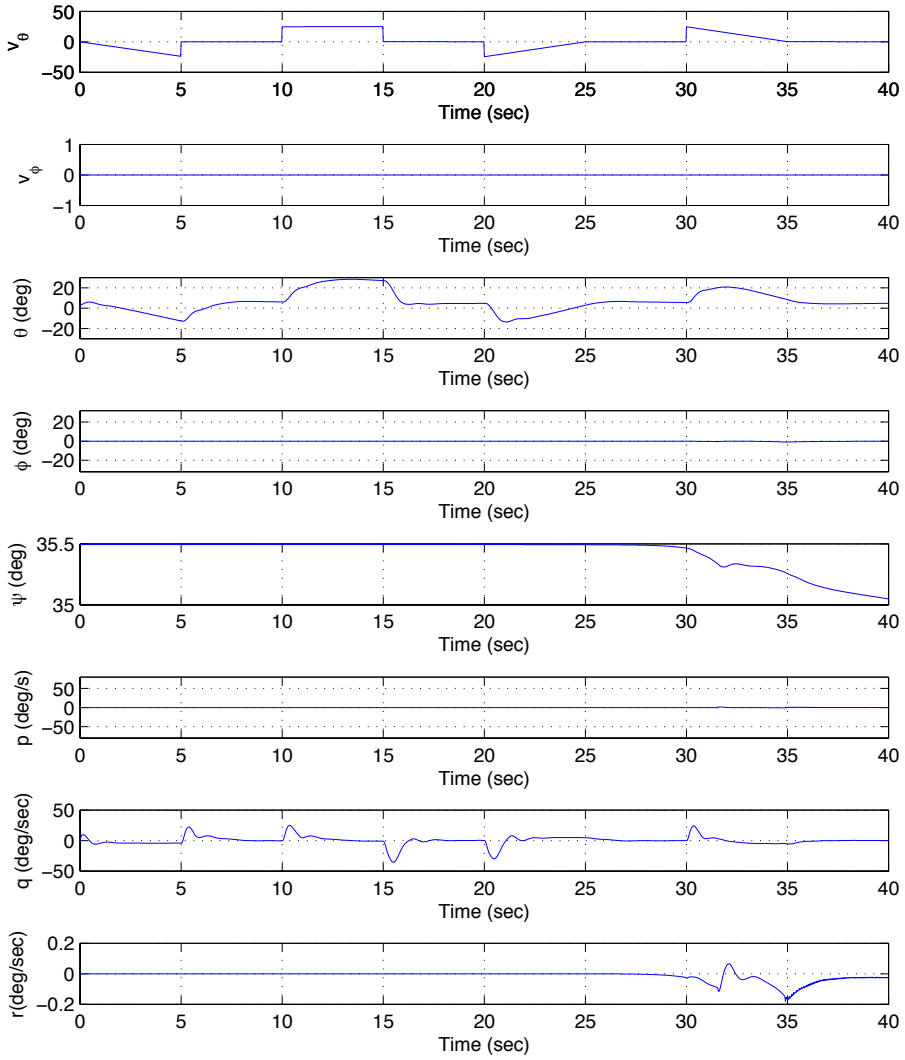

Figure C.20: States for Minimum Rate Control Allocation Method - Simulation 7

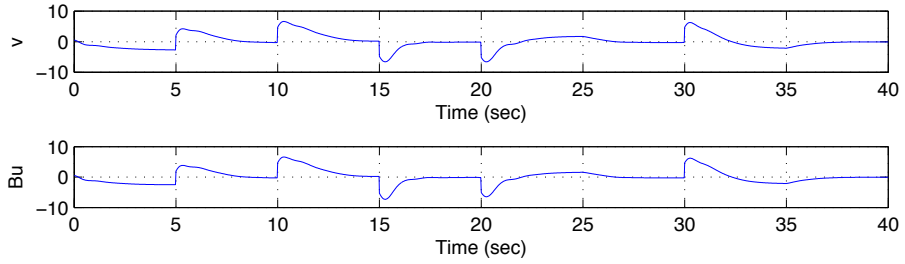

Figure C.21: v,Bu for Minimum Rate Control Allocation Method - Simulation 7

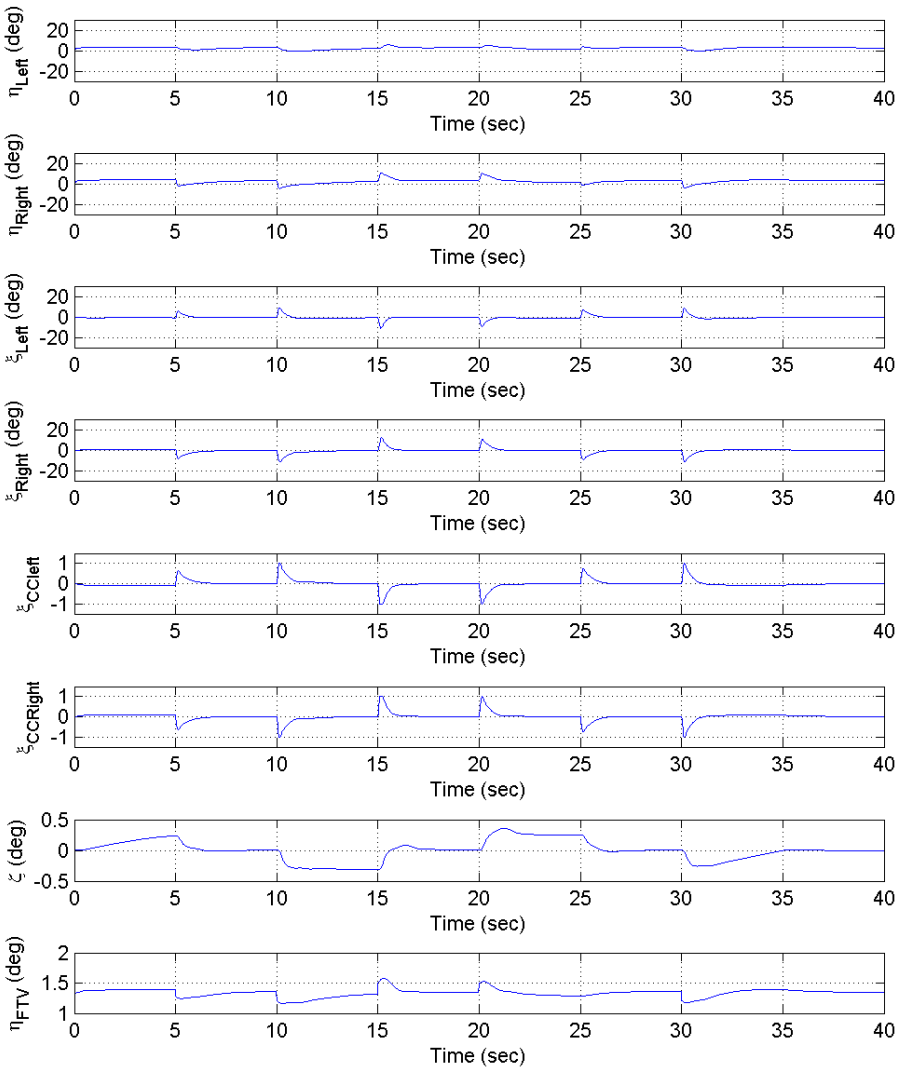

Figure C.22: Effector distribution for Rate Deflection Control Allocation Method - Simulation 8

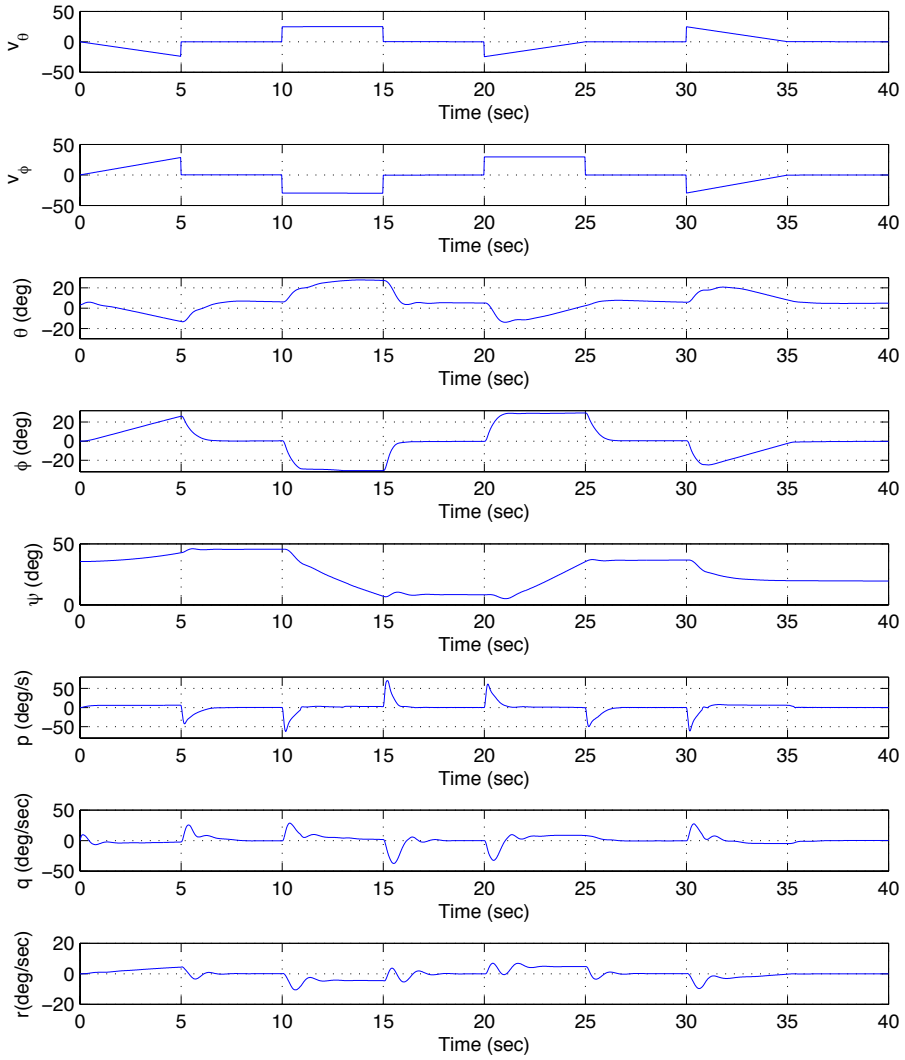

Figure C.23: States for Minimum Rate Control Allocation Method - Simulation 8

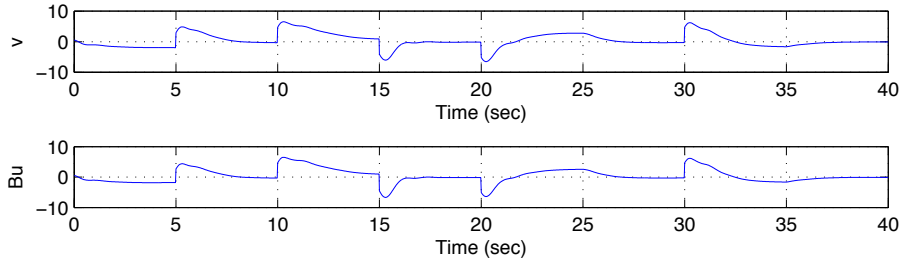

Figure C.24: v,Bu for Minimum Rate Control Allocation Method - Simulation 8

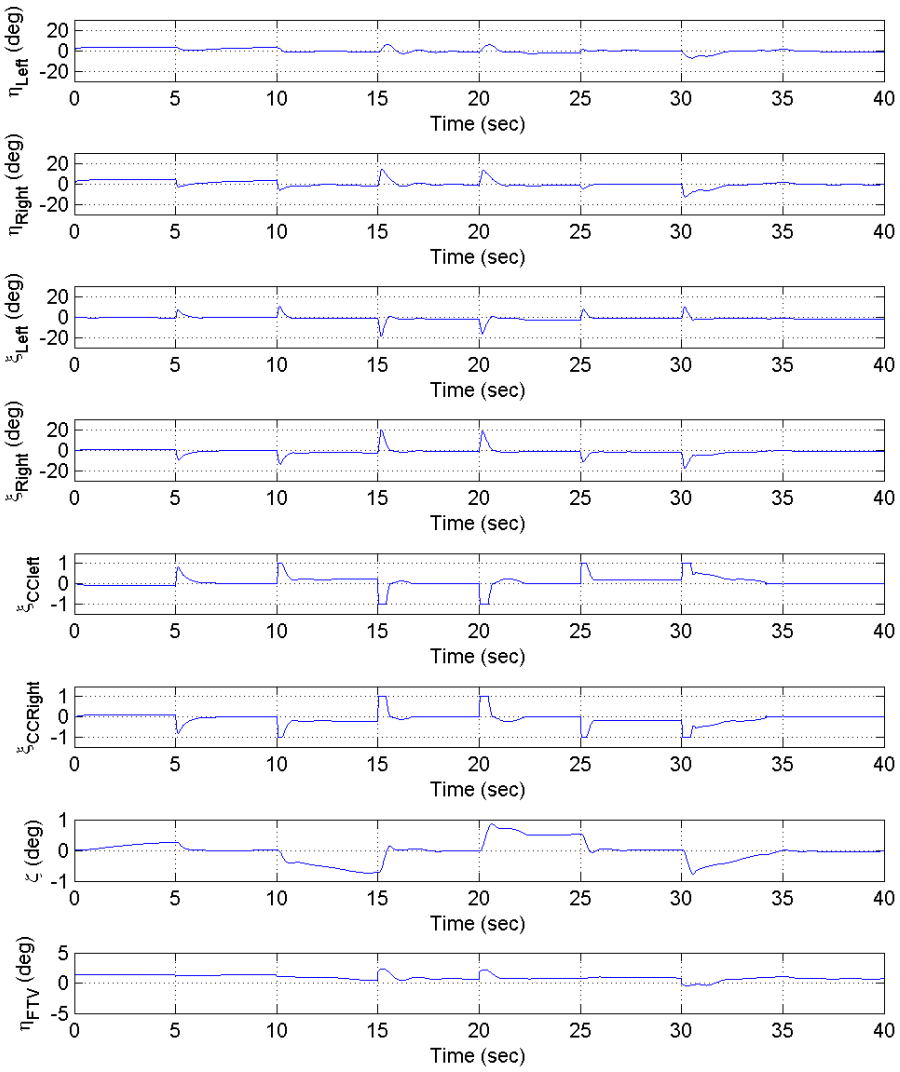

Figure C.25: Effector distribution for Rate Deflection Control Allocation Method - Simulation 9

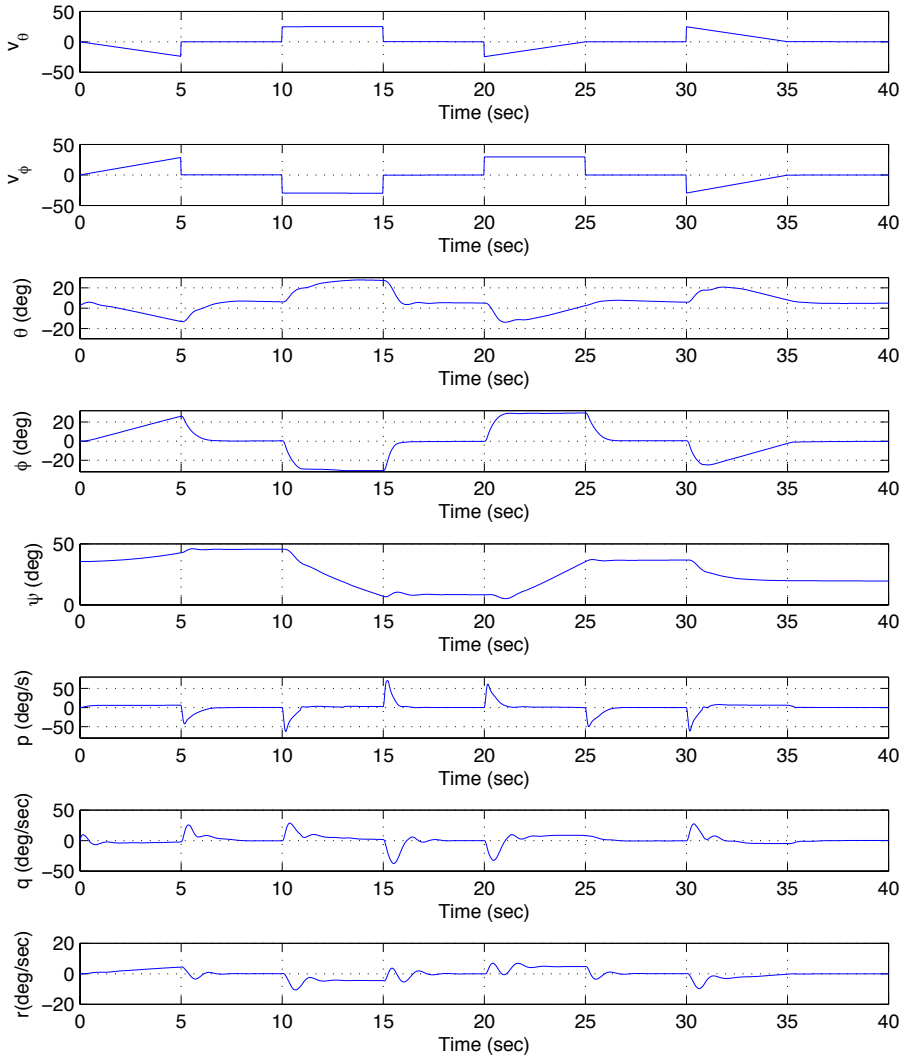

Figure C.26: States for Minimum Rate Control Allocation Method - Simulation 9

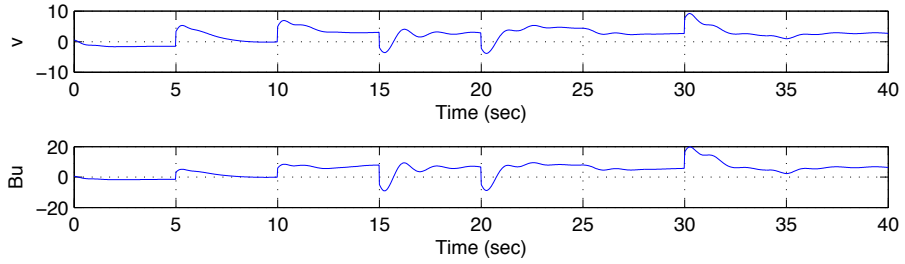

Figure C.27: v,Bu for Minimum Rate Control Allocation Method - Simulation 9

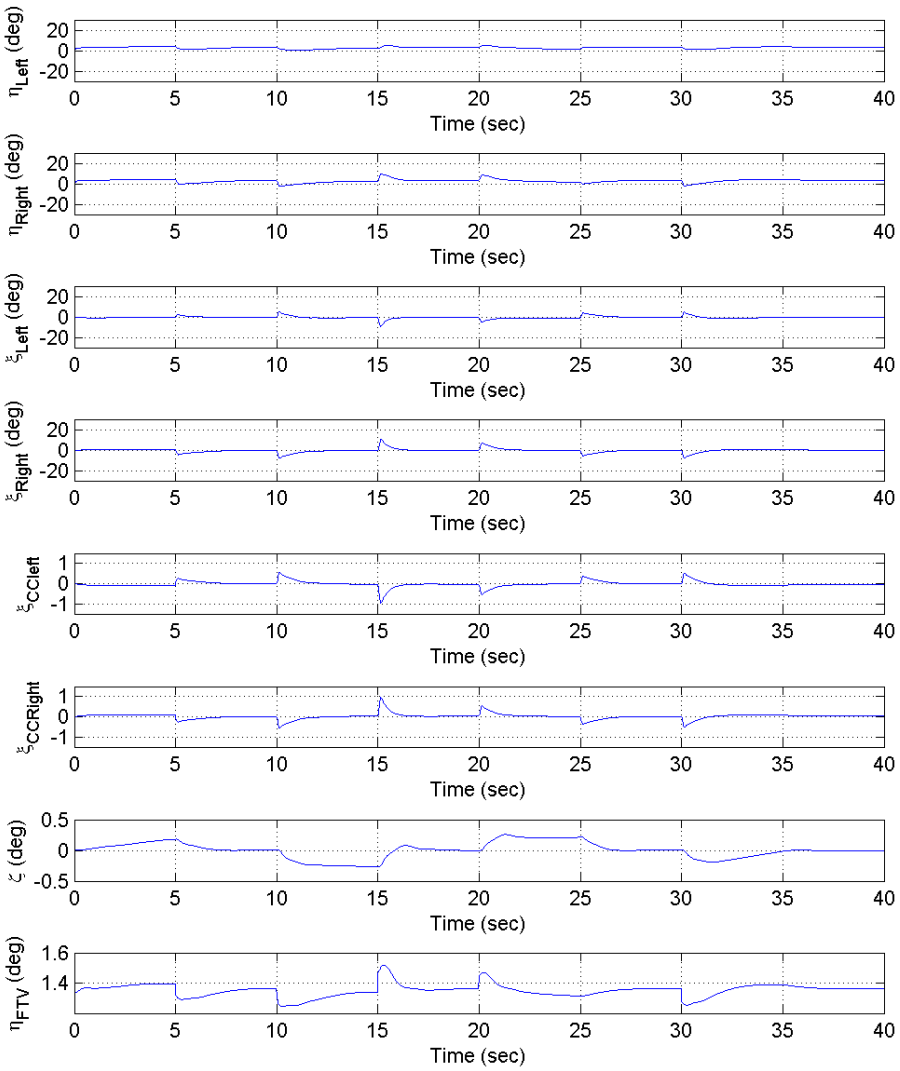

Figure C.28: Effector distribution for Rate Deflection Control Allocation Method - Simulation 9

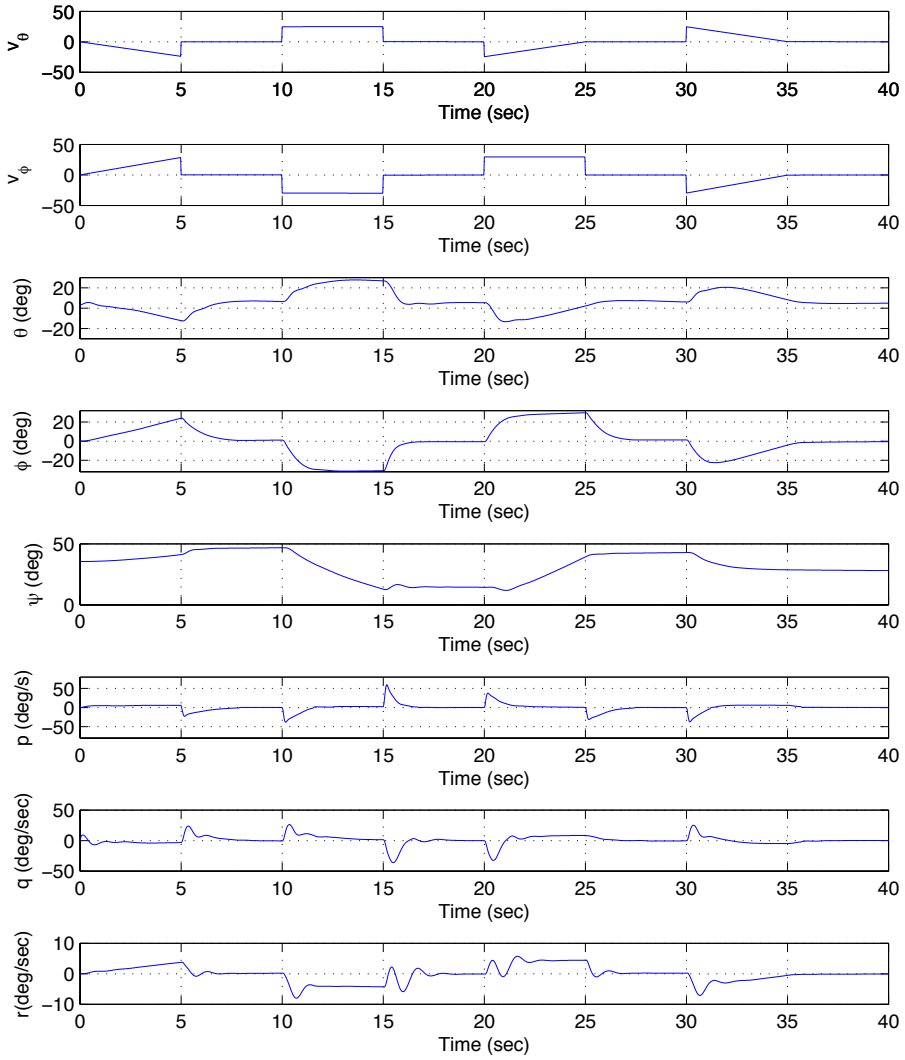

Figure C.29: States for Minimum Rate Control Allocation Method - Simulation 9

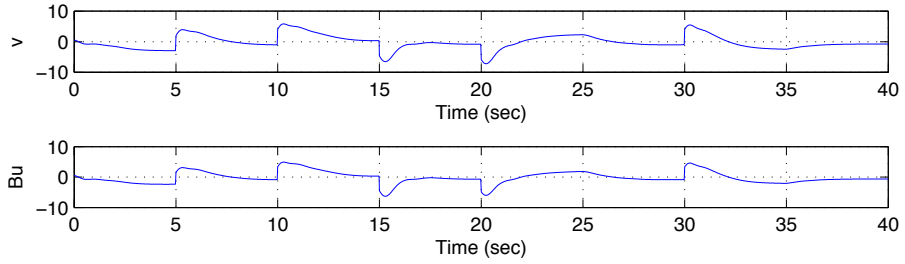

Figure C.30: v,Bu for Minimum Rate Control Allocation Method - Simulation 9

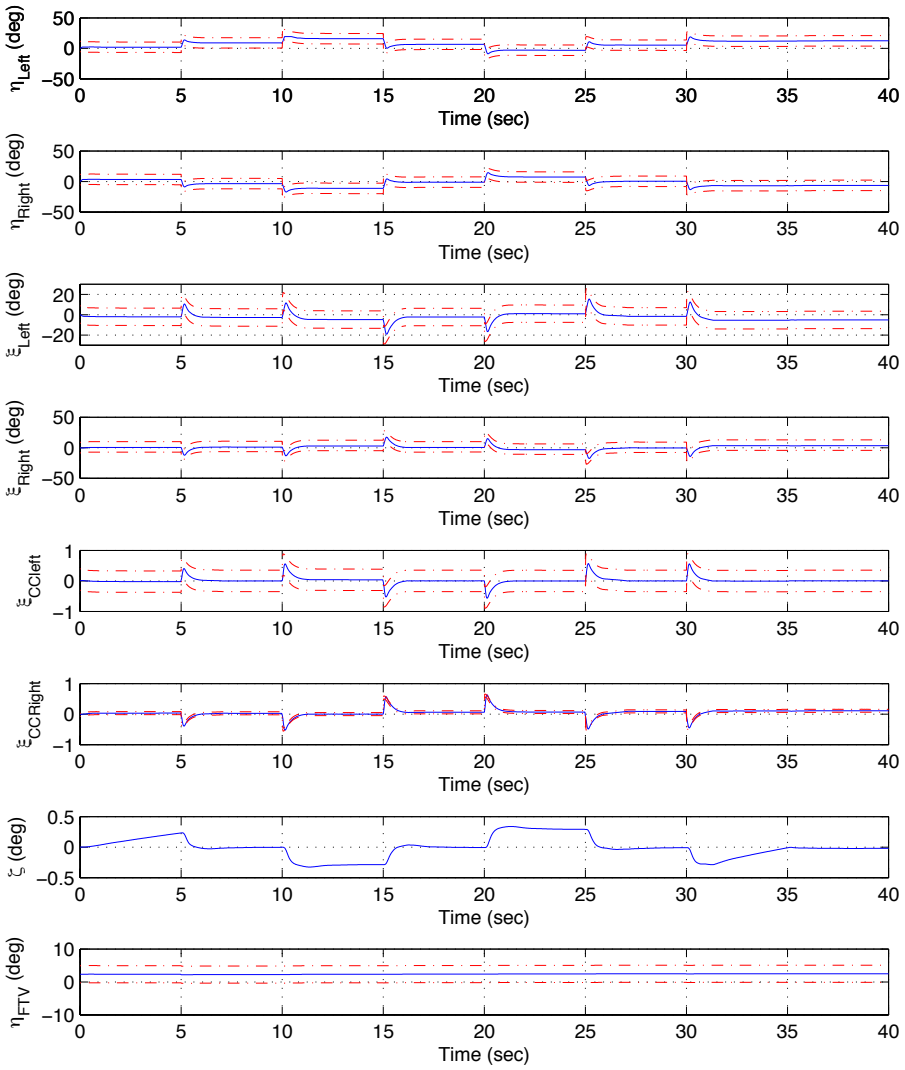

Figure C.31: Effector distribution for Minimum Deflection Control Allocation Method - Simulation 11

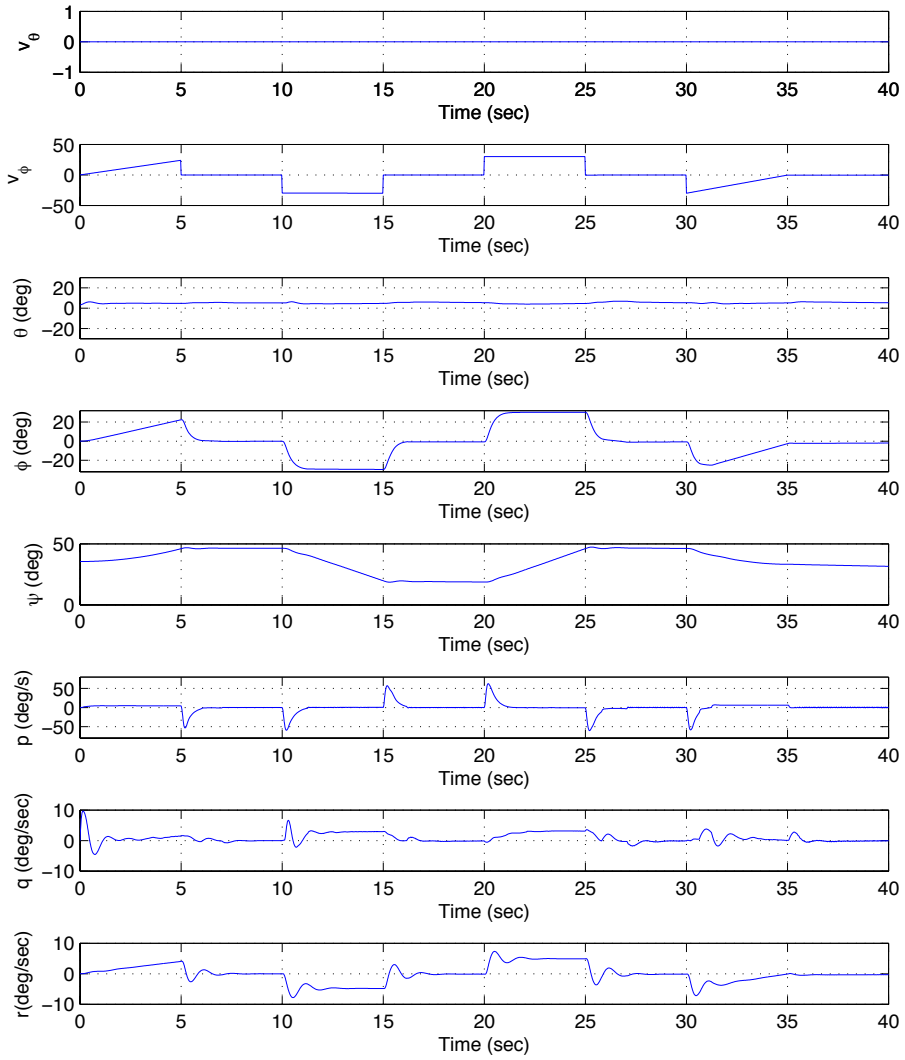

Figure C.32: States for Weighted Control Allocation - Simulation 11

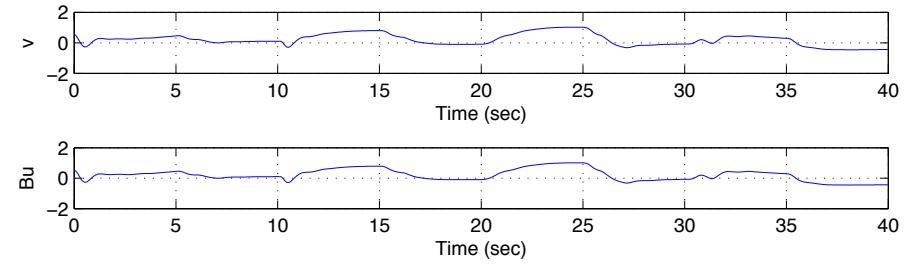

Figure C.33: v,Bu for Minimum Deflection Control Allocation Method - Simulation 11

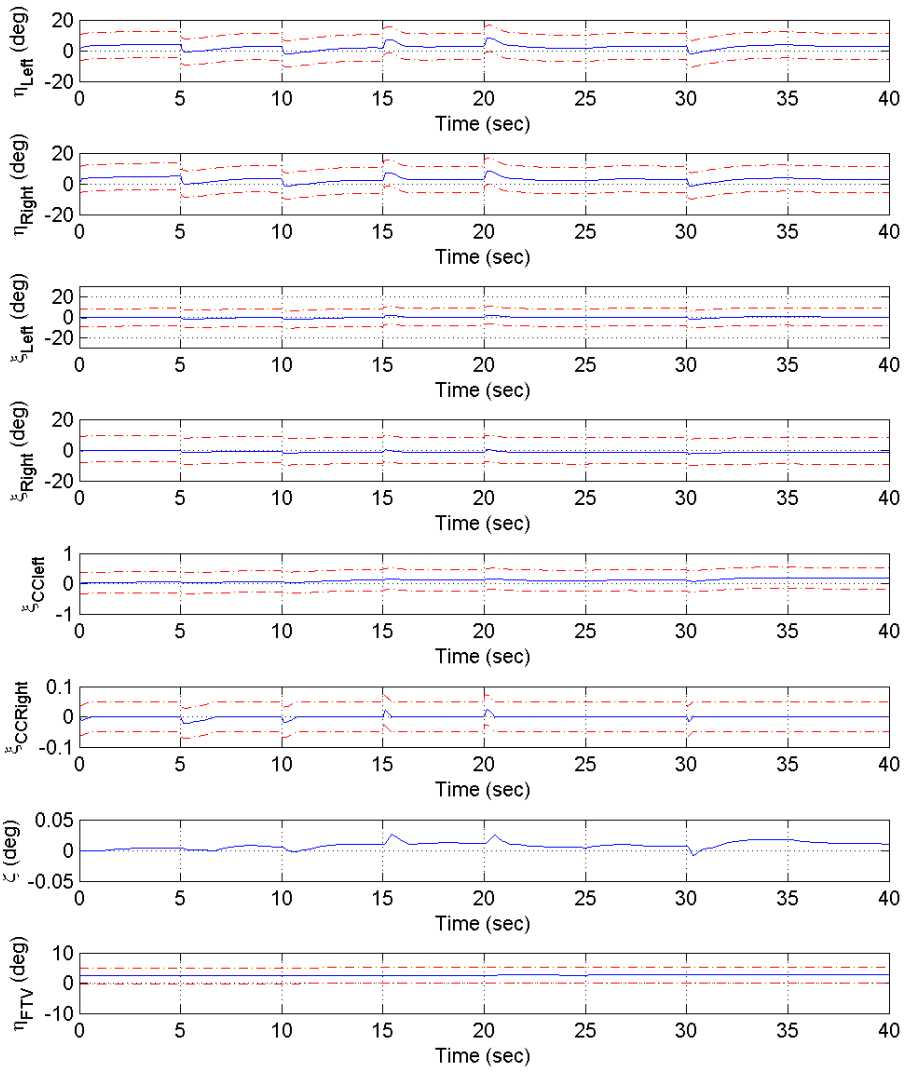

Figure C.34: Effector distribution for Minimum Deflection Control Allocation Method - Simulation 12

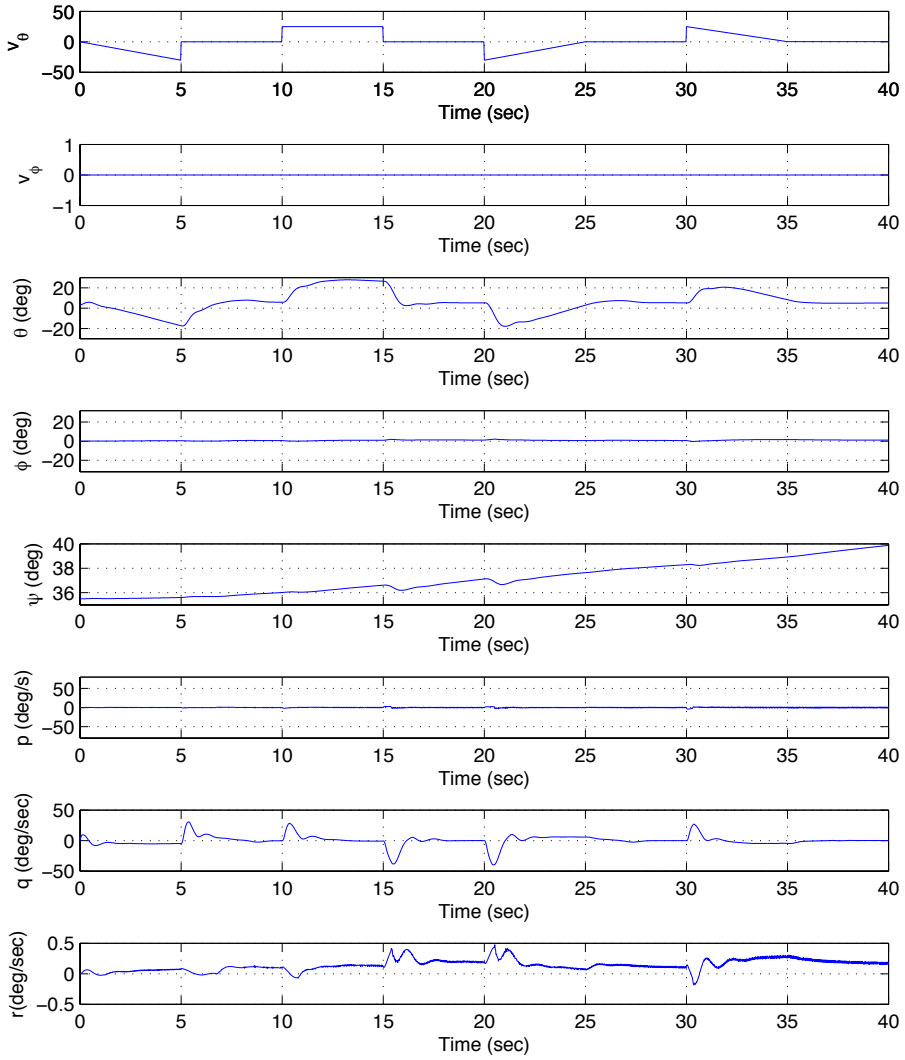

Figure C.35: States for Weighted Control Allocation - Simulation 12

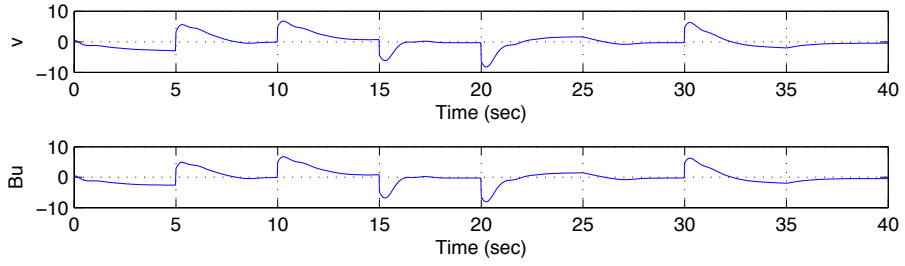

Figure C.36: v,Bu for Minimum Deflection Control Allocation Method - Simulation 12

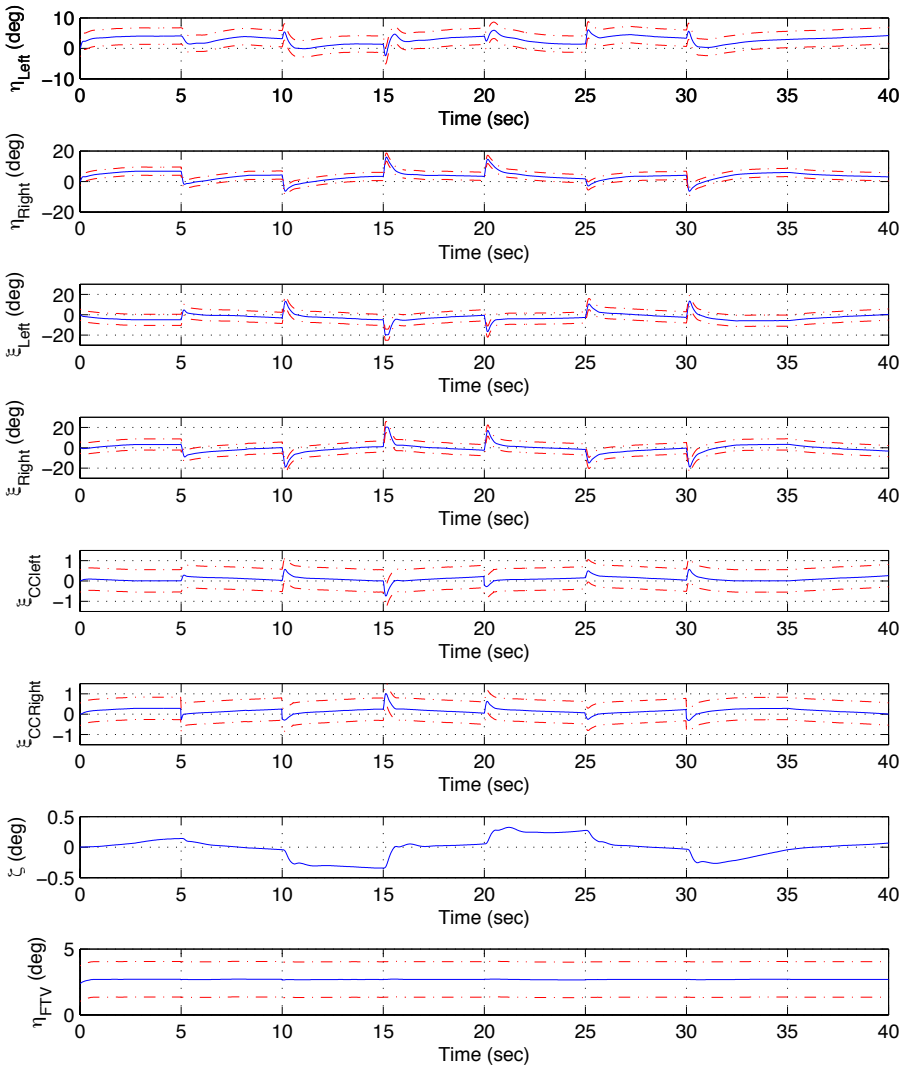

Figure C.37: Effector distribution for Minimum Deflection Control Allocation Method - Simulation 13

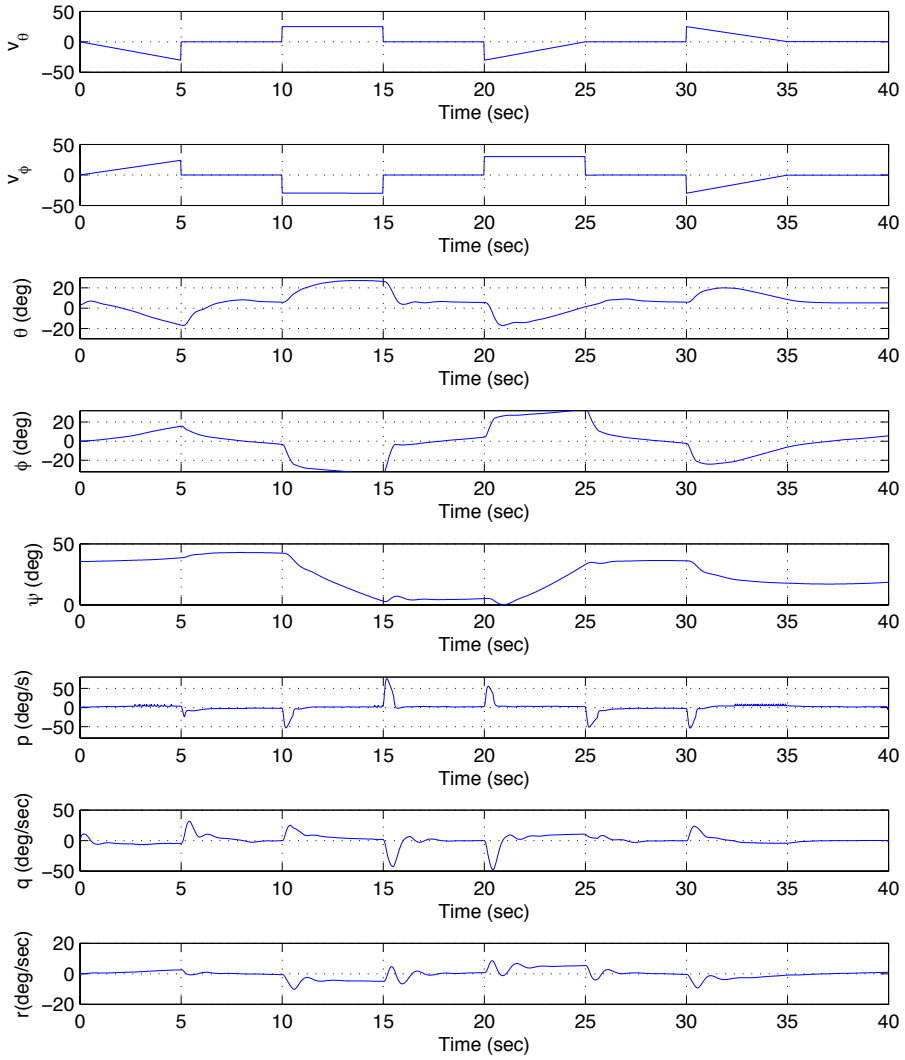

Figure C.38: States for Weighted Control Allocation - Simulation 13

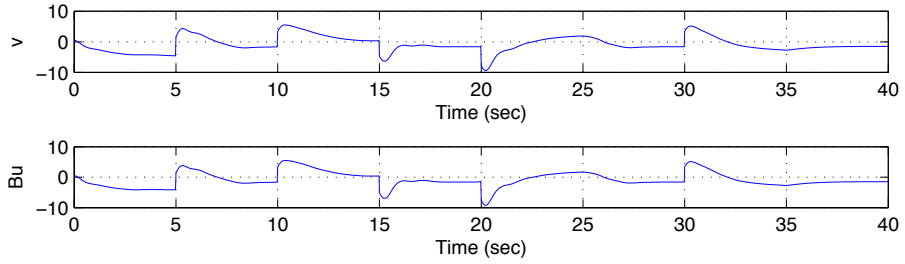

Figure C.39: v,Bu for Minimum Deflection Control Allocation Method - Simulation 13

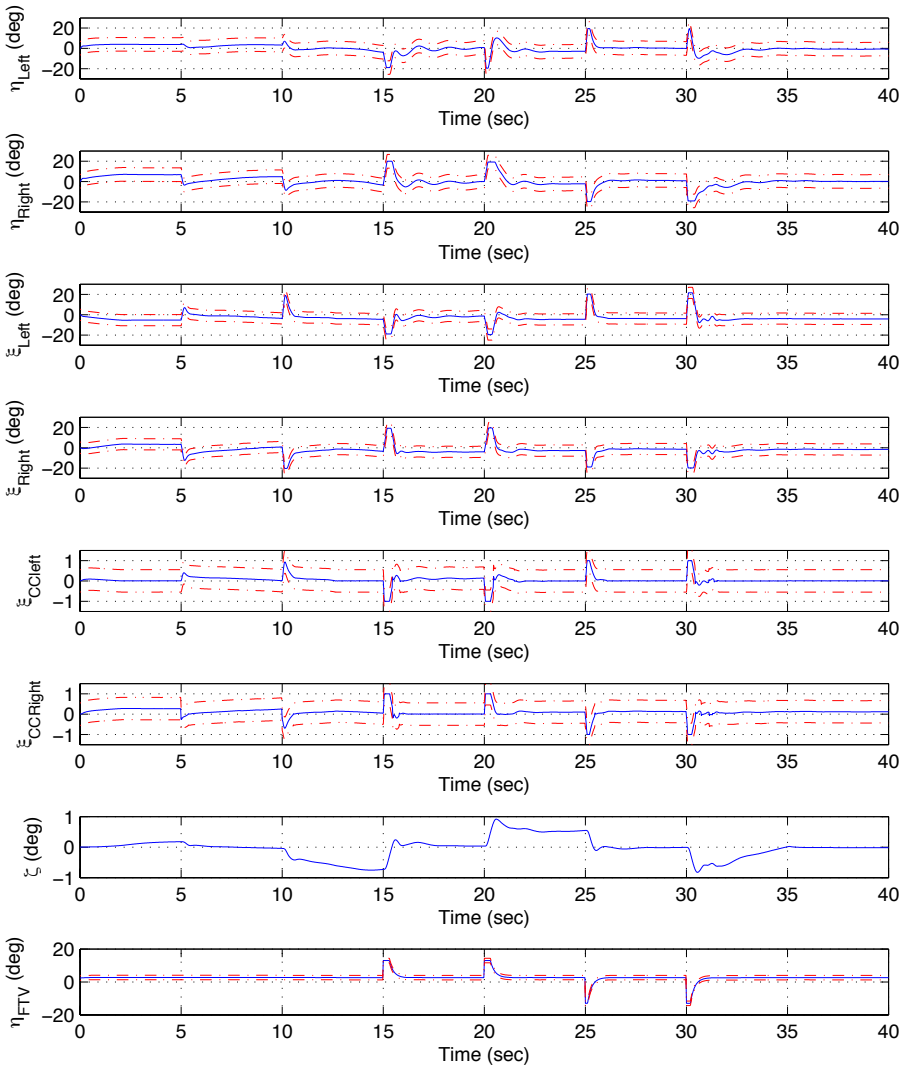

Figure C.40: Effector distribution for Minimum Deflection Control Allocation Method - Simulation 14

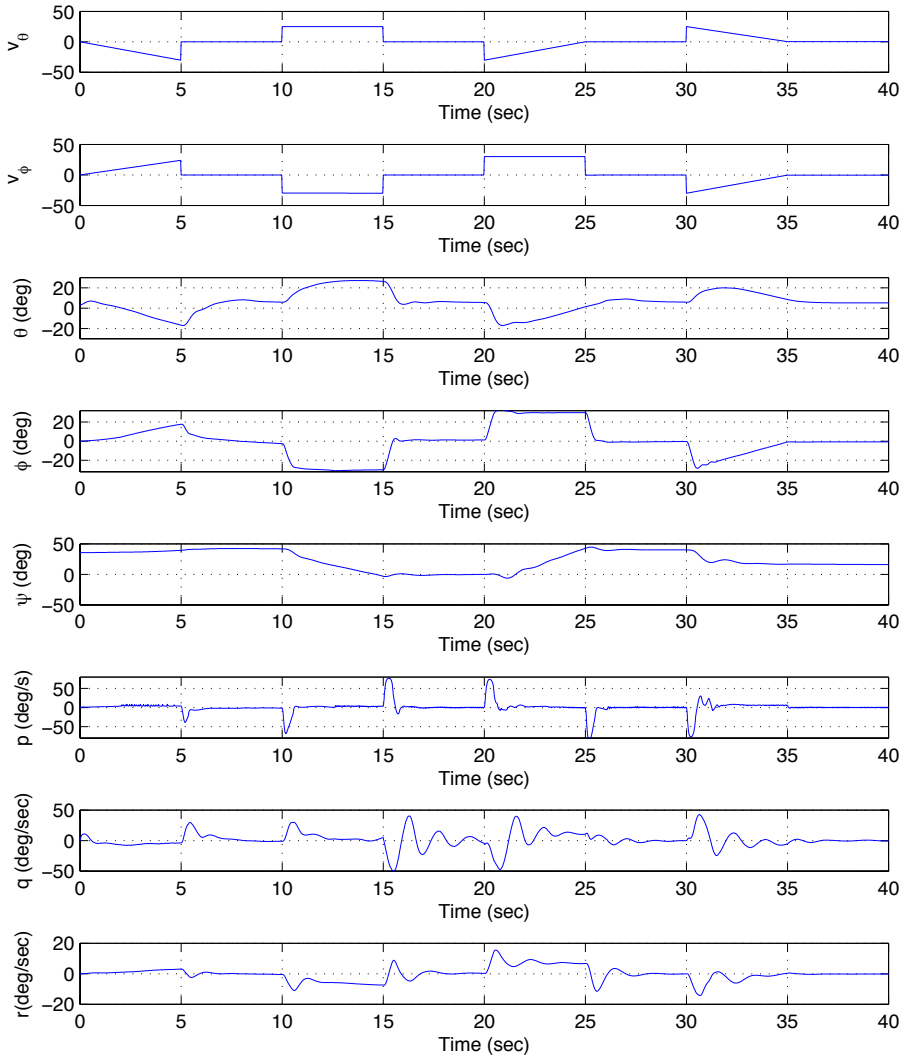

Figure C.41: States for Weighted Control Allocation - Simulation 14

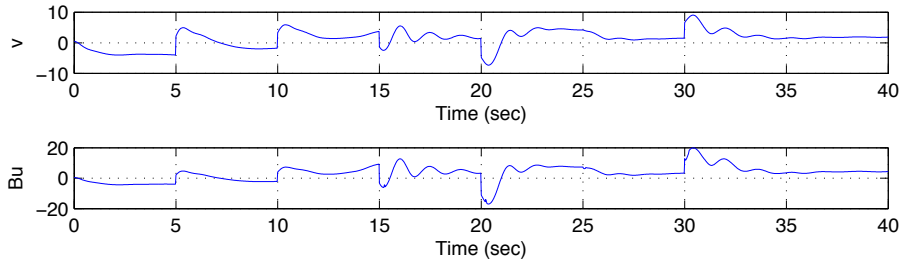

Figure C.42: v,Bu for Minimum Deflection Control Allocation Method - Simulation 14

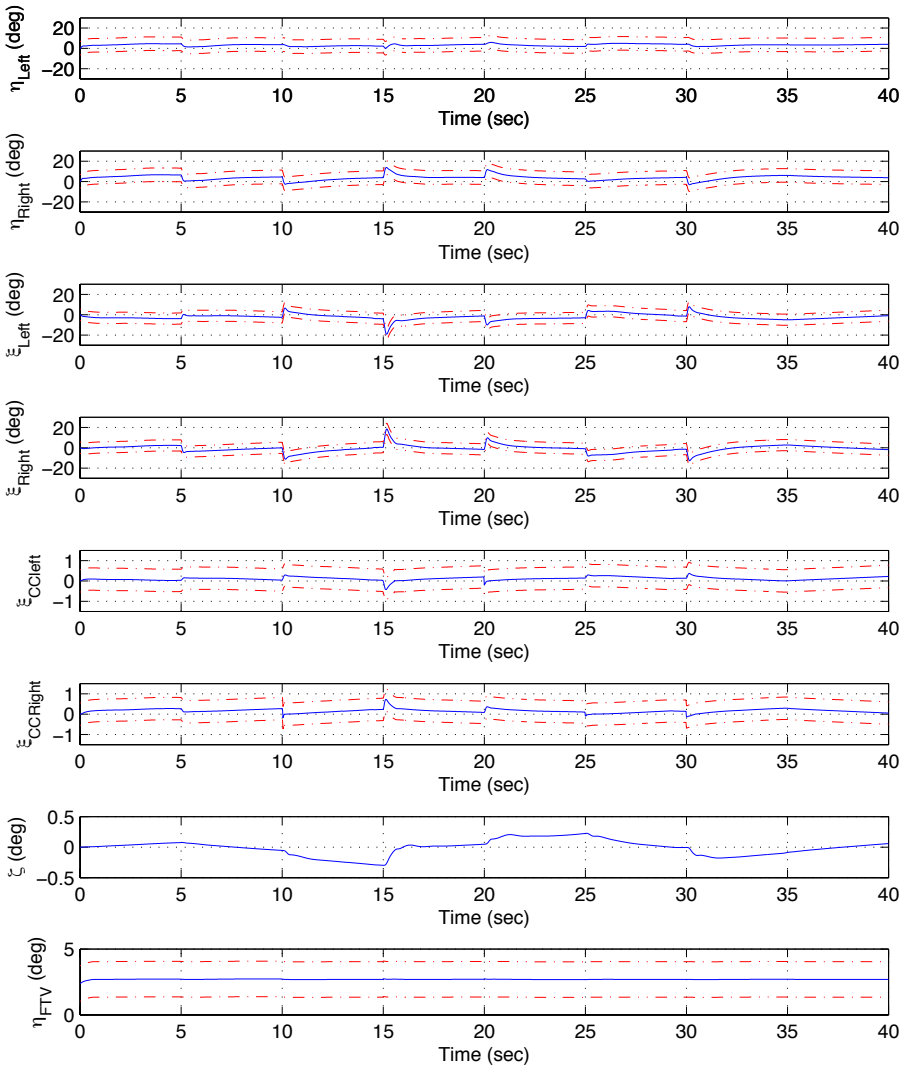

Figure C.43: Effector distribution for Minimum Deflection Control Allocation Method - Simulation 15

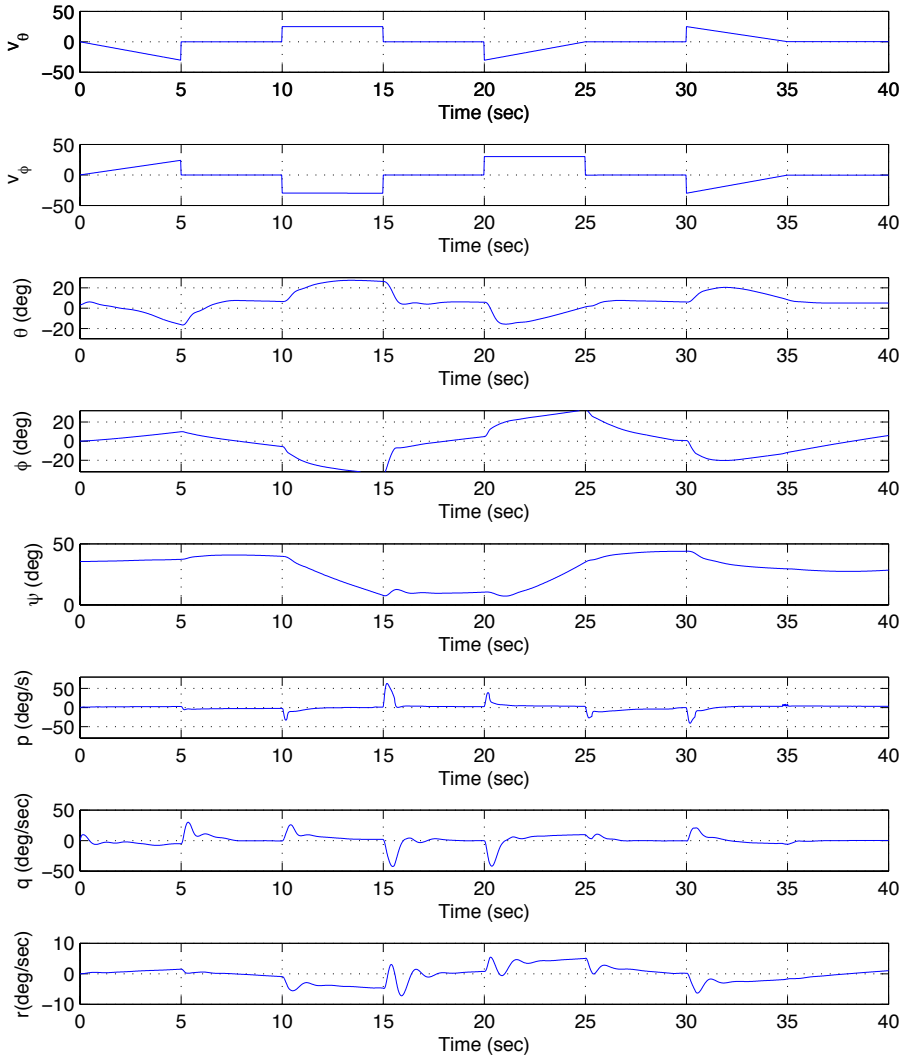

Figure C.44: States for Weighted Control Allocation - Simulation 15

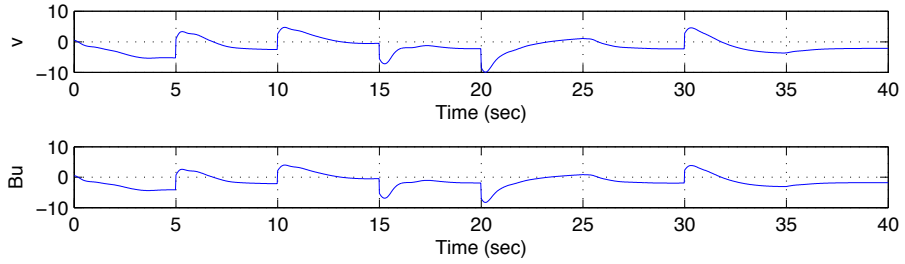

Figure C.45: v,Bu for Minimum Deflection Control Allocation Method - Simulation 15

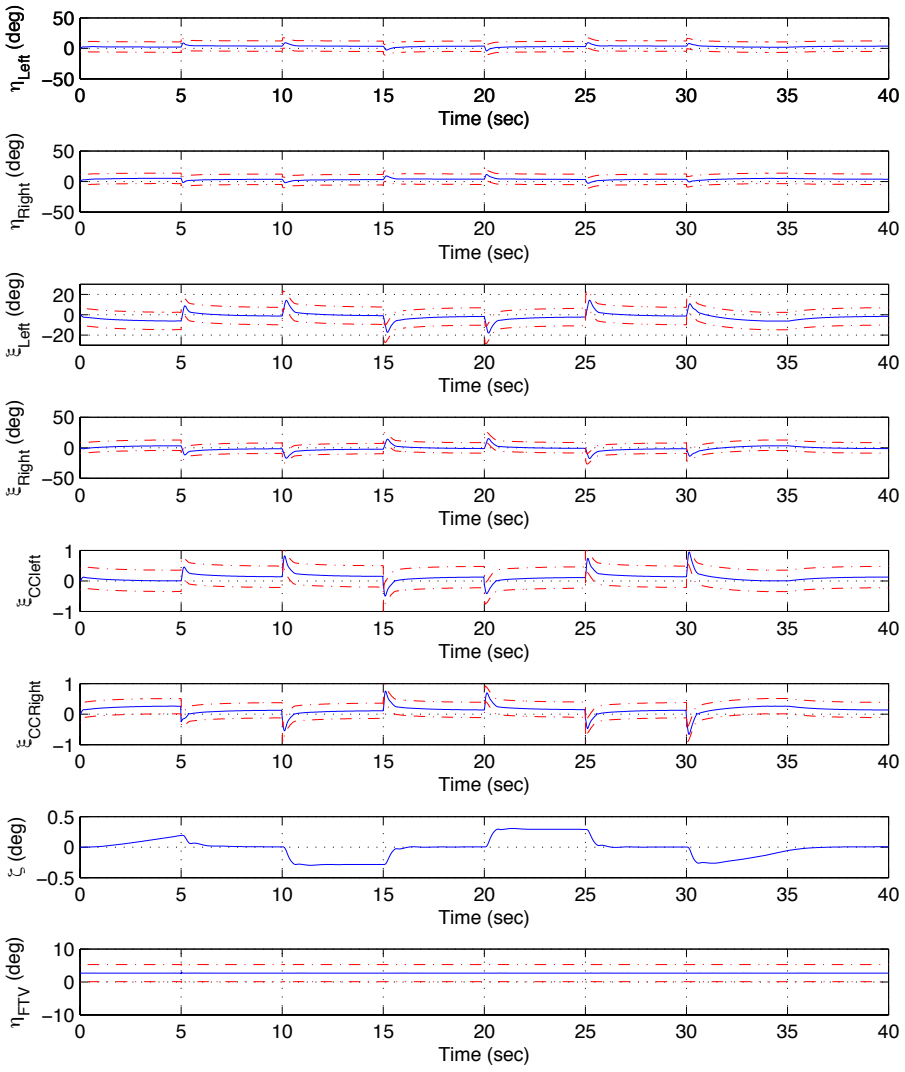

Figure C.46: Effector distribution for Minimax Control Allocation Method - Simulation 16

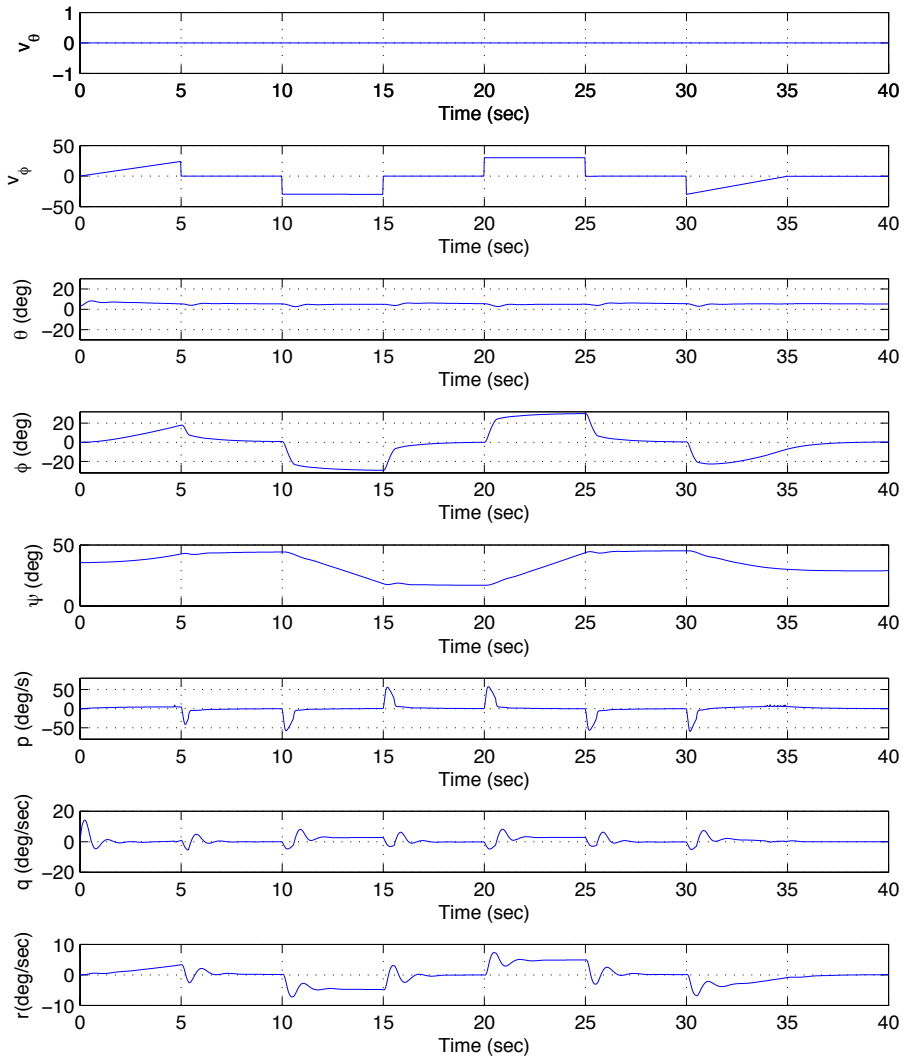

Figure C.47: States for Minimax Control Allocation - Simulation 16

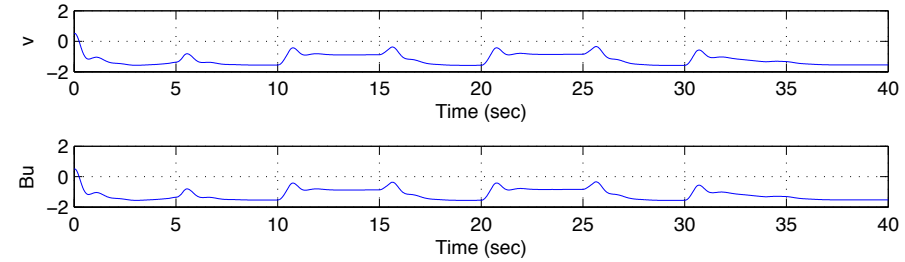

Figure C.48: v,Bu for Minimax Control Allocation Method - Simulation 16

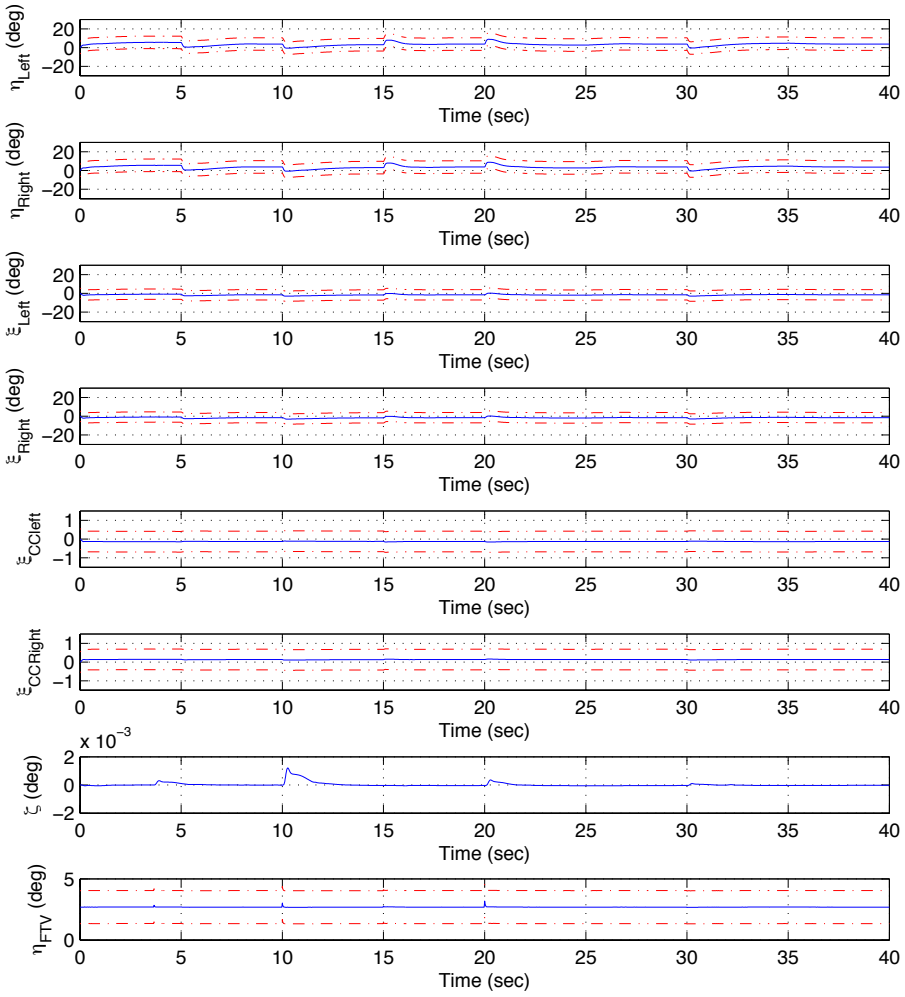

Figure C.49: Effector distribution for Minimax Control Allocation Method - Simulation 17

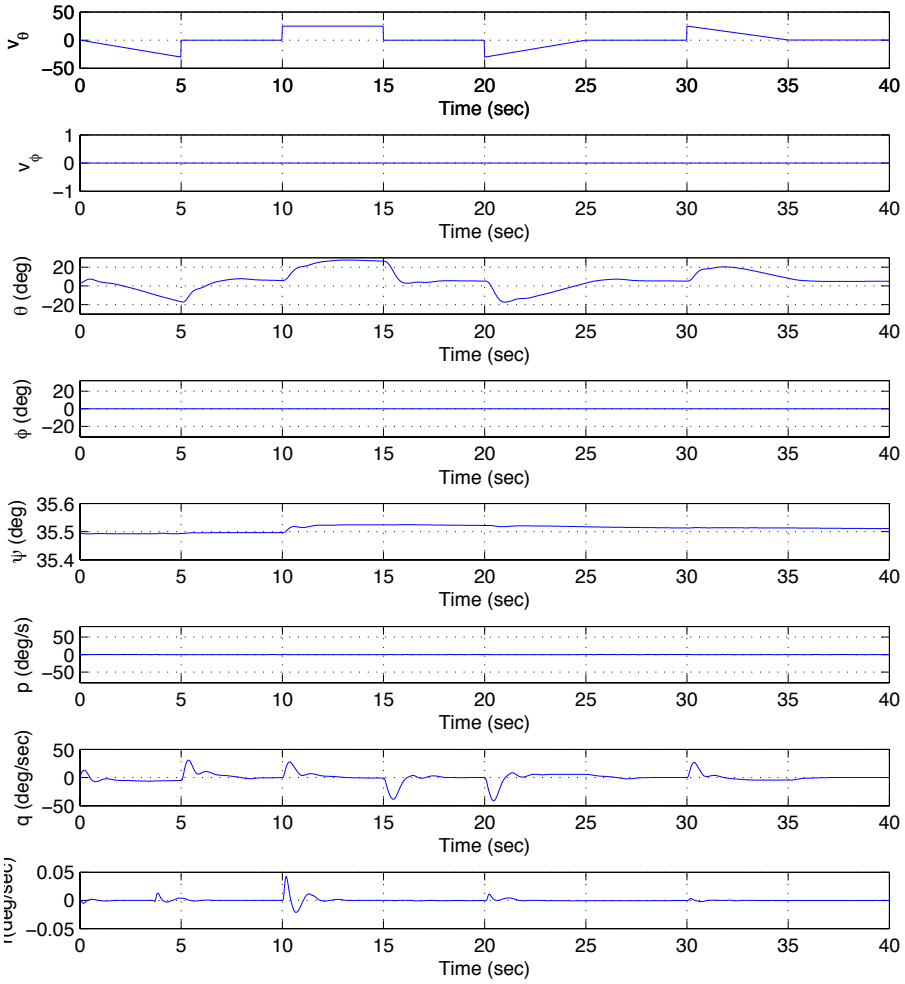

Figure C.50: States for Minimax Control Allocation - Simulation 17

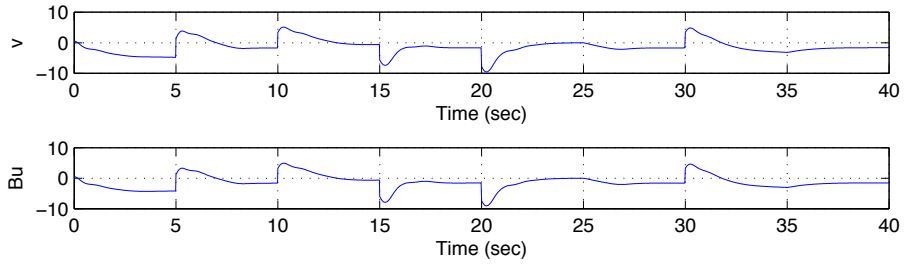

Figure C.51: v,Bu for Minimax Control Allocation Method - Simulation 17

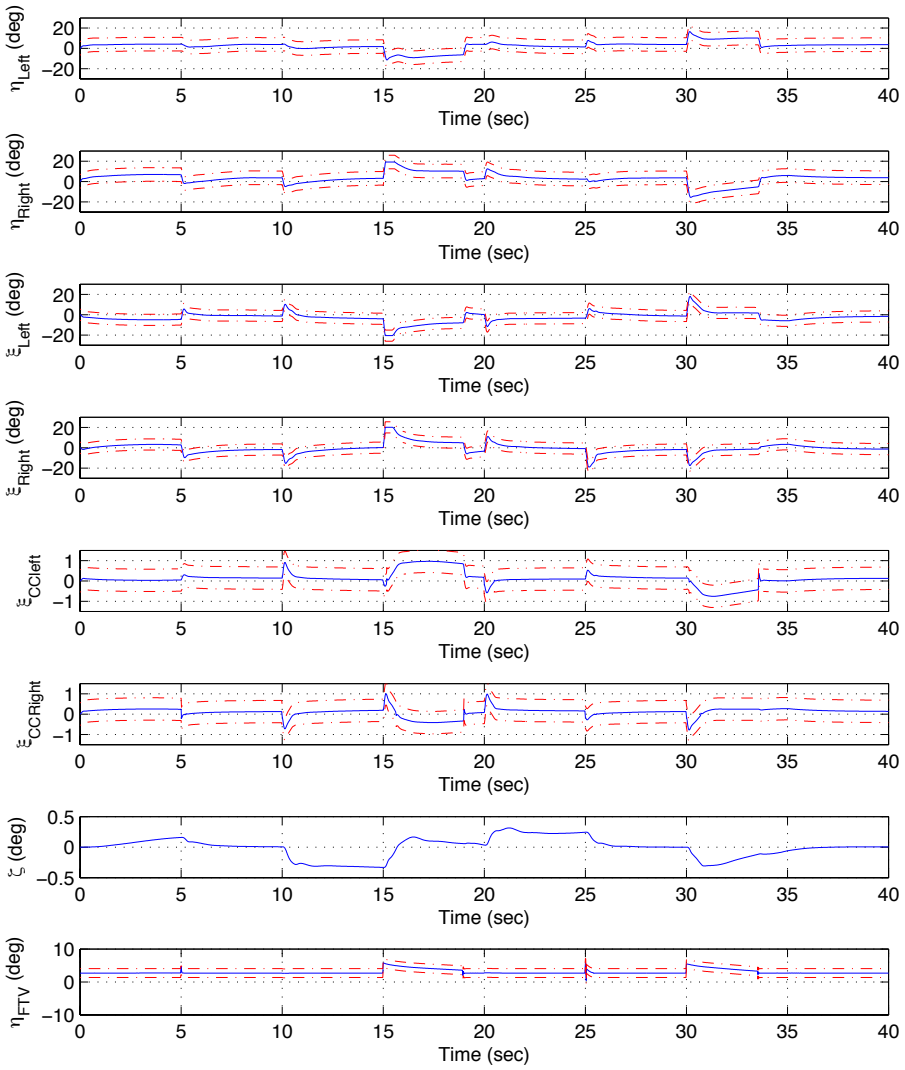

Figure C.52: Effector distribution for Minimax Control Allocation Method - Simulation 18

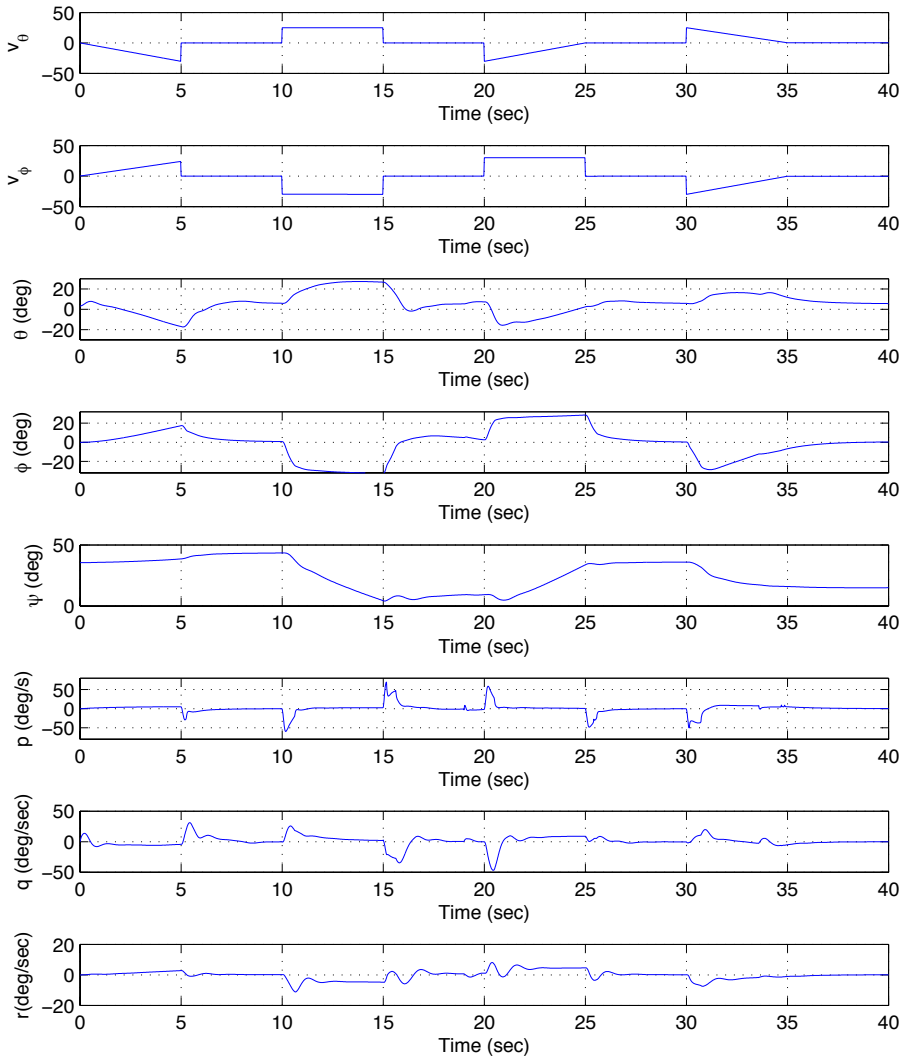

Figure C.53: States for Minimax Control Allocation - Simulation 18

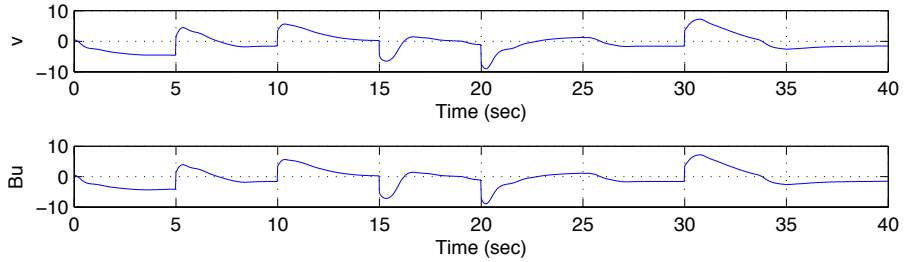

Figure C.54: v,Bu for Minimax Control Allocation Method - Simulation 18

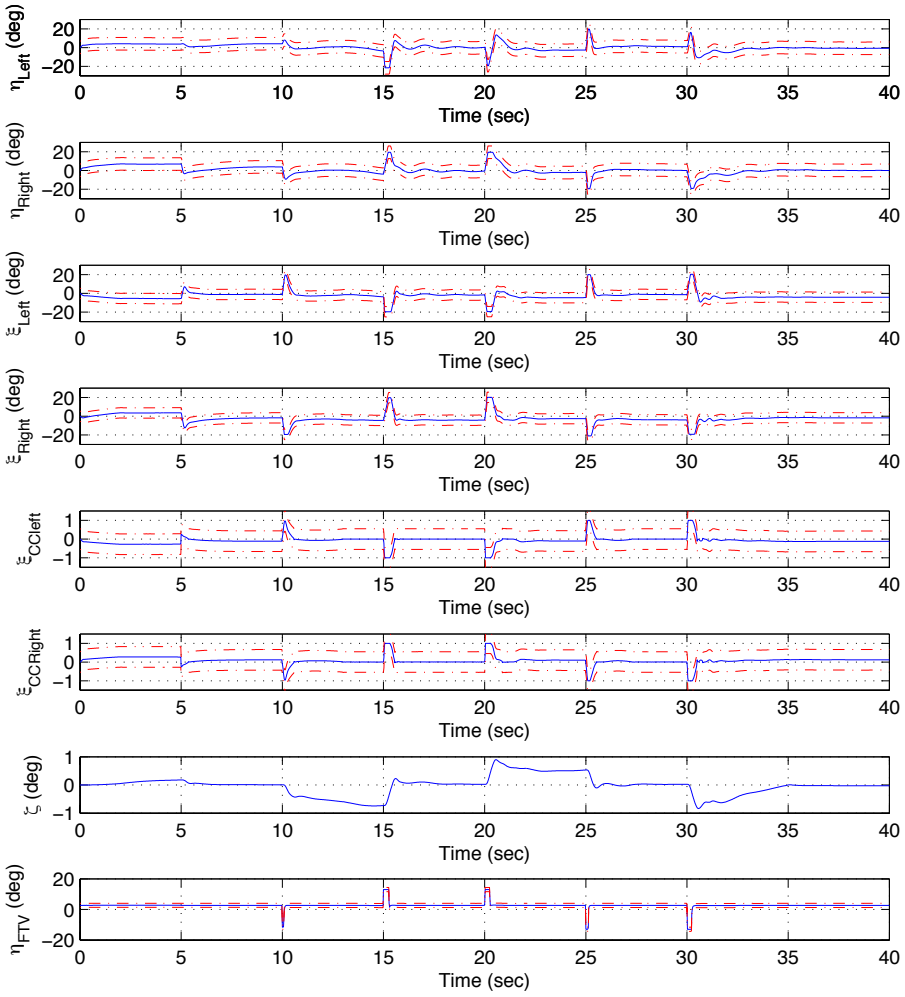

Figure C.55: Effector distribution for Minimax Control Allocation Method - Simulation 19

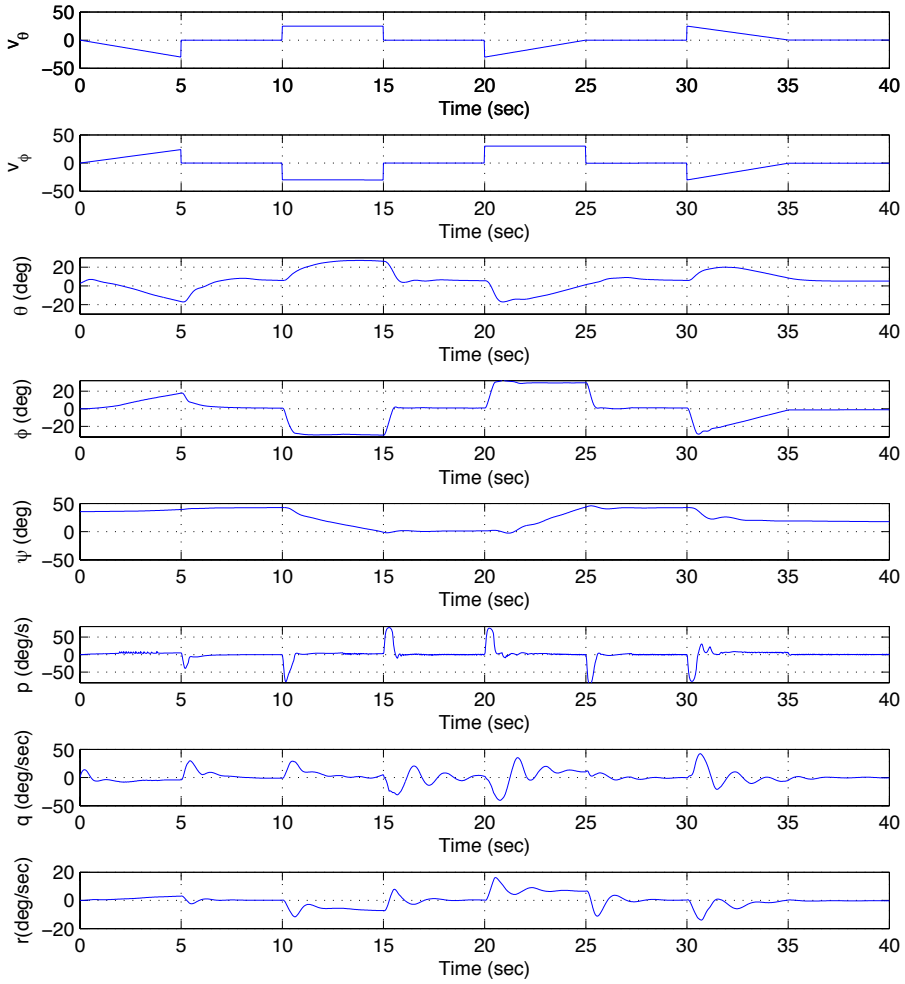

Figure C.56: States for Minimax Control Allocation - Simulation 19

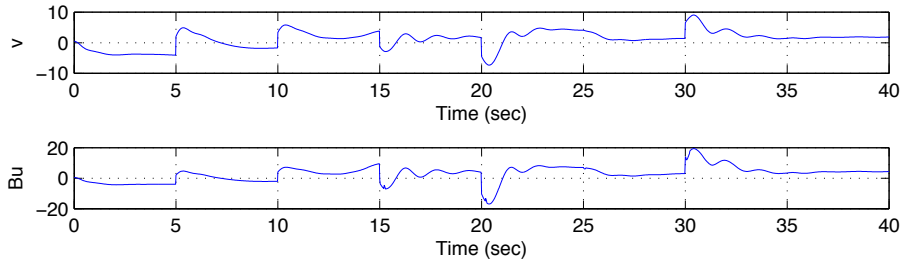

Figure C.57: v,Bu for Minimax Control Allocation Method - Simulation 19

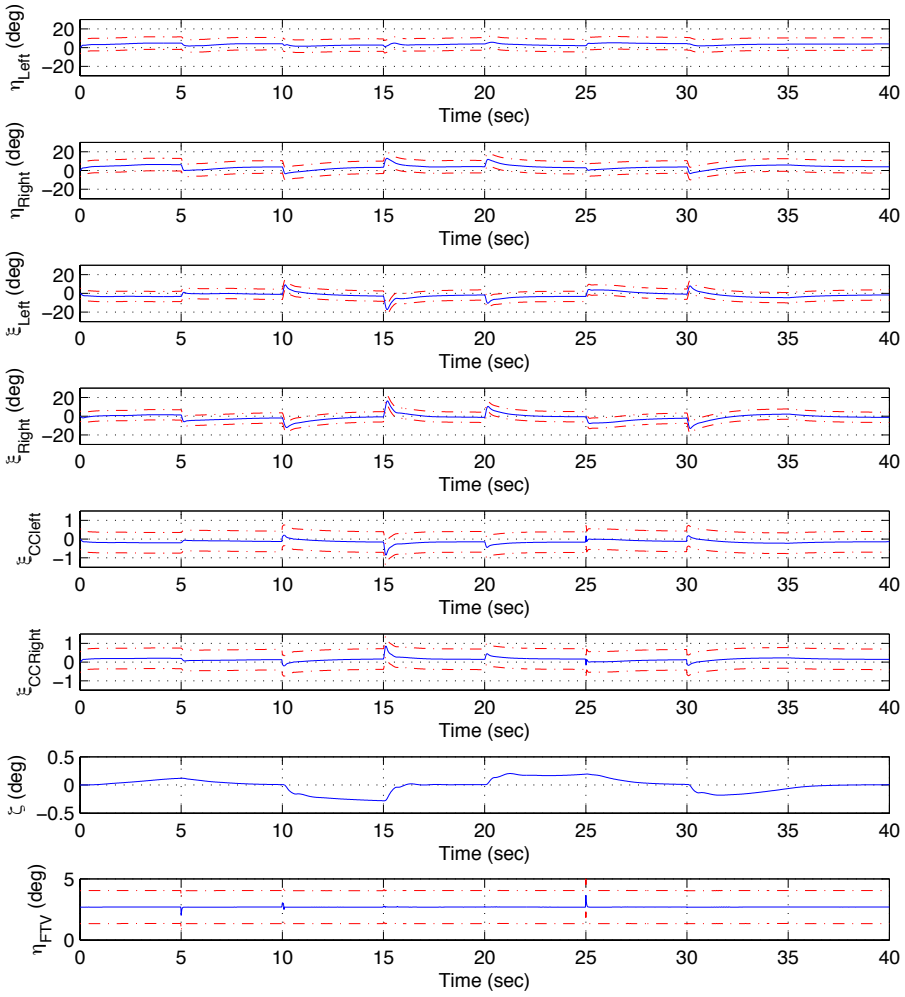

Figure C.58: Effector distribution for Minimax Control Allocation Method - Simulation 20

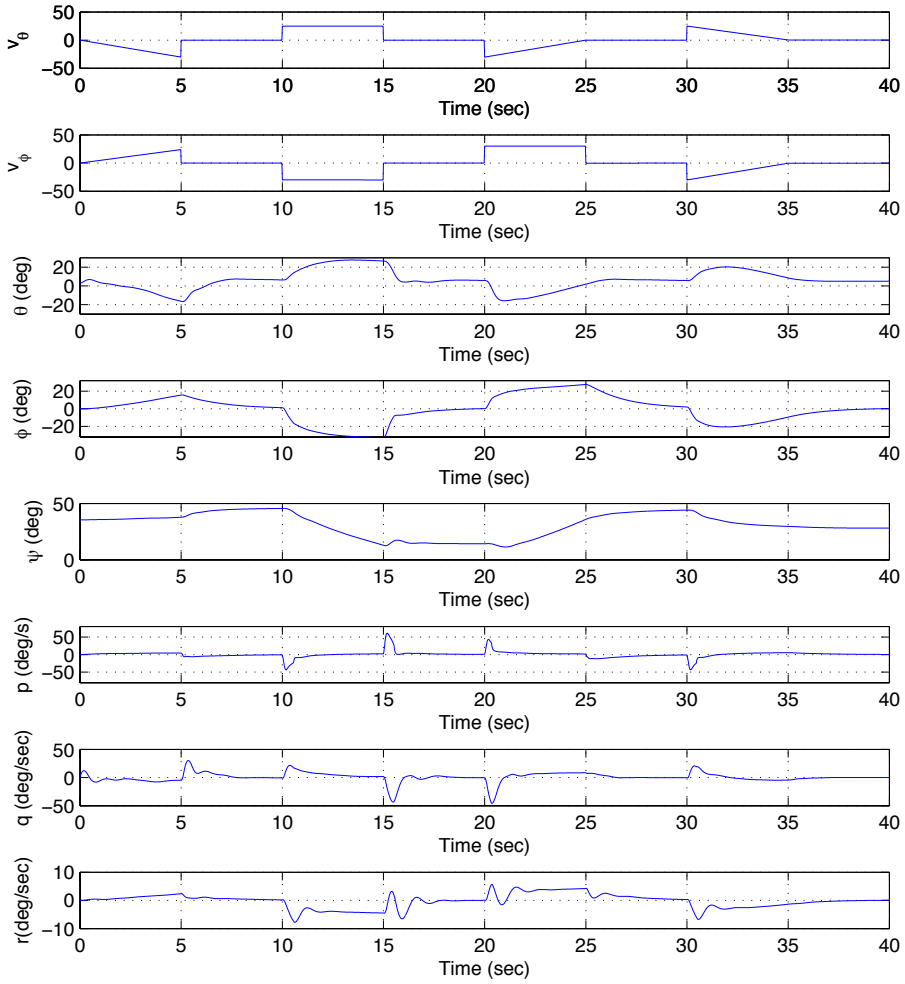

Figure C.59: States for Minimax Control Allocation - Simulation 20

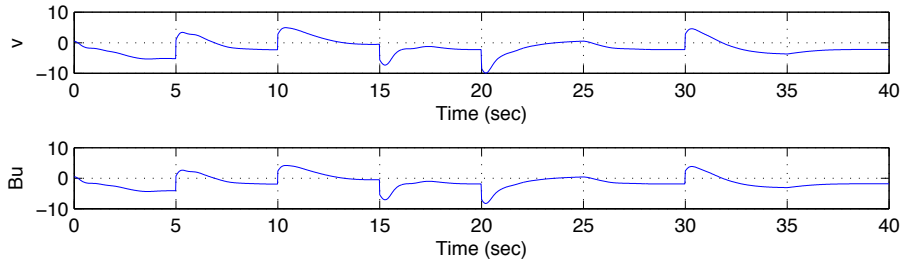

Figure C.60: v,Bu for Minimax Control Allocation Method - Simulation 20

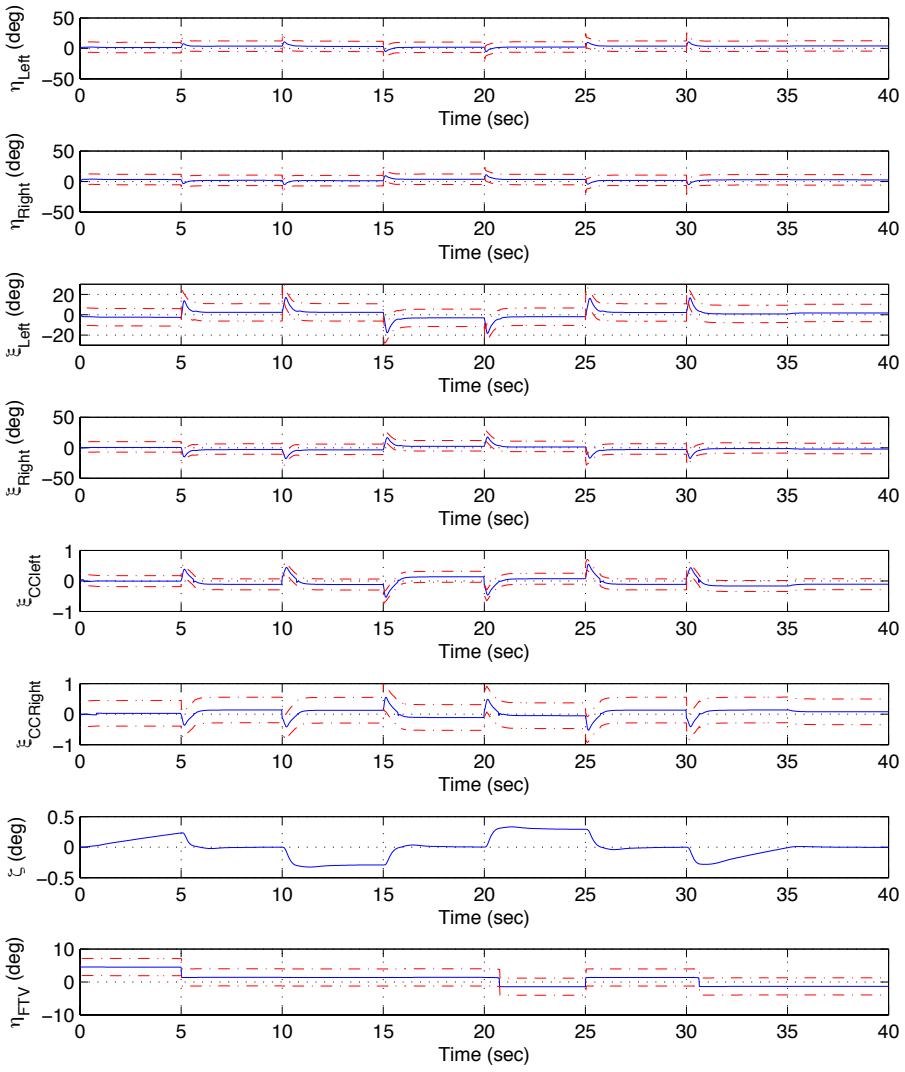

Figure C.61: Effector distribution for Classical Control Allocation Method - Simulation 21

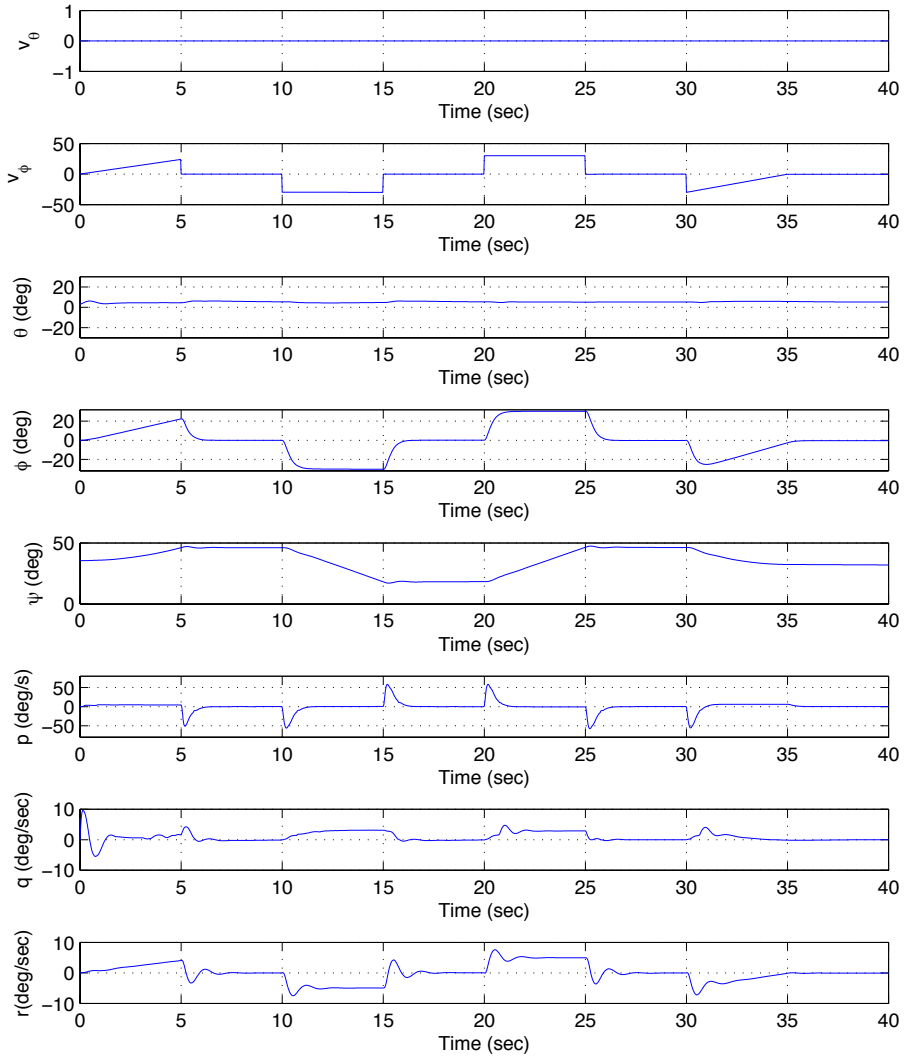

Figure C.62: States for Classical Control Allocation - Simulation 21

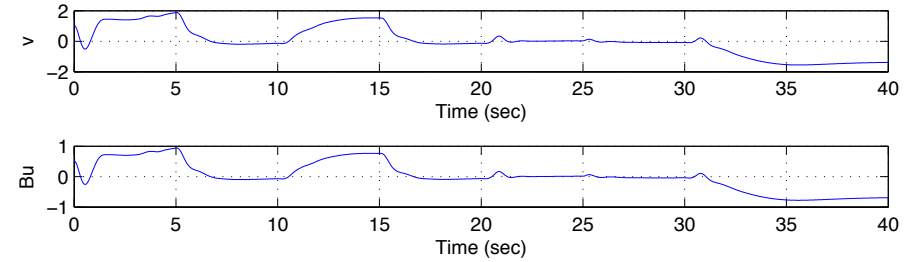

Figure C.63: v,Bu for Minimax Control Allocation Method - Simulation 21

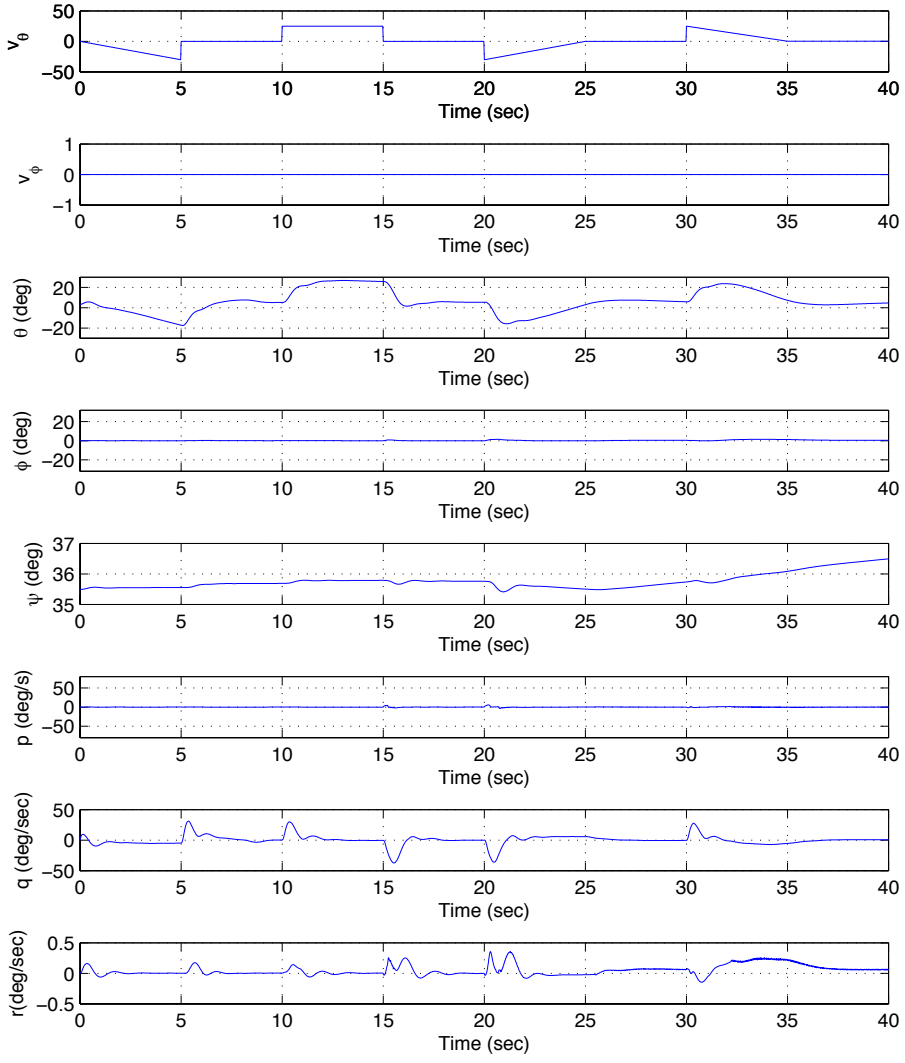

Figure C.64: Effector distribution for Classical Control Allocation Method - Simulation 22

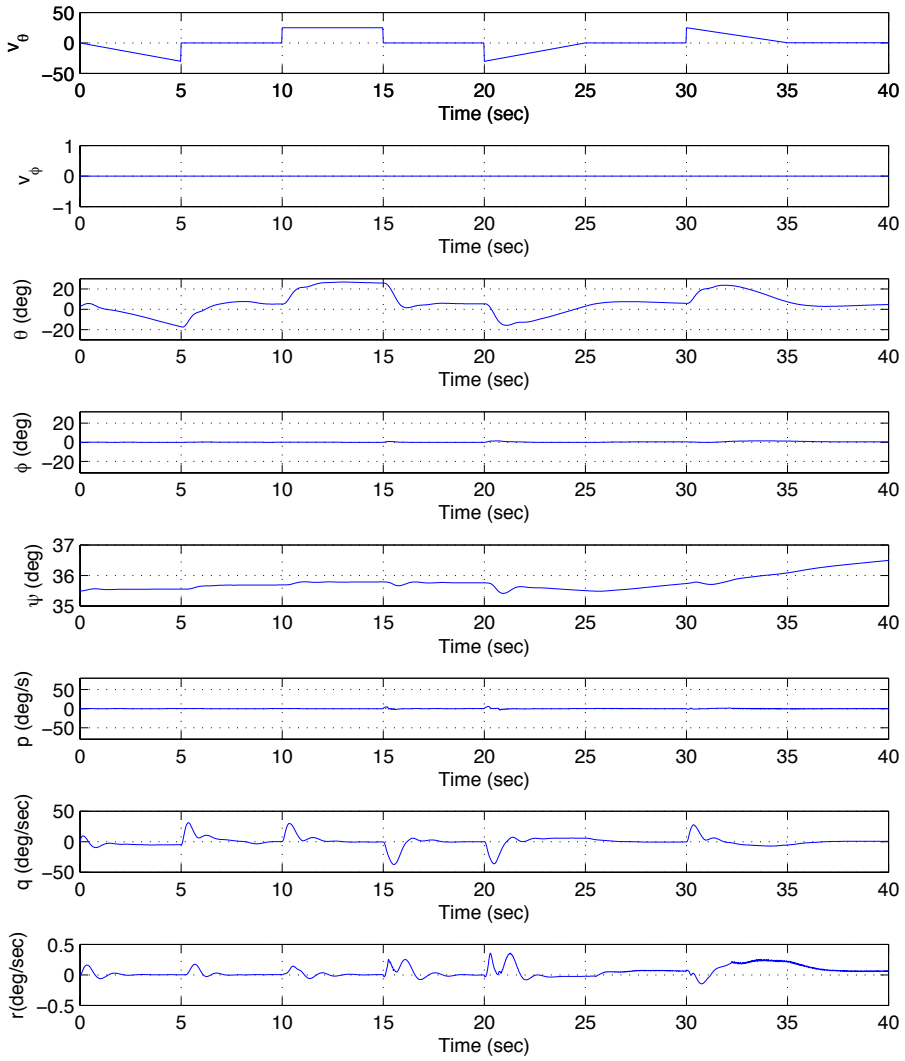

Figure C.65: States for Classical Control Allocation - Simulation 22

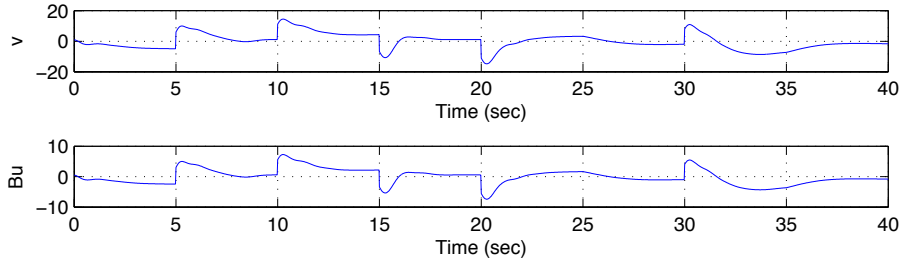

Figure C.66: v,Bu for Minimax Control Allocation Method - Simulation 22

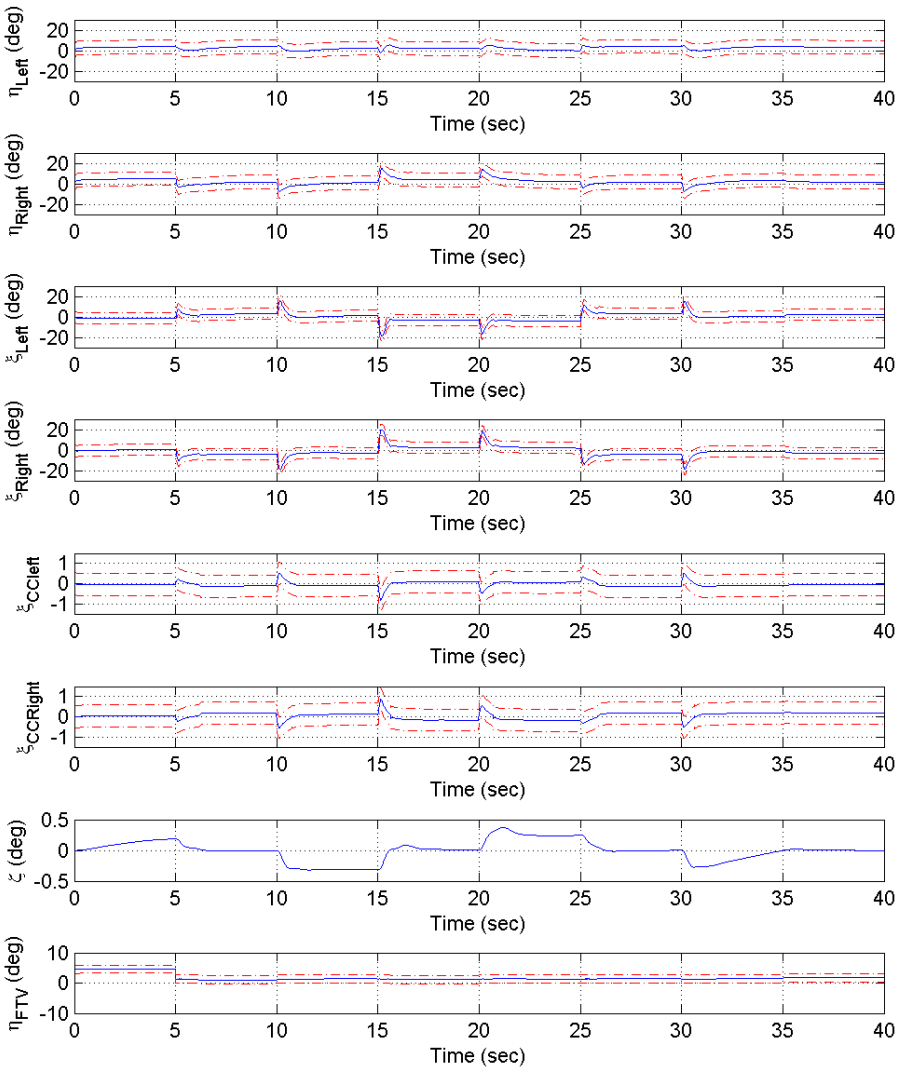

Figure C.67: Effector distribution for Classical Control Allocation Method - Simulation 23

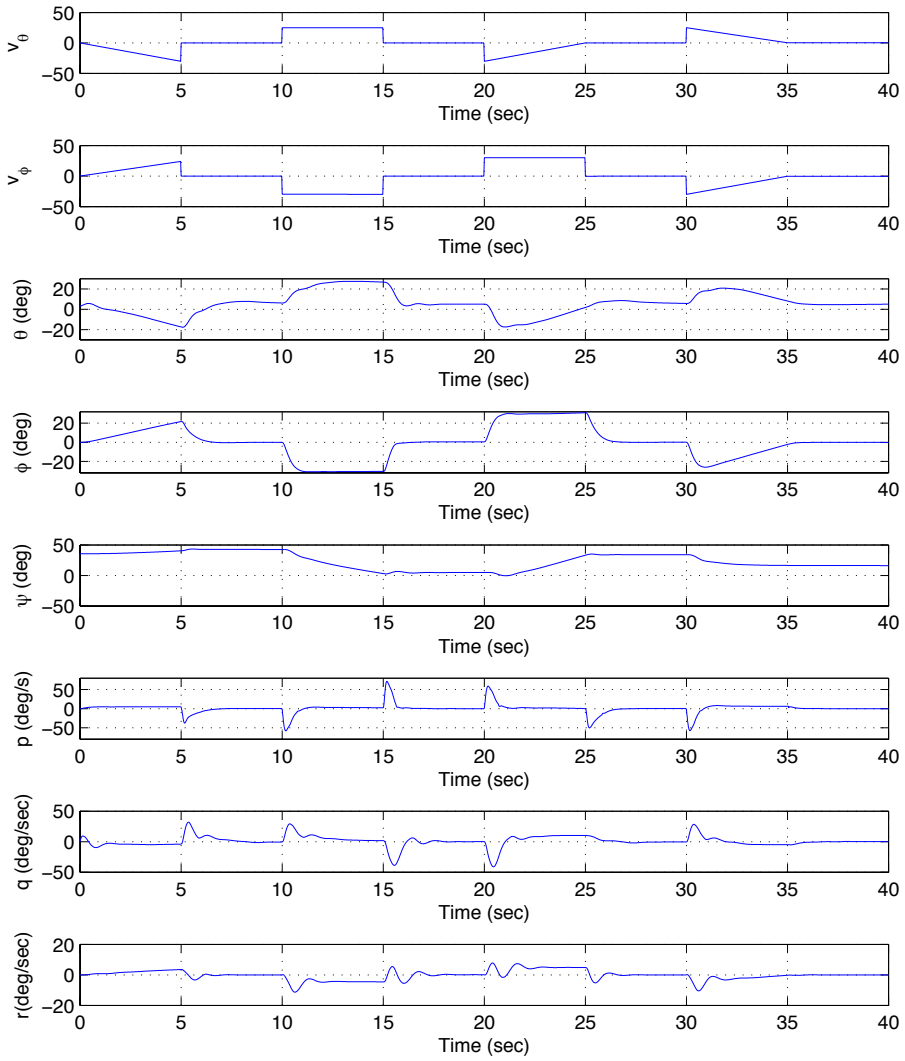

Figure C.68: States for Classical Control Allocation - Simulation 23

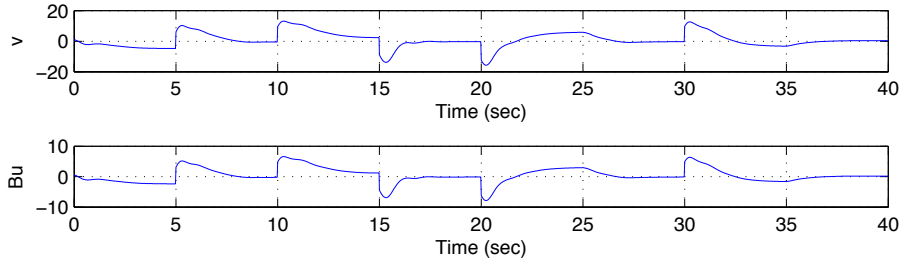

Figure C.69: v,Bu for Classical Control Allocation Method - Simulation 23

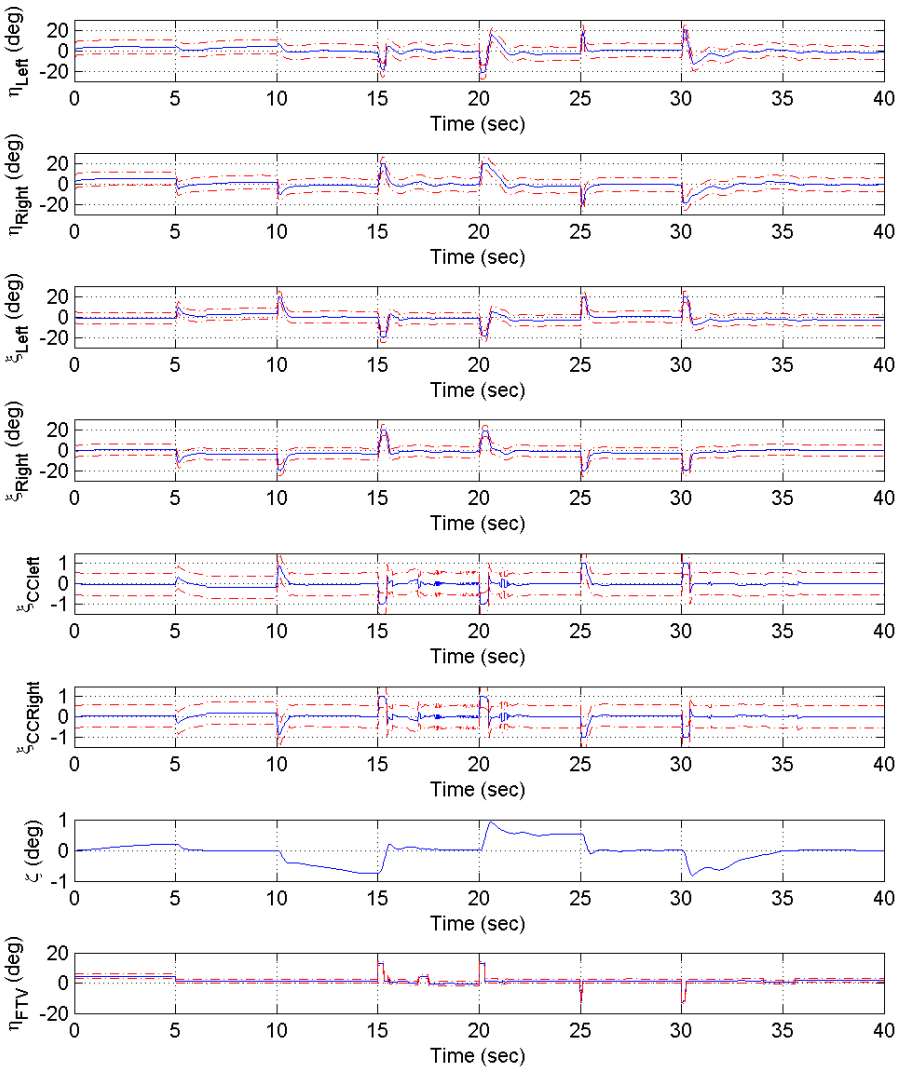

Figure C.70: Effector distribution for Classical Control Allocation Method - Simulation 24

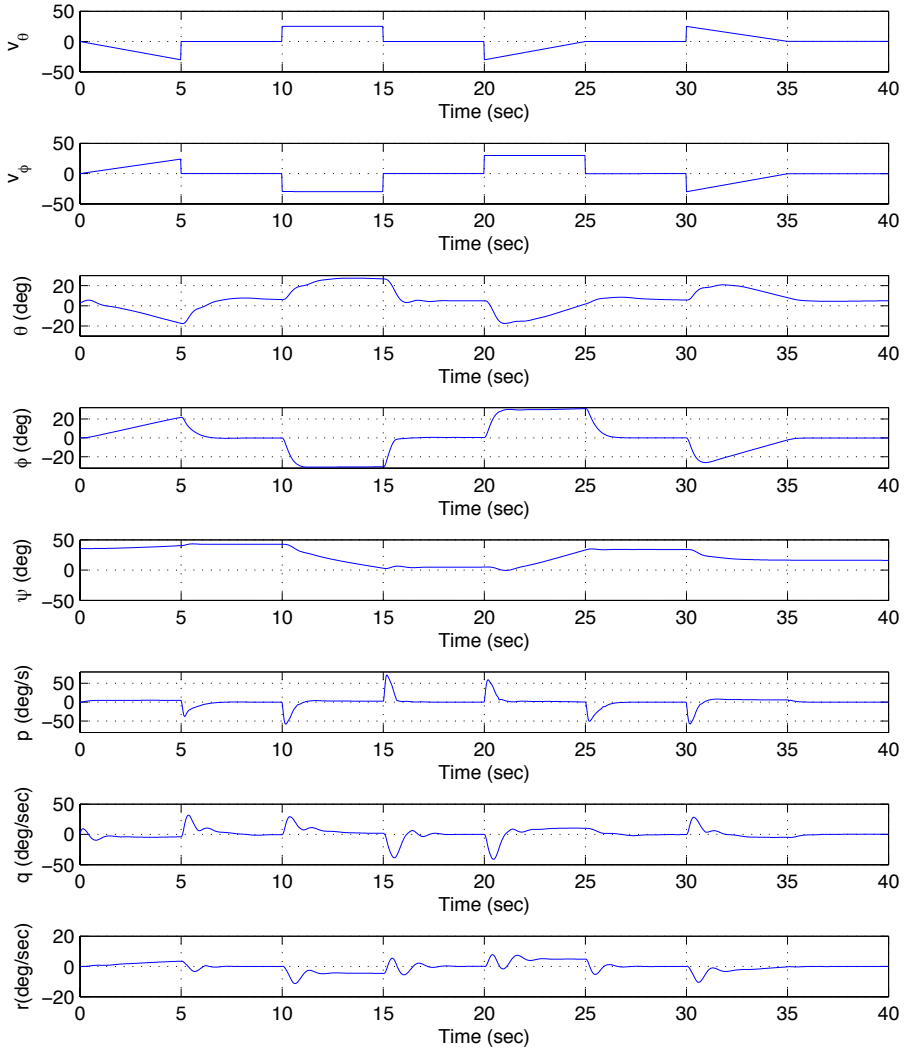

Figure C.71: States for Classical Control Allocation - Simulation 24

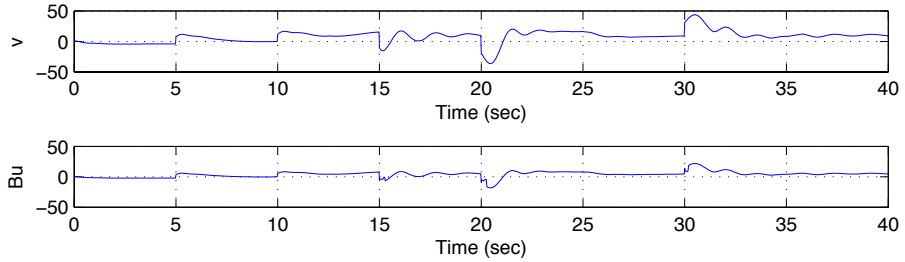

Figure C.72: v,Bu for Classical Control Allocation Method - Simulation 24

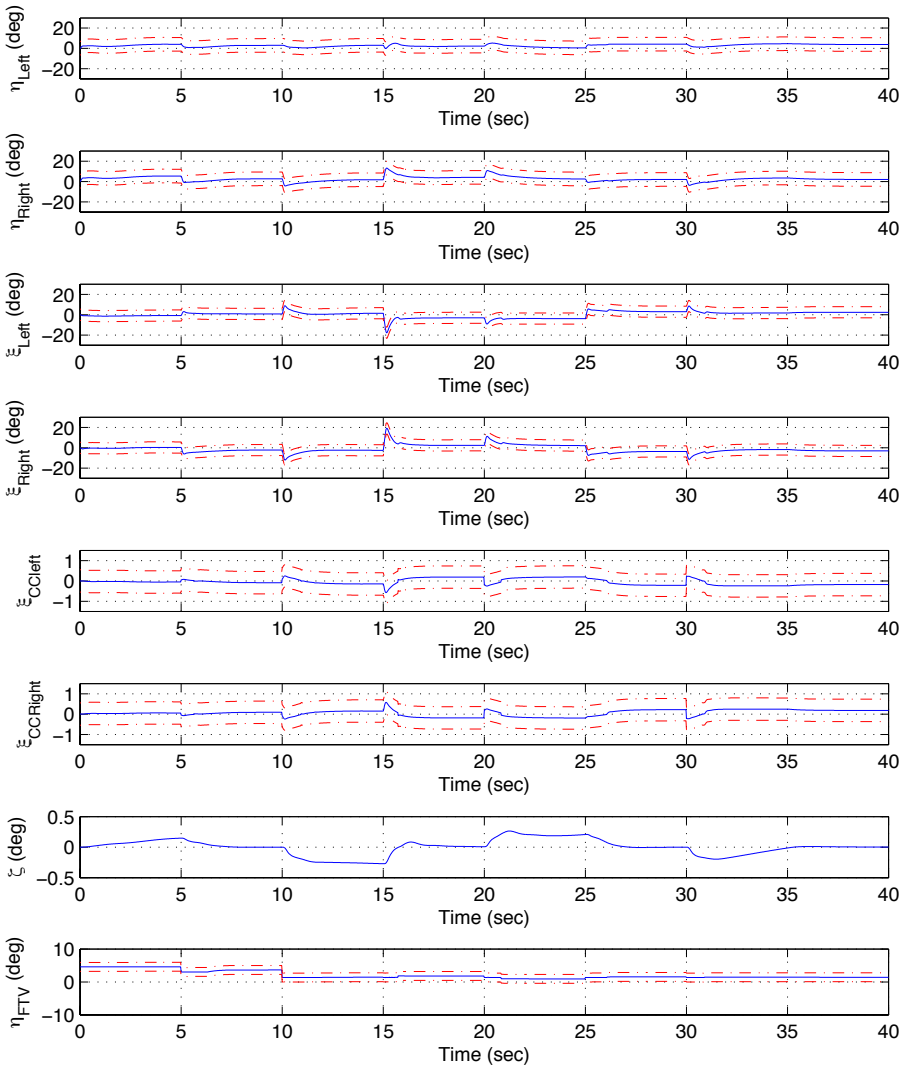

Figure C.73: Effector distribution for Classical Control Allocation Method - Simulation 25

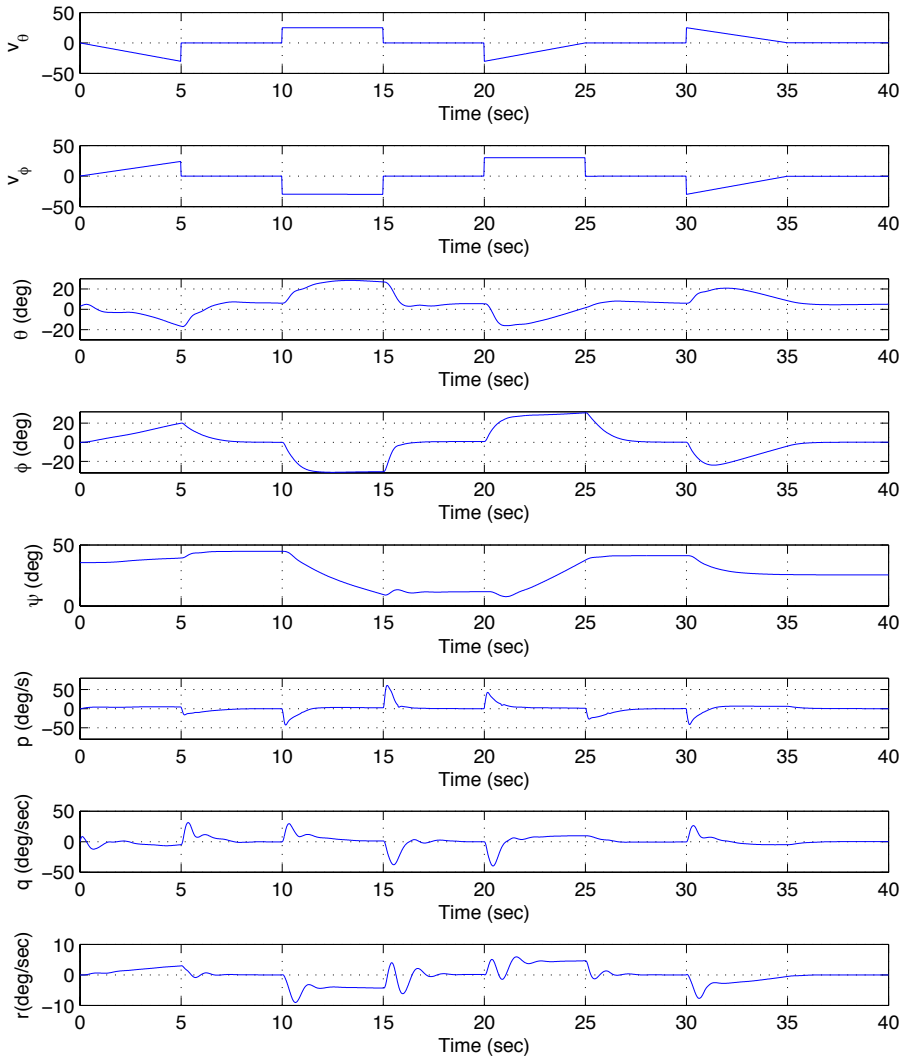

Figure C.74: States for Classical Control Allocation - Simulation 25

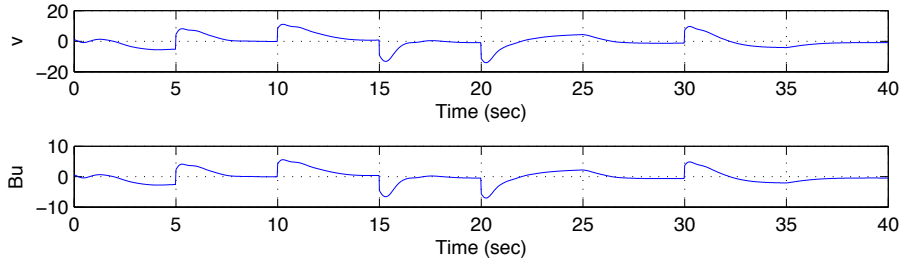

Figure C.75: v,Bu for Classical Control Allocation Method - Simulation 25

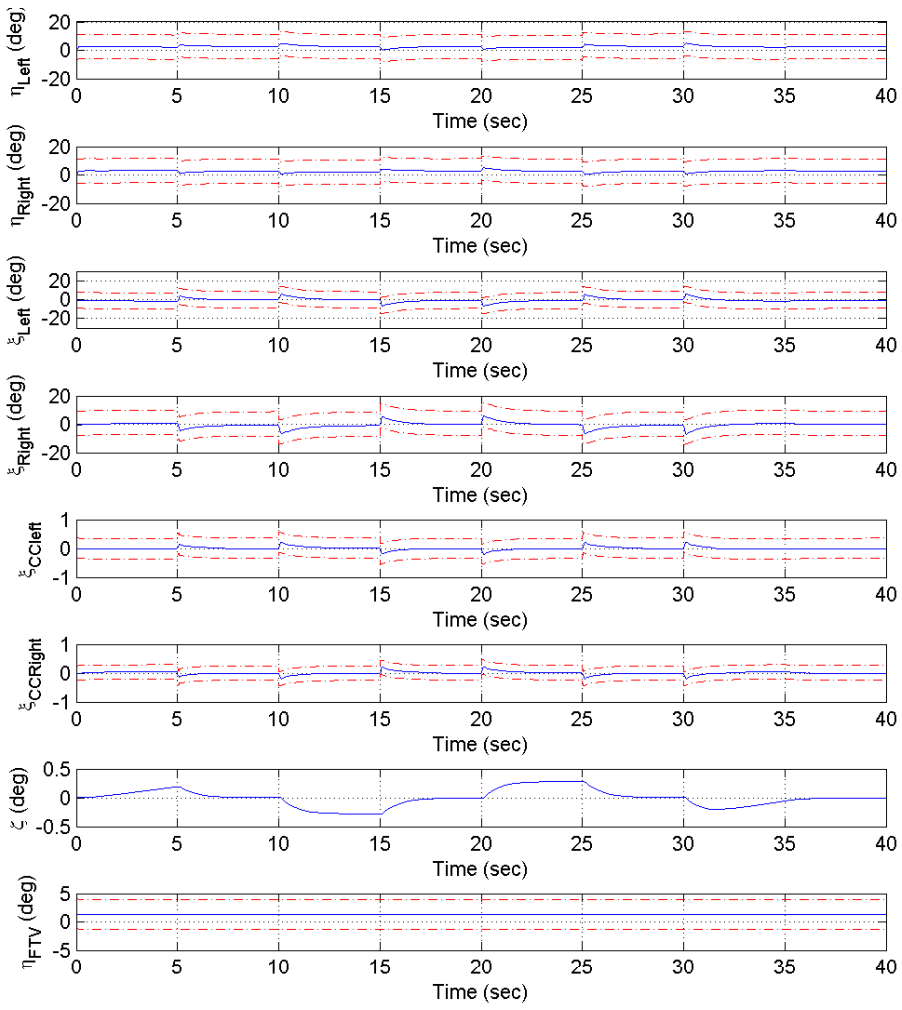

Figure C.76: Effector distribution for Canonical Control Allocation Method - Simulation 26

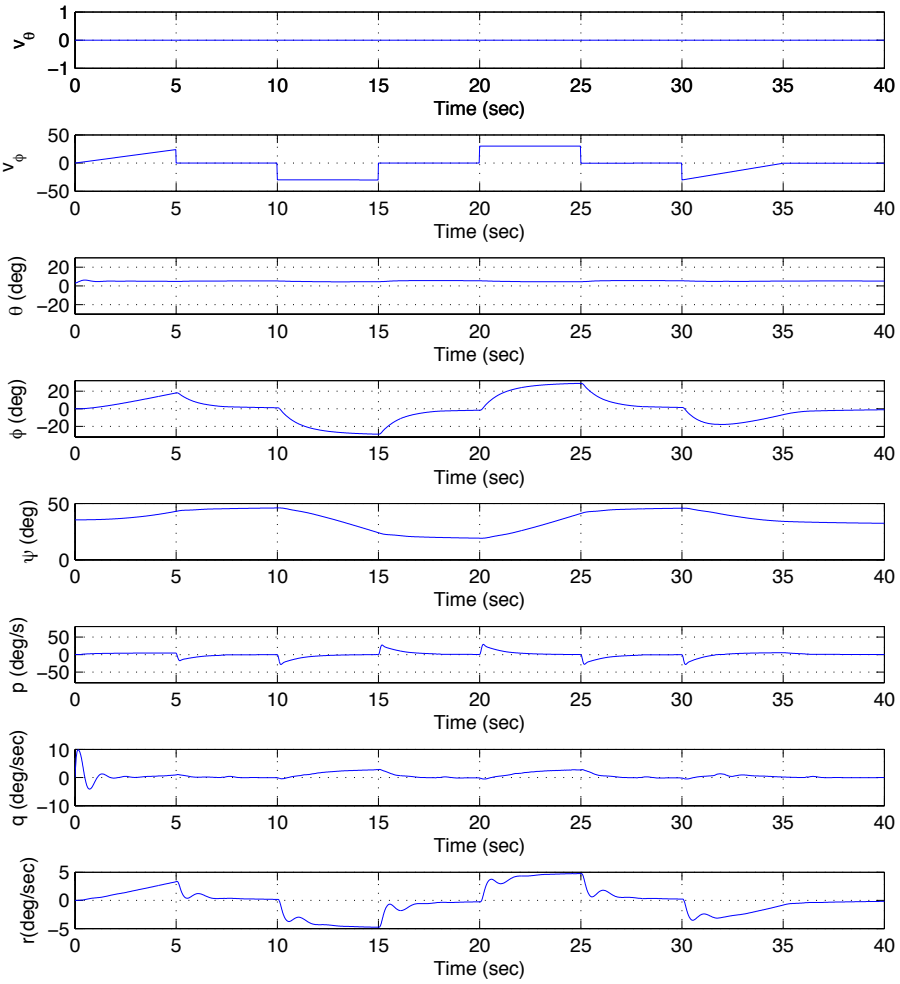

Figure C.77: States for Canonical Control Allocation - Simulation 26

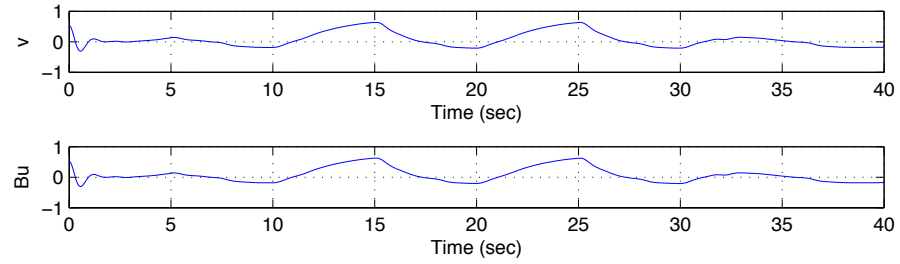

Figure C.78: v,Bu for Canonical Control Allocation Method - Simulation 26

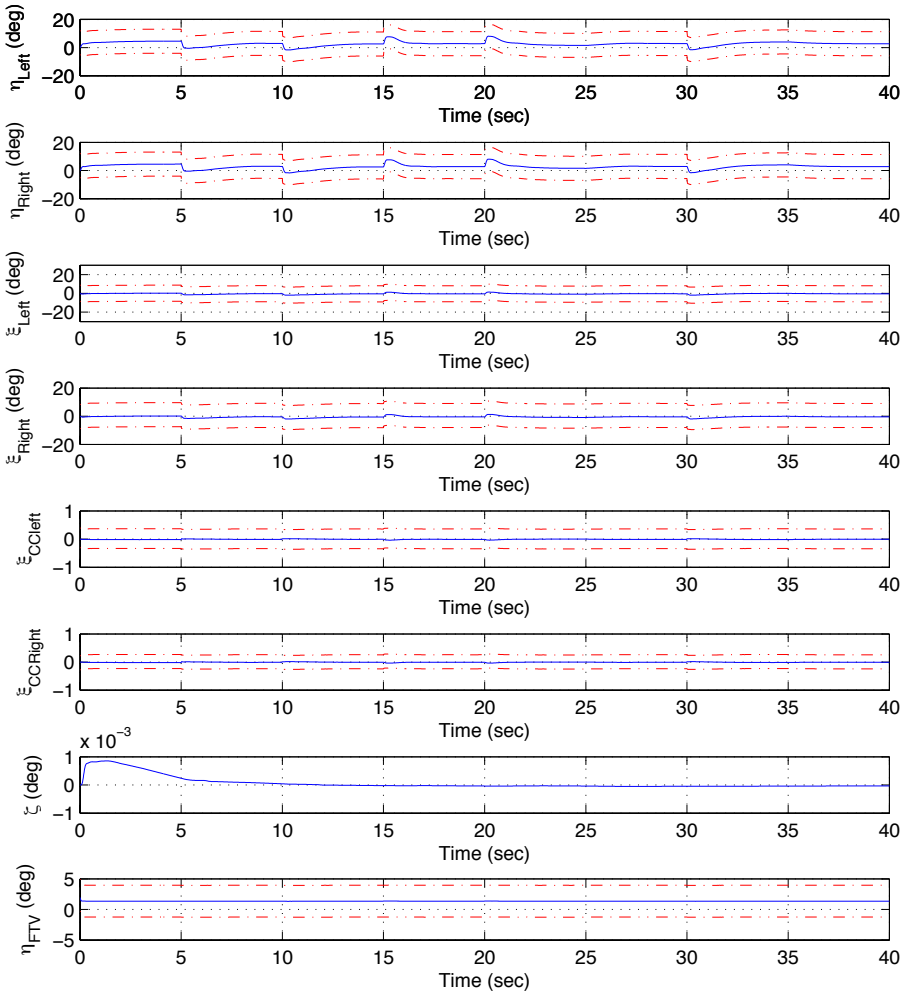

Figure C.79: Effector distribution for Canonical Control Allocation Method - Simulation 27

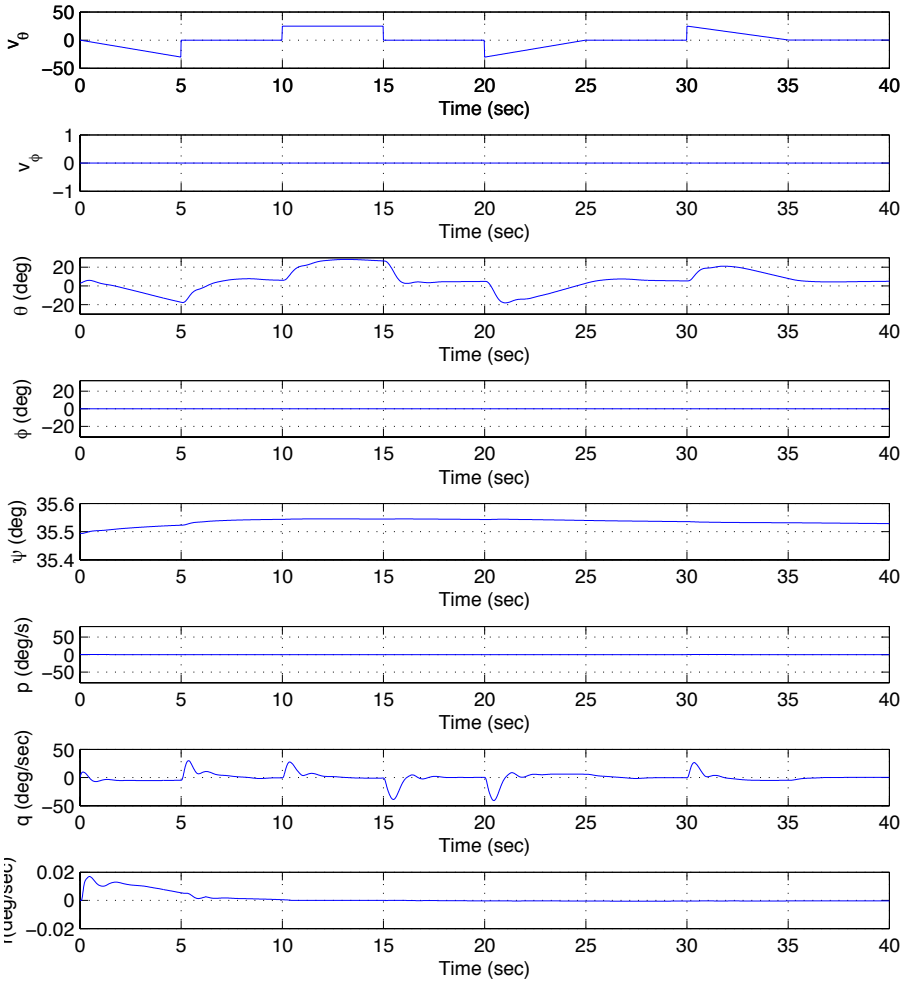

Figure C.80: States for Canonical Control Allocation - Simulation 27

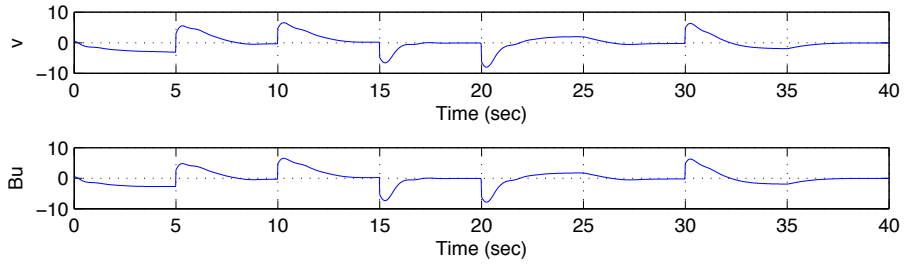

Figure C.81: v,Bu for Canonical Control Allocation Method - Simulation 27

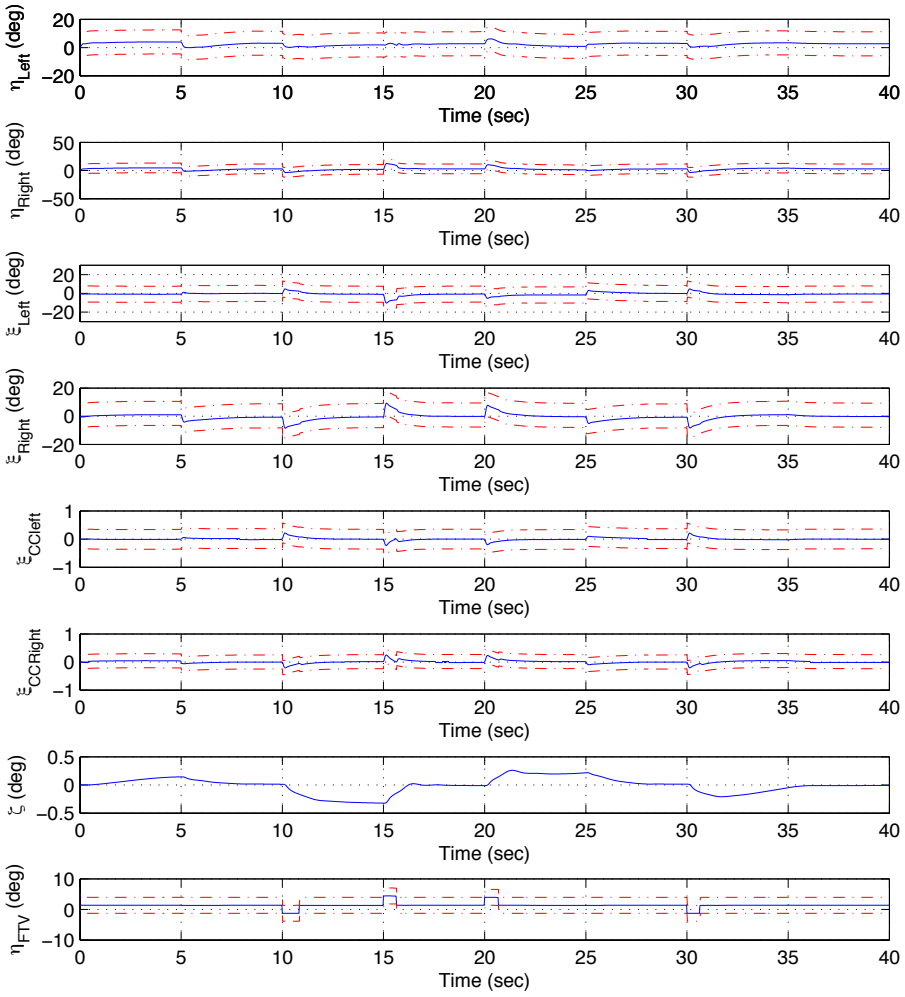

Figure C.82: Effector distribution for Canonical Control Allocation Method - Simulation 28

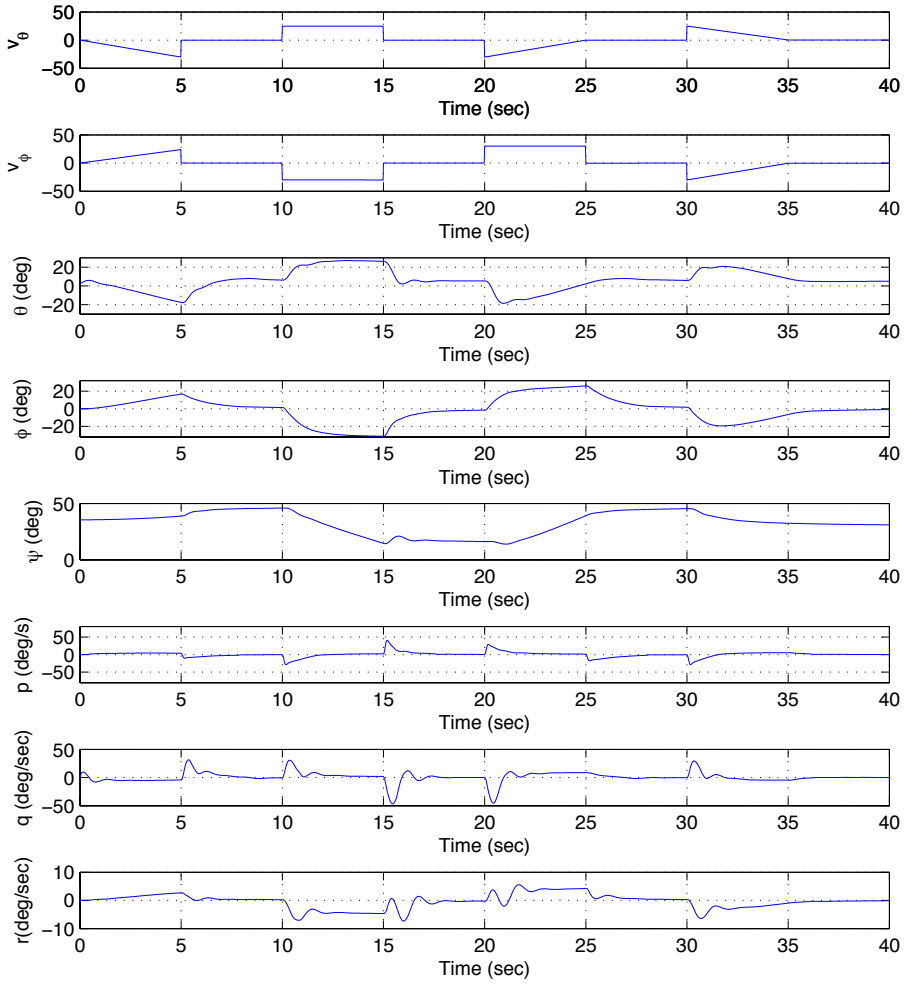

Figure C.83: States for Canonical Control Allocation - Simulation 28

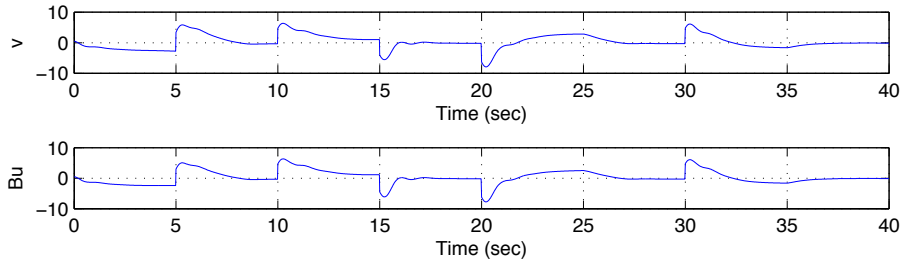

Figure C.84: v,Bu for Canonical Control Allocation Method - Simulation 28

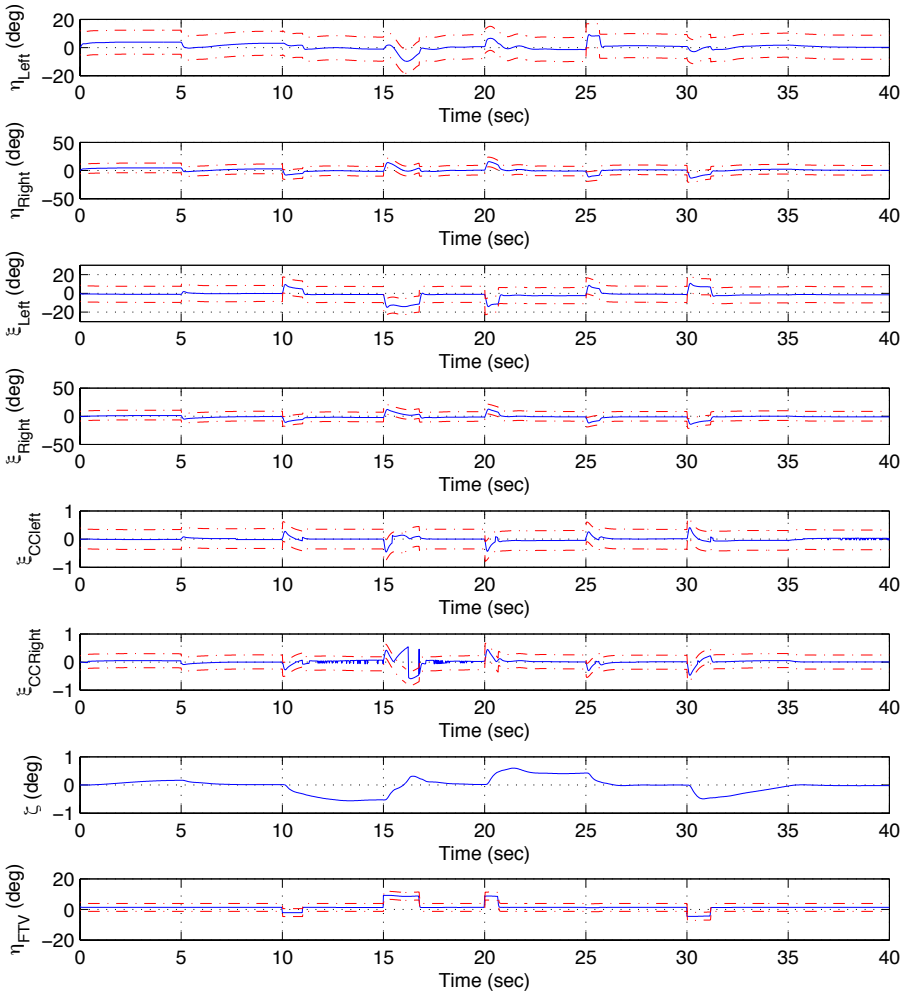

Figure C.85: Effector distribution for Canonical Control Allocation Method - Simulation 29

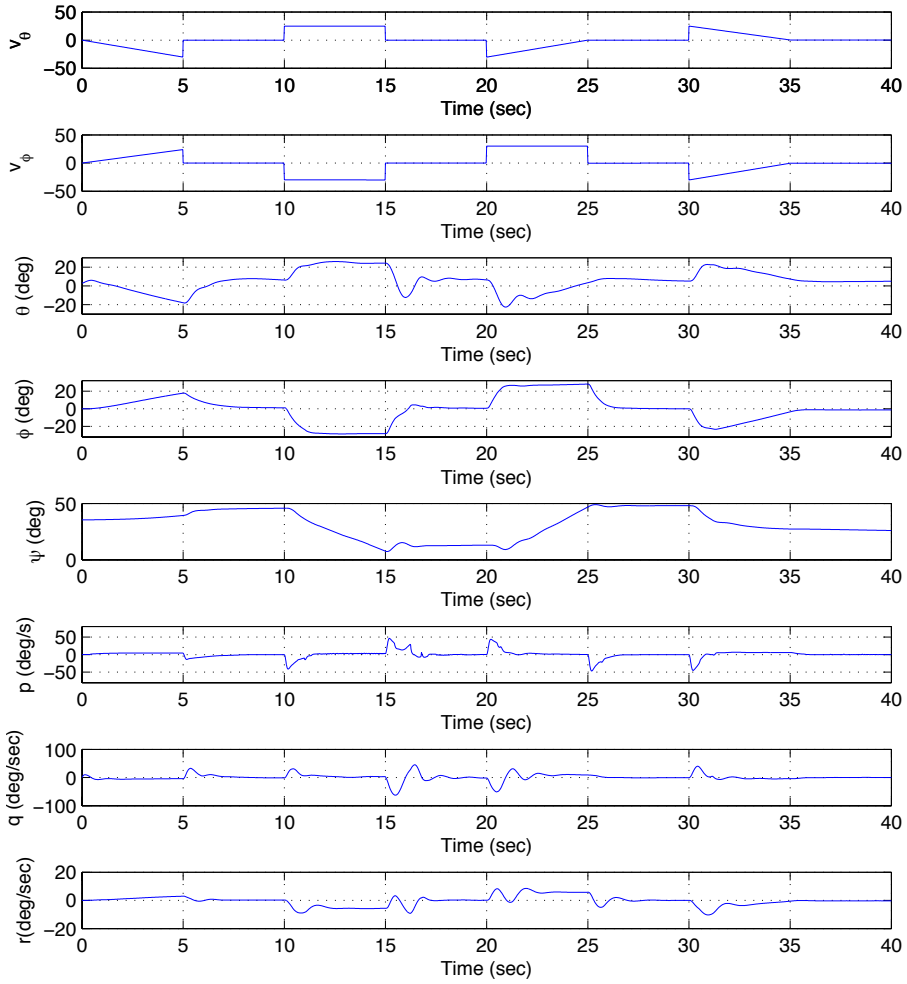

Figure C.86: States for Canonical Control Allocation - Simulation 29

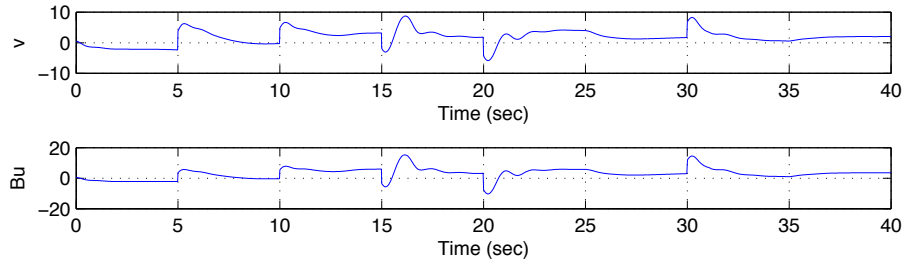

Figure C.87: v,Bu for Canonical Control Allocation Method - Simulation 29

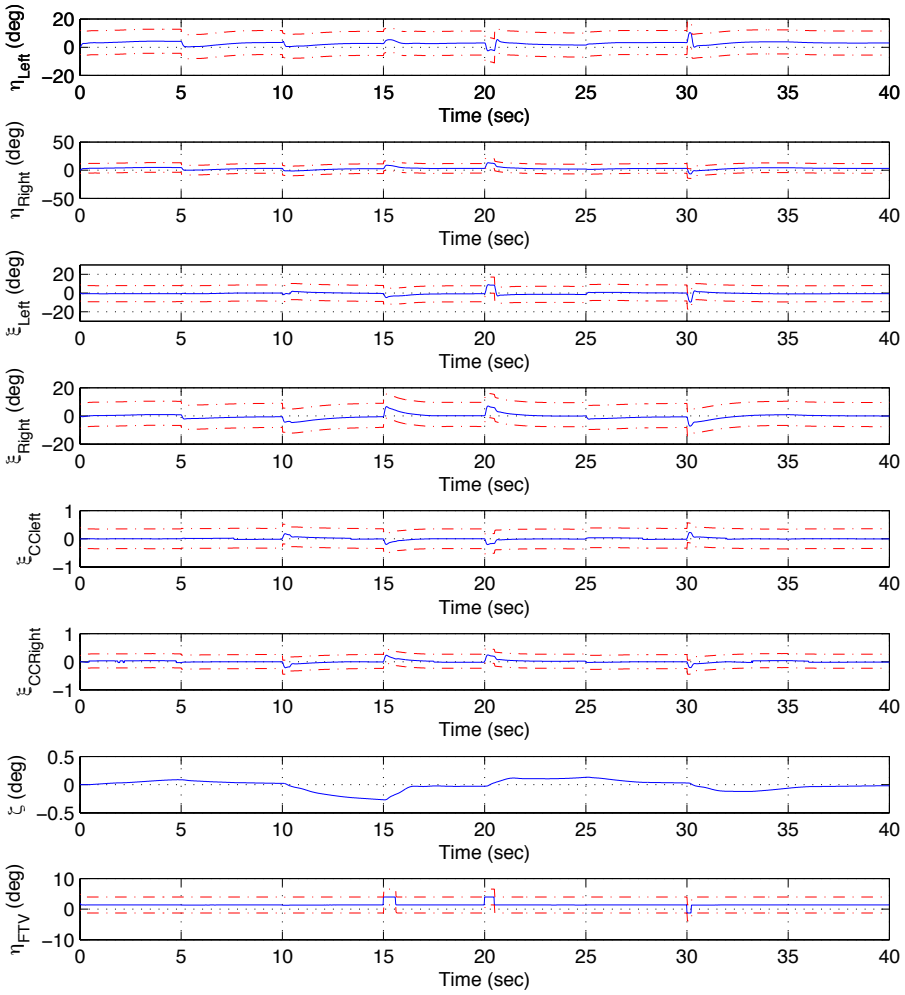

Figure C.88: Effector distribution for Canonical Control Allocation Method - Simulation 30

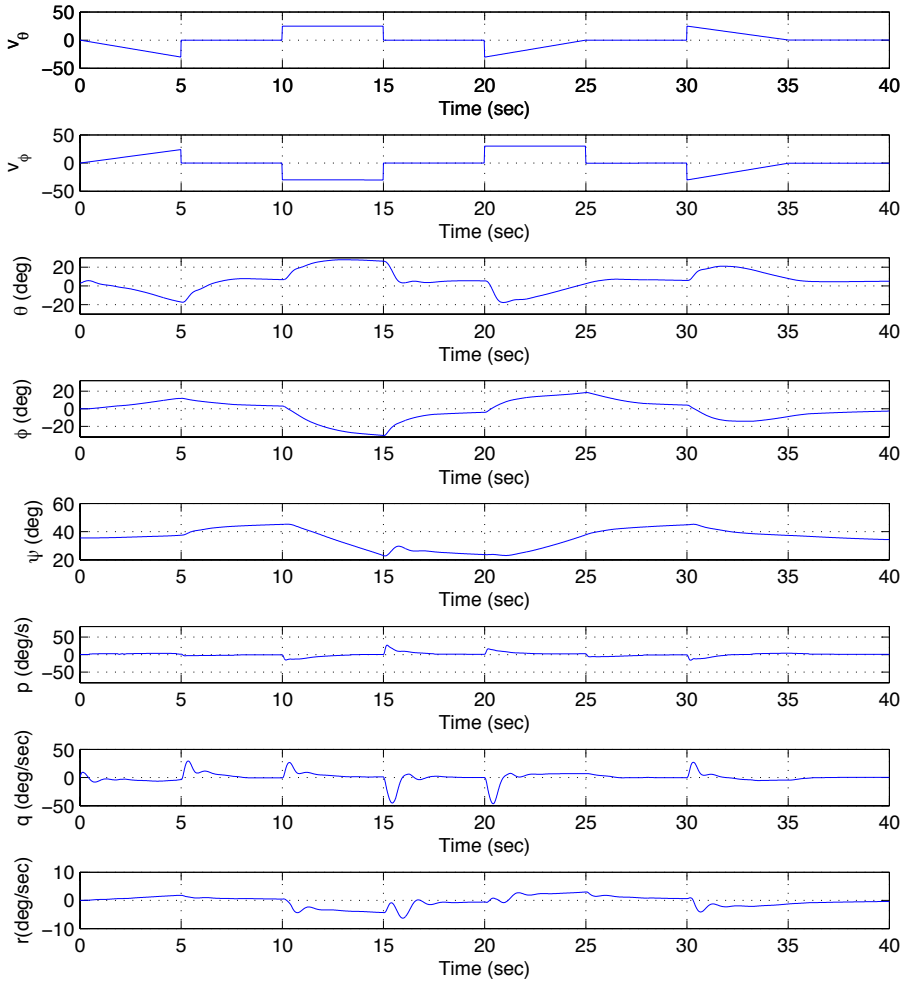

Figure C.89: States for Canonical Control Allocation - Simulation 30

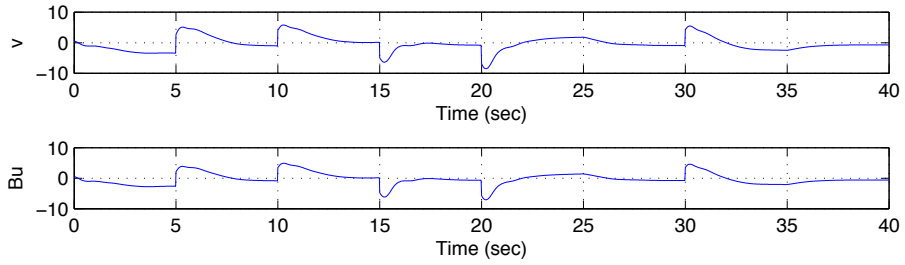

Figure C.90: v,Bu for Canonical Control Allocation Method - Simulation 30

Index

Vita

On the 5^{th} of May 1986 Ramey Jamil and a potted sunflower just happened to come into existence. Ramey Jamil spent his early days seduced by science, technology and all things digital, entranced by the mysteries of the universe and plagued by endless and lingering questions, all the while the sunflower bathed in the sunlight and thought 'forever more'. At the age of 19, Ramey's curiosities led him to Kingston University where he studied aerospace engineering. While he worked hard and long into the nights - the sunflower thought 'forever more'. Ramey finally graduated in 2008 with a BEng 2:1 (hons) - he was elated but his thirst for knowledge had not subdued, he decided to seclude himself in far out village in the middle of nowhere called Cranfield, where he learned at the feet of learned men and was exposed to concepts he had never before imaged - the sunflower thought 'forever more'. For three and half years Ramey endured a journey full of obstacles and hardship, all in the name of knowledge. In 2012 Ramey Jamil left Cranfield University a whole lot wiser and a whole lot older after being crowned *Control Allocation Extraordinaire*. All the while the sunflower remained bathing in the sunlight lost in thought - 'forever more'. If perhaps we understood the reason as to why the potted sunflower had decided to remain bathing in sunlight doing nothing but uttering the thought 'forever more', then we may perhaps understand a great deal more about the intricacies of the universe. But alas we don't and the sunflower shall continue to bath in the sunlight and Ramey shall endure the hardships of academia forever more.